

**Evaluation of Current Descriptions of
Peroxisomal Biogenesis and Inheritance
in *S. cerevisiae*: A Tale of Two Models**



The
University
Of
Sheffield.

Paul Galvin

Thesis submitted to the University of Sheffield in partial
fulfilment of the requirements for the degree of Doctor of
Philosophy

The Department of Molecular Biology and Biotechnology

The University of Sheffield

July 2017

Abstract

The peroxisome is an organelle conserved across Eukaryota. Ever since their discovery, the scientific consensus regarding the processes through which peroxisomes are formed and are inherited has changed several times. It is now known that peroxisomes are either produced through fission of pre-existing ones or *de novo* from the endoplasmic reticulum (ER). However, the relative importance of these processes and the conditions in which they occur is still a subject of much debate. This has led to the proposal of several models attempting to explain the situation, predominantly supported through evidence gathered studying the budding yeast *Saccharomyces cerevisiae*.

An evaluation of some of the proposals of these models in yeast is the main thread of this study. One such model proposed that the division and inheritance of peroxisomes are coupled processes guaranteeing that the same number of peroxisomes is maintained through multiple generations; another suggested that the *de novo* synthesis of peroxisomes occurs continuously in *S. cerevisiae* by the fusion of previously unrecognised heterotypic vesicles, an observation which disagrees with much of the other evidence gathered regarding the process in the organism.

To address these questions, a system of imaging multiple generations of *S. cerevisiae* cells was necessary, alongside the creation of a computer-assisted workflow to analyse and quantify these and other images of peroxisomes and cells.

Results from the long time-lapse live-cell imaging experiments show that the behaviour of peroxisomes is complex and that a direct relationship between division and inheritance is hard to demonstrate in practice, especially with techniques currently available. Moreover, live-cell experiments in conjunction with computer-quantified images corroborated previous evidence regarding the process of *de novo* synthesis and demonstrated the lack of *de novo* synthesis in cells already containing peroxisomes.

Overall, this study shows the usefulness of live cell imaging and computerised analysis for studying peroxisomes. It showcases what can currently be concluded using these techniques for studying this organelle in *S. cerevisiae*, examines the limitations of the restrictions of spatial and temporal resolutions, and explores what progress is necessary to decipher the peroxisome biogenesis and inheritance situation in the future.

Acknowledgements

I would first like to acknowledge Pete Artymiuk for giving me the opportunity to pursue a PhD. Pete sadly passed away only a few months after I started, and I was fortunate to be picked up by Jeremy Craven, who has been my supervisor since. I subsequently ended up in Ewald Hettema's lab, where I was welcomed by everyone there.

So I would like to thank Jeremy for his support and guidance as my supervisor, and for giving me some direction after the loss of Pete and since. I would like to thank Ewald for acting as a second supervisor, for welcoming me into his lab and group and for his guidance and knowledge concerning all things peroxisomes. I would like to thank the rest of E28: Alison, Jimmy, Jamie, John, Joanne, Nadal, Lakhan, Murtakab, Don and Georgia (and anyone else I encountered during my time in E28) for their help, advice, support and general chatter. I'd like to particularly recognise: Alison, who took me under her wing when I first showed up to do some experiments - her slightly maverick style of experimentation has stuck with me since (for good or bad!); John, for many hours shared discussing and playing board games; Nadal, who was always willing to lend a hand especially when I really didn't know what I was doing; Lakhan, for our many discussions concerning work, the quirks of the English language, and poignant Hindi and English sayings; and Don, for his optimism. I hope I taught them a thing or two by the end as well.

Thanks to Josh, Lenny, and all the people I've met for an enjoyable time in Sheffield. I would also like to thank Katy for her continued encouragement and companionship, and my parents for their support even though they almost certainly didn't know what I was doing.

Contents

Abstract	II
List of Figures	XI
List of Tables	XVI
Abbreviations and Glossary	XVIII
Chapter 1: Introduction	1
Preface.....	1
1.1 The Peroxisome.....	3
1.2 The Peroxisomal Disorders	5
1.2.1 The Peroxisomal Biogenesis Disorders (PBDs)	5
1.2.2 Single Peroxisomal Enzyme Deficiencies	9
1.3 Peroxisomal Biogenesis	10
1.3.1 Peroxisomal Membrane Protein Import	11
1.3.2 Peroxisomal Matrix Protein Import.....	12
1.3.3 Fission of Peroxisomes.....	14
1.3.4 New Peroxisome Formation.....	14
1.4 Peroxisome Inheritance.....	21
1.5 Time-Lapse Live Cell Imaging, Image Processing and Quantification	25
1.5.1 Time-Lapse Live Cell Imaging.....	25
1.5.2 Image Analysis of Peroxisomes	31
1.6 Research Scope and Questions	36
1.6.1 Vesicle Fusion Model.....	36
1.6.2 Yeast Population Control.....	37

1.6.3 Outline of Thesis	38
Chapter 2: Materials and Methods	40
2.1 <i>S. cerevisiae</i> Strains	40
2.2 DNA Manipulation	40
2.2.1 Polymerase Chain Reaction (PCR).....	40
2.2.2 Agarose Gel Electrophoresis	41
2.2.3 Gel Extraction and DNA Purification	41
2.2.4 Plasmid Isolation (Miniprep)	42
2.2.5 Restriction Enzyme Digestion.....	42
2.3 Chemical Reagents	42
2.4 Primers	42
2.5 Plasmids	46
2.6 Culture Media.....	49
2.7 <i>Saccharomyces cerevisiae</i> Experimental Procedures.....	51
2.7.1 General Growth Procedure.....	51
2.7.2 High Efficiency Transformation	51
2.7.3 One Step Transformation	51
2.7.4 Yeast Genomic DNA Isolation.....	52
2.8 <i>Escherichia coli</i> Experimental Procedures	53
2.8.1 <i>E. coli</i> Strains.....	53
2.8.2 <i>E. coli</i> General Growth Procedure	53
2.8.3 Production of Electro-competent <i>E. coli</i> Cells.....	53
2.8.4 <i>E. coli</i> Transformation.....	54

2.8.5 Electroporation of <i>E.coli</i>	54
2.9 Microscopy and Imaging.....	55
2.9.1 Microscopy	55
2.9.2 Flourescent Proteins.....	55
2.9.3 Preparation of Agarose Pads for Optimal Growth Conditions.....	56
2.9.4 Microfluidic System.....	56
2.9.5 Microscope Software and Modules.....	59
2.10 Making New mNeonGreen Plasmids and Genomically Integrated Strain.....	60
2.10.1 Creation of Original mNeonGreen Plasmid	60
2.10.2 Replacing the Promoter.....	60
2.10.3 Creating a Genomically Integrated mNeonGreen Strain	61
2.11 Computational Work.....	64
2.11.1 FIJI.....	64
2.11.2 SnapGene and SerialCloner	64
2.12 Image Processing Pathways.....	65
2.13 Analysing Peroxisome Image Data.....	67
2.13.1 Introduction	67
2.13.2 Pathway of Analysis	67
2.13.3 Python Code for Peroxisomal Analysis.....	72
2.14 Analysing Cell Data.....	73
2.14.1 Introduction	73
2.14.2 Pathway of Analysis	73
2.14.3 Python Code for Cell Image Analysis	76

Chapter 3: Re-evaluation of Vesicle Fusion Model of Peroxisome Biogenesis in <i>S. cerevisiae</i>	77
3.1 Introduction	77
3.2 Re-evaluation of the Role of Pex1 and Pex6 in Peroxisome Biogenesis	80
3.3 Fission of Peroxisomes in Absence of Dynamin-Related Proteins Vps1 and Dnm1	83
3.4 Asymmetric Division of BiFC Marker and Peroxisomal Matrix Marker	87
3.5 Re-examination of the Vesicle Fusion Model	91
Chapter 4: Development of Live Cell Imaging and Image Analysis	92
4.1. Introduction	92
4.2 Experimental Requirements	92
4.3 Decreasing Total Light Exposure	94
4.3.1 Locating a New Fluorescent Protein	95
4.3.2 Increasing the Amount of Fluorescent Protein	97
4.3.3 Summary	98
4.4 Fluorescent Protein Expression	99
4.4.1 Ensuring Uniform Expression	100
4.5 Computational Analysis of Live Cell Images	102
4.5.1 Introduction	102
4.5.2 TrackMate	102
4.5.3 Manual Cell Segmentation	105
4.5.4 Matching Peroxisomes to Cells	106
Chapter 5: Evaluating the KPPC Model Using One Cell	108
5.1 Introduction	108
5.2 Data Acquisition and Handling	110

5.3 Analysis of the Images.....	112
5.4 In-depth Analysis of One Cell.....	114
5.4.1 Evaluation of Peroxisome Detection and Tracking in One Cell.....	116
5.5 Peroxisome Detection	117
5.6 Peroxisome Tracking	127
5.6.1 “The Private Life of Peroxisomes” - Tracking Peroxisomes in Cells A and E over Twenty Frames	127
5.6.2 Summary of Peroxisome Tracking.....	134
5.7 Peroxisomal Fission and <i>De novo</i> Synthesis	138
5.8 Insights into Peroxisomal Behaviour from Cells A and E in Cluster 1	141
5.9 Regarding the KPPC Model Using Cell A from Cluster 1	143
5.10 Summary.....	144
Chapter 6: Analysis of Cell Cluster and Clusters	146
6.1 Cluster 1.....	147
6.1.1 General Trends	147
6.1.2 Cell A and Buds	148
6.1.3 Cell B and Buds.....	150
6.1.4 Cell C and Buds	151
6.1.5 Cell D and Bud	152
6.1.6 Cell G and Bud	152
6.1.7 Summary of Behaviour	152
6.2 Peroxisomal Inheritance in Other Cell Clusters	157
6.3 Evaluation of the KPPC Model from Analysis of All Clusters	163
6.3.1 Further Discussion Regarding the KPPC Model.....	167

6.4 Closing Remarks.....	172
Appendix A: Data Structures and Terminology in Image Processing	173
Appendix B: FIJI Pointers	175
B.1 Scripting in FIJI.....	175
B.2 Tips and Tricks in FIJI.....	176
B.3 FIJI Tips for Manual Cell Outlining	176
Appendix C: Image Processing Techniques	177
C.1 Rolling Ball Algorithm	177
C.2 Z Projection.....	177
C.3 Difference of Gaussians (DoG)	178
C.4 Conversion to 8-bit	179
C.5 Maximum Finder Algorithm.....	180
C.6 Auto Local Threshold.....	180
Appendix D: Programs Utilising Peroxisomal and Cell Image Analysis Methods. 181	
D.1 Program to Co-localise Two Different Fluorescent Markers	181
D.2 Program to Analyse Number of Peroxisomes Per Cell.....	184
D.3 Program to Analyse Genome Wide Screen of Peroxisomal Mutants.....	191
Appendix E: Resolution Limits	196
Appendix F: Re-evaluation of the role of Pex1 and dynamin-related proteins in peroxisome membrane biogenesis.....	197
Appendix G: 100 Frame-Montage of Cell A	214
Appendix H: Non-annotated Versions of Figures 6.6 and 6.7a-e for KPPC Model 215	

Appendix I: Cluster Lineages and Graphs of Peroxisomal Number Per Frame For Each Cell in Clusters 2-5 for Evaluation of Yeast Peroxisome Population Control Model.....	219
References	233

List of Figures

Figure 1.1 Basic structure of a peroxisome.	3
Figure 1.2. Diagram of peroxisomal membrane protein import and involved peroxins.....	12
Figure 1.3. Model of peroxisomal matrix protein import and involved peroxins	13
Figure 1.4. Growth and division model of peroxisome biogenesis	16
Figure 1.5. Maturation model of peroxisome biogenesis	16
Figure 1.6 Vesicle fusion model of peroxisome biogenesis	18
Figure 1.7. Mammalian model for peroxisome biogenesis.	18
Figure 1.8. Examples of peroxisome distribution in wild-type <i>S. cerevisiae</i> in contrast with <i>inp2</i> and <i>inp1</i> mutant cells.....	22
Figure 1.9. The KPPC model of peroxisome population control as proposed by Knoblach et al., 2013.....	24
Figure 1.10. Two methods of live-cell imaging utilising agarose pads.	26
Figure 1.11. Comparison of live-cell imaging using the glass-bottomed dish vs. cell culture chamber over an 8-hour experiment.....	27
Figure 1.12. Outline of Definite Focus Module	29
Figure 1.13. Experiments before and after hardware-assisted focusing using Definite Focus module.	29
Figure 1.14. Interplay between the factors affecting live cell imaging.....	30
Figure 1.15. Images are made up of grids of numbers	33
Figure 1.16. Example of thresholding.....	34
Figure 1.17. Proposed scenarios showing number of peroxisomes against time over 3 cell divisions.	38
Figure 2.1. Stages of making a plasmid via homologous recombination in <i>S. cerevisiae</i>	46

Figure 2.2. Microfluidic System equipment used in live-cell imaging.....	57
Figure 2.3. Cell culture chamber within the microfluidic plate.	58
Figure 2.4. Cell trapping mechanism using the elastic ceiling of the cell chamber.....	59
Figure 2.5. Map of the plasmid pAUL15 demonstrating the various regions contained on the plasmid.....	61
Figure 2.6. A map of the plasmid pAUL15 demonstrating the region between the PTS1 and PGK terminator that is cut by HindIII.....	62
Figure 2.7. A map of the plasmid pAUL19 demonstrating the various regions contained on the plasmid. NAT = clonNAT resistance sequence.	62
Figure 2.8. Initial image processing pathway.....	65
Figure 2.9. Example of raw image data.....	66
Figure 2.10. Peroxisomal and cellular channels following pre-processing.....	66
Figure 2.11. Peroxisomal image processing pathway.....	67
Figure 2.12. Example of a Gaussian blur.....	68
Figure 2.13. Peroxisomal channel from Figure 2.10 after difference of Gaussians filter and conversion to 8-bit images.....	69
Figure 2.14. Peroxisomal image from Figure 2.13 with overlay of detected maxima	69
Figure 2.15. Peroxisomal image from Figure 2.13 that has been subjected to automatic thresholding (becoming a binary image).....	70
Figure 2.16. Peroxisomal image from Figure 2.15 with overlay of detected particles, as denoted by the yellow border around an object	70
Figure 2.17. Section of Figure 2.9 showing peroxisomal image processing starting from the raw image data	71
Figure 2.18. Cell image processing pathway. Images of cells are first converted to 8-bit images before being subjected to an automated local thresholding, before conversion to mask..	74

Figure 2.19. Processing of cell images.....	75
Figure 2.20. Section of Figure 2.9 showing processing of cell images starting from raw image data	76
Figure 3.1 Vesicle fusion model of peroxisome biogenesis	78
Figure 3.2. Colocalisation of Pex11 and Pex13 in <i>WT</i> , <i>pex1</i> , <i>pex6</i> and <i>pex1/pex6</i> cells.....	82
Figure 3.3. Box plot representing the measured distances between the centre of each fluorescent Pex11-RFP and the nearest neighbouring Pex13-GFP spot for each of the strains	82
Figure 3.4. Possible course of events of <i>de novo</i> synthesis in <i>vps1/dnm1</i> cells according to the vesicle fusion model.....	83
Figure 3.5. Stills of a time-lapse video of <i>vps1/dnm1</i> cells with galactose-inducible Pex19 expressing HcRed-PTS1 from a plasmid.....	84
Figure 3.6. Stills of a time-lapse video of <i>vps1/dnm1</i> cells with galactose-inducible Pex19 (same as Figure 3.5) showing division of single large peroxisome upon cytokinesis...	85
Figure 3.7. Images of haploid <i>WT</i> cells expressing Pex2-VN, Pex14-VC, and HcRed-PTS1 from a plasmid.....	88
Figure 3.8. Images of diploid <i>vps1</i> cells expressing Pex13-VN, Pex14-VC and HcRed-PTS1.	89
Figure 3.9. Video stills taken from a video of <i>vps1</i> diploid cells expressing Pex13-VN, Pex14-VC and HcRed-PTS1	90
Figure 4.1. Signal strength as the only remaining aspect to optimise	94
Figure 4.2. Comparison between pAUL3 plasmid (HIS promoter) and the pAUL15 plasmid (TPI promoter)	98
Figure 4.3. Variable levels of mNeonGreen-PTS1 expressed (from plasmid pAUL15) in diploid <i>WT</i> cells grown on glucose for 4 hours.	99
Figure 4.4. Example of <i>WT S. cerevisiae</i> cells expressing mNeonGreen-PTS1 (green) from the genome.....	101

Figure 4.5. Schematic of TrackMate workflow.....	103
Figure 4.6. A schematic diagram of the linking of objects together to make tracks	104
Figure 4.7. Example of output from the TrackMate algorithm	104
Figure 4.8. Manual cell outlining in FIJI.....	106
Figure 5.1. Examples of cells growing sub-optimally due to the effects of phototoxicity when imaged at 30 or 150 second intervals for 8 hours	109
Figure 5.2. Acquisition and cropping of data.....	110
Figure 5.3. Progression of the growth of Cluster 1 from the original mother cell ('Cell A').	114
Figure 5.4. Montage of Cell A between frames 22 and 41	115
Figure 5.5. Example of frame-by-frame breakdown used to evaluate peroxisome tracking ability of the TrackMate algorithm	116
Figure 5.6. YZ projection of frame 28-30	119
Figure 5.7. YZ projection of frames 32 and 33	120
Figure 5.8. (following 5 pages). Frames 22-41 of Cell A in Cluster 1.....	121
Figure 5.9. Frames 32 and 33 showing splitting of peroxisome '4' into '4' and '43' and corresponding intensity values.	139
Figure 5.10. <i>imp2</i> cell showing <i>de novo</i> synthesis of peroxisomes and corresponding increases in intensity values	140
Figure 6.1 Representation of the lineage for all the cells that are present in this cluster....	147
Figure 6.2. Graph of number of peroxisomes per cell for all the cells in Cluster 1	154
Figure 6.3a-e (above and previous page). Individual graphs of mother cells (A, B, C, D and G) and their bud cells.	156
Figure 6.4. Average difference in the number of peroxisomes in mother cells in frames relative to when a bud first becomes visible	161

Figure 6.5. Average number of peroxisomes in a bud relative to when the bud first appears..	162
Figure 6.6. Comparison of number of peroxisomes in the mother 10 frames prior to bud appearing and number of peroxisomes in bud 20 frames after it has appeared.	164
Figure 6.7. Representation of events using the peroxisomal number data.....	166
Figure 6.8a and b. a) Number of frames between buddings and b) Number of frames since buds appeared before they start producing buds themselves.....	171
Figure A.1. Examples of different types of image data structure.....	174
Figure C.1. Example of three Gaussian functions	179

List of Tables

Table 1.1. Peroxins identified in <i>S.cerevisiae</i> and <i>Homo sapiens</i>	7
Table 1.2. The single peroxisomal enzyme deficiencies	9
Table 2.1. Yeast strains used in this study	40
Table 2.2. Primers used in this study.....	43
Table 2.3. Plasmids used in this study.....	47
Table 2.4. Media used in this study.....	49
Table 2.5. <i>E. coli</i> strains used in this study.....	53
Table 2.6. Fluorescent proteins used in this study	55
Table 3.1. Key contrasting points between the growth and division model and the vesicle fusion model	79
Table 3.2. Proposed role of Pex1 and Pex6 in vesicle fusion model, how this was tested, and the results expected in line with either the vesicle fusion or growth and division model	80
Table 3.3. Role of Vps1 and Dnm1 in peroxisomal fission in the vesicle fusion model, how this was tested, and the results expected in line with either the vesicle fusion or growth and division model.....	83
Table 4.1. Comparison of EGFP and mNeonGreen fluorescent proteins	97
Table 5.1. Image data acquired, assigned name in analysis and filename in external media	110
Table 5.2. Summary of TrackMate's detection of peroxisomes in Cells A and E across the twenty frames examined in detail (Figure 5.8)	121
Table 5.3. Tracks assigned to peroxisomes in Cells A and E over the course of the twenty frames by the TrackMate algorithm	135
Table 5.4 (next page). Manual interpretation of tracks that each peroxisome is assigned to over time.....	135

Table 5.5. Peroxisome numbers in Cell A, and Cells C and E at the start and end of their respective buddings.....	143
Table 6.1. Proposal of KPPC model and expected observations.	146
Table 6.2. Frame when each cell is present, along with any buds they produce.....	147
Table 6.3. Buds of Cell A do not make more peroxisomes until after they have finished budding.....	150
Table 6.4 (next page). The correlation between peaks in the number of peroxisomes in a mother cell and when buds first appear.....	159
Table 6.5. Proposal of KPPC model, expected observations for this analysis and actual results.	165

Abbreviations and Glossary

Abbreviation	Meaning
λ	Lambda – used to denote wavelength of light
2TY	2x Tryptone, Yeast Extract media (for bacterial growth)
2D; 3D; 4D; 5D	2-dimensional; etc. – used in this instance to refer to types of image data. 2D only has XY dimensions, 3D has XYZ/XYC/XYT dimensions, etc.
AAA+ ATPase	ATPases Associated with diverse cellular Activities
ATP	Adenosine Triphosphate
BiFC	Bimolecular fluorescence complementation – technique to show interaction between two proteins using fragments of fluorescent proteins that only become visible when brought together. See also VN-; VC-
CCD; EMCCD	Charge-coupled Device; Electron Multiplying CCD – types of digital camera used in fluorescence microscopy to detect incoming photons
CFP	Cyan Fluorescent Protein – derived from the original GFP from <i>Aequorea victoria</i> (Demachy et al., 2005)
CMOS	Complementary metal–oxide–semiconductor – type of digital camera used in fluorescence microscopy to detect incoming photons
DAB	3,3'-Diaminobenzidine – used as a stain of nucleic acids and proteins
DAPI	4',6-diamidino-2-phenylindole – blue fluorescent stain
DoG	Difference of Gaussians – type of filtering technique whereby one image convolved with a Gaussian function is taken away from the same image convolved with a Gaussian function of smaller radius
DRP	Dynamain-related Protein – Dynamins are a group of proteins involved in scission of vesicles
EC	Extinction Coefficient – a measure of how strongly a substance absorbs light of a given wavelength
EDTA	Ethylenediaminetetraacetic acid – used to sequester metal ions in solution
EUROSCARF	European <i>Saccharomyces cerevisiae</i> Archive for Functional Analysis
GFP; EGFP	Green Fluorescent Protein; Enhanced GFP – the first fluorescent protein widely studied, and its

	engineered variant used in fluorescence microscopy to this day (Tsien, 1998)
ER	Endoplasmic Reticulum
GAL1 promoter	Promoter of the Galactose 1 gene used to give conditional expression of downstream sequences (only active in presence of galactose)
HE	High-efficiency (i.e. HE transformation)
HIS	Can be used to refer to the amino acid Histidine; the HIS3 gene that is used for selection and also the promoter of the HIS3 gene that is used to give moderate constitutive expression of downstream sequences
IR	Infra-red – wavelengths of light in excess of 700nm
IRD	Infantile Refsum disease – one of the peroxisomal biogenesis disorders (PBDs). Less severe than Zellweger Syndrome
LAP	Linear Assignment Problem – algorithm used by TrackMate to link objects together to make tracks
LED	Light-emitting Diode
LEU	Can be used to refer to the amino acid Leucine or the LEU2 gene that is used for selection
LiAc	Lithium acetate – used to permeabilise the yeast cell membrane in DNA transformation
MFA2 terminator	Terminator of the Mating pheromone a-factor gene used on plasmids
mPTS	Membrane Peroxisome Targeting Signal – proteins possessing this are recognised by Pex19 in the cytosol and brought to the peroxisomal membrane
mRFP	Monomeric Red Fluorescent Protein – engineered form of a red fluorescent protein from <i>Discosoma</i> (DsRed) (Campbell et al., 2002)
mNG	mNeonGreen fluorescent protein – Brightest fluorescent protein to date, engineered from a yellow protein in <i>Branchiostoma lanceolatum</i> (Shaner et al., 2013)
N/A	Not Applicable
NALD	Neonatal Adrenoleukodystrophy - one of the peroxisomal biogenesis disorders (PBDs). Least severe of the PBDs
NAT	nourseothricin N-acetyl transferase, a protein encoded by the natMX gene which inactivates the antibiotic nourseothricin (also known as clonNAT)
NB	<i>Nota bene</i> – ‘note’

nm	Nanometres
OD₆₀₀	Optical Density at 600nm – used to measure turbidity of yeast culture and therefore amount of growth
pAUL; pAS; pEH	Plasmid nomenclature used in the laboratory to distinguish between plasmids and their origins
PBDs	Peroxisomal Biogenesis Disorders
PCR	Polymerase Chain Reaction
PEG	Polyethylene glycol
PEX; Pex	Peroxin – a protein associated with biogenesis of peroxisomes.
PGK terminator	Terminator of the Phosphoglycerate kinase gene used on plasmids
PMP	Peroxisomal Membrane Protein
PTS	Peroxisomal Targeting Signal – protein with a PTS are targeted to peroxisomes. There are two types – the C-terminal PTS1, and the N-terminal PTS2.
QY	Quantum Yield, also Phi (Φ) – given as a ratio between 0 and 1, this is probability that a molecule will emit a photon for every 1 photon absorbed
RCDP	Rhizomelic Chondrodysplasia Punctata – brain disorder characterised by shortening of the rhizomelia (proximal bones). RCDP1 is a PBD associated with mutation in PEX7.
RING (finger)	Really Interesting New Gene (finger) – a zinc finger domain of a protein usually involved in ubiquitination
ROI	Region of Interest – term used in FIJI for objects that have been found via automated processing or manually outlined. Their properties can be stored in an ROI Manager
RNA; mRNA	Ribonucleic acid; messenger RNA
TEF1 promoter	Promoter of the Translation Elongation Factor 1 gene used to give high levels of expressions of downstream sequences
TE	Tris and EDTA-containing buffer used in elution of DNA
TPI1 promoter	Promoter of the Triose Phosphate Isomerase 1 gene used to give high levels of expressions of downstream sequences
UV	Ultra-violet – wavelengths of light between 10 and 400nm

URA	Can be used to refer to the nucleobase Uracil or the URA3 gene that is used for selection
VN-; VC-	N-terminal half of Venus fluorescent protein; C-terminal half of Venus fluorescent protein; See also BiFC
WT	Wild-type – yeast strain with no mutations (excluding auxotrophic mutations necessary for selection)
YPD	Yeast Peptone Dextrose – a complete media (containing all amino acids, sugars and other nutrients) necessary for yeast growth
ZS	Zellweger Syndrome – the most severe of the peroxisomal biogenesis disorders (PBDs)
µm	Micrometres or microns

A Note on Nomenclature

When referring to genes and proteins in *S. cerevisiae*, the standard convention of nomenclature has changed over time. Traditionally genes were written in all uppercase (e.g. PEX19), and proteins with just the first letter capitalised with a ‘p’ afterwards to denote protein (e.g. Pex19p). However, over time the ‘p’ has been dropped (e.g. Pex19), and this form is used in this body of work. Denoting mutant strains are shown through the use of italicised lower case letters, and are sometimes followed by the Greek uppercase delta (e.g. *pex19* or *pex19Δ*). The delta is not used in this study.

Both genes and proteins in mammalian cells are denoted with capital letters (e.g. PEX19 could refer to both the gene and its protein product).

Chapter 1: Introduction

Preface

The defining feature of eukaryotic organisms is the presence of a multitude of membrane-bound organelles, each performing a specialised cellular task. This compartmentalisation in separate membrane-bound structures gives rise to the complexity of Eukaryotic life compared with the other two domains of Bacteria and Archaea.

The discovery and elucidation of knowledge relating to organelles is intrinsically linked to developments in microscopy. The original light microscopes were used to describe cells in the 1660s and 1670s but it was not until the 1800s that organelles were initially described. The nucleus and vacuole were the first organelles to be designated and led to the proposition of cell theory in 1838 by Schleiden and Schwann (Mullock and Luzio, 2005). Mitochondria were recorded in 1842, and their ubiquity in cells was recognised by 1894 (Ernster and Schatz, 1981). In 1898 Camillo Golgi outlined the Golgi apparatus after staining cells with silver nitrate and osmium tetroxide (Golgi, 1898).

Observation of other organelles smaller than the Golgi or mitochondria had to wait until the development of improved microscopes, notably electron microscopy, which only became commercially available in 1939. Biochemical experiments in the 1940s led Charles de Duve in 1949 to hypothesise the existence of membrane bound compartments containing hydrolytic enzymes and he labelled them lysosomes (De Duve et al., 1955). They were directly observed by electron microscopy in 1955 (Novikoff et al., 1956).

Continuing advancements in microscopy techniques, most notably fluorescence microscopy in the 1990s, has allowed greater insight into cellular processes, particularly *in vivo*. After the discovery of organelles, the next questions were of their function in the cell, and their maintenance and persistence over generations. Biogenesis and inheritance of organelles are two processes that are intrinsically linked. Before each cell division, organelles increase in size, are divided, and separated into daughter cells. The necessity of this for some organelles is obvious; the nucleus carries DNA and therefore is vital to the continuation of nearly all cellular processes, and mitochondria and chloroplasts also possess a small amount of DNA which is critical for their function (Warren and Wickner, 1996). Additionally, the endoplasmic reticulum (ER) is the major site of lipid and protein synthesis, which via vesicle-mediated transport are eventually moved to other organelles. As membranes cannot be

synthesised *de novo*, in line with the proposition ‘*omnis membrana e membrana*’ (Blobel, 1980), inheritance of at least a portion of the ER is necessary. The requirement of inheritance of other cytoplasmic organelles is less obvious; if a cell does not inherit an organelle derived entirely from another (e.g. in the way that the Golgi is derived entirely from the ER), then the daughter cell should be able to make a new one *de novo* (Fagarasanu and Rachubinski, 2007). *De novo* formation of organelles has been demonstrated but many studies have shown the presence of dedicated organelle inheritance mechanisms (Fagarasanu et al., 2007; Hoepfner et al., 2001; Rossanese et al., 2001; Weisman, 2003). It can therefore be implied that manufacturing organelles anew is energetically costly and inheritance mechanisms are evolutionary advantageous.

This thesis is concerned with one organelle - the peroxisome; the biogenesis and inheritance of which has been a subject of much debate. Previous studies have outlined several theories and mechanisms surrounding the biogenesis and inheritance of peroxisomes, particularly in the budding yeast *Saccharomyces cerevisiae*. Although considerable research has been done in this area, much of it has focused on outlining individual proteins involved in the processes, and where they fit into or modify the current model(s). The focus of this thesis is to step away from individual proteins and to instead approach the study of peroxisomes biogenesis and inheritance using long-term live-cell imaging over several cell cycles, alongside computer-aided, quantitative approaches to analysing these and other image data of peroxisomes in *S. cerevisiae*. A great advantage of studying peroxisomes over other organelles is that they are relatively easy to observe - appearing as small, dot like objects under the florescent microscope, compared with for example, the string-like network of the ER. This attribute lends itself well to automatic recognition and counting techniques utilising computer software. Building on the existing yeast techniques, a method of imaging yeast populations over long periods was developed, along with means of processing and analysing different types of microscopy data.

In the following sections of this introduction the current state of knowledge concerning peroxisomes and their biogenesis and inheritance is outlined, predominantly in *S. cerevisiae*, and also the particular aspects of yeast peroxisome biogenesis and inheritance that will be addressed.

1.1 The Peroxisome

Peroxisomes were first described after the observation of membrane-enclosed cytoplasmic spheres in kidney electron micrographs that did not resemble any of the then agreed upon cell organelles, and were originally labelled as *microbodies* (Rhodin J., 1954). Subsequent studies in the 1960's found that these microbodies contained various enzymes involved in the production and breakdown of hydrogen peroxide, and it is from this that *peroxisomes* take their name (de Duve, 1969; De Duve and Baudhuin, 1966).

Nearly all eukaryotic organisms possess peroxisomes, from unicellular micro-organisms to higher plants and animals (Hua and Kim, 2016). Notable exceptions to this are protozoan parasites in the genera *Giardia* and *Trichomonas*, and parasitic amoebas of the genus *Entamoeba*, where no evidence of peroxisomes has been found (Hawkins et al., 2007; Parsons et al., 2001).

A peroxisome's structure consists of an inner protein-containing matrix, sometimes with a crystalline core, surrounded by a single lipid bilayer, and measuring between 0.1-1 μ m in diameter (van den Bosch et al., 1992; Zaar et al., 1991)(Figure 1.1). In contrast to mitochondria and chloroplasts, peroxisomes do not contain any transcription/translation machinery or DNA and import all proteins post-translationally (Schrader and Yoon, 2007).

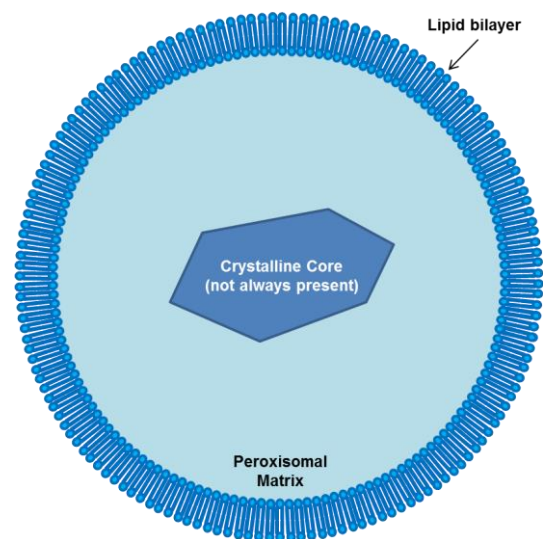


Figure 1.1 Basic structure of a peroxisome.

The proteins within the peroxisomal matrix perform various metabolic functions. Characteristically (but not universally), these are: (i) enzymes involved in the β -oxidation of fatty acids (Wanders and Waterham, 2006); (ii) oxidases involved in the production of hydrogen peroxide (del Rio et al., 1992); and (iii) enzymes carrying out the reduction of reactive oxygen species - notably the enzyme catalase, which performs hydrogen peroxide breakdown (Hettema and Motley, 2009; Pieuchot and Jedd, 2012).

However, the enzymatic content of peroxisomes varies wildly between cell types and also between species. In certain instances this caused peroxisomes to be originally identified as

different organelles, and some of these names are still commonly in use (Gabaldon, 2010). In Kinetoplastea, a protist group containing the parasites *Trypanosoma* and *Leishmania*, the peroxisome contains a majority of the enzymes in the glycolytic pathway and is still referred to as a *glycosome* (Haanstra et al., 2015; Michels et al., 2006). In plants, there are three described types of peroxisome: unspecialised peroxisomes; leaf peroxisomes that perform photorespiration; and *glyoxysomes* which are involved in the glyoxylate cycle in germinating seeds (Hayashi et al., 2000). All these peroxisome-like bodies are linked by conserved protein import machinery, a shared mechanism of fission by dynamin-like proteins and a similar pathway of biogenesis (Gabaldon, 2010; Michels et al., 2005; Parsons et al., 2001).

In humans, peroxisomes are found in all cell types, except for red blood cells (Berger et al., 2016; Wanders and Poll-The, 2015), and are especially prevalent in liver and kidney cells (Islinger et al., 2010).

1.2 The Peroxisomal Disorders

The importance of peroxisomes in humans is illustrated through the presentation of disorders in patients whose peroxisomes have defects to their normal metabolic function or biogenesis.

The first disorder now known to be associated with peroxisomes, Zellweger Syndrome (ZS), was outlined in the mid 1960's and early 1970's before the link between peroxisomes and the symptoms had been established. ZS was recognised and outlined by its namesake, Hans Zellweger, and colleagues, as a condition manifesting in infants and presenting as cranial abnormalities alongside deformities in the brain, liver, eyes and skeleton (Passarge and McAdams, 1967; Poznanski et al., 1970). It was only in 1973 that a link between ZS and peroxisomes was established by a group reporting the lack of peroxisomes in the hepatocytes and renal proximal tubule cells of ZS patients (Goldfischer et al., 1973). Since then, ZS has been joined by several related disorders: neonatal adrenoleukodystrophy (NALD), infantile Refsum disease (IRD) and rhizomelic chondrodysplasia punctata type 1 (RCDP1); collectively these are known as the peroxisomal biogenesis disorders (PBDs) (Braverman et al., 2013). In addition, defects in multiple peroxisomally-located enzymes have also been reported; these form the group of single matrix enzyme deficiencies (Wanders, 2014).

1.2.1 The Peroxisomal Biogenesis Disorders (PBDs)

The PBDs are all autosomal recessive disorders that arise from a defect in one or more of a set of proteins called peroxins, which in turn are encoded by PEX genes (Distel et al., 1996). The peroxins are each in some way responsible for the correct biogenesis and maintenance of a peroxisome; a patient with one of these disorders will have cells with an inadequate number of functional peroxisomes (Waterham and Ebberink, 2012). There are currently 31 identified PEX genes, each involved in either peroxisome generation, peroxisome membrane or matrix protein import, or peroxisome abundance (Smith and Aitchison, 2013). These functions are outlined in Table 1.1.

The PBDs are predominantly caused by a mutation in one of a set of 14 PEX genes (Braverman et al., 2016). Mutations in PEX1 account for between 60-70% of all cases, with PEX6 (~10%), PEX10, PEX12, and PEX26 making up the majority of the remaining cases (Ebberink et al., 2011; Yik et al., 2009). Of the four PBDs mentioned earlier, three originally described as separate entities - ZS, NALD, and IRD – show overlapping clinical phenotypes

and are now considered Zellweger Syndrome Spectrum (ZSS) type-disorders. RCDP1 is phenotypically distinct from the other disorders and remains classified separately (Weller et al., 2003).

The phenotypic differences across the ZSS are poorly defined, especially between the milder NALD and IRD forms. ZS is the most severe, characterised by cranial abnormalities, severe neurological dysfunction, and failure to thrive; consequently most infants die within the first year of life (Schutgens et al., 1986; Wilson et al., 1986). Cells in these infants presenting with a severe ZS phenotype will be entirely absent of peroxisomes. NALD and IRD presentations are more varied and less severe, with NALD patients surviving into their teens and some IRD patients into adulthood (Steinberg et al., 2006). Cells in patients with these milder phenotypes may have a low number of functional peroxisomes (Waterham and Ebberink, 2012), or a heterogeneity of functional peroxisomes both between different cells and different tissues, a phenomenon which is called peroxisomal mosaicism (Gootjes et al., 2004; Pineda et al., 1999).

Symptoms shared by all three include: hepatic disease; retinopathy; variable central nervous system (CNS) development delay; and progressive hearing loss, all of which present within the first few months of life (Wanders and Waterham, 2005). Owing to these overlapping clinical features, the term ‘peroxisome biogenesis disorders in the Zellweger spectrum’ (PBD-ZSD) has been recently proposed, with clinical definitions ranging from mild to severe (Braverman et al., 2016).

1.2.1.1 Rhizomelic Chondrodysplasia Punctata Type 1

The phenotypically distinct RCDP1 arises from a mutation in PEX7 (Waterham and Ebberink, 2012), which recognises peroxisome targeting signal 2 (PTS2) possessing proteins and directs them to the peroxisome (Motley et al., 2002; Purdue et al., 1997)(the mechanism is discussed in section 1.3.2). Only a small subset of proteins are directed to the peroxisomes via the PTS2 pathway, and consequently this gives rise to a phenotype that is clinically distinct from the other PBDs (Unselde et al., 1997). Notably, patients have short stature and facial abnormalities, arising from defects in bone structure. Expected lifespan of RCDP1 patients is varied but most usually die within the first 10 years of life (Steinberg et al., 2006; Wanders and Waterham, 2005).

Table 1.1. Peroxins identified in *S.cerevisiae* and *Homo sapiens*

NB Pex9 is not listed due to it being a misidentified open reading frame in *Yarrowia lipolytica*; it appears to be a Pex26 orthologue (Kiel et al., 2006).

Peroxi n	S. cerevisia e	H. sapien s	Process	Description
Pex1	✓	✓	Peroxisome matrix protein import	AAA+ ATPase that forms heterodimer with Pex6 and is responsible for recycling Pex5 from the peroxisomal membrane. Mutations in human PEX1 are by far the most common cause of PBDs.
Pex2	✓	✓	Peroxisome matrix protein import	RING finger complex peroxisomal membrane protein along with Pex10 and Pex12. Responsible for ubiquitination of Pex5.
Pex3	✓	✓	Peroxisome membrane protein import; Peroxisomal inheritance	Responsible for correct insertion of peroxisomal membrane proteins into the membrane via interaction with Pex19. Interacts with Inp1 to form anchor between cortical ER and peroxisome in peroxisomal retention. Required for de novo formation of peroxisomes.
Pex4	✓		Peroxisome matrix protein import	Part of ubiquitin conjugation complex with Pex22 that is required for ubiquitination of Pex5.
Pex5	✓	✓	Peroxisome matrix protein import	Receptor that recognises PTS1 containing proteins in the cytosol and brings them to the peroxisomal membrane; interacts with Pex14 to release protein cargo into peroxisomal matrix.
Pex6	✓	✓	Peroxisome matrix protein import	AAA+ ATPase that forms heterodimer with Pex1 and is responsible for recycling Pex5 from the peroxisomal membrane. Mutations in human PEX6 are second most common cause of PBDs.
Pex7	✓	✓	Peroxisome matrix protein import	Receptor that recognises PTS2 containing proteins in the cytosol and brings them to the peroxisomal membrane.
Pex8	✓		Peroxisome matrix protein import	Organises the importomer complex by bridging the docking complex and the RING finger complex; interacts with Pex5 and Pex7.
Pex10	✓	✓	Peroxisome matrix protein import	RING finger complex peroxisomal membrane protein along with Pex2 and Pex12. Responsible for ubiquitination of Pex5.
Pex11	✓	✓	Peroxisome proliferation	Elongates peroxisomal membrane to allow for fission of peroxisomes.
Pex12	✓	✓	Peroxisome matrix protein import	RING finger complex peroxisomal membrane protein along with Pex2 and Pex10. Responsible for ubiquitination of Pex5.
Pex13	✓	✓	Peroxisome matrix protein import	Forms part of docking complex with Pex14 and Pex17. Interacts and docks Pex5 and Pex7 at the peroxisomal membrane.
Pex14	✓	✓	Peroxisome matrix protein import	Forms part of docking complex with Pex13 and Pex17. Interacts and docks Pex5 and Pex7 at the peroxisomal membrane; responsible for translocation of cargo into peroxisomal matrix.
Pex15	✓		Peroxisome matrix protein import	Associates with the Pex1/Pex6 heterodimer, and anchors the complex at the peroxisomal membrane. Homologous to human PEX26.
Pex16		✓	Peroxisomal membrane protein import	Membrane receptor for Pex3; implicated in recruiting other peroxisomal membrane proteins to the ER. Required for de novo formation of peroxisomes.
Pex17	✓		Peroxisome matrix protein import	Forms part of docking complex with Pex13 and Pex14.
Pex18	✓		Peroxisome matrix protein import	Interacts with Pex7 in the PTS2 import pathway. Partial redundancy with Pex21.

Pex19	✓	✓	Peroxisomal membrane protein import	Chaperone responsible for import of class 1 peroxisomal membrane proteins (containing mPTS) from the cytosol. Interacts with Pex3 to insert proteins into the peroxisomal membrane. Aids Pex3 exit from the ER and therefore required for de novo formation of peroxisomes.
Pex20			Peroxisome matrix protein import	Found in <i>Yarrowia lipolytica</i> , it is a cofactor of Pex7 in the PTS2 import pathway.
Pex21	✓		Peroxisome matrix protein import	Interacts with Pex7 in the PTS2 import pathway. Partial redundancy with Pex18.
Pex22	✓		Peroxisome matrix protein import	Part of ubiquitin conjugation complex with Pex4 that is required for ubiquitination of Pex5.
Pex23		✓	Peroxisomal proliferation	Found in <i>Yarrowia lipolytica</i> , and a human homologue has been described (Jeynov et al., 2006). Functionally homologous to <i>S. cerevisiae</i> Pex30.
Pex24			Peroxisomal proliferation	Found in <i>Yarrowia lipolytica</i> . Functionally homologous to <i>S. cerevisiae</i> Pex28.
Pex25	✓		Peroxisomal proliferation	Peroxisomal membrane protein that regulates peroxisome size and number. In same family of proteins as Pex11 and Pex27. Paralogue of Pex27, believed to have arisen from whole genome duplication.
Pex26		✓	Peroxisome matrix protein import	Associates with the Pex11/Pex6 heterodimer, and anchors the complex at the peroxisomal membrane. Homologous to yeast Pex15.
Pex27	✓		Peroxisomal proliferation	Peroxisomal membrane protein that regulates peroxisome size and number. In same family of proteins as Pex11 and Pex25. Paralogue of Pex25, believed to have arisen from whole genome duplication.
Pex28	✓		Peroxisomal proliferation	Regulates peroxisome size, number and distribution. In same family as Pex29.
Pex29	✓		Peroxisomal proliferation	ER-resident protein that regulates peroxisome size, number and distribution. Negatively regulates peroxisome size. Role in controlling peroxisome destined vesicles from the ER. Interacts with Pex30. In same family as Pex28.
Pex30	✓		Peroxisomal proliferation	ER-resident protein that regulates peroxisome size, number and distribution. Negatively regulates peroxisome size. Role in controlling peroxisome destined vesicles from the ER. Interacts with Pex29. Partial functional redundancy with its paralogue Pex31.
Pex31	✓		Peroxisomal proliferation	Peroxisomal membrane protein that negatively regulates peroxisome size. Partial functional redundancy with its paralogue Pex31 and related protein Pex32.
Pex32	✓		Peroxisomal proliferation	Peroxisomal membrane protein that negatively regulates peroxisome size. Partial functional redundancy with related protein Pex31.
Pex33			Peroxisome matrix protein import	Identified in <i>Neurospora crassa</i> as part of the docking complex with Pex13 and Pex14.
Pex34	✓		Peroxisomal proliferation	Peroxisomal membrane protein involved in regulation of peroxisomal populations. Interacts with Pex11 family proteins (Pex11/Pex25/Pex27).

Adapted using information from (Sibirny, 2012; Smith and Aitchison, 2013) and the *Saccharomyces* Genome Database (SGD): <http://www.yeastgenome.org>, Cherry et al., 2012).

1.2.2 Single Peroxisomal Enzyme Deficiencies

The single peroxisomal enzyme deficiencies form the other group of diseases associated with peroxisomes. They arise due to a mutation in a protein that is either an enzyme located inside the peroxisomal matrix, or a protein that is involved in the transport of molecules into and out of the peroxisome. A list of these disorders of peroxisomal function is found in Table 1.2.

Table 1.2. The single peroxisomal enzyme deficiencies.

Collated using information in Wanders, 2014.

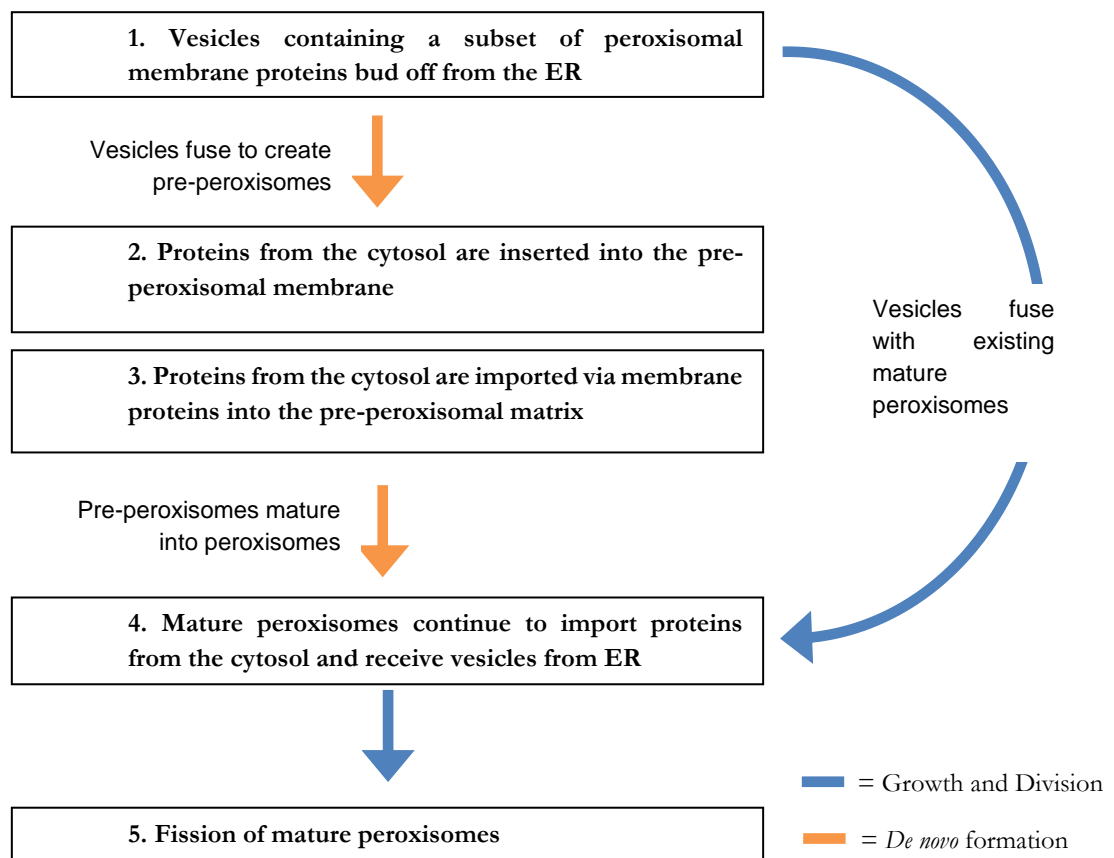
Disorder	Abbreviation	Mutant Gene	Pathway	References
X-linked adrenoleukodystrophy	X-ALD	ABCD1	Fatty acid β oxidation	(Budka et al., 1976; Engelen et al., 2012)
Acyl-CoA oxidase deficiency	ACOX-deficiency	ACOX1	Fatty acid β oxidation	(Ferdinandusse et al., 2007)
D-Bifunctional protein deficiency	DBP- deficiency	HSD17B4	Fatty acid β oxidation	(Ferdinandusse et al., 2006a)
Sterol-carrier-protein X deficiency	SCPx- deficiency	SCP2	Fatty acid β oxidation	(Ferdinandusse et al., 2006b)
2-Methylacyl-CoA racemase deficiency	AMACR-deficiency	AMACR	Fatty acid β oxidation	(Ferdinandusse et al., 2000; Setchell et al., 2003)
Rhizomelic chondrodysplasia punctata Type 2	RCDP2	GNPAT	Etherphospholipid biosynthesis	(Ofman et al., 1998)
Rhizomelic chondrodysplasia punctata Type 3	RCDP3	AGPS	Etherphospholipid biosynthesis	(Wanders et al., 1994)
Refsum disease	ARD/CRD	PHYH/PAHX	Fatty acid α oxidation	(Gerbert A. et al., 1997; Wierzbicki et al., 2002)
Primary Hyperoxaluria Type 1	PH-1	AGTX	Glyoxylate detoxification	(Danpure and Jennings, 1986; Pirulli et al., 2003; Williams et al., 2009)
Bile acid-CoA: amino acid N-acyltransferase deficiency	BAAT-deficiency	BAAT	Bile acid synthesis	(Carlton et al., 2003)
Acatlasemia		CAT	H ₂ O ₂ metabolism	(Ogata, 1991)

1.3 Peroxisomal Biogenesis

Although the PBDs arising from defects in peroxisomal biogenesis are now quite well outlined, the underlying process of peroxisomal biogenesis is still a target of much debate and research. Peroxisome biogenesis is the overarching term for the process of making more peroxisomes, and is performed by peroxins, the group of proteins mentioned earlier (Table 1.1). The first peroxins to be identified were in *Saccharomyces cerevisiae*, based on the inability of two mutants to grow on oleic acid medium. These mutants lacked detectable peroxisomes, and mislocalised peroxisomal matrix enzymes to the cytosol. The genes identified were labelled *pas1* and *pas2* (Erdmann et al., 1989), and are now known in the unified nomenclature as Pex1 and Pex4 respectively (Distel et al., 1996).

Peroxisomes are formed either *de novo* from the ER or by growth and division of pre-existing peroxisomes. An overview of the formation of peroxisomes can be presented as below.

There is still much contention over the relative importance of growth and division versus *de*



de novo synthesis processes, and whether they are mutually exclusive or occur in parallel. As such, there are competing models that emphasise the relative importance of one over the other, and also differ in other key aspects. Such models are described in section 1.3.4. There

are also questions over the relationship between the division of peroxisomes and their subsequent inheritance in *S. cerevisiae*; this is discussed in section 1.4.

Much more generally agreed upon are the underlying mechanisms surrounding peroxisomal membrane protein import, peroxisomal matrix protein import, and peroxisomal fission (steps 2, 3 and 5 respectively); these will be discussed first in sections 1.3.1 through to 1.3.3.

1.3.1 Peroxisomal Membrane Protein Import

As mentioned earlier, all peroxisomal proteins are translated on free polyribosomes (Lazarow, 2003; Lazarow and Fujiki, 1985), and therefore there must be import of these proteins into the peroxisomal membrane and peroxisomal matrix. Peroxisomal matrix proteins require the activity of proteins in the peroxisomal membrane in order to cross the lipid bilayer, and therefore the peroxisomal membrane protein import must occur first. There are two methods of inserting proteins into the peroxisomal membrane: either they are trafficked to the peroxisome via vesicles budding off from the ER, or they are inserted directly into the peroxisomal membrane from the cytosol (Figure 1.2).

In most PEX deletion mutants, peroxisomal matrix proteins are found in the cytosol, but cells still contain membranes with inserted peroxins ('peroxisomal ghosts') (Rucktäschel et al., 2011; Santos et al., 1988). However, in *pex3* and *pex19* mutants in yeast (Hetteema et al., 2000; Koek et al., 2007), and in *pex3*, *pex16* and *pex19* in mammals (Honsho et al., 1998; Kim et al., 2006; Matsuzono et al., 1999; Muntau et al., 2000), cells are devoid of both peroxisomes and peroxisomal membranes, and all membrane proteins are instead rapidly degraded or targeted to other membrane structures like mitochondria (Kim and Hetteema, 2015). For this reason, Pex3, Pex16 and Pex19 are implicated as key to the import of other peroxisomal membrane proteins (PMPs) and/or the formation of peroxisomal membranes.

A majority of PMPs contain a membrane peroxisomal targeting signal (mPTS), which is either a group of positively charged or a mixture of positive and hydrophobic residues that are flanked by a one or two transmembrane domains (Kim and Hetteema, 2015). Proteins possessing an mPTS are recognised and bound in the cytosol by Pex19, which proceeds to deliver these proteins to the peroxisomal membrane (Rottensteiner et al., 2004; Sacksteder et al., 2000). At the peroxisomal membrane, Pex19 interacts with Pex3, and the mPTS-possessing protein is incorporated into the membrane (Fang et al., 2004). The details of exactly how the proteins are inserted remain unclear. The proteins that possess this mPTS have been dubbed Class 1 PMPs; so by extension any peroxisomal membrane protein that

does not contain an mPTS is labelled a Class 2 PMP. Class 2 PMPs are targeted to peroxisomes via the ER (Jones et al., 2004). The only proteins currently known to be imported via this pathway are Pex3, Pex16 and Pex22 (Halbach et al., 2009; Matsuzaki and Fujiki, 2008).

1.3.2 Peroxisomal Matrix Protein Import

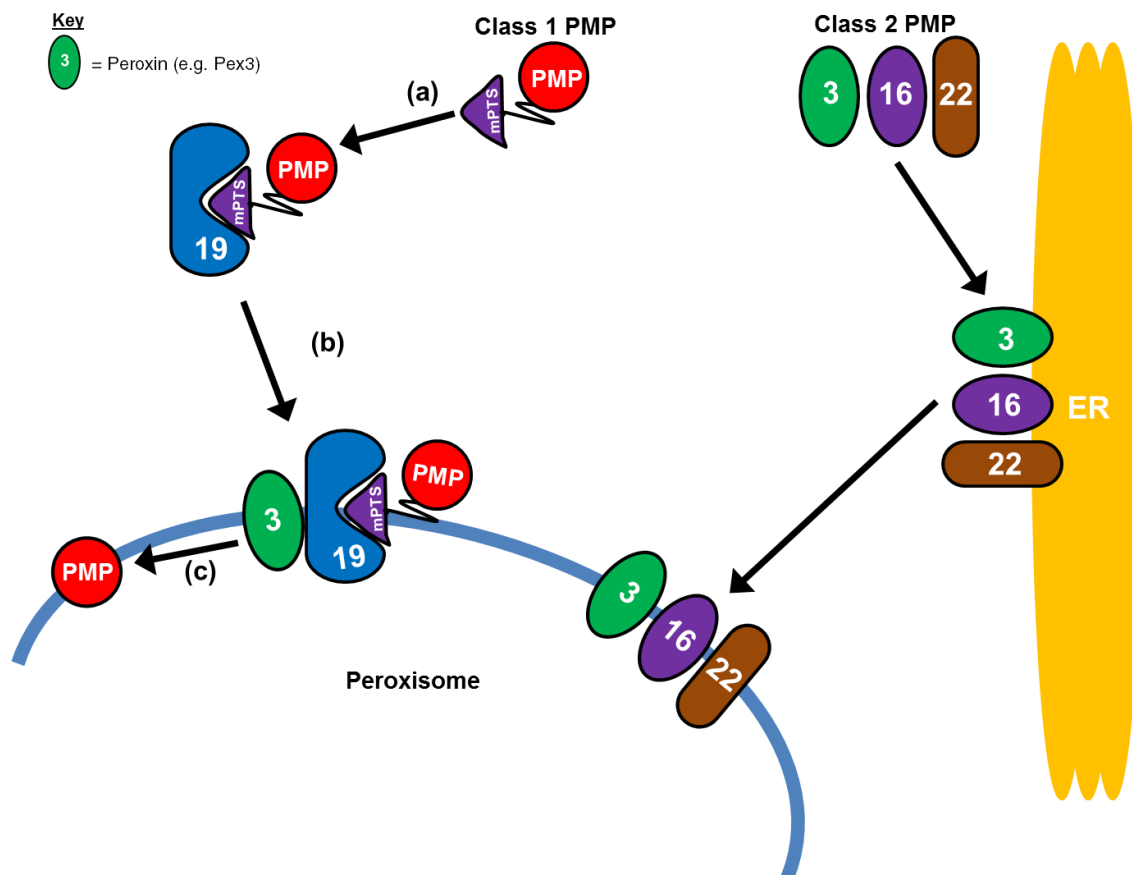


Figure 1.2. Diagram of peroxisomal membrane protein import and involved peroxins. (a) Class 1 peroxisomal membrane proteins (PMPs) possess a membrane peroxisomal targeting signal (mPTS) and are bound by Pex19 in the cytosol; (b) Pex19 and cargo are brought to the peroxisomal membrane where Pex19 interfaces with Pex3; (c) the protein is inserted into the peroxisomal membrane. Class 2 PMPs do not possess an mPTS, and are imported into the peroxisome by first trafficking to the ER.

Import of peroxisomal matrix proteins is an involved process requiring many peroxins (Figure 1.3). All proteins destined for the peroxisomal matrix possess a targeting signal that is recognised by one of two receptor/chaperone proteins in the cytosol. A majority of the matrix proteins possess a peroxisomal targeting signal 1 (PTS1). The PTS1 is a tripeptide C-terminal sequence, ordinarily taking the form of serine-lysine-leucine (S-K-L) (Gould et al., 1989), with some exceptions (Brocard and Hartig, 2006).

Proteins possessing a PTS1 are recognised and bound in the cytosol by the receptor Pex5 (Girzalsky et al., 2010). Pex5 and its protein cargo proceed to the peroxisomal docking machinery, a multipart complex comprising the proteins Pex13, Pex14 and Pex17 (Otera et al., 2002). Pex5 docks into the peroxisomal membrane in complex with Pex14, the protein cargo is then dissociated from Pex5, and the cargo is subsequently released into the peroxisomal matrix. Following this, Pex5 is monoubiquitinated by a ubiquitin ligase complex consisting of Pex2, Pex10 and Pex12, known as the RING finger complex (Platta et al., 2009; Williams et al., 2008), in conjunction with the ubiquitin conjugation complex of Pex4 and Pex22 (El Magraoui et al., 2014). The docking complex (Pex13/14/17) and the RING finger complex (Pex2/10/12) are interconnected by another protein, Pex8; the whole hepta-protein complex is referred to as the importomer (Agne et al., 2003). The monoubiquitination of Pex5 is necessary for it to be subsequently recycled from the peroxisomal membrane by the

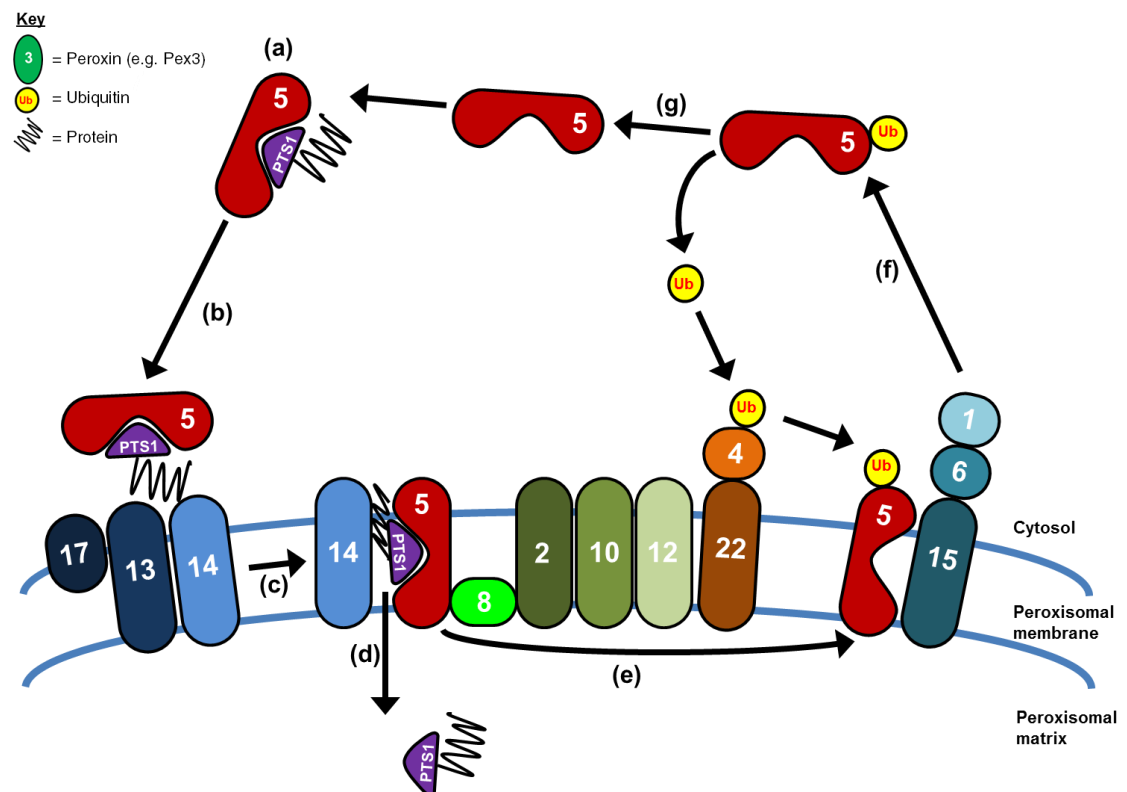


Figure 1.3. Model of peroxisomal matrix protein import and involved peroxins. (a) PTS1 or PTS2 (not shown) containing proteins are bound in the cytosol by Pex5. (b) Receptor and cargo docks with Pex13/Pex14/Pex17. (c) Receptor inserts into membrane in a complex with Pex14 and (d) the protein cargo is released into the peroxisome. (e) Pex5 is monoubiquitinated by the RING finger complex (Pex2/Pex10/Pex12), in conjunction with the ubiquitin conjugation complex (Pex4/Pex22). (f) Monoubiquitinated Pex5 is recycled from the peroxisomal membrane by AAA+ ATPases Pex1/Pex6, which are anchored in the membrane by Pex15. (g) Following deubiquitination, Pex5 is then free to bind further PTS1 containing proteins. PTS2-containing proteins are recognised by Pex7 in the cytosol which docks with Pex13/14/17 with aid of species-specific cofactors. The remainder is the same as the PTS1-Pex5 pathway. Based on Kim and Hettema, 2015.

activity of the AAA+ (ATPases Associated with diverse cellular Activities) ATPases Pex1 and Pex6 (Miyata and Fujiki, 2005; Platta et al., 2005). Following deubiquitination, Pex5 is then free to seek out further PTS1 containing proteins (Miyata et al., 2012).

As mentioned in section 1.2.1.1 with respect to RCDP1, there exists a PTS2 targeting sequence that is recognised by the protein Pex7. There are a comparatively small number of peroxisomal matrix proteins that possess this PTS2, which is a diffusely conserved N-terminal nonapeptide of sequence (R-L/V/I/Q)-XX-(L/V/I/H)-(L/S/G/A)-X-(H/Q)-(L/A) (Lazarow, 2006). The PTS2 is recognised in the cytosol by Pex7 (Marzioch et al., 1994; Rehling et al., 1996), which proceeds to deliver PTS2-possessing proteins to the peroxisomal membrane. At the peroxisomal membrane interface Pex7 interacts with other closely related proteins, which differ depending on the species: Pex18 and Pex21 in *S. cerevisiae* (Purdue et al., 1998); Pex20 in *Y. lipolytica* (Einwächter et al., 2001); and the longer spliced isoform of Pex5 (Pex5pL) in mammals (Otera et al., 2000). The other proteins aid Pex7 in interacting with the importomer complex. The remainder of the import is then identical to the PTS1 pathway.

1.3.3 Fission of Peroxisomes

The mechanism of peroxisomal division via fission consists of elongation, constriction and scission steps. The elongation step is known to be performed by the Pex11 family of proteins (Pex11, Pex25 and Pex27 in yeast, Pex11 α , Pex11 β and Pex11 γ in mammals) (Schrader et al., 2012), but constriction is still a poorly understood process (Knoblach and Rachubinski, 2015). The dynamin related proteins (DRPs) Vps1 and Dmn1 are known to perform the final scission step in yeast (Hoepfner et al., 2001), with Drp1 performing it in mammals (Fujiki et al., 2014).

1.3.4 New Peroxisome Formation

The accepted model for the formation of new peroxisomes has been in flux since they were discovered, and has subsequently given rise to multiple models that attempt to explain how cells goes about this process.

Initial studies of peroxisomal formation led to the conclusion that they formed via budding directly from the ER, as inferred from electron micrographs showing a close relationship between peroxisomes and the ER (Novikoff and Novikoff, 1972). However, subsequent biochemical studies led this view to fall from favour – evidence of direct interaction between

the ER and peroxisomes was inconclusive, and it was later shown that matrix proteins are imported post-translationally from the cytosol (Lazarow, 2003; Lazarow and Fujiki, 1985), as explained in Chapter 1.3.2. This led to the growth and division model where peroxisomes were considered to be autonomous organelles that proliferate exclusively by growth and division of pre-existing ones, with the ER just supplying the membrane lipids (Lazarow and Fujiki, 1985).

The issue was not settled however, as *de novo* formation of peroxisomes was later demonstrated. It was first observed in experiments where the reinstatement of the respective gene in *pex3* and *pex19* mutant *S. cerevisiae* caused peroxisomes to form from the ER (Kragt et al., 2005; Tam et al., 2005). A key experiment in *pex3* mutant yeast expressing Pex3-YFP (Pex3 tagged with yellow fluorescent protein) showed a series of stages of peroxisomal development when Pex3 expression was restored (Hoepfner et al., 2005). Pex3 was observed to appear first in the ER and concentrate into foci - becoming a 'pre-peroxisomal' structure in the ER - before pinching off and maturing through several stages into a fully functioning peroxisome (Hoepfner et al., 2005). This discovery of *de novo* formation was clearly incompatible with a pure growth and division model; the new peroxisomes would have to derive their membrane from a donor organelle (to satisfy the axiom *omnis membrana e membrana* (Blobel, 1980)) and have some capacity to import peroxisome specific machinery. This led to a revision of the growth and division model into its current form whereby a subset of PMPs, including Pex3 and Pex22, first insert into the ER (Fakieh et al., 2013; Halbach et al., 2009) that are then either directed to peroxisomes in the presence of pre-existing peroxisomes, or form the basis of new peroxisomes only if the cell is devoid of them (Figure 1.4)(Halbach et al., 2009; Hetteema and Motley, 2009; Motley and Hetteema, 2007; Nuttall et al., 2011).

The discovery of *de novo* synthesis of peroxisomes also led to a separate, distinct model of peroxisomal formation called the maturation model. In this model, vesicles containing some of the PMPs first bud off from the ER, like in the growth and division model. These vesicles then fuse with each other and the structure develops by importing other PMPs and then matrix proteins from the cytosol before eventually becoming a mature peroxisome (Figure 1.5)(Tabak et al., 2006). The relative contribution of this process to overall peroxisome numbers was unclear.

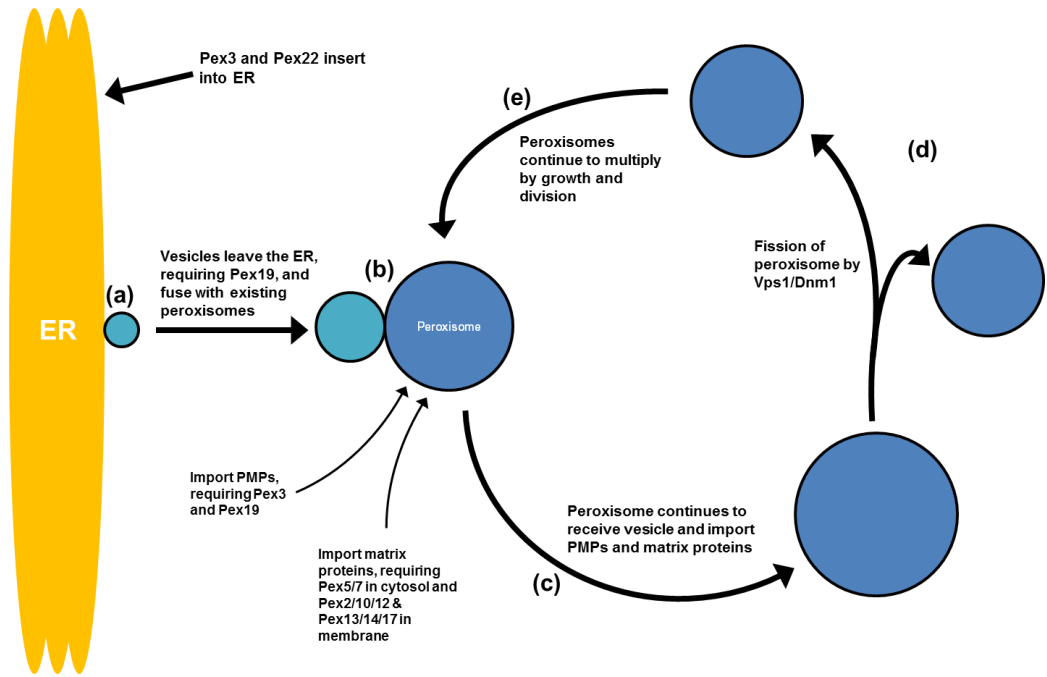


Figure 1.4. Growth and division model of peroxisome biogenesis. Here the PMPs Pex3 and Pex22 first insert into the ER. (a) Pex3, Pex22 and lipids gather at the surface of the ER before pinching off in a vesicle, requiring Pex19. (b) This vesicle fuses with pre-existing peroxisomes or matures into a new peroxisome in the absence of pre-existing peroxisomes. (c) Peroxisomes grow by continuing to receive vesicles from the ER and importing PMPs and matrix proteins from the cytosol (see Figures 1.2 and 1.3 for mechanism). (d) Peroxisomes divide by fission via the action of DRPs Vps1 and Dnm1. (e) Peroxisomes continue to multiply via growth and division.

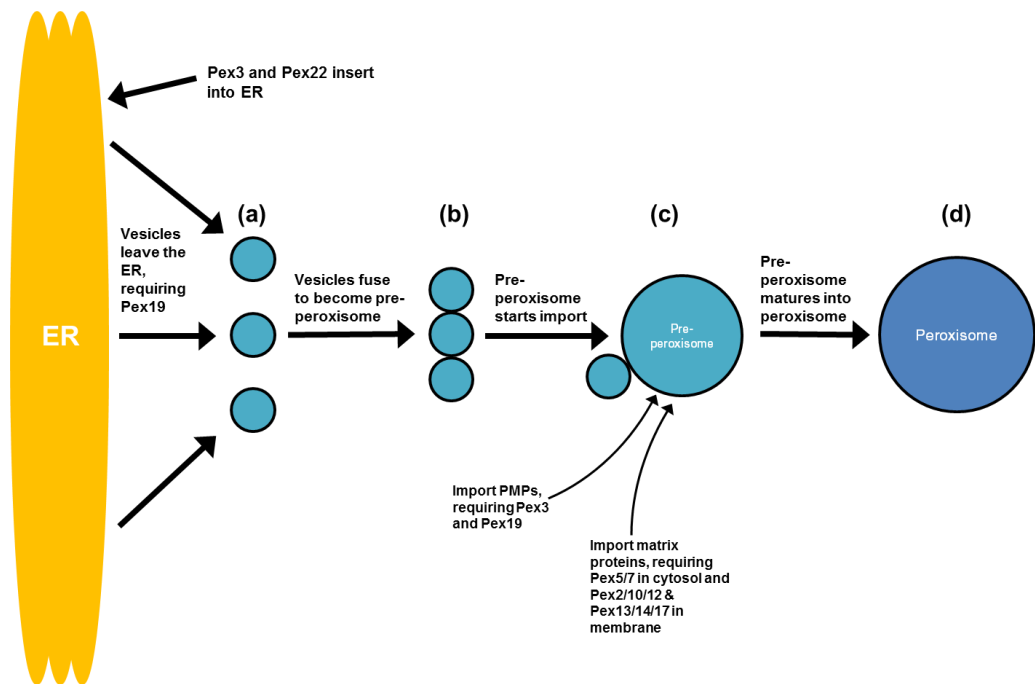


Figure 1.5. Maturation model of peroxisome biogenesis. (a) Lipids and some PMPs gather at the surface of the ER before pinching off in vesicles. (b) Multiple vesicles homotypically fuse together to form a pre-peroxisome. (c) Pre-peroxisome continues to receive vesicles from the ER before importing other PMPs and matrix proteins from the cytosol. Eventually this pre-peroxisome becomes (d) a mature peroxisome.

Subsequent research sought to evaluate the major propositions of the maturation model, and specifically the contribution that *de novo* synthesis played in the peroxisome population. In yeast, the DRPs Dnm1 and Vps1 perform the scission step of peroxisomal fission (Hoepfner et al., 2001; Motley et al., 2008) and consequently mutant *vps1/dnm1* strains generally only contain one large peroxisome which is divided physically upon cytokinesis (Nagotu et al., 2008). Experiments with mutant *vps1/dnm1* cells showed no *de novo* synthesis of peroxisomes even though the *de novo* synthesis machinery was still active (Motley and Hettema, 2007). Dnm1 and Vps1 are not involved in the *de novo* synthesis process as demonstrated by production of peroxisomes in cells that do not inherit any in mutant *vps1/dnm1* cells (Motley et al., 2008). This showed that fission appears to be the predominant form of peroxisome proliferation in yeast, with *de novo* formation only observed in cells completely lacking in peroxisomes. Moreover, *de novo* synthesis of peroxisomes seems to be an intrinsically slow process in yeasts, as shown upon reintroduction of Pex3 in *pex3* mutants, as peroxisomes only appear roughly 5 hours later (Motley and Hettema, 2007). This is much longer than the time needed to complete one cell cycle in good growth conditions (between 90-120 minutes). Logic would dictate that to maintain a population of peroxisomes the yeast should divide them by fission and segregate efficiently (Hettema and Motley, 2009). This evidence pointed to a situation whereby yeast cells multiply their peroxisomes by growth and division under normal conditions (Motley and Hettema, 2007).

The maturation model has subsequently evolved into the recently proposed vesicle fusion model by van der Zand and colleagues (van der Zand et al., 2012)(Figure 1.6). The model advances that there is a continuous stream of vesicles that bud off from the ER, undergo heterotypic fusion, and mature to become fully functioning peroxisomes. Unlike the growth and division model, this is purported to happen both in the presence and absence of pre-existing peroxisomes; consequently advocating *de novo* synthesis of peroxisomes as a continuously occurring process under normal conditions. In the vesicle fusion model all of the peroxisomal membrane proteins insert first into the ER membrane (van der Zand et al., 2010). In the ER membrane the peroxisomal membrane proteins are divided into two subsets before pinching off in separate vesicles. These distinct vesicles subsequently undergo heterotypic fusion via the action of Pex1 and Pex6, after which point they can then start importing peroxisomal matrix proteins from the cytosol. Fission is mediated by Vps1 and Dnm1, and occurs after vesicle fusion (Tabak et al., 2013; van der Zand et al., 2012; van der Zand and Tabak, 2013).

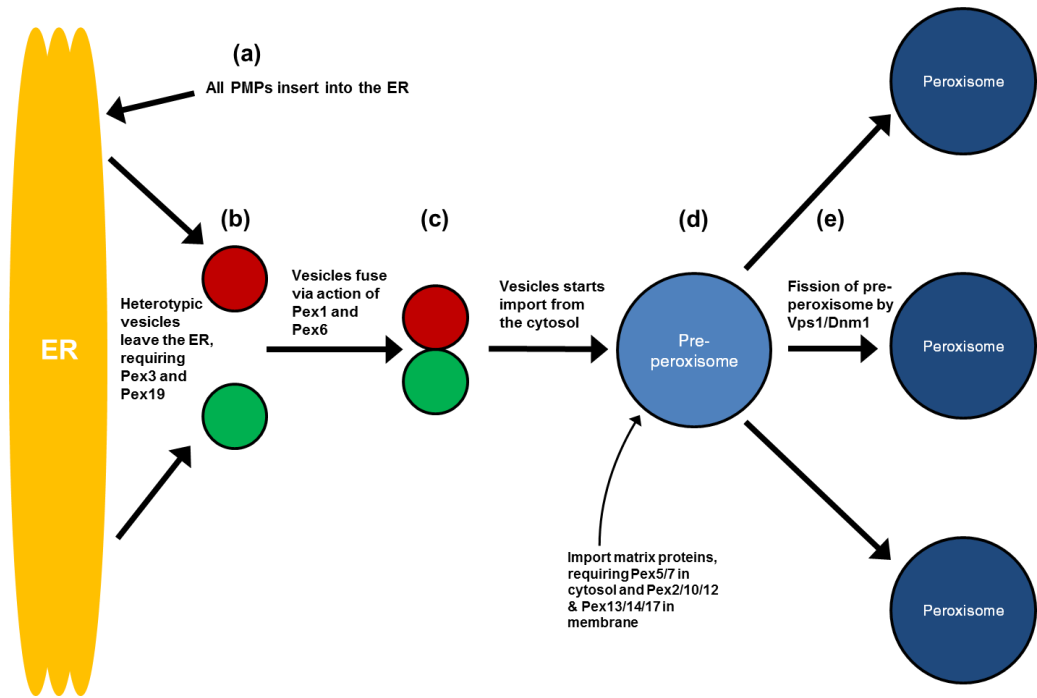


Figure 1.6 Vesicle fusion model of peroxisome biogenesis. (a) All peroxisome membrane proteins first insert into the ER. (b) The PMPs sort into two distinct groups and bud off the ER in separate vesicles. (c) The distinct vesicles undergo heterotypic fusion via action of Pex1 and Pex6. (d) After fusion the structure imports matrix proteins from the cytosol (it already possess all PMPs) and can undergo fission by Vps1 and Dnm1 (e).

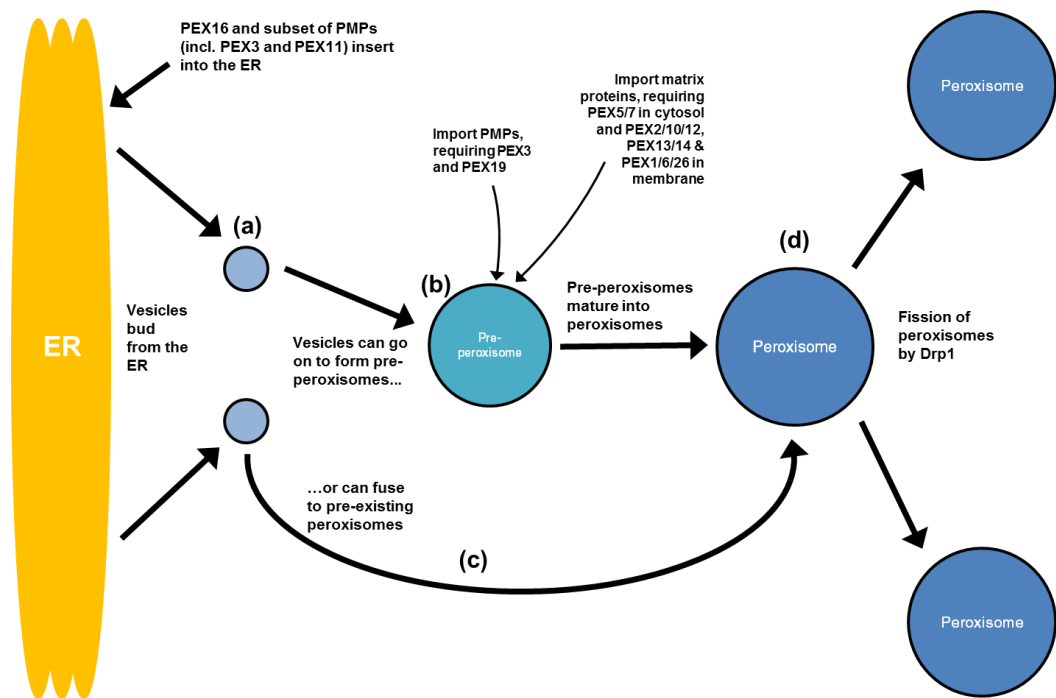


Figure 1.7. Mammalian model for peroxisome biogenesis. PEX16 causes some PMPs, including PEX3 and PEX11, to insert into the ER. (a) Lipids and PMPs gather at the ER surface before pinching off in vesicles. (b) Vesicles can go on to form a pre-peroxisome which imports from the cytosol before maturing into a peroxisome or (c) fuse to pre-existing peroxisomes providing lipids and PMPs to maintain the steady state number. (d) Mature peroxisomes undergo fission via the action of Drp1, aided by PEX11.

The mechanistic differences between this model and the more long-standing growth and division model are numerous (compare Figures 1.4 and 1.6) and have consequences for understanding the role of Pex1 and Pex6, the role of DRPs Vps1 and Dnm1 in peroxisomal fission, and the relative contribution of *de novo* synthesis to overall peroxisome numbers in *S. cerevisiae*. Some of the discrepancies between these two models of peroxisomal biogenesis are questioned as part of this study; the specific aspects addressed in this thesis are outlined in section 1.5.1.

Shifting the focus away from yeast towards other species, a study in mammalian fibroblasts suggested that *de novo* synthesis was active alongside growth and division of pre-existing peroxisomes (Kim et al., 2006). Tracking lipids coming off the ER in these cells appeared to show some vesicles attaching to pre-existing peroxisomes, but most going on to aggregate and form new organelles. Inference from this suggested that *de novo* formation is the principal pathway in mammalian cells and fission is of relatively little importance; although other studies have evidence to the contrary (Delille et al., 2010; Huybrechts et al., 2009). Recent studies show that mammalian PEX16 causes many of the PMPs that can be imported from the cytosol by PEX19 to be instead targeted to the ER (Hua et al., 2015). One group proposes that these PMPs and PEX16 accumulate to form pre-peroxisomal vesicles that could fuse with pre-existing peroxisomes to maintain the steady-state number of peroxisomes, or could go on to form new ones (Hua and Kim, 2016). The relative contribution of this process on maintenance of peroxisomes versus forming peroxisomes *de novo* is not addressed in the study. The proposition is that this occurs in mammalian cells due to the much higher number of peroxisomes they contain (~100-1000) compared with yeast (~2-10), and as a result there is a greater demand on the ER to supply lipids and membrane proteins. They put forward a model with the current understanding of the situation in mammalian cells, although the authors acknowledge it likely a crude representation of the real situation (Hua and Kim, 2016)(Figure 1.7).

In plants, evidence for any distinct *de novo* formation directly from the ER is currently deficient (Hu et al., 2012). The current evidence points to a ‘semi-autonomous’ model of peroxisome biogenesis – PMPs are imported post-translationally, but there are ER derived vesicles that deliver lipids and some PMPs to existing peroxisomes (Cross et al., 2015; Hu et al., 2012).

Taking the above as a whole, it can be assumed that a comprehensive model of peroxisome biogenesis may be problematic. The role of the ER in peroxisome biogenesis across the

different species is undecided. The particulars of which PMPs traffic via the ER, how these PMPs are sorted when they are there, and how the process is regulated depending on cellular conditions is still disputed. The relative importance of *de novo* synthesis versus fission of peroxisomes across species is also unresolved.

1.4 Peroxisome Inheritance

The previous section described how peroxisomes are formed; this section will deal with how they are passed on from one cell generation to the next. The inheritance and biogenesis of organelles are two fundamentally linked processes – for a daughter cell to inherit a sufficient number, the mother cell must grow and divide organelles it already has or create them *de novo*.

Studies of organelle inheritance utilising *S. cerevisiae* as their model organism are widespread. *S. cerevisiae* divides by budding, which is an asymmetric form of cell division. In this process, an initially small bud forms on a mother cell, and grows until it is nearly the size of the mother. In contrast with symmetrically dividing fission yeast or mammalian cells, this means that the active delivery of a share of organelles to the growing bud is necessary. Transport of organelles to the bud is proposed to be a tightly regulated and ordered process, to both retain some organelles in the mother cell, and to ensure the daughter cell receives an adequate number of all the organelles (Fagarasanu and Rachubinski, 2007; Hoepfner et al., 2001; Rossanese et al., 2001). Like many organisms, *S. cerevisiae* utilise the actin filament network in conjunction with myosin motor proteins to move organelles (Vale, 2003).

Organelles in *S. cerevisiae* are moved along actin filaments by the action of the myosins Myo2 and Myo4 (Neuhaus et al., 2016), with the exception of the nucleus which is moved along microtubules via other motor proteins (Huffaker et al., 1988; Jacobs, 1988). Myo2 transports most of the organelles, including mitochondria (Altmann et al., 2008) and peroxisomes (Fagarasanu et al., 2006a), whilst Myo4 is responsible for transporting the cortical ER (Estrada et al., 2003) and also transports mRNAs (Takizawa and Vale, 2000). Organelles attach themselves to the C-terminal cargo binding domain of Myo2 via organelle-specific adapter proteins (Altmann et al., 2008; Fagarasanu and Rachubinski, 2007; Langford, 2002).

In *S. cerevisiae* the peroxisomal membrane protein Inp2 is the adapter linking peroxisomes to Myo2 and is therefore responsible for the inheritance of peroxisomes. This is clearly demonstrated in knockout *inp2* cells, where all the peroxisomes are retained in the mother cell (Fagarasanu et al., 2006a)(Figure 1.8, B). Conversely, overexpression of Inp2 entirely depletes the mother cell's peroxisomes, as all are moved to the bud (Fagarasanu et al., 2006b).

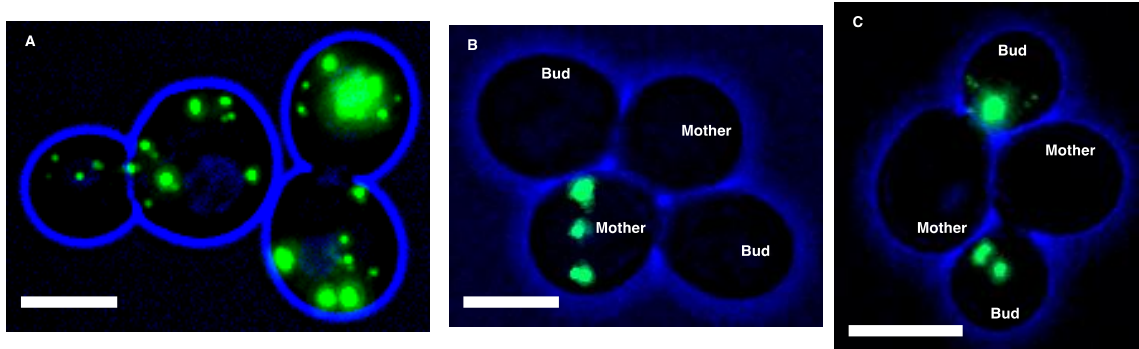


Figure 1.8. Examples of peroxisome distribution in wild-type *S. cerevisiae* in contrast with *inp2* and *inp1* mutant cells. A) WT cells showing peroxisomes distributed between mother and bud cells. B) Cells lacking Inp2 retain all peroxisomes in mother cell. The top mother did not inherit any peroxisomes and consequently could not pass any on; they will form *de novo* in time. C) *inp1* mutant cells cannot retain peroxisomes in the mother and all are moved through to the bud. The mother cells will form peroxisomes *de novo* in time. Brightfield in blue, cells are expressing mNeonGreen-PTS1 (green). Images are maximum intensity projections. Scale bars indicate 5 μ m.

Interestingly, Inp2 protein molecules are present on each individual peroxisome initially in the mother yet only some end up being moved to the bud (Fagarasanu et al., 2010). Inp2 on peroxisomes is degraded upon reaching the bud (Fagarasanu et al., 2006a) and the Inp2 levels on peroxisomes in the mother drop as more are sent to the bud, with transport eventually ceasing (Fagarasanu et al., 2009). In *myo2* point mutants that are unable to bind Inp2, the inheritance of peroxisomes is disrupted and Inp2 levels are elevated (Fagarasanu et al., 2009). This suggests an as yet unidentified feedback mechanism based on the positioning of peroxisomes, using currently unknown signal and machinery (Nuttall et al., 2011).

Alongside inheritance there are retention mechanisms in yeast to ensure the mother maintains some portion of the organelles after cell division. This is achieved through protein tethers, which anchor organelles to the cell periphery or other organelles. Tethers in the bud also prevent backtracking of the organelles into the mother (Boldogh et al., 2004; Fehrenbacher et al., 2004). Both peroxisomes and mitochondria are retained by attaching to the cortical ER (Knoblach et al., 2013; Kornmann et al., 2009), which is in turn connected to the plasma membrane (Manford et al., 2012).

The cortical ER-peroxisome tether is formed of two proteins: Inp1 and Pex3 (Knoblach et al., 2013). Inp1 was identified first as a protein responsible for retaining peroxisomes. In knockout *inp1* populations a substantial proportion of mother cells are bereft of peroxisomes, with the entire peroxisome contingent in the buds (Figure 1.8, C), while overexpression of Inp1 holds all peroxisomes in the mother (Fagarasanu et al., 2005). At the time, the protein that attached Inp1 to the periphery of the cell was undetermined (Fagarasanu et al., 2006b). Subsequently Pex3 was shown to physically interact with Inp1,

establishing Pex3 having a dual role in peroxisomal inheritance and biogenesis (Munck et al., 2009). Inp1 contains two Pex3 binding sites, connecting a Pex3 in the cortical ER membrane with one in the peroxisome membrane (Knoblach et al., 2013).

Despite the opposite functions of retention and transport of Inp1 and Inp2, no interaction between them has been demonstrated (Fagarasanu et al., 2006a). This has led to the proposition that there is a tug-of-war event happening over each peroxisome between the Pex3-Inp1 anchor and the Inp2-Myo2 transport system (Fagarasanu and Rachubinski, 2007; Fagarasanu et al., 2010, 2006b).

Mammalian cells lack identifiable homologues of Inp1 and Inp2, and for a long time the inheritance of peroxisomes was thought to be stochastic (Schrader and Yoon, 2007; Wiemer et al., 1997). As mammalian cells contain hundreds of peroxisomes, and most cells divide symmetrically upon cytokinesis, in theory the active movement of peroxisomes is unnecessary as they could be shared randomly upon division of the mother cell (Jongsma et al., 2015). However, peroxisomes clearly display ordered behaviour in dividing cells. In interphase they are distributed randomly in the cytoplasm, but move into two clusters at the spindle poles in metaphase (Kredel et al., 2009). Previous example associations of peroxisomes and microtubules are numerous, so it is likely that mammalian cells use microtubules for the directed movement of peroxisomes at cell division (Rapp et al., 1996; Schrader et al., 2000; Wiemer et al., 1997). However, save for Pex3 (PEX3) and Myo2 (MYOVB), examples of mammalian homologues for proteins in the yeast system of inheritance have not yet been identified (Jongsma et al., 2015).

In their 2013 study (and reiterated in Knoblach and Rachubinski, 2015), Knoblach et al. connected the processes of peroxisomal division and peroxisomal inheritance in *S. cerevisiae* as a form of peroxisome population control, which in this study will be referred to as the KPPC (Knoblach et al. Peroxisome Population Control) model (Figure 1.9). In the KPPC model, fair segregation of peroxisomes between mother and daughter cells upon cell division is achieved through Inp1-anchored peroxisomes in the mother undergoing fission into two peroxisomes, with one resultant daughter peroxisome being moved into the bud and the other remaining tethered in the mother. This guarantees that both cells receive their fair share of peroxisomes (Knoblach and Rachubinski, 2015). Some of the implications of this assertion are addressed as the main part of this study; these questions are outlined in section 1.6.

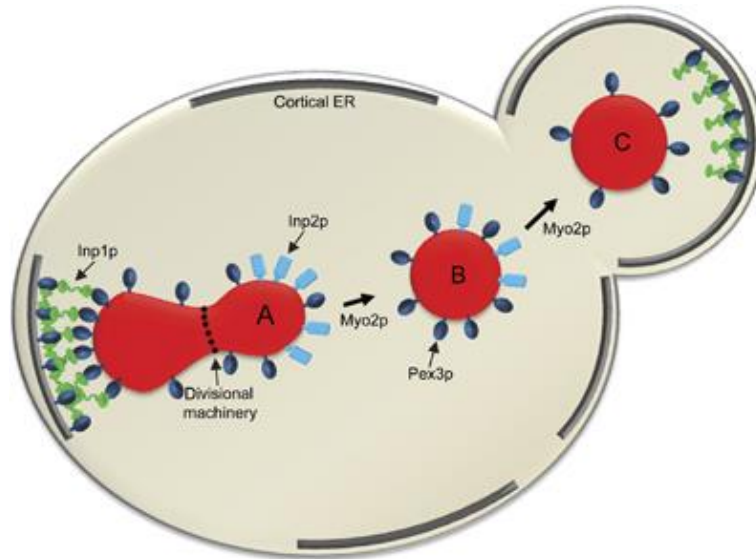


Figure 1.9. The KPPC model of peroxisome population control as proposed by Knoblach et al., 2013. Inp1 tethers peroxisomes in the mother cell via Pex3. Inp2 attaches peroxisomes to Myo2. A) Through the pulling action of Myo2 and the constriction action of the peroxisomal divisional machinery, peroxisomes rupture and are split into two. The process can be asymmetrical. B) The peroxisomes will move to bud via Myo2. C) In the bud, the incoming peroxisomes are tethered to Inp1 for retention. Reproduced from Figure 9 of Knoblach et al., 2013. ©2013 European Molecular Biology Organisation.

1.5 Time-Lapse Live Cell Imaging, Image Processing and Quantification

1.5.1 Time-Lapse Live Cell Imaging

Live cell imaging has been utilised to study peroxisomes for some time (Fagarasanu et al., 2006a, 2005; Knoblach et al., 2013). In this study, even longer-term live cell imaging experiments and image processing techniques are employed to study peroxisomal biogenesis and inheritance to allow for a more in-depth analysis.

There are many challenges associated with time-lapse live-cell imaging that do not arise when acquiring still images. When designing a live cell imaging experiment, many factors must be considered and be finely balanced to acquire the desired experimental data. Two major problems are to maintain healthy, growing cells over the course of one's experiment and the issue of cells moving out of focus over the course of an experiment, a problem called drift.

1.5.1.2 Maintaining Growth by Providing Optimal Growth Conditions

To image cells over many cell generations requires them to be actively growing and dividing. Cells will not grow if they do not have access to sufficient nutrients (e.g. sugars, amino acids, salts and water). This means that imaging on the glass slides that are usually used to mount cells is not feasible for long-term imaging, as nutrients become scarce and the slide dries out quickly.

A tried and tested method of providing cells with more nutrients for long-term imaging is an agarose pad, which is agarose that is dissolved in experiment-appropriate media and left to solidify. This sits on top of cells (on glass slides with small wells, or in a glass-bottomed dish) keeping them supplied with water and nutrients, and is transparent, allowing cells to be imaged through the agarose (Figure 1.10). However, the agarose pad dries out over time which reduces the cells' access to nutrients and water. The drying out of an agarose pad also adds to the drift in the sample (explored in the next section). They are therefore not ideal for imaging for very protracted periods of time, such as overnight.

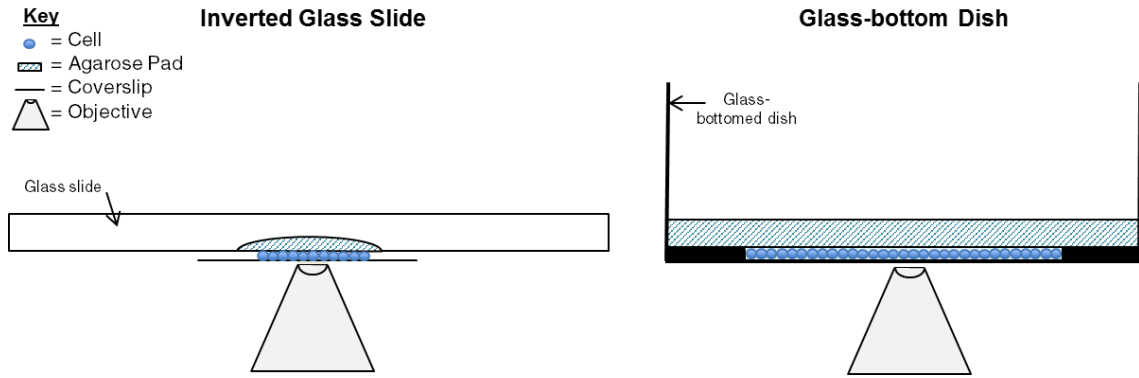


Figure 1.10. Two methods of live-cell imaging utilising agarose pads.

A system more suited to imaging for extended periods is a cell culture chamber, in conjunction with a microfluidic controller. Cell culture chambers are a glass-bottomed chambers in part of a larger plastic plate with wells for media. Cells are loaded under pressure into the chamber from one of the wells and are trapped between the bottom of the plate and the elastic ceiling. There are capillaries coming from the other wells which can be loaded with the appropriate experimental media. Pressure is supplied to the inlet wells via the microfluidic controller, which is programmable using a desktop computer. A gentle pressure placed on the inlet wells is enough to ensure a fresh supply of media to the cells in the chamber. Therefore, the nutrients surrounding the cells are constantly refreshed, and excreted products are taken away. This leads to better growth than using glass-bottomed dishes (Figure 1.11).

1.5.1.3 Drift in Long Time Lapse Experiments

In long-term time lapse experiments a well-known phenomenon occurs whereby a specimen that was properly in focus at the start of the experiment later becomes blurry and out of focus. This is known as drift. Drift of a specimen can occur in both XY (lateral) and Z (axial) planes. This drift occurs slowly, so it is not noticeable when one is normally taking images on glass slides with a microscope.

Lateral drift is caused by cells moving in the XY direction, which can occur through slides drying out or if the cells have not been mounted correctly initially. When using cell culture chambers, where cells are trapped between the glass bottom of plate and an elastic ceiling (shown in Figure 2.4), the problem of lateral drift is essentially eliminated. However, axial drift remains a major problem. This drift in the axial plane is called focus drift. Focus drift can occur for a variety of reasons. It is particularly an issue for high-magnification oil-immersion lenses, like the 100x magnification objectives used to image yeast.

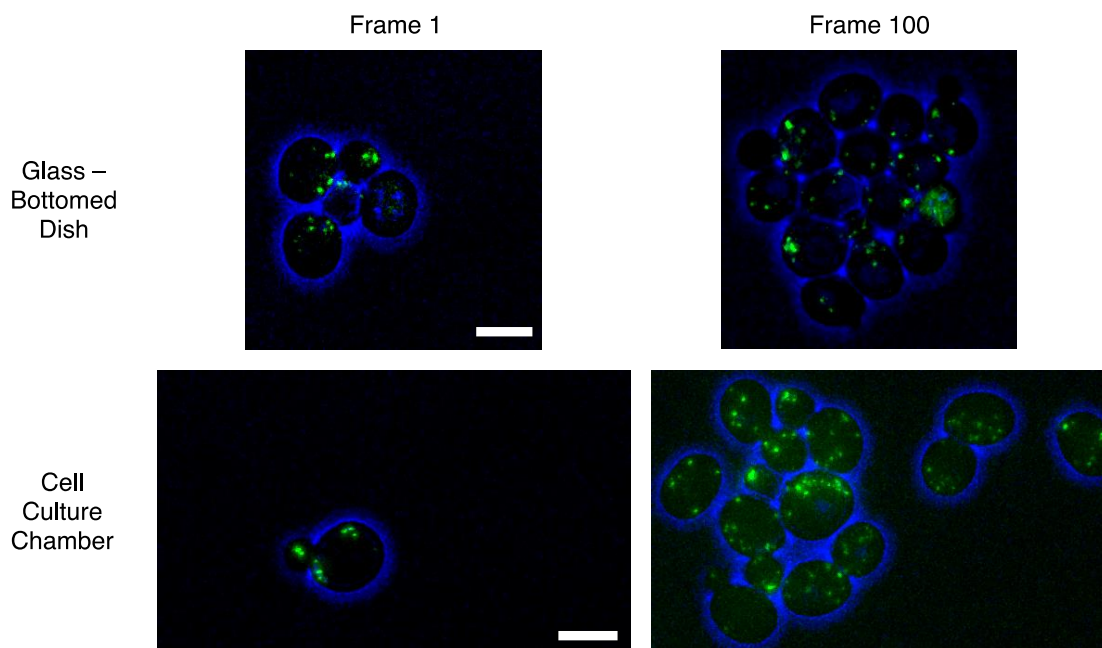


Figure 1.11. Comparison of live-cell imaging using the glass-bottomed dish (top panels) vs. cell culture chamber (bottom panels) over an 8-hour experiment. Although some growth clearly occurs in the glass-bottomed dishes, it is far from optimal. Over 8-hours the five original cells in the glass-bottomed dish have grown and divided to give 16 cells, meaning they have undergone between 1-2 cell divisions. On the other hand, the one cell present in the cell culture chamber has undergone 5 cell divisions in the same period, to give rise to a colony of 15 cells. In this study, on average yeast cells present in the glass-bottomed dish at the start of imaging underwent between 1-2 cell divisions whereas yeast cells present in the cell culture chamber at the start of imaging would undergo between 4-6 cell divisions, therefore giving rise to larger colonies over the same period of imaging. Brightfield in blue, green is mNeonGreen-PTS1. Image is maximum intensity projection of 15 Z slices, one stack taken every 5 minutes. Scale bars indicates 5 μm .

The most common cause of focus drift is thermal drift – i.e. fluctuations in temperature. Temperature fluctuations around the specimen can be due to changes in air temperature because of variations in air conditioning or heat from illumination sources, computers, draughts etc. There may also be different expansion and contraction rates of materials surrounding the specimen, leading to changes in distance between the objective and specimen. A change in 1°C can lead to drift of between $0.5\mu\text{m}$ – $1.0\mu\text{m}$ in the axial plane (Silfies et al., 2016).

Correcting Focus Drift

There are two approaches to tackling focus drift: one can either target the source of the focus drift or attempt to correct the focus drift as it happens. Supposing that thermal drift is the major source of focus drift, one way of reducing this is the use of temperature-controlled chambers. These are usually constructed from acrylic glass and surround the whole of the microscope and its components, keeping it at a constant temperature. However, they are expensive and require a lot of space surrounding the microscope.

The alternative is to correct focus drift as it occurs. This can be done using either a software or hardware-based approach.

There have been many software-based approaches developed over the years, and generally they utilise algorithms relying on the fact that specimens being observed have features that create great contrast or have fine detail when in focus. A specimen out of focus will lose this contrast or finer detail. A specimen that has drifted out of focus will be recognised by the software algorithm and it will adjust the objective up or down by a set amount, repeating this process until the specimen is again in focus. The major downside to this is that each iteration requires taking more images for the software to process and compare, and the whole process can take several minutes. After all this, the software algorithms can still erroneously determine that the optimal focal plane is different to the one desired.

Hardware-based approaches are therefore a more robust option for correcting focus drift. Numerous hardware-based focus correction systems are sold by commercial vendors. One example is the Zeiss Definite Focus module. This works in a similar way to most hardware based focus drift correction systems; its method of action is explained in Figure 1.12. A comparison of an experiment with and without a focus correction system in place is shown in Figure 1.13.

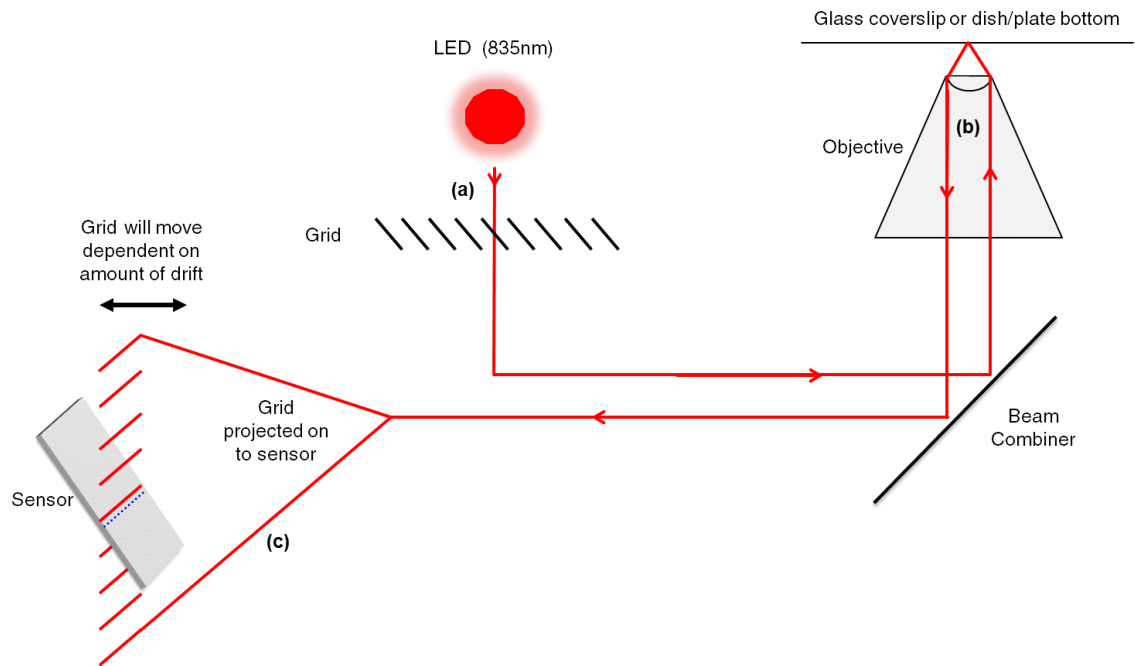
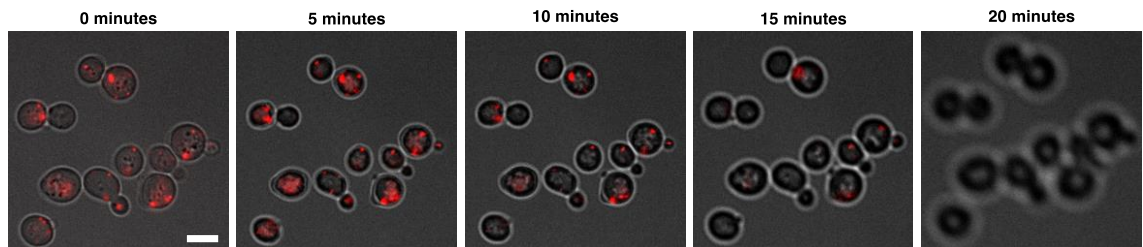


Figure 1.12. Outline of Definite Focus Module. (a) Infrared (IR) light produced by an LED is made into a grid pattern and combined with the normal light path of the microscope by a beam combiner. (b) The IR light is passed through the objective and is reflected by the coverslip-media interface. It passes back to the beam combiner that directs it onto a sensor module. (c) Based on the position of the refracted light interpreted by the sensor, the system establishes the focal point of the specimen (e.g. blue dotted line). If the sensor detects any changes in the reflected light's position then the microscope will be instructed to move the objective in Z to compensate.

Experiment Before Hardware-assisted Focusing



Experiment After Hardware-assisted Focusing

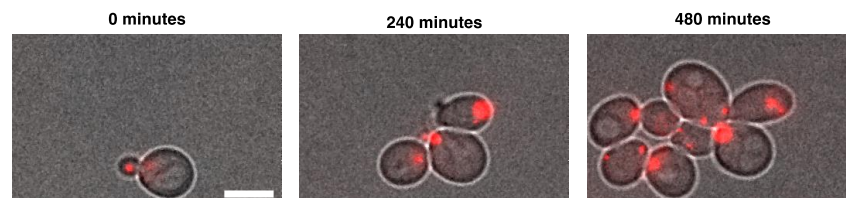


Figure 1.13. Experiments before and after hardware-assisted focusing using Definite Focus module. Top panels show an image experiment without using the focus module. Cells start drifting out of focus almost immediately; by 15 minutes only a few of the peroxisomes are in focus, and by 20 minutes the cells are also out of focus. Bottom panels show an experiment using the focus module. Even after 480 minutes (8 hours) cells are still in focus. Both sets of panels are images in one plane. Times are relative to the start of imaging. Cells are wild-type *S. cerevisiae* expressing HcRed-PTS1. Scale bar indicates 5 μm .

1.5.1.3 Other Considerations of Live Cell Imaging

Any live cell imaging experiment is a compromise between several factors: the overall duration of the movie; the sampling frequency (i.e. how often one image/stack of images is taken); the number of vertical sections (i.e. resolution in Z) and the overall brightness that one wishes to achieve for a good signal to noise ratio (i.e. the strength of signal coming from the fluorescent protein) (Figure 1.14).

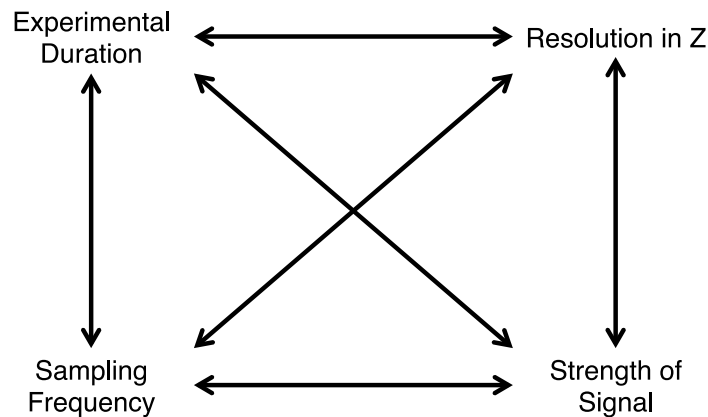


Figure 1.14. Interplay between the factors affecting live cell imaging. A live cell imaging experiment is a compromise between all the factors. There is a limit to the total amount of light fluorophores and cells can receive before succumbing to photobleaching and phototoxicity. At these limits, wanting to increase one factor will mean decreasing one or more of the others.

In addition, there is an inescapable limitation on live cell imaging that must be contended with: the total amount of light that a cell can be exposed to without causing either a) severe photobleaching of the fluorescent protein or b) the disruption of key cellular processes. Photobleaching is the phenomena whereby a fluorophore is damaged in some way over the course of an experiment so that it no longer fluoresces and as such that they can no longer be detected over the background (White and Stelzer, 1999). Cells are sensitive to light and overexposure can cause cells to either arrest in the cell cycle or expire entirely; this damage via light exposure is called phototoxicity (Hoebe et al., 2007). Consequently, one must put limits on the factors listed above to ensure that cells are not exposed to excessive light levels and the experiment falls foul to photobleaching and/or phototoxicity.

There is no single superlative set of values to use for the frame rate, total experimental duration etc. They are linked together in a complex manner and will vary depending on the sample being imaged, the process one wishes to image, and the physical setup of the imaging system one is utilising. In order to study peroxisomes over time for this work, several

compromises and developments of live cell imaging had to be made. These are explored in Chapter 4.

1.5.2 Image Analysis of Peroxisomes

1.5.2.1 Introduction and Brief History

Peroxisomes have some history of being analysed in an automated fashion, with the first work starting in the early 1980's (Beier and Fahimi, 1985). For example, a study with DAB stained rat hepatocytes utilised automatic image analysis to identify changes to peroxisomes after treatment with thyroid hormone. Approximately 31,000 peroxisomes were counted and variables such as their number, size, optical density and perimeter were measured. Manual counting confirmed the accuracy of the automatic analysis (Kerckaert et al., 1989). Later experiments using immunogold staining allowed more quantitative automatic analysis of individual peroxisomal proteins (Beier and Fahimi, 1992; Fahimi et al., 1996). These early investigations demonstrated the usefulness of automatic image analysis for this organelle. Later studies used live *S. cerevisiae* cells and fluorescence microscopy to quantify peroxisomes (Niemisto et al., 2006). Very large screens looking into peroxisomal biogenesis have also been analysed in an automated fashion. In one screen Pot1-GFP (a peroxisomal matrix protein) was expressed in 4775 unique deletion mutant *S. cerevisiae* strains (Saleem et al., 2010). The authors developed their own image analysis method which identified 211 genes linked to peroxisomal biogenesis based on factors such as abnormal Pot1-GFP localisation, reduced GFP fluorescence levels and disrupted transport of peroxisomes to daughter cells. Studies such as those above set precedent for automated analysis of images containing peroxisomes, and show that peroxisomes lend themselves well to automated analysis.

The pathway through which one turns raw image data into biologically meaningful measurements such as number, area, shape or location etc. will vary dependant on both what one wants to measure and the nature of the data (Eliceiri et al., 2012).

1.5.2.2 Image Processing Programs

Extracting meaningful information from one's images is predominantly performed with the aid of an image processing program. There exist many such programs: those that have multi-purpose applications; ones tailored to a particular problem; script-orientated programs; GUI-orientated ones; commercially designed applications sold alongside microscopes by companies such as Zeiss, Nikon, and GE; open-source programs such as BioImageXD

(Kankaanpää et al., 2012), Icy (de Chaumont et al., 2012) and CellProfiler (Carpenter et al., 2006); etc.

The oldest and most popular of the open-source programs is ImageJ, first released in 1997 (Collins, 2007; Schneider et al., 2012). ImageJ has great extensibility, and can perform a wide variety of both common and specialised tasks. FIJI (Fiji Is Just ImageJ) is an implementation of ImageJ bundled with many plugins and features tailored for use in microscopy analysis, particularly for the life sciences (Schindelin et al., 2012). Additionally, FIJI has support for writing scripts in the Java, Ruby and Python programming languages – increasing the level of control and customisation the user has over the analysis.

1.5.2.3 Image Acquisition and Image Makeup

In nearly all microscopy techniques the images are acquired using a digital camera attached to the microscope. The digital camera contains within it an image sensor, which will be a type of either a charge-coupled device (CCD) or a complementary metal–oxide–semiconductor (CMOS). An image sensor is a two-dimensional grid of individual units that accrue electrical charge in proportion to the amount of light they receive. These units within an image sensor are correctly referred to individually as either a ‘photosite’ or ‘photosensor element’, although microscope companies and users nearly universally refer them to as pixels. When the image sensor is exposed to light, photons arriving at a particular pixel will cause it to accrue charge. The length of time the image sensor is exposed to light is the exposure time of an image. After the exposure time has elapsed, the charge of the pixel at each site in the image sensor is read and this value becomes the intensity of that pixel in a digital image (Figure 1.15). The range of values that each pixel can hold is known as the dynamic range of a camera. Each image is therefore made up of a grid of numbers arising from the intensity of light in a discrete area of the sample being imaged.

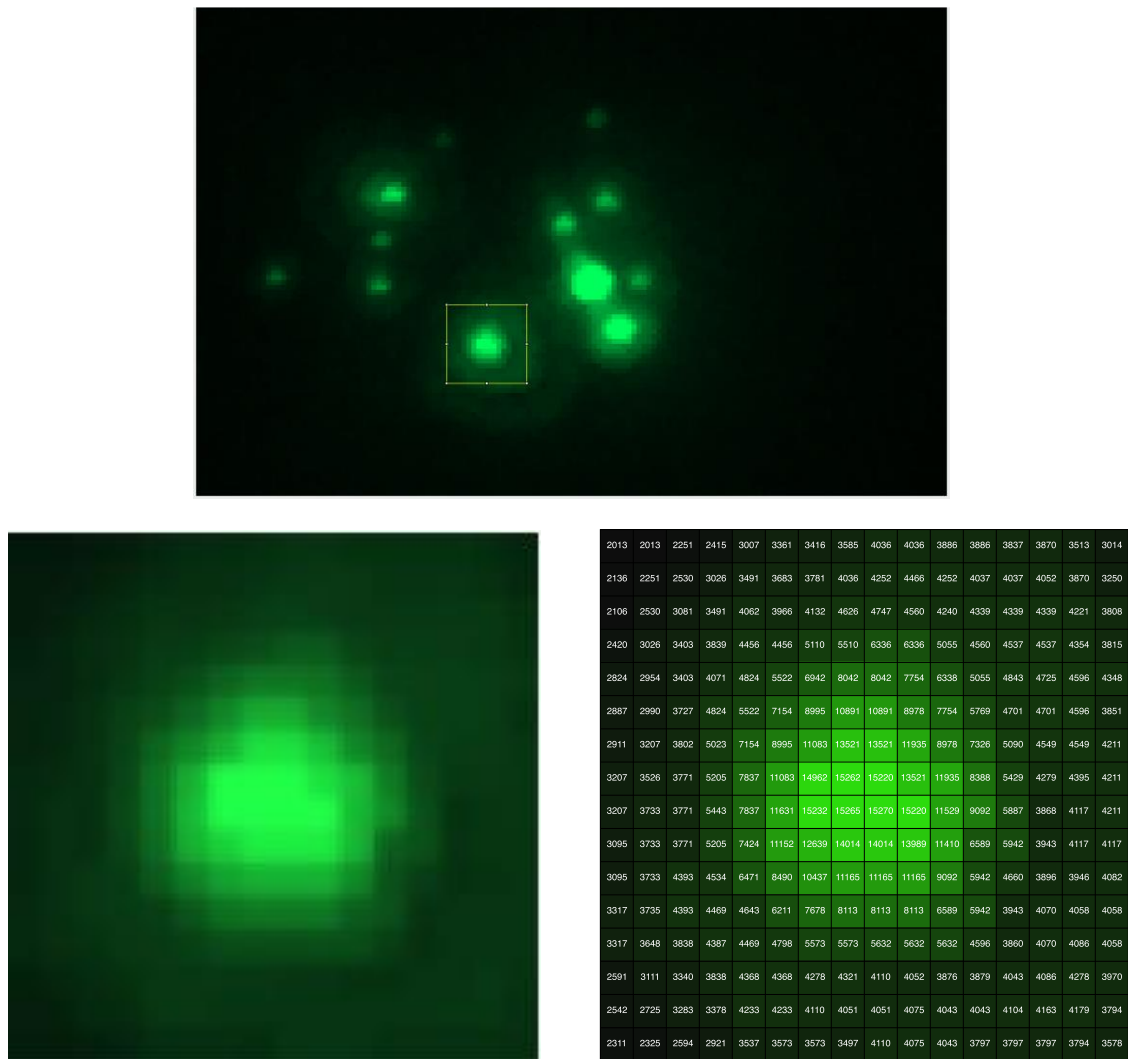


Figure 1.15. Images are made up of grids of numbers. Top) A maximum intensity projection of peroxisomes in yeast expressing mNeonGreen-PTS1. B) A magnified section of the highlighted area of the image A. Individual pixels can be made out. C) The individual values of each pixel have been extracted using FIJI; they are the numbers making up the grid. The background colours show how the original image can be reconstructed from the intensity values; the lowest value has been coloured black, moving towards green at the highest value, resembling the peroxisome on the left.

1.5.2.4 Image Processing and Analysis Basic Techniques

Computer image processing and analysis involves transforming this grid of numbers into quantifiable measurements that are biologically meaningful. This process can be summarised in the following stages:

1. Pre-processing – Use of filters and other methods to improve desired qualities of an image
2. Segmentation – Dividing an image into separate features (i.e. cells or peroxisomes)

3. Feature Extraction – Measurement of objects (‘features’) to obtain quantitative data (i.e. position of peroxisomes, area and position of cells etc.)

This process may be better understood if explained in reverse. To obtain measurements from an image (feature extraction), first the computer has to decide what the objects to be measured actually are. This involves the computer going through some process of assigning pixels to become defined objects called features. The process of dividing an image into separate features is called segmentation. There are many techniques that can be used to segment an image, and the methods utilised depend on the quality of the original image and the desired end point of the segmentation. Before segmentation, the image may be ‘pre-processed’, which is the term used when the pixel content (i.e. values of the pixels) are modified.

The pre-processing step consists of removing noise, reducing background and excluding other un-desired features of an image. Pre-processing usually involves the use of filters and feature enhancement algorithms to achieve this. Removing noise often uses filters that recalculate pixel values based on the intensity of surrounding pixels. As real objects often constitute many pixels of a similar intensity, changing a pixel’s value to the average of its neighbours (for example) will not affect a group of pixels of similar intensity, but will suppress pixels that are dissimilar to their neighbours (like noise).

After pre-processing, the image can be segmented. The simplest form of segmentation is thresholding (Figure 1.16). Thresholding methods classify a pixel as foreground if it is brighter than a certain threshold value, and background if it is not. This threshold value can be chosen by eye, or alternatively several algorithms have been written that allow a computer to decide the threshold value automatically. A few examples of these algorithms include the

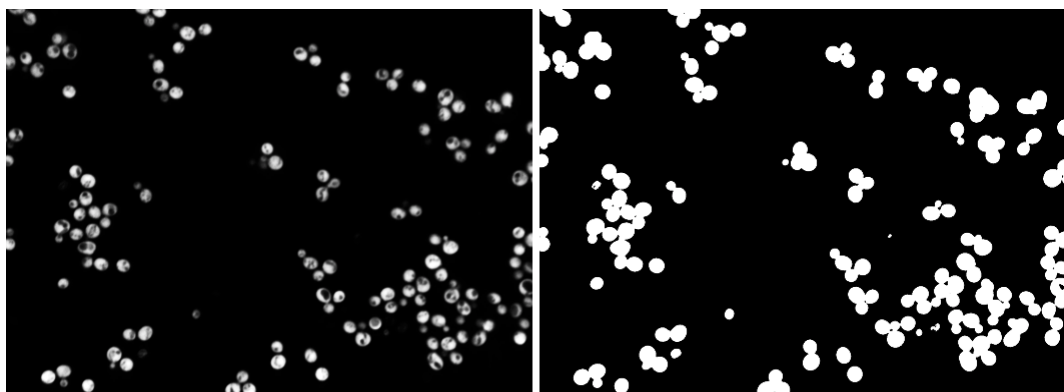


Figure 1.16. Example of thresholding. Image on the left is of *S. cerevisiae* expressing mRFP in the cytosol. Image on the right is thresholding by the computer using the Li Minimum Cross Entropy method.

Li Minimum Cross Entropy method (Li and Lee, 1993)(used in Figure 1.16), the Triangle method (Zack et al., 1977) or Otsu's method (Otsu, 1979). The algorithm that performs best is dependent on the variability of pixel content of the image. In practice, when looking biological images such as those of whole cells, then the correct threshold value is one that identifies the most of whatever feature one wants to measure as foreground, and discards the rest. Performing a threshold on a greyscale image will result in a binary image, with pixels being either one of two numerical values - 0 or 1.

When features are sufficiently segmented, as determined by the user, then feature extraction can be performed and quantifiable data obtained. Some parameters can be set that can refine the scope of analysis if necessary. For example, features below a certain size or a measure of circularity could be disregarded if one was interested in cells of a particular area or shape. These measurements can then be exported for statistical analysis.

The kind of image analysis performed depends on the measurements one wishes to acquire and the nature of the raw image data. In this study, different methods are employed for non-time-lapse and time-lapse data. The processes used to analyse non-time-lapse images can be seen in the Methods chapter (Chapter 2). In Chapter 4 the issue of how to analyse time-lapse images, and the eventual method, is discussed.

1.6 Research Scope and Questions

Having established the background in the literature, this section describes what was aimed to be addressed by this study. In the broadest sense, the main goal of this study at outset was to move toward a more quantitative approach to studying peroxisomal biogenesis and inheritance.

This took the form of evaluating two disputed aspects of peroxisomal biogenesis and inheritance as presented in the literature. The main goal was investigating the link between peroxisomal division and inheritance in *S. cerevisiae* as a form of peroxisomal population control, as put forward by the KPPC model (section 1.6.2).

Developing the live cell imaging and image quantification techniques needed for this main goal also aided in investigating the claims made by the vesicle fusion model of peroxisomal formation as set out by van der Zand et al., 2012 (section 1.6.1).

1.6.1 Vesicle Fusion Model

As outlined in section 1.3.4, the vesicle fusion model (van der Zand et al., 2012) is a proposal for yeast peroxisome formation (Figure 1.6). Many of its claims disagree with much of the literature and with the more long-standing growth and division model in several ways, but notably in three key aspects:

- 1) That Pex1 and Pex6 are required for the fusion of the heterotypic vesicles that gives rise to a peroxisomal structure with a fully functioning importomer complex (Figure 1.6c).
- 2) That the dynamin-related proteins Vps1 and Dnm1 act after this Pex1/6-mediated fusion event to divide the peroxisomal structure to give rise to multiple peroxisomes (Figure 1.6e).
- 3) That this vesicle fusion and subsequent fission gives rise to new peroxisomes by *de novo* synthesis, even in the presence of pre-existing peroxisomes.

Investigating these claims required the creation of a system of live cell imaging yeast over time. By following mutant *vps1/dnm1* cells over time, could the *de novo* synthesis of large, undivided peroxisomes be seen (i.e. Figure 1.6, but without step e)? Could other time-lapse imaging unearth the presence of *de novo* synthesis occurring in the presence of pre-existing peroxisomes? Development of image quantification techniques were also necessary to

examine whether the lack of Pex1 and Pex6 affected the localisation of peroxisomal membrane proteins. The first section of this study will address these points.

1.6.2 Yeast Population Control

The second section and main body of this study will address the proposition of the KPPC model that peroxisomal division and inheritance are coupled processes, as outlined at the end of section 1.4 (Figure 1.9).

The KPPC model makes two strong assertions: the first is that there is an establishment of a ‘steady state’ number of peroxisomes in the mother – the number of peroxisomes in the mother that are divided and passed on to the bud - that is reset once per cell cycle (Knoblauch et al., 2013). The second, as mentioned previously, is that every peroxisome is split, with one half retained by the mother cell and the other inherited by the bud, to guarantee an equitable share of peroxisomes (Knoblauch and Rachubinski, 2015).

These claims can be investigated quantitatively using time-lapse live-cell imaging and computer aided image analysis to establish the number of peroxisomes within a cell over time. Could this ‘steady state’ number be seen in a relationship between the number of peroxisomes in the mother at the start of bud formation and the number in the bud at the end, after splitting off from the mother? Can following the number of peroxisomes over time show a signature of when the proliferation of peroxisomes occurs? For example, does it occur at the end of the cell cycle (Figure 1.17a) or instead over its whole course (Figure 1.17b)? Or is the division and inheritance of peroxisomes so inexorably coupled as to occur so very rapidly that no real increase can be seen (Figure 1.17c)? Barring the latter situation, if the proliferation of peroxisomes can be detected, does it show a doubling of peroxisomal number in a mother cell, followed by a halving due to inheritance as predicted by the KPPC model?

Not only was there a goal to establish overall peroxisomal number per cell, but there was also desire to track individual peroxisomes over the course of multiple cell divisions, in order to aid in understanding peroxisomal behaviour. This would help ascertain whether each peroxisome is indeed divided, with one half subsequently inherited, as suggested by the KPPC model. Previous studies have used live cell imaging to track the positions of peroxisomes over one cell division but not over multiple generations (Fagarasanu et al., 2006a, 2005; Knoblauch et al., 2013).

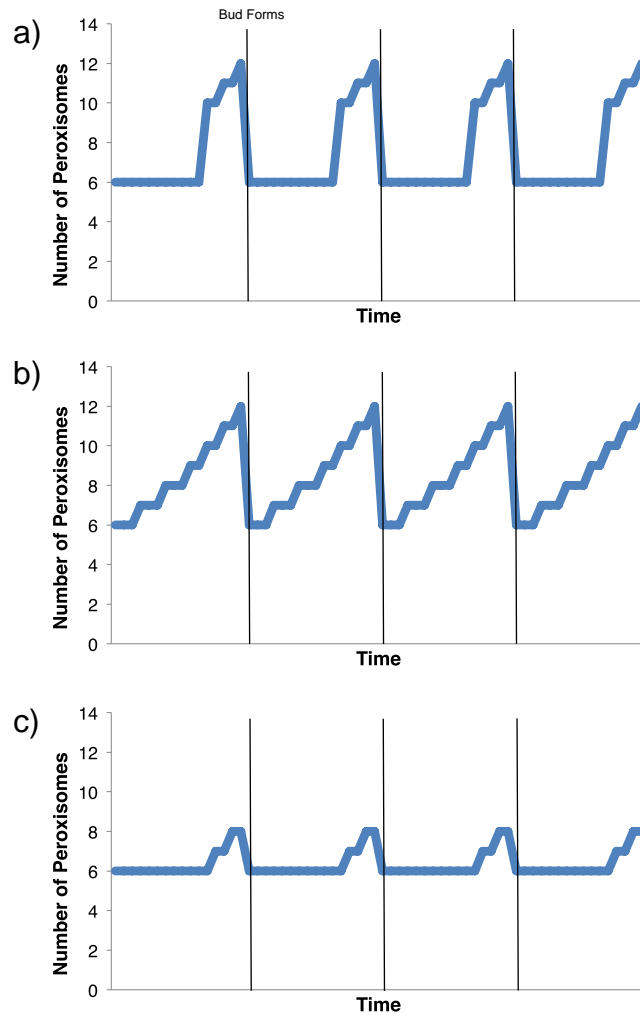


Figure 1.17. Proposed scenarios showing number of peroxisomes against time over 3 cell divisions. a) Graph representing noticeable increase of peroxisomes just before the bud inherits them. b) Graph representing gradual increase of peroxisomes over the entire course of a cell cycle before a daughter cell inherits them. c) Graph representing only a small increase in number of peroxisomes over the course of the cell cycle as they divided and inherited within a small time frame. Black lines indicate when a new bud starts forming. Numbers are illustrative.

1.6.3 Outline of Thesis

To address these models, a system of live cell imaging and image analysis was needed. Some of the important considerations of time-lapse live-cell imaging have already been outlined in section 1.5.1. Methods developed to analyse images for the vesicle fusion model (van der Zand et al., 2012) are outlined in Chapters 2.12-2.14. The claims of the vesicle fusion model (van der Zand et al., 2012), are then addressed in Chapter 3. Chapter 4 discusses the improvements to the live cell imaging setup necessary to probe the questions raised in 1.6.2 above. Chapters 5 and 6 are the culmination of this body of work, and evaluate the extent to which establishing peroxisomal number per cell and tracking individual peroxisomes was a

success, and the bearing this had on answering some of those questions above regarding the KPPC model.

Chapter 2: Materials and Methods

2.1 *S. cerevisiae* Strains

Strains used for this study are shown below in Table 2.1.

Table 2.1. Yeast strains used in this study

S. cerevisiae strain	Genotype	Source
BY4741 (WT)	MAT α , his3 Δ leu2 Δ met15 Δ ura3 Δ	European Saccharomyces cerevisiae Archive for Functional Analysis (EUROSCARF)
BY4742 (WT)	MAT α , his3 Δ leu2 Δ lys2 Δ ura3 Δ	EUROSCARF
dnm1 vps1	his3 Δ leu2 Δ lys2 Δ ura3 Δ yll001w::KanMX ykr001c::lox <i>S.pombe</i> HIS5 lox	Hettema Lab
inp1	his3 Δ leu2 Δ lys2 Δ ura3 Δ ymr204c::KanMX	Hettema Lab
inp2	his3 Δ leu2 Δ lys2 Δ ura3 Δ ymr163c::KanMX	Hettema Lab
Diploids (WT)	his3 Δ leu2 Δ ura3 Δ	Hettema Lab
FY1679-08A (WT)	MATA ura3-52 leu2 Δ 1 trp1 Δ 63 his3 Δ 200 GAL2	EUROSCARF
FY1679-06C (WT)	MAT α ura3-52 leu2 Δ 1 trp1 Δ 63 his3 Δ 200 GAL2	EUROSCARF
pex1	BY4742 pex1 Δ ::kanMX4	EUROSCARF
pex6	BY4742 pex6 Δ ::kanMX4	EUROSCARF
pex1/6	BY4742 pex1 Δ ::kanMX4 pex6 Δ ::HIS5	Produced in this study for Motley et al., 2015
vps1/dnm1 with galactose-inducible Pex19	BY4742 dnm1 Δ ::kanMX4 vps1 Δ ::loxP :His3MX6 -pGAL1 -3HA -PEX19	Produced in this study for Motley et al., 2015
WT expressing Pex2-VN and Pex14-VC	FY1679-08A PEX14-VC::HIS5 PEX2-VN::TRP1	Produced in this study for Motley et al., 2015
Vps1 expressing Pex13-VN and Pex14-VC	FY1679-08A PEX14-VC::HIS5 PEX13-VN::TRP1 vps1 Δ ::LEU2	Produced in this study for Motley et al., 2015
WT expressing mNeonGreen from the genome	BY4742 TPI-mNeonGreen-PTS1-clonNAT::TRP5	This study

2.2 DNA Manipulation

2.2.1 Polymerase Chain Reaction (PCR)

Polymerase chain reaction was performed with various enzymes depending on the application. Standard cloning was performed either with Velocity (Bioline), Accuzyme (Bioline) or Q5 (New England Biolabs) DNA polymerases, all of which are high fidelity

enzymes with both 5-3' and 3-5' proofreading activity. MyFi DNA polymerase (Bioline) was used to clone clonNAT-containing sequences, and was found to be more reliable and robust for cloning this particular sequence over any other polymerase that was utilised. MyTaq polymerase (Bioline) was used when checking proper integration of sequences into the *S. cerevisiae* yeast genome. Nearly all reactions were performed to the manufacturer's protocols for temperature and extension times (mins/kb). The exception was when performing a PCR using the clonNAT sequence. Below is the outline of a clonNAT PCR using MyFi enzyme:

- 1. 3 minutes at 95°C for initial denaturation of DNA**
- 2. 30 seconds at 95°C for denaturation of DNA**
- 3. 30 seconds at 55°C for annealing of the primers**
- 4. 3 minutes at 72°C for elongation**
- 5. 10 minutes at 72°C for final extension**

Steps 2-4 were repeated for 30 cycles.

2.2.2 Agarose Gel Electrophoresis

Agarose gel electrophoresis was used to analyse DNA from PCR reactions. 1% (w/v) high-resolution standard agarose was prepared in 0.5x TBE (0.1M Tris-base, 0.1M Boric acid, 10mM EDTA, at pH 8), using a microwave to dissolve the agarose in the TBE buffer. Once dissolved the agarose was left to cool slightly before 3µl of ethidium bromide was added, and the gel was poured. After solidifying, the gel was placed into a tank containing 0.5x TBE buffer. 6x loading dye was added to the samples that will be loaded to a 1x final concentration. A 1kb DNA ladder was used for reference. After loading, the agarose gels were run at either 100V for 30 minutes or 90V for 40 minutes. Gels were then viewed under a UV transilluminator.

2.2.3 Gel Extraction and DNA Purification

To perform a gel extraction of DNA in agarose, first the band of interest was excised from the agarose gel using a scalpel, usually whilst on a UV transilluminator following the appropriate safety procedures. The subsequent DNA extraction was performed using a Qiagen DNA extraction kit following the manufacturer's instructions.

2.2.4 Plasmid Isolation (Miniprep)

Overnight 5ml *Escherichia coli* cultures expressing plasmid of interest in ampicillin-containing media were first harvested. Isolation of plasmids from the culture was performed using miniprep kits from Bioline, Sigma Aldrich or Qiagen, following the manufacturer's instructions.

2.2.5 Restriction Enzyme Digestion

Digestion of plasmids using restriction enzymes was performed to facilitate the integration of DNA fragments from PCR, or to check integration of DNA into a plasmid after high-efficiency transformation. Each restriction digest contained 5µl of 10x 'CutSmart' buffer from NEB, 5µl of plasmid and 1µl of each restriction enzyme. The reaction volume was made up to 50µl using dH₂O. The reaction tube was then left at 37°C for a minimum of 1 hour, but generally overnight. Resultant reaction mixture was checked for complete digestion by loading a small amount onto an agarose gel.

2.3 Chemical Reagents

Sigma Aldrich supplied a majority of chemical reagents. New England Biolabs supplied the restriction enzymes. PCR enzymes were either from Bioline or New England Biolabs. Plasmid mini prep kits came from Bioline, Qiagen or Sigma. Gel extraction kits came from Qiagen. Components for making media were supplied by Formedium or Fisher Scientific.

2.4 Primers

All primers used were ordered from Sigma Aldrich, as dry powder. Primers were designed to have an 18-24 nucleotide homologous flanking region to the vector, and a similar size region of homology to start of target sequence for PCR. Sequences for *S. cerevisiae* homologous recombination were obtained from the Saccharomyces Genome Database (SGD) or from Addgene.

A table of primers used is listed in Table 2.2.

Table 2.2. Primers used in this study

Primer Name	Forward/Reverse	Description	5'→3' Sequence
VIP 119	Forward	M13 Forward	CTGACTGGGTGGAAGGCAAGAGAGCCCCGAAAGCTTACA TTTTATGTTAGGAAACAGCTATGACCATG
VIP 120	Reverse	M13 Reverse	CAACACCAATAACGCCATTTAATCTAAGCGCATCACCAACAT TTTCTGGCGTTTTCCAGTCACGACG
VIP 2249	Forward	Recombine anything from YCP vectors	GAATTGTAATACGACTCACTATAGGGCGAATTGACGTTGTA AAACGACGGCCAG
VIP 2250	Reverse	Recombine anything from YCP vectors	GGGAACAAAAGCTGGGTACCGGGCCCCCTCGAGCACAC AGGAAACAGCTATGACCATG
VIP 2543	Forward	His-BFP	AATGAGCAGGCAAGATAAACGAAGGCAAAGAGCTCAAATG TCTGAATTGATTAAGAGAAT
VIP 2544	Reverse	BFP-PTS1-PGK	AAAAAATTGATCTATCGATAAGCTTTTAGAGTTTTGAGTGCA GTGGGTTCAATTTGTGTCCTAACTTAGA
VIP 2546	Forward	HIS-tdTomato	AATGAGCAGGCAAGATAAACGAAGGCAAAGAGCTCAAATG GTGAGCAAGGGCGAGGAGGTC
VIP 2547	Reverse	tdTomato-PTS1-PGK	AAAAAATTGATCTATCGATAAGCTTTTAGAGTTTTGAGTGCA GTGGCTTGACAGCTCGTCCATGCCGTA
VIP 2548	Forward	Pex3-TurboGFP	AGCTCGTTTTCTCAAGCCTGGACTTTCTAGAGTCGACGG AGCAGGGGCGGAATGGAGAGCGACGAGCGGC
VIP 2549	Reverse	TurboGFP-PGK	AAAAAATTGATCTATCGATAAGCTTGCATGCCTGCAGGTC ATTCTTCACCGGCATC
VIP 2550	Forward	Pex3-CopGFP	AGCTCGTTTTCTCAAGCCTGGACTTTCTAGAGTCGACGG AGCAGGGGCGGAATGCCAGCTATGAAAATTGAATGT
VIP 2551	Reverse	CopGFP-PTS1-PGK	AAAAAATTGATCTATCGATAAGCTTGCATGCCTGCAGGTTA AGCAAAGCAATTGGAGTTTTAA
VIP 2655	Forward	Pex3-mNeonGreen	TCGTTTTCTTCAAGCCTGGACTTTCTAGAGTCGACGGAGC AGGGGCGGAATGGTGAGCAAGGGCGAGGAG
VIP 2656	Reverse	mNeonGreen-PGK	AAAAAATTGATCTATCGATAAGCTTGCATGCCTGCAGGTC ATTACTTGACAGCTCGTC
VIP 2659	Forward	HIS-mNeonGreen	AATGAGCAGGCAAGATAAACGAAGGCAAAGAGCTCAAATG GTGAGCAAGGGCGAGGAGGAT
VIP 2764	Forward	HIS-SacI-AAAA-mNeonGreen	GAGCAGGCAAGATAAACGAAGGCAAAGAGCTCAAATGG TGAGCAAGGGCGAGGAGG
VIP 2765	Reverse	mNeonGreen-PTS1-HindIII-PGK	AAAAAATTGATCTATCGATAAGCTTTTAGAGTTTTGAGTGCA GTGGCTTGACAGCTCGTCCATGCC
VIP 2766	Forward	GAL-SacI-AAAA-mNeonGreen	CTTTAACGTCAAGGAGAAAAAAGCTATAGAGCTCAAATGG TGAGCAAGGGCGAGGAGG
VIP 2767	Reverse	mNeonGreen-PTS1-HindIII-MFA2	CAAAAATTAAGCGATAACACAGGCGGGATCTTAGAGTTTTG AGTGCAGTGGCTTGACAGCTCGTCCATGCC
VIP 2992	Forward	GAL-BFP	CTTTAACGTCAAGGAGAAAAAAGCTATAAGCTCAAATGTCTG AATTGATTAAGAGAAT
VIP 2993	Reverse	BFP-PTS1-MFA2	CAAAAATTAAGCGATAACACAGGCGGGATCTTAGAGTTTTG AGTGCAGTGGTTCAATTTGTGTCCTAACTTAGA
VIP 2998	Forward	HIS-AAAA-mCherry	AATGAGCAGGCAAGATAAACGAAGGCAAAGAGCTCAAATG GGTGAGCAAGGGCGAGGAGGATAAC
VIP 2999	Reverse	mCherry-PTS1-PGK	AAAAAATTGATCTATCGATAAGCTTTTAGAGTTTTGAGTGCA GTGGCTTGACAGCTCGTCCATGCC
VIP 3000	Reverse	mCherry-PGK	AAAAAATTGATCTATCGATAAGCTTCTACTTGACAGCTCGT CCATGCC
VIP 3015	Forward	TPI-AAAA-mNeonGreen	CTATAACTACAAAAACACATACATAAACGAGCTCAAATG GTGAGCAAGGGCGAGGAGG

VIP 3028	Forward	TPI-AAAA-mCherry	CTATAACTACAAAAACACATACATAAACGAGCTCAAAAATG GTGAGCAAGGGCGAGGAGG
VIP 3048	Forward	TPI-AAAA-BFP	CTATAACTACAAAAACACATACATAAACGAGCTCAAAAATG CTGAATTGATTAAGAGAAT
VIP 3049	Reverse	BFP-PGK	AAAAAATTGATCTATCGATAAGCTTTTAGTTCAATTTGTGTC CTAACTTAGA
VIP 3071	Forward	mCherry-clonNAT	GAGGGCCGCCACTCCACCGCGGCATGGACGAGCTGTAC AAGTAGCAGCTGAAGCTTCGTACGC
VIP 3072	Forward	mNeonGreen- PTS1-clonNAT	ATGGGCATGGACGAGCTGTACAAGCCACTGCACTCAAACT CTAGCAGCTGAAGCTTCGTACGC
VIP 3073	Forward	BFP-PTS1-clonNAT	TCTAAGTTAGGACACAAATTGAACCCACTGCACTCAAACT CTAGCAGCTGAAGCTTCGTACGC
VIP 3074	Reverse	clonNAT-PGK	GTAAGGATGGGGAAAGAGAAAAGAAAAAATTGATCTATC GATAGCATAGGCCACTAGTGGATCTG
VIP 3093	Forward	BFP-clonNAT	CGTTATTGTGACTTGCCTTCTAAGTTAGGACACAAATTGAAC TAACAGCTGAAGCTTCGTACGC
VIP 3103	Forward	DMA2 KO for PUG/PAC system	GCAACGCATTGTATACGTTTGAAGCTTTCAGCAAAGGATAT ACCGTGGAACAGCTGAAGCTTCGTACGC
VIP 3104	Reverse	DMA2 KO for PUG/PAC system	GGTCAAAGAAAATACACAGTTTAAAAATAAAGAAAAACCAC CGAACTCCGCATAGGCCACTAGTGGATCTG
VIP 3105	Forward	1kilobase upstream DMA2	TACCTGTCATCGGAGGGGTGTTTCATGCCATGGGTGGTATG GCTGCGCAA
VIP 3130	Forward	M13 to recombine TRP5	TGCTCCAAAAAGGGACATAGCACACCGACAGACCATGTCA GAACAGTAAAACGACGGCCAGT
VIP 3131	Reverse	M13 to recombine TRP5	TAGTTAAAAAGCTAAATAAAAGCGTTTCTTATCAGATATTAC TCACAGGAAACAGCTATGAC
VIP 3210	Forward	HIS-SacI-AAAA- mKate2	AATGAGCAGGCAAGATAAACGAAGGCAAAGAGCTCAAAAAT GGTTTCTGAACTCATCAAGAAAAAC
VIP 3211	Forward	TPI-SacI-AAAA- mKate2	CTATAACTACAAAAACACATACATAAACGAGCTCAAAAATG GTTTCTGAACTCATCAAGG
VIP 3212	Forward	HIS-SacI-AAAA- mRuby2	AATGAGCAGGCAAGATAAACGAAGGCAAAGAGCTCAAAAAT GGTGTCCAAAGGAGAGGAGTTAATC
VIP 3213	Forward	TPI-SacI-AAAA- mRuby2	CTATAACTACAAAAACACATACATAAACGAGCTCAAAAATG GTGTCCAAAGGAGAGGAG
VIP 3214	Reverse	mKate2-PTS1-PGK	AAAAAATTGATCTATCGATAAGCTTTTAGAGTTTTGAGTGCA GTGGTCTGTGTCCCAACTTAGATGGC
VIP 3215	Reverse	mKate2-PGK	AAAAAATTGATCTATCGATAAGCTTTTATCTGTGTCCCAACT TAGATGG
VIP 3216	Reverse	mRuby2-PTS1-PGK	AAAAAATTGATCTATCGATAAGCTTTTAGAGTTTTGAGTGCA GTGGCTTATACAATTCATCCATACC
VIP 3217	Reverse	mRuby2-PGK	AAAAAATTGATCTATCGATAAGCTTTTACTTATACAATTCATC CATACC
VIP 3300	Forward	M13F(-40)-EcoR1- SacI-ZRT1(+500bp)	GTTTTCCAGTCACGACGAATTCGAGCTCCAAATTAGTCAA ATGCACTAG
VIP 3301	Reverse	ZRT1-BamH1-Xba- Sall-GSSG-mRuby2	CTCCTCTCCTTTGGACACCATTCCAGAAGATCCGTGACTC TAGAGGATCCAGCCCACTTACCGATCAAAGC
VIP 3302	Forward	M13F(-40)-EcoR1- SacI-TNA1(+500bp)	GTTTTCCAGTCACGACGAATTCGAGCTCCAGCCGGGCATA CTCGGGATC
VIP 3303	Reverse	TNA1-BamH1-Xba- Sall-GSSG-mRuby2	CTCCTCTCCTTTGGACACCATTCCAGAAGATCCGTGACTC TAGAGGATCCATACATGTACTTAACTCAGG
VIP 3304	Forward	M13F(-40)-EcoR1- SacI- PHO88(+500bp)	GTTTTCCAGTCACGACGAATTCGAGCTCGCAGAAAAAGAA ATAAACCGC
VIP 3305	Reverse	PHO88-BamH1- Xba-Sall-GSSG- mRuby2	CTCCTCTCCTTTGGACACCATTCCAGAAGATCCGTGACTC TAGAGGATCCTTCAGCCTTAACACCAGCGTTACC

VIP 3306	Forward	M13F(-40)-EcoR1-SacI-ERG25(+500bp)	GTTTTCCCAGTCACGACGAATTCGAGCTCCACTACCACTGCCTCCCTTCG
VIP 3307	Reverse	ERG25-BamH1-Xba-Sall-GSSG-mRuby2	CTCCTCTCCTTTGGACACCATTCCAGAAGATCCGTGACTCTAGAGGATCCGTTAGTCTTCTTTTGAGC
VIP 3308	Forward	M13F(-40)-EcoR1-SacI-MDH1(+500bp)	GTTTTCCCAGTCACGACGAATTCGAGCTCCCAAATCCGCATGTACCTGGG
VIP 3309	Reverse	MDH1-BamH1-Xba-Sall-GSSG-mRuby2	CTCCTCTCCTTTGGACACCATTCCAGAAGATCCGTGACTCTAGAGGATCCTTTACTAGCAACAAAGTTGAC
VIP 3310	Forward	M13F(-40)-EcoR1-SacI-ISU1(+500bp)	GTTTTCCCAGTCACGACGAATTCGAGCTCCTAGGTCTAATATTGTTATTG
VIP 3311	Reverse	ISU1-BamH1-Xba-Sall-GSSG-mRuby2	CTCCTCTCCTTTGGACACCATTCCAGAAGATCCGTGACTCTAGAGGATCCCGATAACATGGTTGGAGTGTTC
VIP 3312	Forward	M13F(-40)-EcoR1-SacI-ACO2(+500bp)	GTTTTCCCAGTCACGACGAATTCGAGCTCCGTTCCGTAGAAATCATG
VIP 3313	Reverse	ACO2-BamH1-Xba-Sall-GSSG-mRuby2	CTCCTCTCCTTTGGACACCATTCCAGAAGATCCGTGACTCTAGAGGATCCTTCGTTTCTTCGTATATTACC

2.5 Plasmids

All plasmids in this study were produced using homologous recombination in *S. cerevisiae* (Figure 2.1). All plasmids contained a separate origin of replication for *S. cerevisiae* and *E. coli*, ampicillin resistance marker for selection in *E. coli*, and an amino acid selectable marker, which allowed the *S. cerevisiae* to grow on media that lacked that particular amino acid (or uracil). Most often used were LEU2 and URA3 genes, but HIS5 was also occasionally utilised. Elsewhere on the plasmid was the gene of interest to be expressed, usually a fluorescent protein, or protein with fluorescent tag. Upstream of the gene of interest was a promoter, usually HIS, TPI or GAL1 (giving moderate, high, and inducible levels of expression, respectively). Downstream of the gene was a terminator that increases the efficiency of the mRNA translation, usually either PGK or MFA2. A list of plasmids produced during this study is documented in Table 2.3.

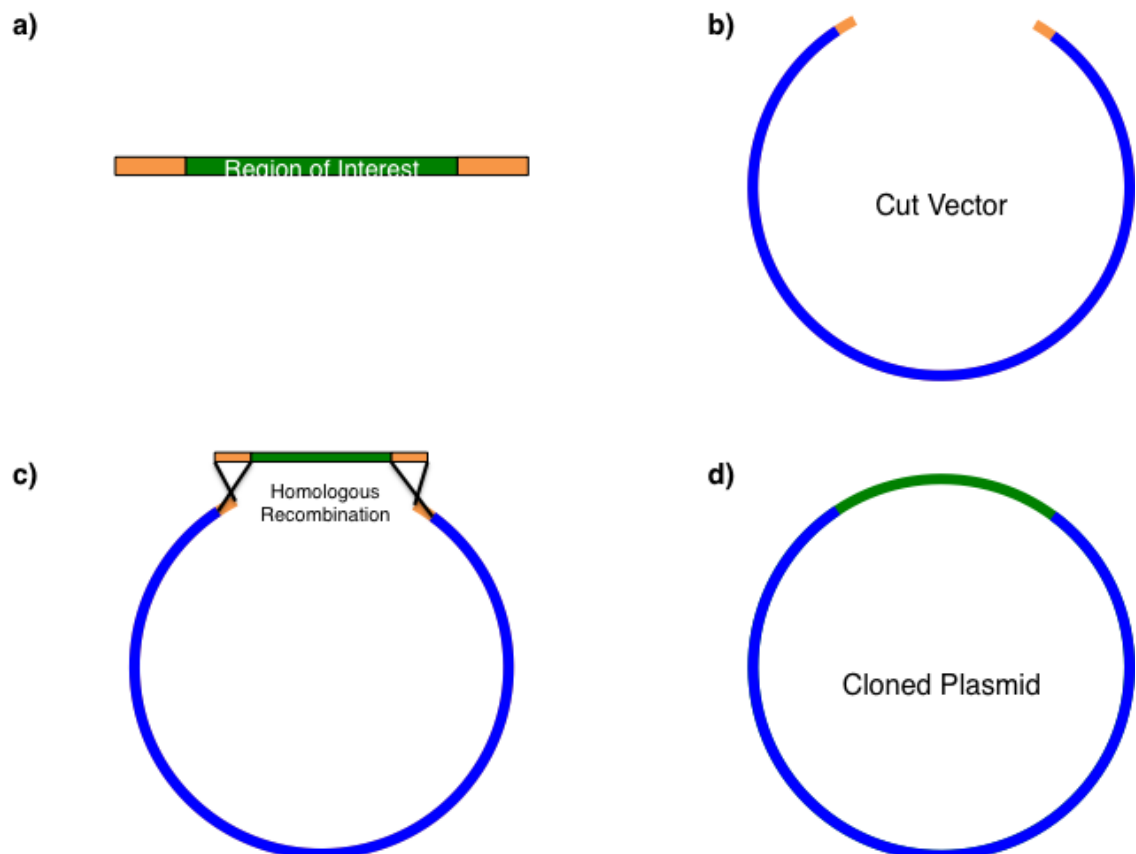


Figure 2.1. Stages of making a plasmid via homologous recombination in *S. cerevisiae*. a) The region of interest is amplified using the polymerase chain reaction (PCR). PCR product is produced using primers with homology to region of interest and 18-24 nucleotide flanking regions (orange) with homology to target. b) Vector plasmid is cut using appropriate restriction enzymes. Region of homology to PCR product in orange. c) PCR product and cut vector are introduced to *S. cerevisiae* plus reagents (see 2.7.2 for high-efficiency transformation protocol), and recombination occurs between homologous regions of the DNA. d) The PCR product is integrated into the vector producing the new plasmid.

Table 2.3. Plasmids used in this study.

Plasmid Name	Promoter	Description	Selection	Source
pAUL1	HIS	BFP-PTS1	URA	This study
pAUL2	GAL	Pex3-mNG	URA	This study
pAUL3	HIS	mNG-PTS1	URA	This study
pAUL4	HIS	mNG-PTS1	LEU	This study
pAUL7	GAL	mNG-PTS1	URA	This study
pAUL8	GAL	mNG-PTS1	LEU	This study
pAUL9	GAL	BFP-PTS1	URA	This study
pAUL10	GAL	BFP-PTS1	LEU	This study
pAUL11	HIS	mCherry	URA	This study
pAUL12	HIS	mCherry-PTS1	URA	This study
pAUL13	HIS	mCherry	LEU	This study
pAUL14	HIS	mCherry-PTS1	LEU	This study
pAUL15	TPI	mNG-PTS1	URA	This study
pAUL16	TPI	mCherry	URA	This study
pAUL17	TPI	mCherry-PTS1	URA	This study
pAUL18	TPI	BFP	URA	This study
pAUL19	TPI	mNG-PTS1	clonNAT + URA	This study
pAUL20	TPI	BFP-PTS1	clonNAT + URA	This study
pAUL21	TPI	BFP	clonNAT + URA	This study
pAUL22	HIS	BFP-PTS1	HIS	This study
pAUL23	HIS	mNG-PTS1	HIS	This study
pAUL24	HIS	mCherry-PTS1	HIS	This study
pAUL25	TPI	mCherry	LEU	This study
pAUL26	SP6	mKate2	HIS	Addgene
pAUL27	SP6	mRuby2	HIS	Addgene
pAUL28	HIS	mKate2-PTS1	LEU	This study
pAUL29	TPI	mKate2-PTS1	LEU	This study
pAUL30	TPI	mKate2	LEU	This study
pAUL31	HIS	mRuby2-PTS1	LEU	This study
pAUL32	TPI	mRuby2-PTS1	LEU	This study
pAUL33	TPI	mRuby2	LEU	This study
pAUL34	HIS	mKate2-PTS1	URA	This study
pAUL35	TPI	mKate2-PTS1	URA	This study
pAUL36	TPI	mKate2	URA	This study
pAUL37	HIS	mRuby2-PTS1	URA	This study
pAUL38	TPI	mRuby2-PTS1	URA	This study

pAUL39	TPI	mRuby2	URA	This study
pAUL40	ZRT1	ZRT1-mRuby2	LEU	This study
pAUL41	TNA1	TNA1-mRuby2	LEU	This study
pAUL42	PHO88	PHO88-mRuby2	LEU	This study
pAUL43	ERG25	ERG25-mRuby2	LEU	This study
pAUL44	MDH1	MDH1-mRuby2	LEU	This study
pAUL45	ISU1	ISU1-mRuby2	LEU	This study
pAUL46	ACO2	ACO2-mRuby2	LEU	This study
pAUL47	TPI	mNG-PTS1	LEU	This study
pAUL48	ZRT1	ZRT1-mRuby2	URA	This study
pAUL49	TNA1	TNA1-mRuby2	URA	This study
pAUL50	PHO88	PHO88-mRuby2	URA	This study
pAUL51	ERG25	ERG25-mRuby2	URA	This study
pAUL52	MDH1	MDH1-mRuby2	URA	This study
pAUL53	ISU1	ISU1-mRuby2	URA	This study
pAUL54	ACO2	ACO2-mRuby2	URA	This study
pAUL55	TPI	BFP-PTS1	URA	This study
pAUL56	TPI	BFP-PTS1	HIS	This study
pAUL57	TPI	mNG-PTS1	HIS	This study
pAUL58	ZRT1	ZRT1-mNG	URA	This study
pAUL59	TNA1	TNA1-mNG	URA	This study
pAUL60	PHO88	PHO88-mNG	URA	This study
pAUL61	ERG25	ERG25-mNG	URA	This study
pAUL62	MDH1	MDH1-mNG	URA	This study
pAUL63	ISU1	ISU1-mNG	URA	This study
pAUL64	ACO2	ACO2-mNG	URA	This study
pEH001	HIS	GFP-PTS1	URA	Ewald Hettema
pEH100	TPI	HcRed-PTS1	URA	Ewald Hettema
pEH117	TPI	GFP	LEU	Ewald Hettema
pAS5	HIS	HcRed-PTS1	URA	Alison Motley
pAS27	GAL	HcRed-PTS1	URA	Alison Motley
pAS28	GAL	HcRed-PTS1	LEU	Alison Motley
pAS62	GAL	Pex3-RFP	URA	Alison Motley
pAS63	HIS	HcRed-PTS1	LEU	Alison Motley
pAS212	N/A	Tet vector	HIS	Alison Motley

2.6 Culture Media

Culture media was made as described in Table 2.4. All media was sterilised by autoclaving. Addition of agar at 2% was used to make plates.

Yeast Peptone Dextrose is a complete media and requires no addition of amino acids. YM1

Table 2.4. Media used in this study.

Media	Ingredients
Yeast Peptone Dextrose (YPD)	1% Yeast extract, 2% Peptone, 2% Glucose
YM1	0.5% Ammonium sulphate, 0.17% Yeast nitrogen base, 2% Glucose/Galactose/Raffinose. Adjusted to pH 6.5 using NaOH
YM2	0.5% Ammonium sulphate, 0.17% Yeast nitrogen base, 1% Casamino acids, 2% Glucose/Galactose/Raffinose. Adjusted to pH 6.5 using NaOH
2TY for E. coli	1.6% Tryptone, 1% Yeast extract, 0.5% NaCl

is a yeast minimal media, and stocks of the appropriate amino acids (Leucine, Histidine, Tryptophan, Methionine, Lysine) and/or Uracil, were added as needed to 1x final concentration. Amino acids (and Uracil) were prepared in 100x stocks, and were added after the media was autoclaved and cooled to at least 50°C. YM2 is a more complete yeast media due to the inclusion of casamino acids that contains all the essential amino acids barring tryptophan (which is destroyed in the original acid digest of casein used to produce casamino acids). Uracil was added as determined by the experimental requirements.

Glucose was the carbon source used in both YM1 and YM2 media in a majority of cases. Galactose was occasionally used as the carbon source as determined by experimental requirements, for example for expressing proteins with the GAL1 promoter. Raffinose was occasionally for cell growth prior to switching cells to galactose-containing media, as the presence of raffinose does not actively suppress the GAL1 promoter, unlike the presence of glucose.

Drop-out media was also used, supplied by Formedium, which was added to YM1 media before autoclaving, and contained all the amino acids except for the ‘dropped out’ ones. For example, Leucine drop out contains all the amino acids except Leucine. This was sometimes used in place of YM2 and the addition of amino acids.

Nourseothricin (trade name *clonNAT*) was used as a selection antibiotic for *S. cerevisiae*, and was added to a final concentration of 100µg/ml.

2TY media was used for *E. coli* growth. Ampicillin for *E. coli* selection was added post-autoclaving, to a final concentration of 75µg/ml.

2.7 *Saccharomyces cerevisiae* Experimental Procedures

2.7.1 General Growth Procedure

Cells were grown shaking at 30°C in appropriate liquid media, or on agar plates containing 2% glucose at either 30°C or left on the bench at room temperature. Yeast were placed into 30% glycerol in cryo-tubes and deposited at -80°C for long-term storage.

2.7.2 High Efficiency Transformation

This technique required the use of pre-prepared stocks of sterile 1M lithium acetate (LiAc) at pH7.5, 10xTE (0.1M Tris-HCl, 0.01M EDTA, pH7.4) and 50% Polyethylene glycol (PEG) 3350 reagents. Solutions of 1x TE/LiAc (0.5ml 10xTE, 0.5ml 1M LiAc, 4ml dH₂O) and 40% PEG (0.5ml 10xTE, 0.5ml 1M LiAc, 4ml PEG3350) were prepared from the stock solutions. Cells were grown overnight in the appropriate media and then diluted to OD₆₀₀ = 0.1 and inoculated into a necessary volume of media (5ml was required for each transformation). The culture was then left to grow shaking at 30°C until mid-log phase, at roughly OD₆₀₀ = 0.5. The culture was then centrifuged at 3000rpm for 10 minutes and the supernatant was discarded. The pellet was washed in 1x TE/LiAc and transferred to microcentrifuge tubes. These were centrifuged for 2500rpm for 5minutes. The supernatant was again discarded, and the resultant pellet was again washed in 1x TE/LiAc, and spun again at 3000rpm for 3 minutes. The pellet was re-suspended in 50µl/transformation 1x TE/LiAc and separated into microcentrifuge tubes. Added to each microcentrifuge tube was 5µl of linearised vector, 5µl of PCR product, and 5ul ssDNA (herring sperm, Sigma Aldrich). Added to this was 350ul of 40% solution of PEG3350. The mixture was then vortexed and left at room temperature for 30 minutes. The microcentrifuge tubes were then placed into a water bath at 42°C for 15 minutes. Following centrifugation at 10000rpm for 30 seconds, the pellet was resuspended in 50µl 1x TE for plating on appropriate selection agar, and left to grow at 30°C for 2 days.

2.7.3 One Step Transformation

Cells were grown overnight in the appropriate media. 200µl of culture was centrifuged at 10000rpm for 30 seconds, and the supernatant was discarded. 1µl of plasmid was added, and the mixture was vortexed. 50µl of one-step buffer (0.2M lithium acetate pH5.0, 40% Polyethylene glycol 3350, 100mM DTT) and 5µl ssDNA (herring sperm, Sigma Aldrich) was added. This was mixed by vortexing. The resultant mixture can be left at room temperature

for several hours to improve efficiency of transformation. After incubation at 42°C in a water bath, the reaction mixture was plated onto appropriate selection agar, and left to grow at 30°C for 2 days.

2.7.4 Yeast Genomic DNA Isolation

Cells for DNA extraction were either grown overnight in appropriate liquid media, or scraped from an agar plate, and were subsequently washed in 1ml dH₂O. After a short centrifugation, the supernatant was discarded and the cells were re-suspended in the remaining volume. 200µl pre-prepared TENT'S (20mM Tris/HCl at pH8.0, 1mM EDTA, 100mM NaCl, 2% Triton X-100, 1% SDS) solution, 200µl glass beads (measured using a 200ul pipette tip) and 200µl of phenol/chloroform solution was added to the tube. Tubes were then placed into a bead beater at full speed for 45 seconds. After bead beating, samples were centrifuged at 12000x g for 30 seconds. To this mixture a further 200µl TENT'S solution was added, and the sample vortexed. The mixture was then centrifuged for 5 minutes at 12000x g, and the supernatant transferred to a new microcentrifuge tube. To this was added 200µl of phenol/chloroform solution, and the sample was again centrifuged for 5 minutes at 12000x g. 300µl of the supernatant was removed and placed into another fresh tube. To this was added 30µl of 3M sodium acetate at pH5.2 and 750µl of absolute ethanol. DNA was precipitated by leaving tubes at -20°C for at least 30 minutes. Samples were then spun at maximum speed for 15 minutes. Pellets were washed in 70% ethanol solution and the previous centrifugation step was repeated. After removing the ethanol solution, the pellets were re-suspended in 200µl of 1xTE at pH8.0 containing 5µg/ml RNAse and incubated at room temperature for 10 minutes. To this solution was added 20µl NaAc and 550µl absolute ethanol, and the DNA was again left to precipitate at -20°C for at least 30 minutes. Again the sample was centrifuged at maximum speed for 15 minutes, followed by the 70% ethanol wash step and 15 minute maximum speed centrifugation. The pellets were then left to dry completely. The dry pellet was then re-suspended in 50µl 1x TE at pH8 and can be stored at -20°C until required.

2.8 *Escherichia coli* Experimental Procedures

2.8.1 *E. coli* Strains

DH5 α was the only *E. coli* strain used in this study. It is outlined in Table 2.5 below.

Table 2.5. *E. coli* strains used in this study.

E. coli strain	Genotype	Source
DH5 α	supE44 DlacU169 (f80 lacZ DM15) hsdR17 recA1 endA1 gyrA96 thi-1 relA1	Laboratory stock

2.8.2 *E. coli* General Growth Procedure

E. coli were grown in 2TY liquid media, shaking at 37°C, or on 2TY agar plates at 37°C. *E. coli* agar plates were sometimes placed in the fridge at 4°C for short term storage. Ampicillin was added to final concentration of 75 μ g/ml for plasmid selection.

2.8.3 Production of Electro-competent *E. coli* Cells

DH5 α cells were first inoculated into an overnight culture of 2TY, and left to proliferate overnight shaking at 37°C. The following morning, a 1L flask containing 2TY was inoculated with a volume of cells from the overnight culture so that the starting OD₆₀₀ = 0.1. Cells were left to grow shaking at 37°C until OD₆₀₀ = 0.5 was reached. Cells were then separated into centrifuge flasks to be spun at 3000rpm for 10 minutes at 4°C. The 2TY supernatant was discarded, with care being taken not to disturb the pellets. The pellets were re-suspended in 500ml of 10% (w/v) of pre-prepared glycerol solution using 10ml pipettes. Cells were spun as before, supernatant discarded, and resuspended this time in 250ml of 10% glycerol. Cells were spun for a third time at 3000rpm, 15 minutes, 4°C before then being re-suspended in 50ml 10% glycerol. Cells were spun as before, but resuspended in 0.7ml 10% glycerol and transferred to a microcentrifuge tube. 40 μ l aliquots were taken into tubes sitting on ice, before being snap frozen in liquid nitrogen and placed into the -80°C freezer for long-term storage.

2.8.4 *E. coli* Transformation

One aliquot of *E. coli* cells in a microcentrifuge tube was thawed on ice. 1µl of plasmid was added to the tube. The tube was gently mixed and left on ice for 30 minutes. The cells were then heat shocked by placing the tube into the water bath at 42°C for 90 seconds, and then back onto the ice for 5 minutes. 900µl of 2TY media was added to the tube, and the cells were left to recover at 37°C for 30 minutes. Cells were then spun at 12000x g for 1 minute, supernatant was removed, and the cells were re-suspended in the remaining volume. The cells were then plated onto agar containing ampicillin for selection, and left overnight at 37°C.

2.8.5 Electroporation of *E. coli*

One aliquot (40µl) of electro-competent DH5α cells were added to 10µl of diluted (1µl DNA/9µl dH₂O) gDNA. This was then transferred to an electroporation cuvette (Fisher), and mixed by pipetting up and down. Cells were then pulsed using an electroporator set at 'EC2'. 1ml 2TY was added to the electroporation cuvette, mixed, and then the cell solution was transferred to a microcentrifuge tube. Cells were then left to recover at 37°C for 30 minutes. The tubes were then centrifuged at 5000 rpm for 5 minutes, supernatant removed, with care being taken not to disturb the pellet. The cells were then plated onto agar containing ampicillin for selection, and left overnight at 37°C.

2.9 Microscopy and Imaging

2.9.1 Microscopy

The microscope used in this study was a Zeiss Axio Observer microscope (widefield) with a 100x 1.45 NA α Plan-Fluar objective with an electron-multiplying charge-coupled device (EMCCD) camera supplied by Rolera. Fluorescence filter cubes are supplied by Zeiss or Chroma, and consist of DAPI, HE (high-efficiency) GFP, Texas Red and GFP/Texas Red bandpass filters. The microscope is also equipped with a Definite Focus Module (Zeiss). Light source is a HXP120 mercury arc lamp (OSRAM).

2.9.2 Fluorescent Proteins

Fluorescent proteins were expressed as protein tags, or on their own, with or without the inclusion of a signal sequence tag.

The predominant fluorescent protein employed in this study was mNeonGreen (Allele Biotechnology), which is a bright monomeric yellow-green fluorescent protein. Proteins are summarised in the Table 2.6:

Table 2.6. Fluorescent proteins used in this study. Adapted from ‘Fluorescent Protein Properties’, <http://www.fpyis.org/FP.html> (Thorn and Lambert, 2017).

Protein	λ_{ex} (nm)	λ_{em} (nm)	Extinction Coefficient	Quantum Yield	Brightness	Maturation Speed
mNeonGreen	506	517	116000	0.8	92.8	Very Fast
EGFP	488	507	56000	0.6	33.6	Fast
HcRed	590	637	160000	0.04	6.4	Very Slow
mCherry	587	610	72000	0.22	15.8	Medium
mRuby2	559	600	113000	0.38	43	Slow
BFP	402	457	52000	0.63	32.8	Medium
mKate2	588	633	62500	0.4	25	Fast

2.9.3 Preparation of Agarose Pads for Optimal Growth Conditions

2.9.3.1 Using Glass Slides

Roughly square wells were prepared by using tape on glass slides. A heat block was turned on in preparation to keep the agarose warm after melting. 0.1g of agarose was weighed out and placed into a 15ml plastic tube before adding 5ml of suitable growth media. The agarose was then dissolved in the microwave. The hot agarose and media mixture was then pipetted into the wells created by the tape on the glass slides. Another glass slide was placed on top of the wells, creating a flat square of agarose in the well. The agarose was then left to cool for approximately 20 minutes. The top glass slide was then removed, cells were mounted on the agarose, and a coverslip was placed on top.

2.9.3.2 Using Glass Bottom Dishes

The glass dishes used were 35mm ‘ μ -Dish’ supplied by Ibidi. The agarose was prepared as above. The warm agarose was then pipetted or poured into a glass bottomed dish and left to set, which formed a small ‘plug’ of agarose in the dish. After the agarose had set, this plug was then lifted up and excised from the dish completely using a scalpel. Cells were pipetted into the well in the dish underneath. The agarose plug was reinserted after pipetting cells into the dish. If it was necessary, gently pressing with the back of a pipette tip on the agarose plug was performed to help level out the cells.

2.9.4 Microfluidic System

A system more suited to imaging for extended periods was a cell culture chamber, in conjunction with a microfluidic controller (Figure 2.2). The cell culture chamber is a glass-bottomed chamber in part of a larger plastic plate with wells for media. The microfluidic controller is a device that generates pressurised air and is connected to the microfluidic plates via series of tubing and a specially made manifold (Figure 2.2a and Figure 2.2b). The pressurised air is used to pump media and cells into the culture chambers in the plates, and a vacuum keeps the plate sealed. The microfluidic controller itself is controlled by software on a connected desktop computer. In this study, a CellASIC ONIX Microfluidic System (Merck Millipore) with Y04C-02 Microfluidic Plates (Merck Millipore) was used. Software was downloaded from www.merckmillipore.com.

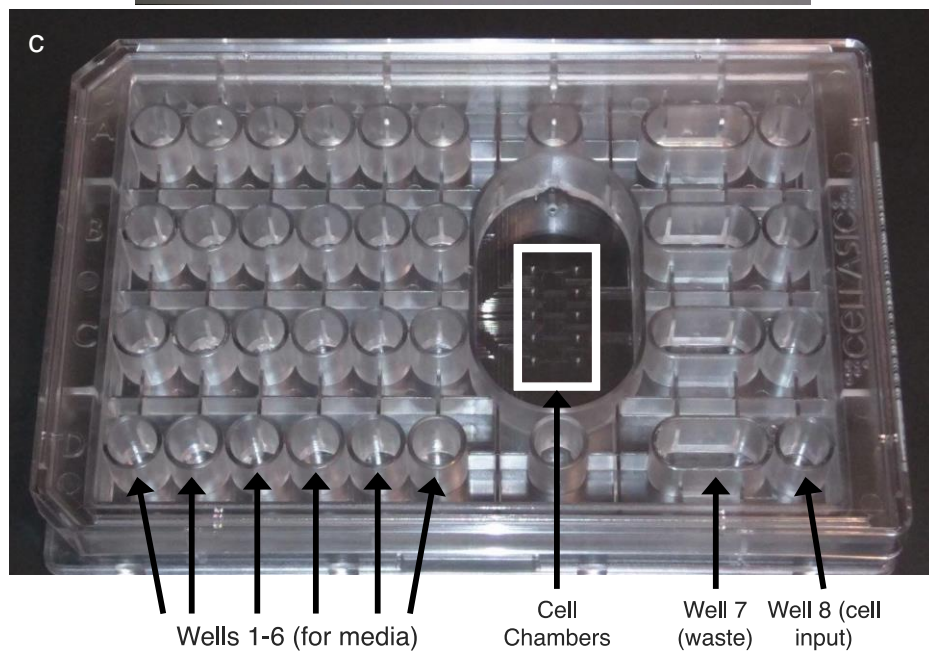
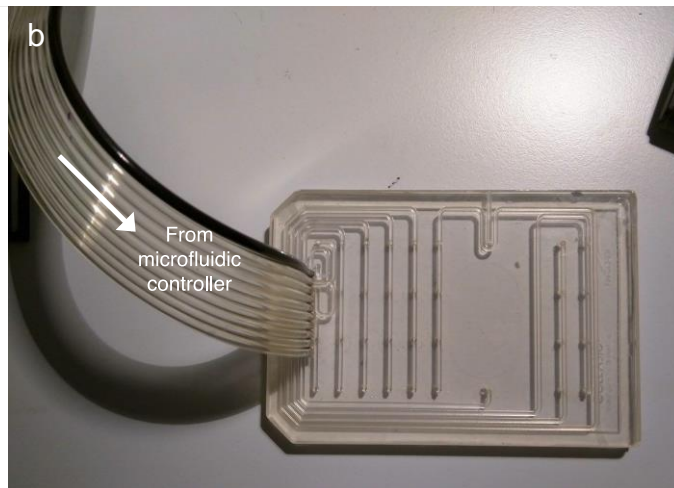


Figure 2.2. Microfluidic System equipment used in live-cell imaging. a) Microfluidic controller. b) Gasket that connects the microfluidic system to the microfluidic plates. c) Microfluidic plate.

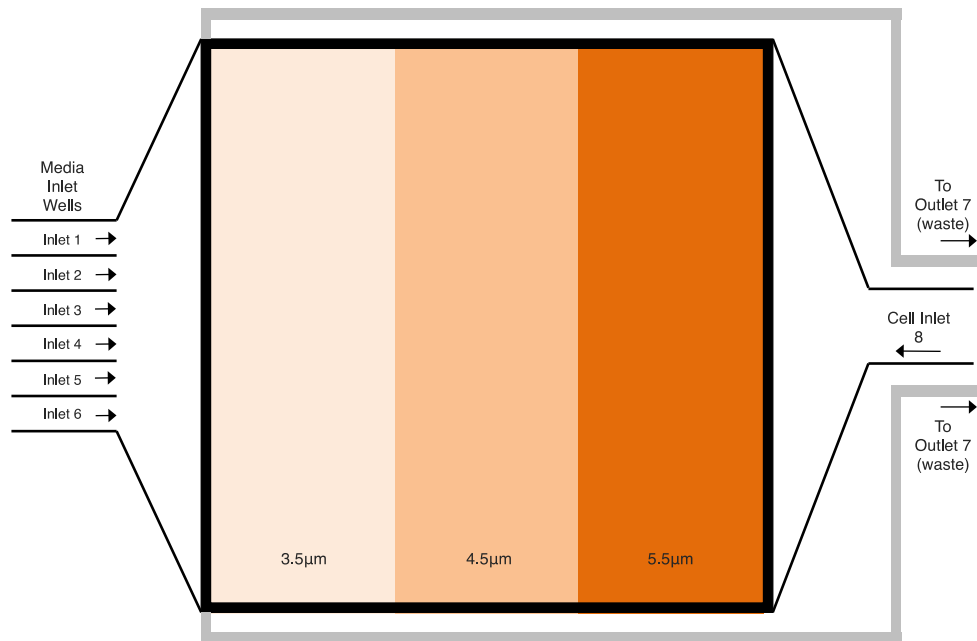


Figure 2.3. Cell culture chamber within the microfluidic plate. The chamber measures 3x3mm with different ceiling heights of 3.5µm, 4.5µm and 5µm for trapping cells. Media comes in via inlet wells 1-6, cells via inlet 8 and waste goes out to well 7.

The Y04C-02 Microfluidic Yeast Plates are four chambered cell culture plates specifically designed for use with haploid yeast cells and can fit onto a standard multiwell plate stage adapter (Figure 2.2c). Each chamber within the plate measures 3.0 x 3.0mm, each with three different ceiling heights of 3.5µm, 4.5µm and 5.5µm for trapping cells (Figure 2.3). Each chamber is fed with six inlet wells for media (1-6), one inlet well for loading cells (8) and an exit well for waste (7).

Before any experiment 350µl of desired media - predominantly 2% glucose-containing YM2 media, although 2%-galactose containing YM2 was used for some experiments in Chapter 4 - was loaded into wells 1-6 and cells were loaded into cell 8. Well 7 remained empty as this was the waste outlet well. The manifold gasket was then sealed to the plate by placing it on the plate and activating the Microfluidic Controller's vacuum. Gentle downward force was applied until an indicator light on the controller showed when the plate was sealed. The cells were loaded into the cell culture chamber under pressure (8psi for 5 seconds). The elastic ceiling within the cell culture chamber traps the cells (Figure 2.4). The manufacturer recommends washing out un-trapped cells by flowing one or more inlet wells at 5psi for minutes. The software was then programmed to direct media into the wells for the duration of the experiment via controlling the amount of pressure to each of the 1-6 inlet wells. This gentle pressure placed on the inlet wells is enough to ensure a fresh supply of media to the cells in the chamber. Therefore, the nutrients surrounding the cells are constantly refreshed, and excreted products are taken away.

It should be noted that focusing in Z was not attempted before the media flow into the cell culture chamber had commenced; changes in the flow of media into the chamber disrupts the focus in Z and would have to be readjusted if performed beforehand.

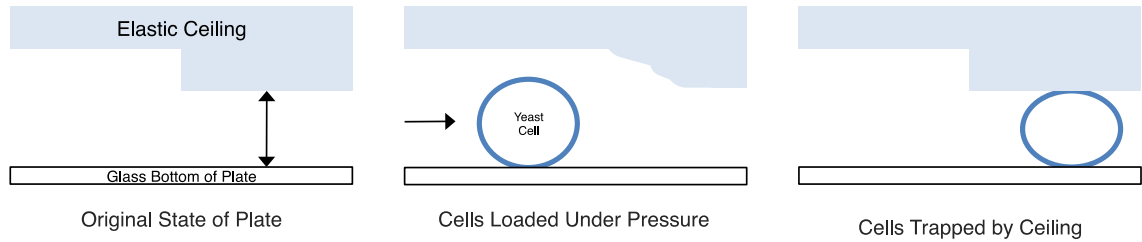


Figure 2.4. Cell trapping mechanism using the elastic ceiling of the cell chamber.

2.9.5 Microscope Software and Modules

The microscopy software supplied with the Zeiss Axio Observer microscope was ZEN, which eventually included the Definite Focus (explained in Chapter 1.5.1.3) and Tiles and Positions modules. Tiles and Positions enabled multiple locations to be visited in the same live-cell imaging experiment. This meant that many (usually 9, in a grid) sites could be visited one after another in the live cell imaging experiments, which was a more efficient use of microscopy time and resources (media, live-cell imaging plates etc.).

2.10 Making New mNeonGreen Plasmids and Genomically Integrated Strain

2.10.1 Creation of Original mNeonGreen Plasmid

An mNeonGreen-expressing bacterial plasmid was obtained from a commercial vendor (Allele Biotechnology).

E. coli were transformed with this plasmid and selected on ampicillin (Chapter 2.8.4). A few colonies were isolated and a miniprep was performed (Chapter 2.2.4) to get a high concentration of the plasmid for future yeast work. Primers were designed (VIP 2764 (F) and VIP 2765 (R), Table 2.2) to clone the sequence from this plasmid into another yeast plasmid with homology to the 20bp at the N and C termini of the gene, along with the reverse primer containing the PTS1 targeting sequence (PLHSL). PCR was performed using the *E. coli* expressing plasmid as a template with Q5 DNA Polymerase. After running PCR product on an agarose gel, the product was transferred into the cut pAS5 target vector (SacI/HindIII) via yeast homologous recombination in a high efficiency transformation (Chapter 2.7.2, plasmid table 2.2). Yeast genomic DNA isolation was performed (Chapter 2.7.4), followed by transformation in *E. coli* (Chapter 2.8.4), isolation and miniprepping (Chapter 2.2.4) to get the finished plasmid (pAUL3, Table 2.3). This plasmid was then used as a base for cloning mNeonGreen for other purposes.

2.10.2 Replacing the Promoter

A PCR reaction was performed using the mNeonGreen-PTS1 expressing plasmid (pAUL3) as a template, VIP 2765 (Table 2.2) as the reverse primer, and a forward primer with homology to C-terminus of the TPI promoter on the target vector (VIP 3015, Table 2.2). This PCR product was transformed into cut pEH101 as target vector in a high efficiency transformation using yeast homologous recombination (Chapter 2.7.2, plasmid Table 2.2). Again, yeast genomic DNA isolation was performed (Chapter 2.7.4), followed by transformation in *E. coli* (Chapter 2.8.4), isolation and miniprepping (Chapter 2.2.4) to get a concentration of the plasmid (pAUL15, Table 2.3). The map of this finished plasmid can be seen in Figure 2.5.

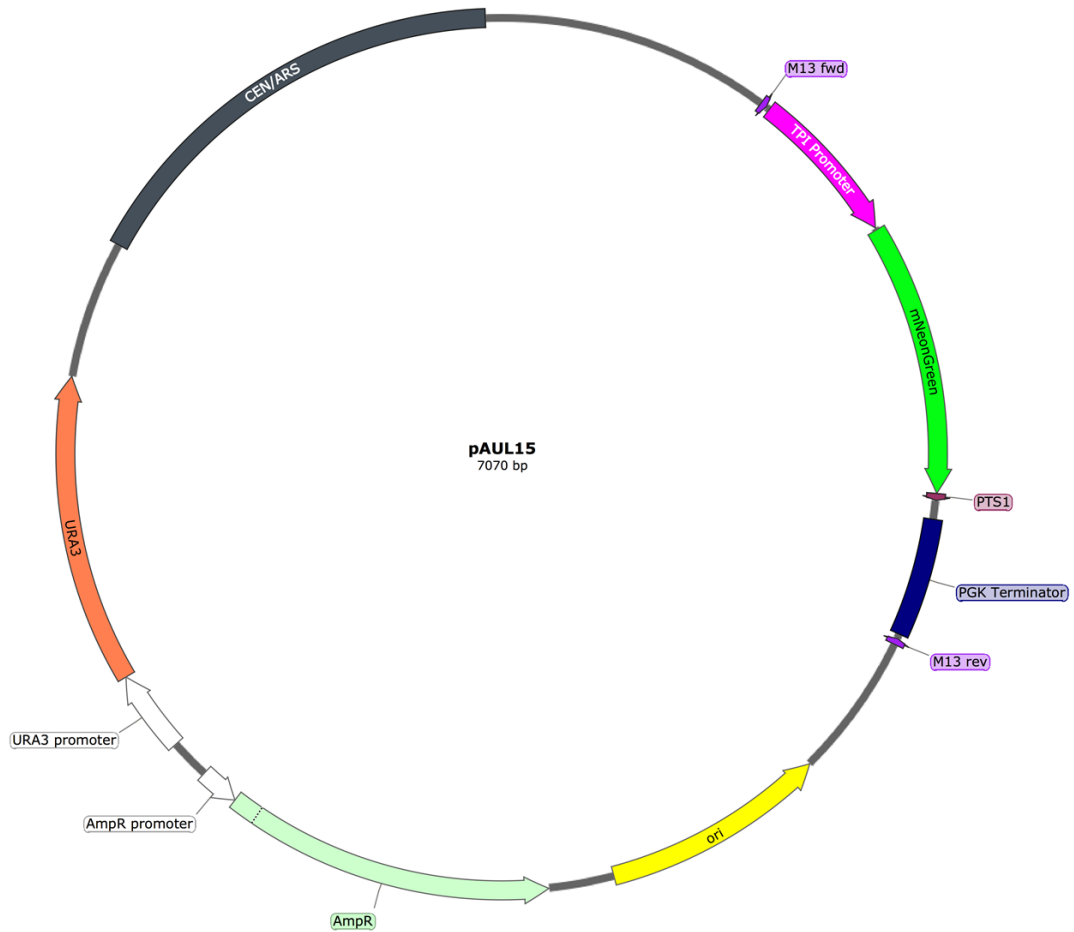


Figure 2.5. Map of the plasmid pAUL15 demonstrating the various regions contained on the plasmid. CEN/ARS = centromere, required for the plasmid to be maintained through generations. Ori = E.coli origin of replication. URA3 = codes for Orotidine-5'-phosphate decarboxylase (part of the uracil biosynthesis pathway), which allows yeast to grow on media lacking uracil. M13 fwd and M13 rev = sites were standard sequencing primers M13 anneal to the plasmid.

2.10.3 Creating a Genomically Integrated mNeonGreen Strain

First a PCR was performed with a plasmid that contained the clonNAT sequence as the template using primers VIP 3071 and VIP 3074 (Table 2.2) and the DNA polymerase MyFi. Meanwhile, the plasmid pAUL15 was cut using only HindIII. This cut the plasmid between the end of the PTS1 sequence and the start of the PGK terminator (Figure 2.6). The PCR product and cut vector were combined in a high-efficiency transformation (Chapter 2.7.2). The product of this homologous recombination is displayed in Figure 2.7. The transformed yeast cells were checked under the fluorescence microscope for expression of the fluorescent protein, along with selection on clonNAT to ensure that the

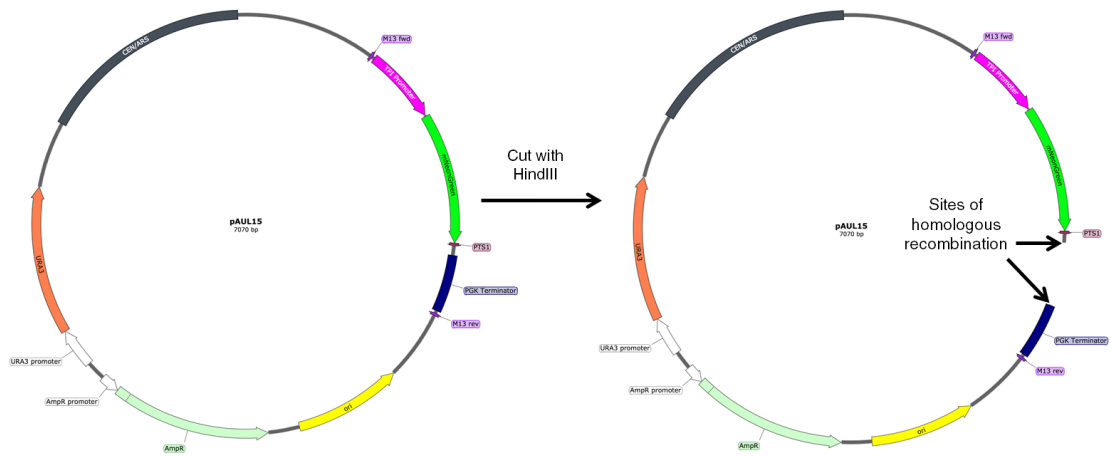


Figure 2.6. A map of the plasmid pAUL15 demonstrating the region between the PTS1 and PGK terminator that is cut by HindIII. The clonNAT resistance sequence is inserted by homologous recombination at this location.

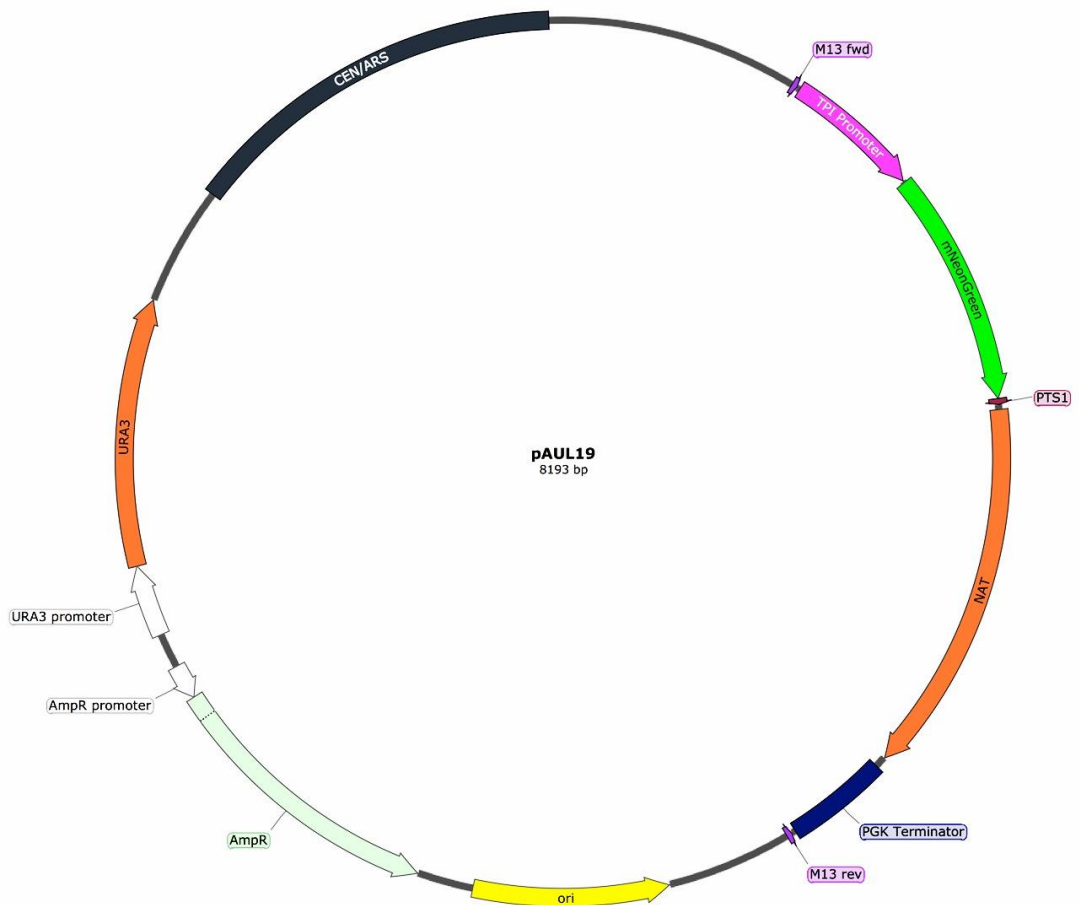


Figure 2.7. A map of the plasmid pAUL19 demonstrating the various regions contained on the plasmid. NAT = clonNAT resistance sequence.

resistance gene was expressing. This new plasmid was isolated from the yeast via the yeast genomic DNA isolation (Chapter 2.7.4), and then transformed into *E. coli* (Chapter 2.8.4), isolated and minipreped (Chapter 2.2.4).

This new plasmid (pAUL19, Figure 2.7) was then used as the template a PCR using the 'M13 forward' and 'M13 reverse' primers with MyFi DNA polymerase, which amplified the entire coding region on the plasmid. These primers have 5' ends homologous to flanking regions of the TRP5 gene for integration into the genome. The entire PCR product was then loaded onto a gel for subsequent gel extraction (see Chapter 2.2.3). This step was necessary because the PCR reaction tube still contains a small amount of the original template plasmid. Performing a high efficiency transformation using the PCR reaction mixture from the tube would inevitably cause some of the yeast to be transformed with the original plasmid and not with the PCR product as desired. The extracted PCR product was then transformed into yeast via homologous recombination in a high efficiency transformation (Chapter 2.7.2), and the yeast were screened for fluorescence.

2.11 Computational Work

The bulk of this work was carried out on machines running Linux Mint 22 (for computational analysis) utilising the bash shell, or on Windows 7 machines (microscopy). Scripts were written in the Python 2.7 programming language for image analysis using FIJI and data manipulation, and also some shell scripts were written for general-purpose tasks. The Matplotlib plotting library (a Python extension) was used to produce some figures (Hunter, 2007), and jplot was used for some others (Jeremy Craven, University of Sheffield). External programs used were FIJI, SnapGene and SerialCloner.

2.11.1 FIJI

FIJI is an open source, widely available and widely used image processing program, and is an extension of ImageJ (Schindelin et al., 2012). FIJI supports scripts written in its macro language, or in several of the other supported languages including (but not limited to) Python, Java and Ruby. FIJI features many plugins and tools that are extremely useful in image analysis, and there is a vast range of other tools not bundled on a new install that can be downloaded as required. It is available at <http://imagej.net/Fiji/Downloads>. Several pieces of information would have been useful to know before starting to use FIJI and these have been documented in Appendix B.1 and B.2.

2.11.2 SnapGene and SerialCloner

SnapGene and SerialCloner are programs used to manipulate DNA sequences. SnapGene was also used to create some figures in section 2.10. They can be downloaded from <http://www.snapgene.com/> and http://serialbasics.free.fr/Serial_Cloner.html respectively.

2.12 Image Processing Pathways

All image manipulation was performed using FIJI, either manually or using scripts. Commands in FIJI will be described with how to access those commands via the menus (e.g. Menu X > Set of Functions Y > Function Z), but it should be noted that most processing was performed using commands written as Python scripts. Extracts from these Python programs will be shown at the end of the relevant sections, and the whole scripts will be contained within the Appendix section, and referenced in the text.

The workflow of the initial processing of any image is described in Figure 2.8. These initial steps are concerned with getting the image data into a format that was more manageable for further processing. First, the raw image data (e.g. Figure 2.9) was opened. If data consisted of stacks and hyperstacks they were first separated into their respective channels, as a different analysis would be performed depending on the channel (these terms are explained in Appendix A). The use of a plugin called 'Bio-formats' (Plugins > Bio-Formats > Bio-Formats Importer) allowed opening of the original hyperstack and splitting into separate channels straight away.

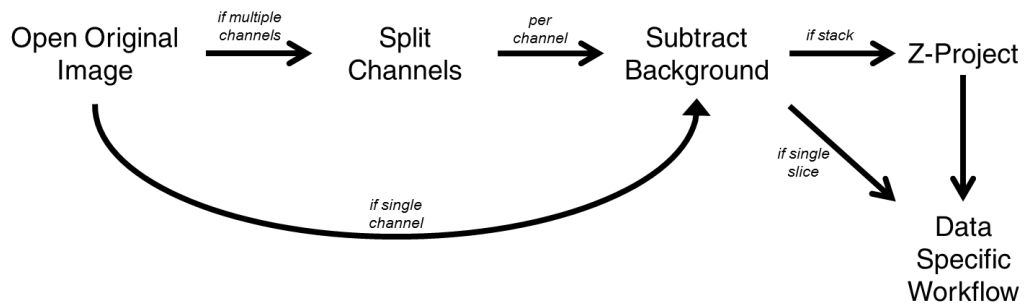


Figure 2.8. Initial image processing pathway. Raw image data is opened, and split into multiple channels if necessary. Then for each channel, a background subtraction is performed. If the image data is a stack, this is then Z-projected. After this, the pathway of image processing diverges depending on the data being analysed. These stages and the terms used here are explained in the text.

Two stages of pre-processing were consistent across all types of image (Figure 2.8). The first stage was subtracting the background (Process > Subtract Background). This is based on the 'rolling ball' algorithm as described in Sternberg, 1983 (although the algorithm now actually uses a rolling paraboloid). See Appendix C.1 for explanation of the rolling ball algorithm. For peroxisomes a radius of 1 pixel was chosen for the rolling ball algorithm, and for cells a radius of 50 pixels was chosen.

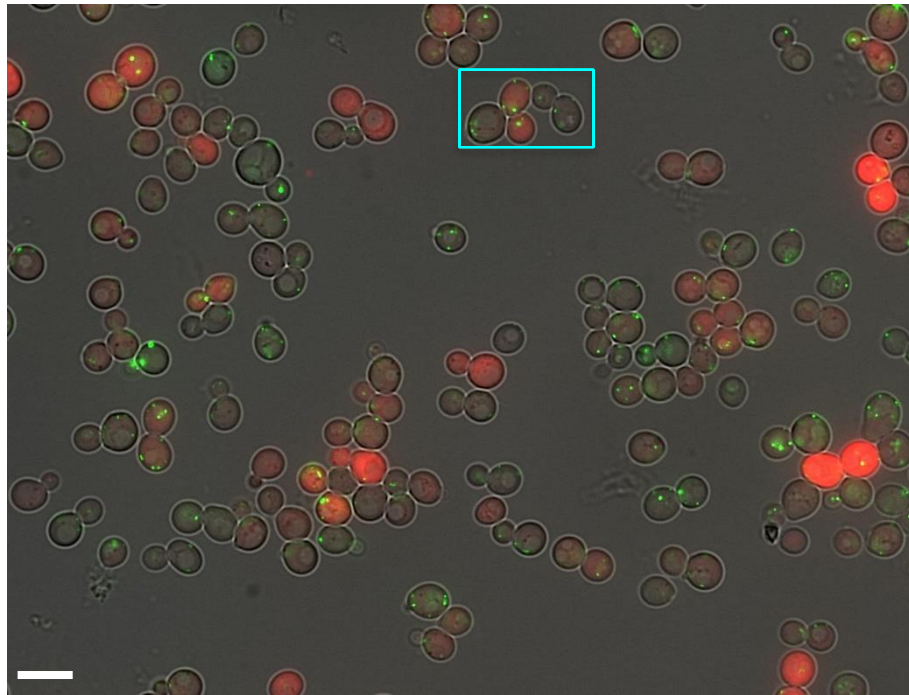


Figure 2.9. Example of raw image data. This is one Z section (slice 6 of 11) of an image in 3 channels: brightfield (grey), cytosolic mCherry (red) and mNeonGreen-PTS1 (green). This image would be split immediately into its three constitutive channels via the Bio-formats plugin. Processing is performed on the green and red channels only. Cells are WT expressing mCherry and mNeonGreen-PTS1 from two different plasmids. Note the varied intensities of both green and red signals in different cells. Cyan box indicates section of image used in Figures 2.17 and 2.20 showing processing for peroxisomal and cell channels, respectively. Scale bar indicates 5 μm .

If the image was a stack, then it was Z-projected (Image > Stacks > Z Project) (Figure 2.10). See Appendix C.2 for an explanation of Z projection and the different types of Z projection used. For cells, the sum slices method was used, and either sum slices or maximum intensity projection was used for peroxisomal images. After this stage, the processing of images diverged depending on whether the image is of cells or peroxisomes.

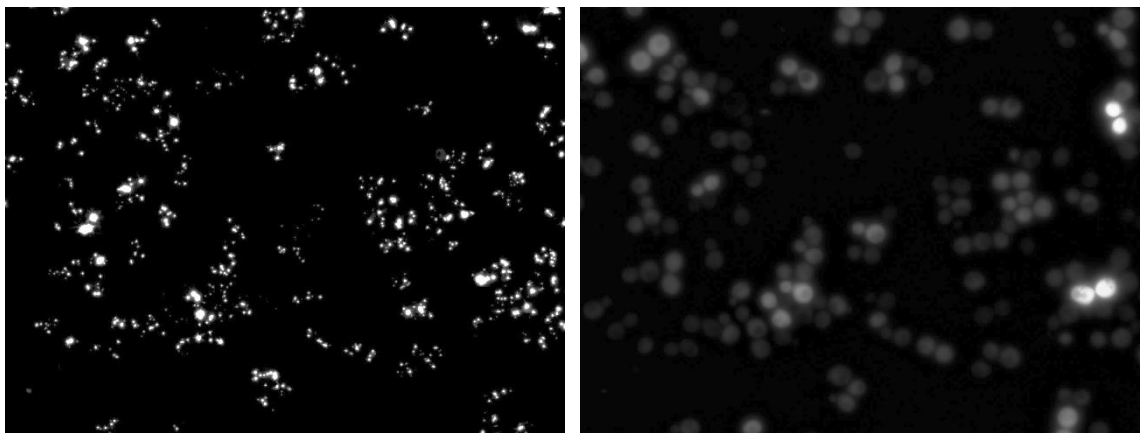


Figure 2.10. Peroxisomal and cellular channels following pre-processing. These two images are derived from the raw image data in Figure 2.9 following the first stages of pre-processing. Both images have had a background subtraction followed by a Z-projection (both by the sum slices method in this instance). The peroxisomal channel, originally green in Figure 2.9, is on the left, and red channel from Figure 2.9 showing cells containing the fluorescent protein in the cytosol are the image on the right.

2.13 Analysing Peroxisome Image Data

2.13.1 Introduction

Peroxisomes are visualised using fluorescent protein targeted to peroxisomes. The fluorescent protein was usually targeted to the peroxisome by adding the signal sequence PTS1 on to the C-terminal end of the fluorescent protein. For a list of fluorescent proteins used in this study, see Chapter 2.9.2. The PTS1 on the fluorescent protein is recognised in the cytosol and imported into the peroxisomal matrix by Pex5 (see Chapter 1.3.2).

Peroxisomes in wild-type cells labelled with fluorescent protein appear as round, circular objects on a 2D image. The technique of processing, segmenting and analysing peroxisome image data is based on maximising the contrast provided by the fluorescent label against the (non-fluorescent) background and then segmenting the image based on the maximum points in an image, or by detecting objects of a certain size and circularity. The workflow of this analysis is outlined in Figure 2.11.

2.13.2 Pathway of Analysis

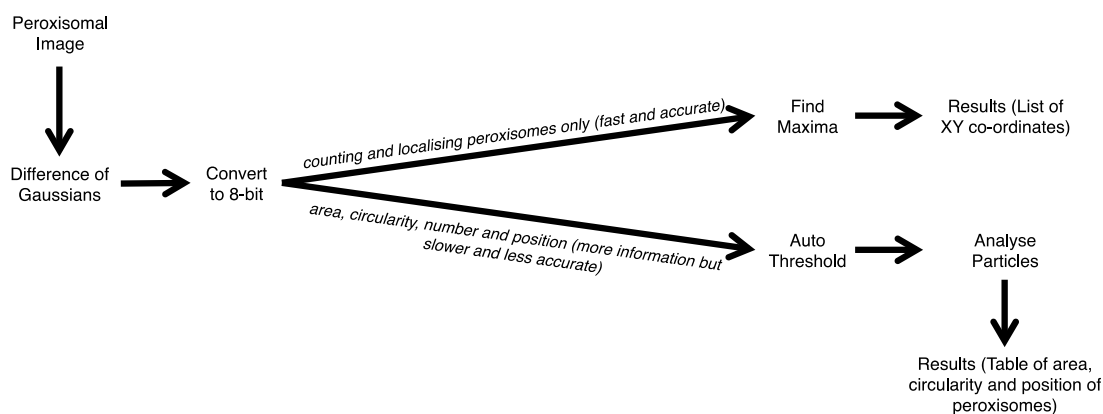


Figure 2.11. Peroxisomal image processing pathway. Peroxisomal image data is subjected to a difference of Gaussians filter, and converted to 8-bit images. At this point, if only number and position of peroxisomes is required, a maxima-finding algorithm can be used to obtain the XY co-ordinates of the peroxisomes from the image. If more information is desired, the images can be thresholded and the ‘Analyze Particles’ command can be utilised to obtain information such as the area, circularity, position and number of peroxisomes. The downside of this is that it is slower and less accurate for number and position than a maxima-finding algorithm. Figure 2.17 shows an example of the peroxisomal image processing from start to finish.

The main technique of enhancing peroxisomes in an image was the use of a difference of Gaussians (DoG) filter. The methodology behind a DoG filter is explored in Appendix C.3.

In FIJI, there exists no single command to perform a DoG filter. Instead, one has to duplicate an image (Image > Duplicate), before performing a Gaussian blurring (Process > Filters > Gaussian Blur) on each of the two resultant images. One image was blurred with a sigma (radius) of two, and another with a sigma of one (Figure 2.12). The more blurred image (i.e. one blurred with the sigma of two) is subtracted from the less blurred one using the image calculator function of FIJI (Process > Image Calculator), completing the DoG technique (Figure 2.13).

Example Python code used to perform the DoG filter is shown in section 2.12.3.

After a DoG filter, images are converted to 8-bit (Image > Type > 8-bit). This is explained in Appendix C.4.

After this, depending on the image quality and the desired measurements, the pathway of image analysis could diverge. If only the number and position of peroxisomes was required, then no more pre-processing was needed, and the maxima finding algorithm could be utilised on this image to 'segment' it into a series of points (Process > Find Maxima) (Figure 2.14). The theory behind the maxima finding algorithm is explored in Appendix C.5. The series of maxima was then deposited to a file by saving all the XY co-ordinates of the image (Analyze > Tools > Save XY Coordinates).

Alternatively, if the image was of a sufficient quality, or more information was desired, then the image was thresholded and then segmented using analyse particles. Thresholding an image is explained earlier (accessed via Image > Adjust > Auto Threshold); the thresholding algorithm that was determined to work the best on peroxisomal images is the Triangle

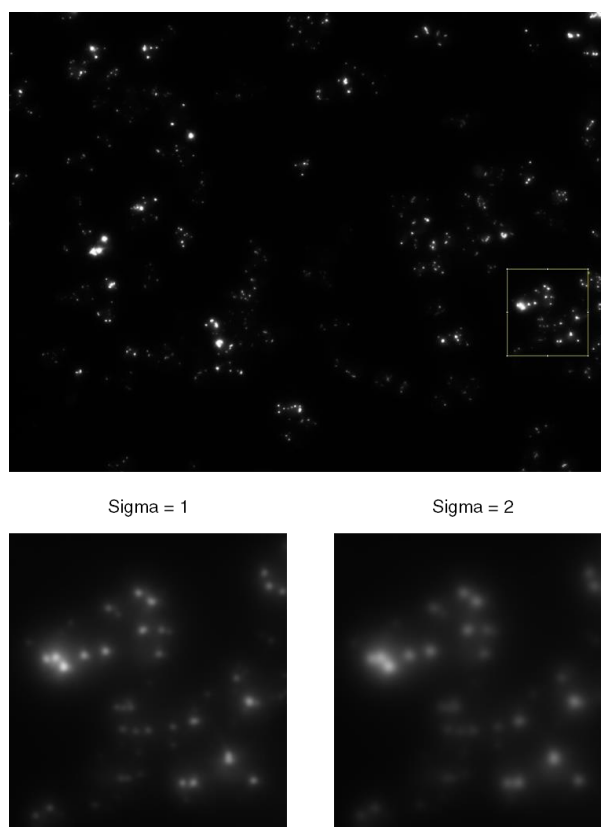


Figure 2.12. Example of a Gaussian blur. Top image is the same as the peroxisomal image from Figure 2.10. Yellow box highlights a small section of the image that is used in the bottom two panels. Left bottom image has been Gaussian blurred with a sigma of 1, and the right with a sigma of 2. One can see that the right image appears more blurred than the one on the left.

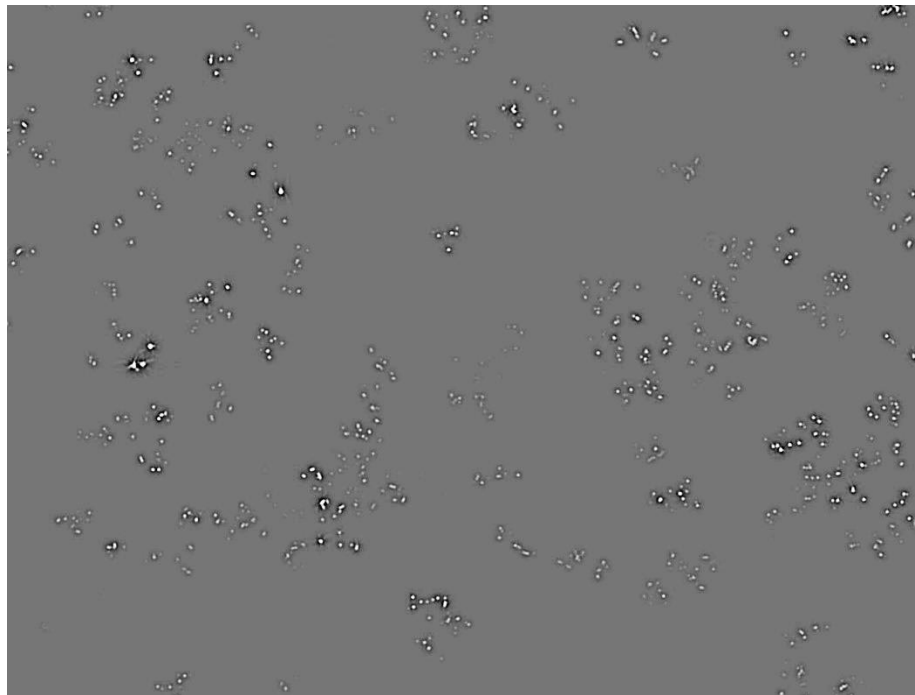


Figure 2.13. Peroxisomal channel from Figure 2.10 (left panel) after difference of Gaussians filter and conversion to 8-bit images. The maxima finder algorithm can then be used immediately on this image to get positions of the peroxisomes (Figure 2.14).

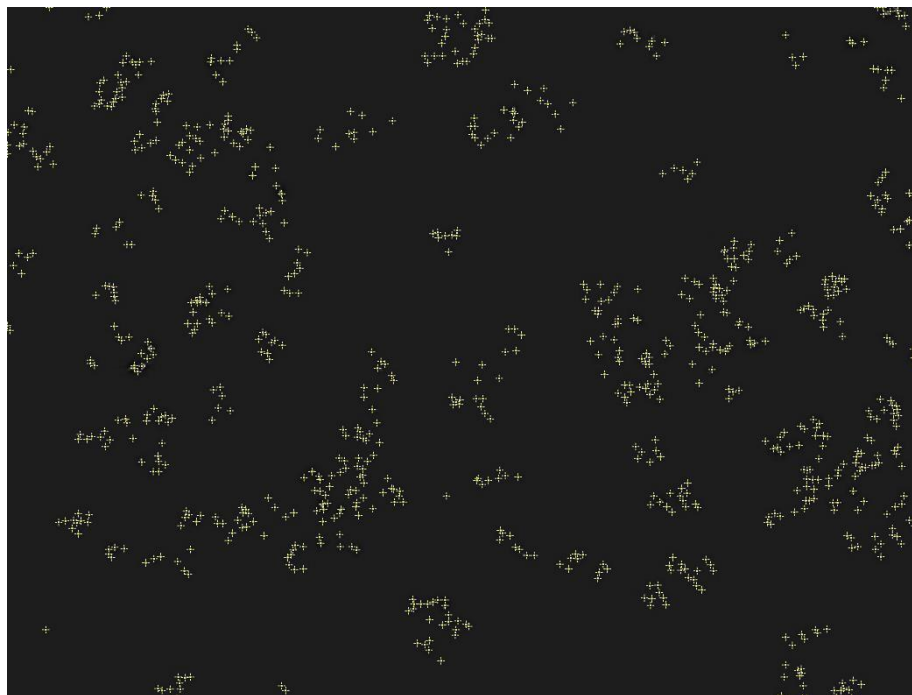


Figure 2.14. Peroxisomal image from Figure 2.13 with overlay of detected maxima. The co-ordinates of these maxima can then be extracted.

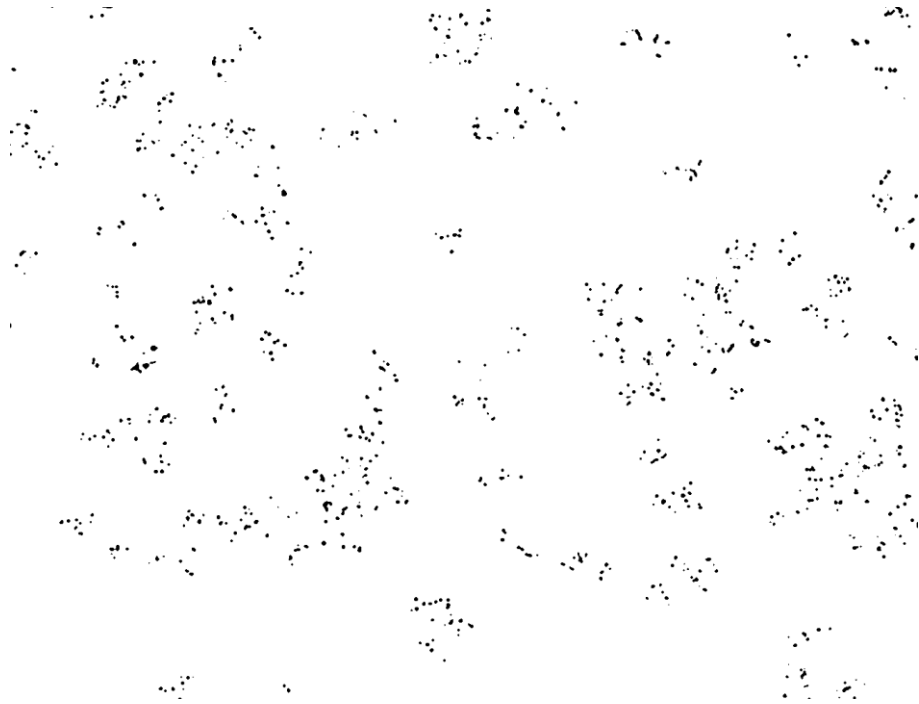


Figure 2.15. Peroxisomal image from Figure 2.13 that has been subjected to automatic thresholding (becoming a binary image). The particle analyser can then be used on this image.

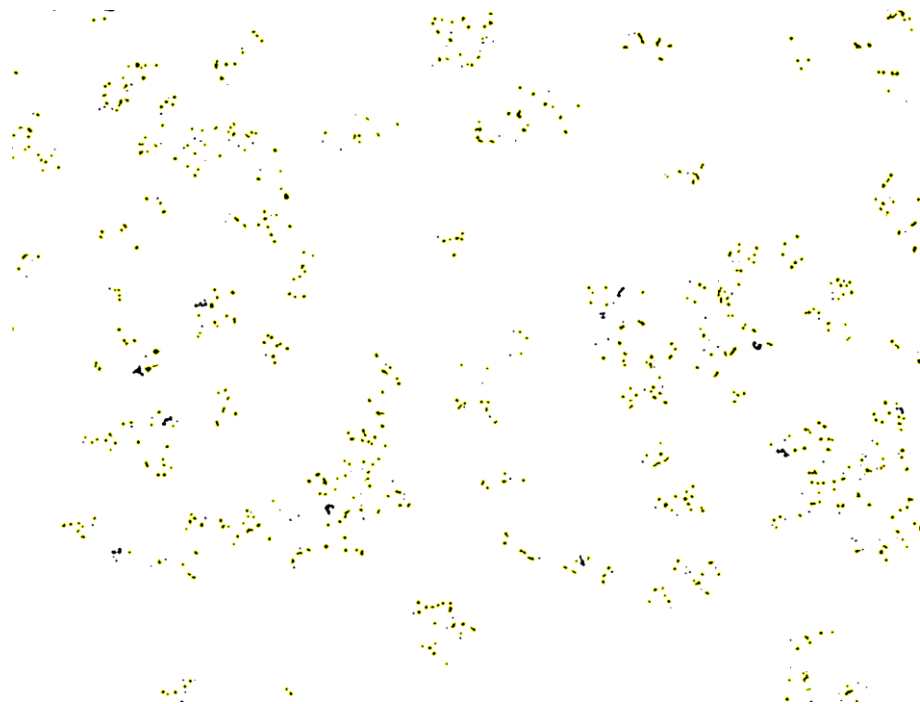


Figure 2.16. Peroxisomal image from Figure 2.15 with overlay of detected particles, as denoted by the yellow border around an object. Note how clusters of peroxisomes become one large object and are therefore erroneously detected as just one object instead of multiple – this can be seen more easily in Figure 2.17. The maxima finder method is more accurate in this regard for peroxisomal number and position.

method (Zack et al., 1977)(Figure 2.15). Particle analysis is then performed on the image to segment it (Analyze > Analyze Particles). The particle analyser tool looks for objects in an image that satisfy both user defined size (area) and circularity criteria. As peroxisomes are small, values of between 10-100 pixels² for area and a circularity of between 0.5 – 1 (where 1 is a perfect circle) are used (Figure 2.16). This generates a list of ‘Regions of Interest’ (ROIs). The properties of each ROI are recorded in a table. The measurements that the particle analyser gathers are pre-set via the ‘Measurements’ command in FIJI (Analyze > Set Measurements). The area, circularity and position of each peroxisome was recorded in this manner. To acquire the intensity data of each peroxisome (which is not possible on this binary image), the ROIs in the results table can be used to refer to those regions on the original (un-processed) image, and intensity values (mean, maximum, and minimum) can be gathered.

The result of this processing is either a list of XY co-ordinates of all the peroxisomes in an image, or a more extensive table containing information regarding a peroxisome’s area, circularity and position. Figure 2.17 gives an example of this entire image processing procedure for isolating peroxisomes on a section of Figure 2.9 containing a few cells.

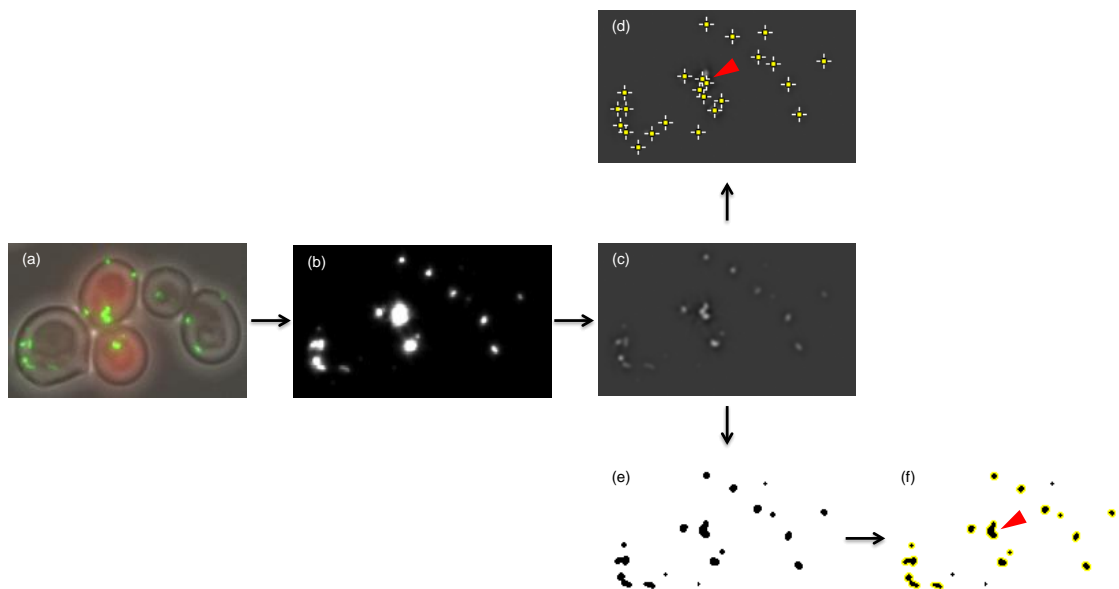


Figure 2.17. Section of Figure 2.9 showing peroxisomal image processing starting from the raw image data. (a) Raw image. (b) Peroxisomal channel has been extracted and subtract background and Z-projection steps have been performed (Figure 2.10, left). (c) Image after a DoG filter (Figure 2.13). Processing can subsequently diverge to (d) or (e) and (f). (d) DoG image with overlay of detected maxima (Figure 2.14). (e) DoG image after automated thresholding (Figure 2.15). (f) Thresholded image from (e) with overlay of detected particles from the particle analyser, as denoted by the yellow border around an object (Figure 2.16). Compare (d) and (f) and note how clusters of peroxisomes become one object with the particle analyser method but are separate objects using the maxima finder method (red arrows). The maxima finder method therefore is more accurate for determining peroxisomal number and position.

2.13.3 Python Code for Peroxisomal Analysis

Below is the Python code written for this purpose that can be executed in FIJI that performs the processing steps from background subtraction through to saving the XY co-ordinates in the maxima finding method, followed by the particle analyser method (which is the same up to the 'Find Maxima' line). Comments in green explain each line. The whole program is shown in Appendix D.2.

```
def PEROXISOME_ANALYSIS (ImageTitle, which_channel, directory): # MAXIMA FINDER METHOD

    imp_perox1 = IJ.selectWindow(ImageTitle+" - C=%d"%(which_channel))

    IJ.run(imp_perox1, "Subtract Background...", "rolling=1 sliding stack") # Subtract Background command, with radius of rolling
    # paraboloid of 1, for every image in Z stack
    IJ.run(imp_perox1, "Z Project...", "projection=[Sum Slices] copy") # Z projection, sum slices method

    SUM_image = str("SUM_"+ImageTitle+" - C=%d"%(which_channel))

    imp_perox1 = IJ.selectWindow(SUM_image) #<-----
    imp_perox2 = IJ.run("Duplicate...", " ") # |
    # |
    imp_perox1 = IJ.selectWindow(SUM_image) # |
    IJ.run(imp_perox1, "Gaussian Blur...", "sigma=1") # |
    # |
    imp_perox2 = IJ.selectWindow(SUM_image+"-1") # |
    IJ.run(imp_perox2, "Gaussian Blur...", "sigma=2") # |-----> Difference of Gaussians filter
    # |
    # |
    ic = ImageCalculator() # |
    imp1 = WindowManager.getImage(SUM_image) # |
    imp2 = WindowManager.getImage(SUM_image+"-1") # |
    imp3 = ic.run("Subtract", imp1, imp2) #<-----

    imp3 = IJ.selectWindow(SUM_image)

    IJ.run(imp3, "8-bit", "") # Conversion to 8-bit image
    IJ.run(imp3, "Find Maxima...", "noise=3 output=[Single Points]") # Maxima finder, noise tolerance of 3, output as
    # single points in centre of maxima

    IJ.selectWindow(SUM_image)
    IJ.run("Close", "")

    imp4 = IJ.selectWindow(SUM_image+" Maxima")

    if not os.path.exists(str(str(directory)+"/Results/")):
        os.makedirs(str(str(directory)+"/Results/"))

    perox_file =
    os.path.normpath(str(str(directory)+"/Results/"+str(ImageTitle).strip()+str(which_channel)+'perox_co_ords_results'+'.txt'))

    IJ.run(imp4, "Save XY Coordinates...", "background=0 invert suppress save=[%s]" %(perox_file)) # Save XY co-ords of picked
    # maxima, 0 is background value (so everything that is 255 is saved, normally Y is inverted unless invert is a flag, suppress means suppress
    # dialog box

    IJ.selectWindow(SUM_image+" Maxima")
    IJ.run("Close", "")

def PEROXISOME_ANALYSIS (ImageTitle): # ANALYSE PARTICLES METHOD

    imp_perox = IJ.openImage (ImageTitle)

    IT = ImageTitle.split('\\')[-1]

    IJ.run(imp_perox, "Subtract Background...", "rolling=3 sliding")
    IJ.run(imp_perox, "Gaussian Blur...", "sigma=1");
    IJ.run(imp_perox, "8-bit", "")
    IJ.run(imp_perox, "Auto Threshold", "method=Triangle white") # Auto Threshold using the Triangle method. White means white objects
    # on a black background

    table1 = ResultsTable() # Generate a new results table
    roiM1 = RoiManager (True)
    ParticleAnalyzer.setRoiManager (roiM1) # This is the table that the results will be stored in

    pa = ParticleAnalyzer (ParticleAnalyzer.ADD_TO_MANAGER+ParticleAnalyzer.EXCLUDE_EDGE_PARTICLES,
    Measurements.AREA+Measurements.CENTER_OF_MASS+Measurements.SHAPE_DESCRIPTOR, table1, 20, 1000, 0.00, 1.0) # Sets parameters for
    # particle analyser, excluding objects on the edge. Measurements taken are area, XY centre, and shape descriptors (of which circularity is
    # one)
    pa.setHideOutputImage (True)
    pa.analyze (imp_perox) # Call particle analyser for image
```

2.14 Analysing Cell Data

2.14.1 Introduction

Automated image analysis of cells required a completely different workflow to that of peroxisomes. Images of cells were acquired using either standard bright-field imaging or by imaging an untargeted fluorescent protein which was dispersed in the cytosol. As mNeonGreen was the fluorescent protein of choice for visualising peroxisomes, the fluorescent proteins used for this cytosolic labelling therefore had to be a different colour. mCherry and mRuby2, both red fluorescent proteins, were utilised for this purpose.

The reasoning behind using a fluorescent protein as a cytosolic label is that *S. cerevisiae* cells do not give very good contrast in normal bright-field imaging. Although this is adequate to identify which cell is which by eye, automated analysis of these images proved problematic as the contrast was too poor to segment the cells correctly. Using a fluorescent protein, the contrast between what is 'cell' and what is background is much clearer, and automated segmentation of cells was much more accurate.

Automated segmentation of cells with cytosolic labelling was straightforward, and required thresholding of the image followed by segmentation using the particle analyser. However, the thresholding occasionally required some correction depending on the data. The workflow of processing these images is shown in Figure 2.18.

2.14.2 Pathway of Analysis

First, the images of the cells were converted to 8-bit images. This was necessary for performing the automatic thresholding. The images of the cells are then thresholded on a local level using the 'Auto Local Threshold' command (Image > Adjust > Auto Local Threshold) (Figure 2.19, top left panel). An explanation of this command is outlined in Appendix C.6. This creates a binary image.

Images are then inverted (Edit > Invert) (Figure 2.19, top right panel). In a binary image, this just swaps white and black around. This is required as the Auto Local Threshold command segments objects in the foreground of the image as white. However, the particle analyser only detects objects in the black section of the image.

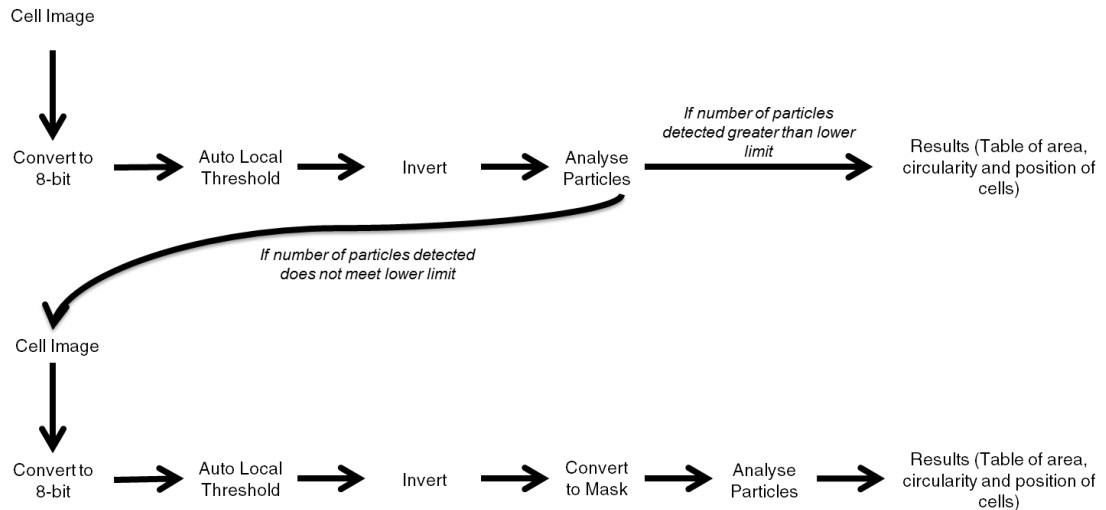


Figure 2.18. Cell image processing pathway. Images of cells are first converted to 8-bit images before being subjected to an automated local thresholding (which is different to normal thresholding, see text), before conversion to mask. Then the particle analyser is called to segment the image into features and extract the measurements (area, position and circularity). If the particle analyser does not detect a certain number of cells, then the program is instructed to discard those measurements and instead return to the original image. The pre-processing then follows the same steps prior to calling the particle analyser, but with the addition of convert to mask, which was found to give rise to correct segmentation of the image. These stages and terms will be explained in the text. Figure 2.20 shows an example of the cell image processing from start to finish.

The particle analyser then is called (*Analyze > Analyze Particles*) to segment the image and extract the measurements (Figure 2.19, bottom panel). This also functions as a checkpoint for this image processing. It was noticed that occasionally the ‘Auto Local Threshold’ algorithm segmented the image with the cells as background (when they should be the foreground). This checkpoint functions by comparing the number of features actually detected by the particle analyser versus a user-defined reasonable estimate of the number of features that were expected to be found. This reasonable estimate is a very conservative lower bound of the number of cells that should be found by the particle analyser in an image, and exists purely to instruct the program to repeat the pre-processing with an additional step. For example, for an image that probably contained 30 or so cells, this lower bound would be set at 10. The reason that this number is not zero is that when the particle analyser was called on this incorrectly segmented image, it would still locate some objects but they would clearly not be cells.

If the number of features detected did not meet the minimum limit, then the measurements were discarded and the processing returned to the original image. The second round of pre-processing was the same until just before the ‘Analyze Particles’ step. Before this, the image was converted to mask to correct for the incorrect thresholding

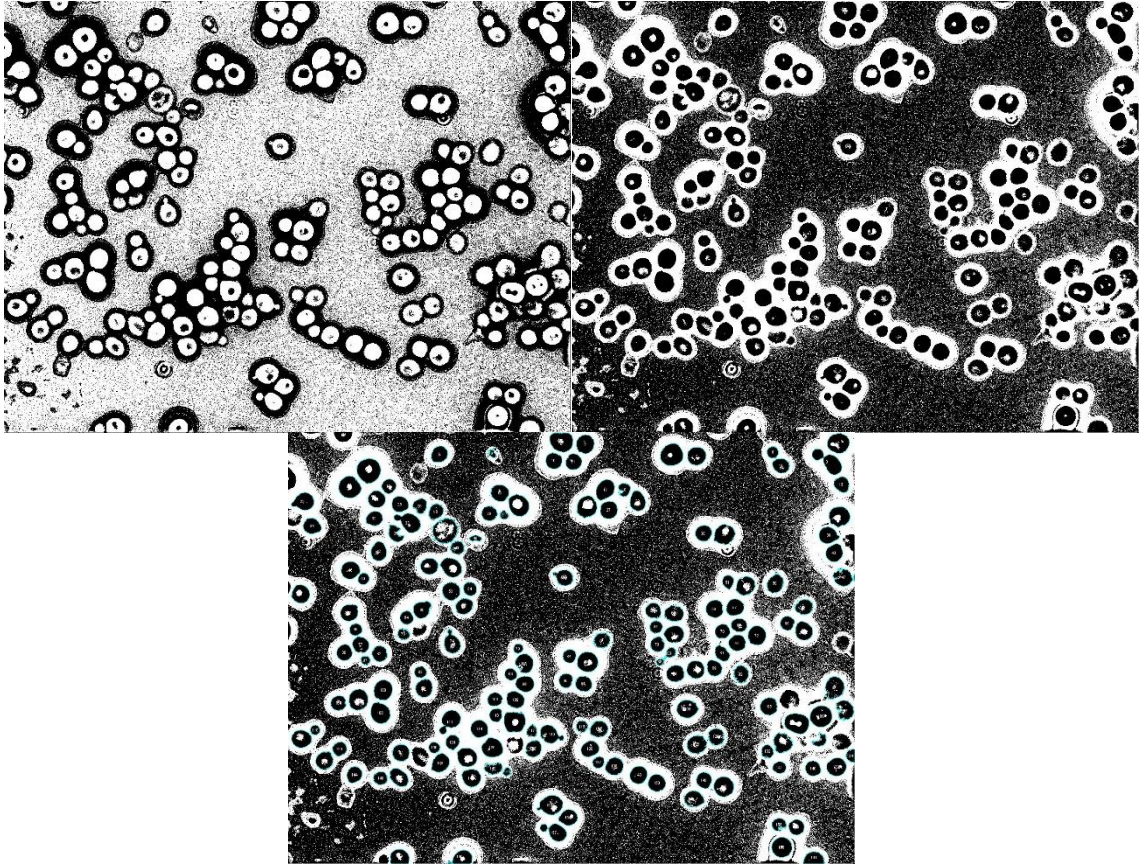


Figure 2.19. Processing of cell images. Top left) Resultant binary image after Auto Local Threshold method, 'Mean' algorithm with radius 10, is applied to cell image from Figure 2.10. Top right) Left image after inversion. Bottom) Image from top right with an overlay of detected particles, as denoted by the blue outline surrounding the object.

(Process > Binary > Convert to Mask). This normally converted an image to binary. However, in an image that is already binary it inverts the values of each pixel. This gave rise to a correctly segmented image.

As when segmenting the peroxisomal images, the Analyze Particles command is given an area and circularity of objects to look for. The area and circularity specified are different as cells are clearly larger than peroxisomes but are also generally less akin to a circle and more ovoid in shape (so a lower restriction on the minimum circularity is set).

The end point of this processing is a results table of ROIs with area, position and circularity measurements. Figure 2.20 gives an example of this entire image processing procedure for processing and segmenting cells on a section of Figure 2.9 containing only a few cells.

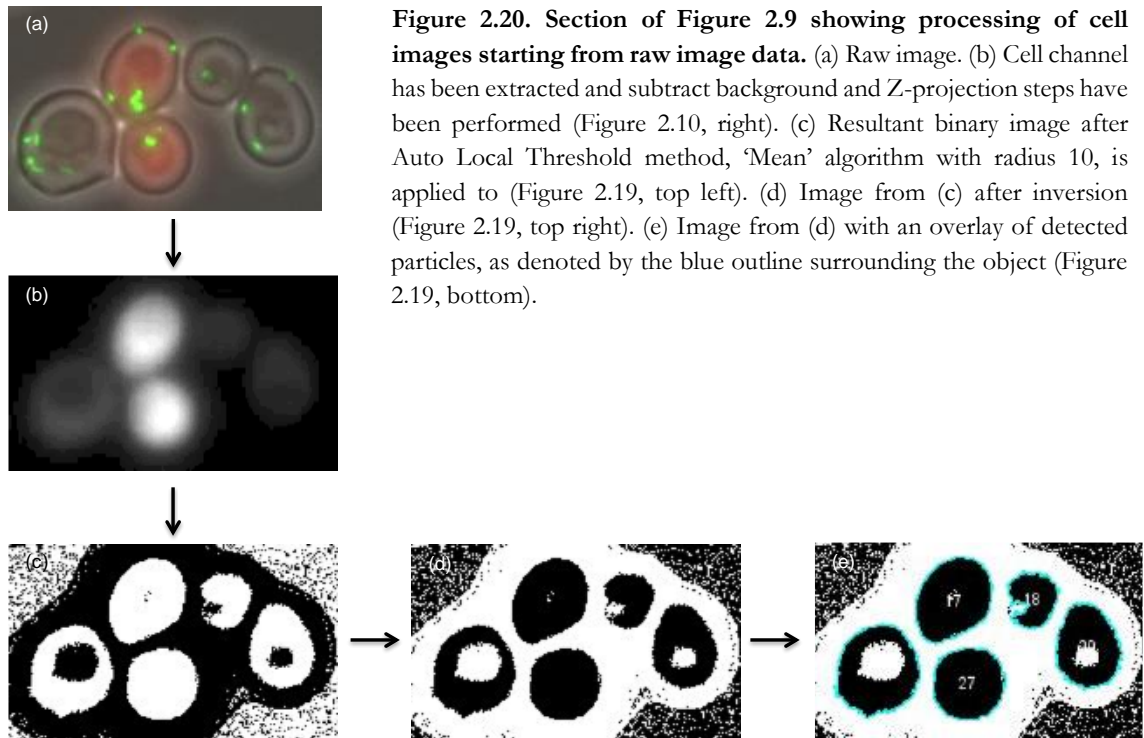


Figure 2.20. Section of Figure 2.9 showing processing of cell images starting from raw image data. (a) Raw image. (b) Cell channel has been extracted and subtract background and Z-projection steps have been performed (Figure 2.10, right). (c) Resultant binary image after Auto Local Threshold method, ‘Mean’ algorithm with radius 10, is applied to (Figure 2.19, top left). (d) Image from (c) after inversion (Figure 2.19, top right). (e) Image from (d) with an overlay of detected particles, as denoted by the blue outline surrounding the object (Figure 2.19, bottom).

2.14.3 Python Code for Cell Image Analysis

Below is the Python code written for this purpose that can be executed in FIJI that performs the processing steps from background subtraction through to calling the particle analyser. Comments in green explain each line. The whole program is shown in Appendix D.2.

```
def@CYTOPLASMIC_PROCESSING(run,ImageTitle,which_channel):@
@
@IJ.run(imp_cyto,@"Subtract@Background...",@"rolling=50@sliding@stack")@#####Subtract@Background@command,@with@radius@of@rolling@
paraboliod@of@50,@for@every@image@in@Z@stack@
#####
@imp_cyto=@IJ.selectWindow(ImageTitle+"-@C=@d"%@which_channel))@
@IJ.selectWindow(ImageTitle+"-@C=@d"%@which_channel))@
#####
@IJ.run(imp_cyto,@"Z@Project...",@"projection=[Sum@Slices]@copy")@#####Z@project,@sum@slices@method@
@SUM_image=@Sstr("SUM_"+ImageTitle+"-@C=@d"%@which_channel))@
#####
@imp_cyto=@WindowManager.getImage(SUM_image)@
@IJ.run(imp_cyto,@"8-bit",@"")@#####Conversion@to@8-bit@
@IJ.run(imp_cyto,@"Auto@Local@Threshold",@"method=Mean@radius=10@parameter_1=0@parameter_2=0@white")@#####If@image@doesn't@segregate@well,@consider@
changing@the@radius@
@IJ.run(imp_cyto,@"Invert",@"")@#####Inversion@of@image@
@
@if@run@in@[2]:@#####2nd@attempt@converts@to@mask@and@solves@
problem@of@strange@thresholding@
#####IJ.run(imp_cyto,@"Convert@to@Mask",@"")@
@
@table1=@ResultsTable()@#####Generate@a@new@results@table@
@roim1=@RoiManager(True)@#####This@is@the@table@that@the@results@will@be@
stored@in@
#####ParticleAnalyzer.setRoiManager(roim1)#####
@pa=@ParticleAnalyzer(ParticleAnalyzer.ADD_TO_MANAGER+ParticleAnalyzer.EXCLUDE_EDGE_PARTICLES,@Measurements.AREA+Measurements.CENTER_OF_MASS,@
table1,@500.@00,@10000.@00,@0.35,@1.0)@#####Set@parameters@for@particle@analyser.@Measurements@are@area@and@XY@centre.@
@pa.setHideOutputImage(True)@
#####
@imp_cyto_max=@WindowManager.getImage(SUM_image)@
@pa.analyze(imp_cyto_max)@#####Call@particle@analyser@on@selected@image@
```

Chapter 3: Re-evaluation of Vesicle Fusion Model of Peroxisome Biogenesis in *S. cerevisiae*

3.1 Introduction

This chapter will address the vesicle fusion model as proposed by van der Zand et al., 2012 using the techniques of live-cell imaging and image analysis as outlined in Chapters 2.9-2.14. The vesicle fusion model is first described in Chapter 1.3.4 alongside the maturation model it evolved from (van der Zand et al., 2010), and the more longstanding growth and division model (Hettema and Motley, 2009; Motley and Hettema, 2007; Nuttall et al., 2011). The claims made by the vesicle fusion model will be evaluated in contrast to those made by the growth and division model. The two models will be explained in a little more detail in this introductory section, and in the subsequent sections (3.2-3.4) the discrepancies between the two models will be addressed.

The first and more established theory in the literature is that peroxisomes proliferate principally by growth and division of pre-existing peroxisomes (Motley and Hettema, 2007). The ER provides membrane lipids and a subset of peroxisomal membrane proteins (Pex3 and Pex22) via vesicles that bud from the ER and fuse with pre-existing peroxisomes (Figure 1.4). All other PMPs are inserted directly into the membrane (see Chapter 1.3.1) and all matrix proteins are imported from the cytosol via the action of Pex5 and Pex7, which are recycled from the peroxisomal membrane by the AAA+ ATPases Pex1 and Pex6 (see Chapter 1.3.2). The dynamin-related proteins (DRPs) Dnm1 and Vps1 perform fission on mature peroxisomes. Importantly, peroxisomes only form *de novo* from the ER when there are no peroxisomes present in the cell. In the absence of pre-existing peroxisomes, the vesicles that bud off from the ER mature slowly into peroxisomes.

Contrasting with this growth and division model is the vesicle fusion model (van der Zand et al., 2012)(Figure 3.1). In this model, all peroxisomal membrane proteins insert first into the ER (Figure 3.1(a)). These sort into two distinct groups of proteins: one containing the RING finger complex proteins (Pex2/10/12) and Pex11; the other containing members of the docking complex (Pex13/14/17). These bud off in separate vesicles from the ER (Figure

3.1(b)). These vesicles undergo heterotypic fusion via Pex1 and Pex6 (Figure 3.1(c)). Notably, the fusion of these heterotypic vesicles is posited to take place under both the re-introduction of peroxisomes in cells that are lacking them and in the presence of pre-existing peroxisomes (Tabak et al., 2013; van der Zand et al., 2012; van der Zand and Tabak, 2013); consequently the *de novo* synthesis of peroxisomes is always occurring under normal conditions. The peroxisomal structure post-heterotypic fusion has a fully functioning importomer complex, and can therefore import peroxisomal matrix proteins from the cytosol. DRPs Dnm1 and Vps1 act to perform fission after this heterotypic fusion but before the peroxisomal structure has matured fully into a peroxisome (Figure 3.1d)(Tabak et al., 2013; van der Zand et al., 2012; van der Zand and Tabak, 2013).

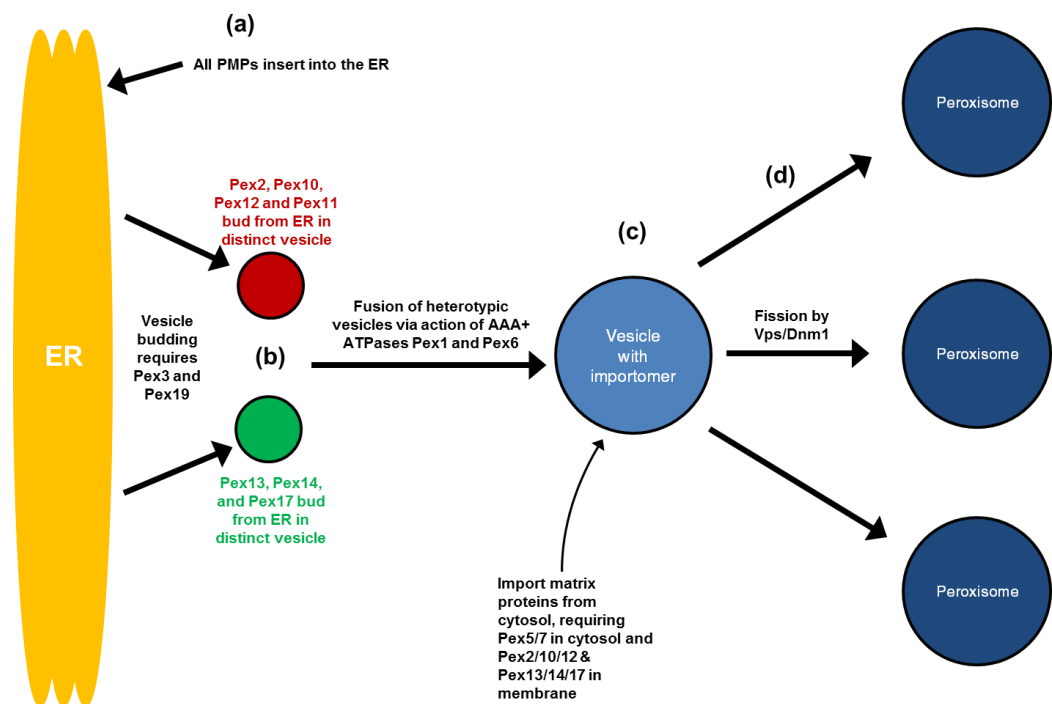


Figure 3.1 Vesicle fusion model of peroxisome biogenesis. (a) All peroxisomal membrane proteins first insert into the ER. (b) These PMPs are sorted into distinct vesicles containing either RING finger proteins Pex2/Pex10/Pex12 and Pex11 or docking complex of Pex13/Pex14/Pex17 and bud off from the ER, requiring Pex3 and Pex19. (c) Heterotypic fusion between vesicles occurs requiring the activity of AAA+ ATPases Pex1 and Pex6, forming a vesicle with a fully functioning importomer complex, meaning it can import matrix proteins from the cytosol. (d) Fission by Vps1 and Dnm1 occurs after the Pex1 and Pex6 mediated vesicle fusion event. This figure is a more detailed version of Figure 1.6.

Clearly there are several differences between the two models, of which three in particular are addressed in this chapter. These are summarised in Table 3.1. Investigating the apparent disparity between the two models is performed by evaluation of the methods and conclusions in van der Zand et al., 2012 using live-cell imaging and image quantification. All of the research forming this investigation is contained within Motley et al., 2015 (see Appendix F).

Table 3.1. Key contrasting points between the growth and division model and the vesicle fusion model.

Process	Growth and Division Model	Vesicle Fusion Model
Role of Pex1 and Pex6	To recycle Pex5 from the peroxisomal membrane only	Perform heterotypic fusion of vesicles containing Pex2, Pex10, Pex11 and Pex12 with vesicles containing Pex13, Pex14, and Pex17
Fission by Vps1 and Dnm1	Mature peroxisomes only undergo fission	Fission occurs on pre-peroxisomes that have not yet imported matrix proteins from the cytosol
De novo synthesis of peroxisomes	De novo synthesis of peroxisomes only occurs in absence of pre-existing peroxisomes	De novo synthesis of peroxisomes occurs continuously even in presence of pre-existing peroxisomes

3.2 Re-evaluation of the Role of Pex1 and Pex6 in Peroxisome Biogenesis

According to the vesicle fusion model, Pex1 and Pex6 are required for the fusion of the heterotypic vesicles after they leave the ER (van der Zand et al., 2012). A majority of the evidence in the literature instead points to the functions of Pex1 and Pex6 as being involved in the recycling of Pex5 from the membrane (see Figure 1.3 for reminder).

The role of Pex1 and Pex6 in peroxisome biogenesis was investigated by comparing the extent to which the colocalisation of Pex11 and Pex13 - two PMPs that are reputedly in different ER-derived vesicles according to the vesicle fusion model (Figure 3.1b) - was altered in *pex1*, *pex6* and *pex1/6* mutant backgrounds when compared with WT cells. The experiment and expected results are summarised in Table 3.2 below.

Table 3.2. Proposed role of Pex1 and Pex6 in vesicle fusion model, how this was tested, and the results expected in line with either the vesicle fusion or growth and division model.

Proposed Role of Pex1 and Pex6 in Vesicle Fusion Model	Experiment	Result Expected in line with Vesicle Fusion Model	Result Expected in line with Growth and Division Model
Perform heterotypic fusion of vesicles containing Pex2, Pex10, Pex11 and Pex12 with vesicles containing Pex13, Pex14, and Pex17.	Evaluate to what extent vesicle fusion is disrupted by absence of Pex1, Pex6 or Pex1 and Pex6 by measuring the colocalisation of Pex11-mRFP and Pex13-GFP using computerised image analysis.	Significant difference should be observed in colocalisation of Pex11-mRFP and Pex13-GFP between WT cells and knock-out mutants of <i>pex1</i> , <i>pex6</i> and <i>pex1/6</i> .	No significant difference should be observed in colocalisation of Pex11-mRFP and Pex13-GFP between WT and knock-out mutants.

Images were acquired using a 100x magnification lens in single slices in both red and green channels (Figure 3.2). These images were analysed using a program written in Python code for FIJI which is included in Appendix D.1. This program measured the distances between each Pex11-mRFP spot and its nearest neighbouring Pex13-GFP spot.

The results of the computational image analysis are displayed as the box plot in Figure 3.3. The median distance between the centres of fluorescent spots of Pex11-mRFP and the nearest neighbouring Pex13-GFP are 160, 113, 113, and 160 nm in WT, *pex1*, *pex6*, and *pex1/pex6* backgrounds respectively. This is below the minimum resolution of the

microscope setup that was used (i.e. less than the minimum distance required for two objects to be resolved separately) of ~180nm (see Appendix E for explanation of resolution limits). If, as the vesicle fusion model states, Pex1 and Pex6 were involved in the process of localising Pex11 and Pex13 to the same compartment, then one would expect to see a discernible difference in colocalisation between the WT and the mutants. No such difference can be seen and therefore this evidence points to Pex1 and Pex6 not being involved in this process.

This, alongside evidence from several different studies showing that matrix protein import, but not PMP import was affected in the absence of Pex1, further supported the current evidence that Pex1 and Pex6 are factors involved in the import of matrix proteins (Debelyy et al., 2011; Miyata and Fujiki, 2005; Miyata et al., 2012; Platta et al., 2004, 2005). Further evidence is provided in Motley et al., 2015, whereby Pex11-mRFP and Pex13-GFP are shown to colocalise over the extent of elongated peroxisomes in *vps1/dnm1/pex1/atg36* mutant cells, and galactose- inducible Pex11-GFP is shown to localise with pre-existing Pex13-mCherry in mutant *pex1/pex6* cells. Altogether, this evidence points to Pex1 and Pex6 being involved in the import of matrix proteins and not in the fusion of heterotypic ER-derived vesicles as predicted in the vesicle fusion model.

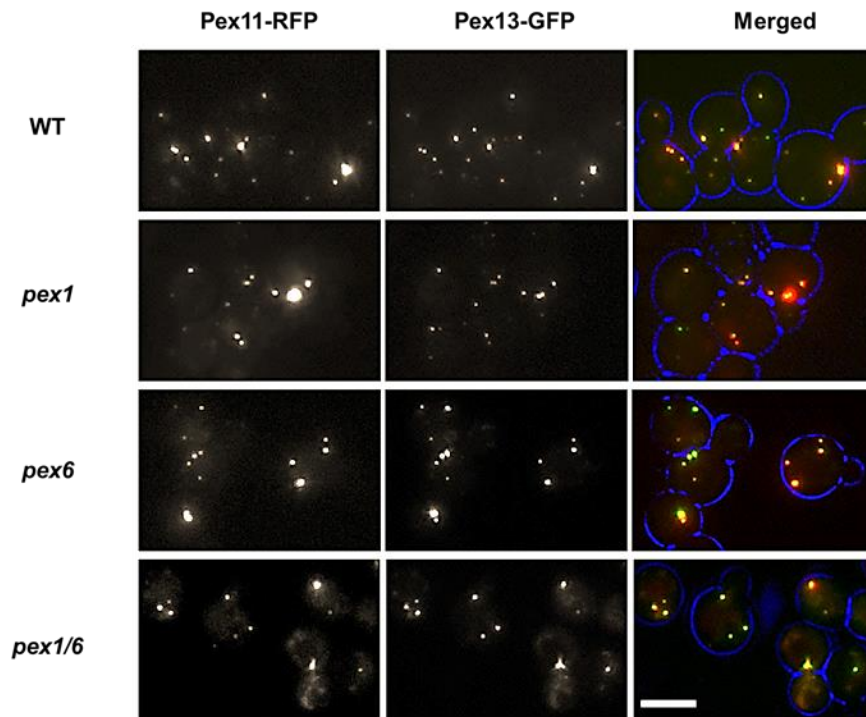


Figure 3.2. Colocalisation of Pex11 and Pex13 in *WT*, *pex1*, *pex6* and *pex1/pex6* cells. These cells are expressing Pex11-RFP and Pex13-GFP from endogenous promoters on plasmids. Imaging was performed after 3 hours growth in logarithmic phase. Images are single slices. Scale bar indicates 5 μm . (Figure 6A from Motley et al., 2015)

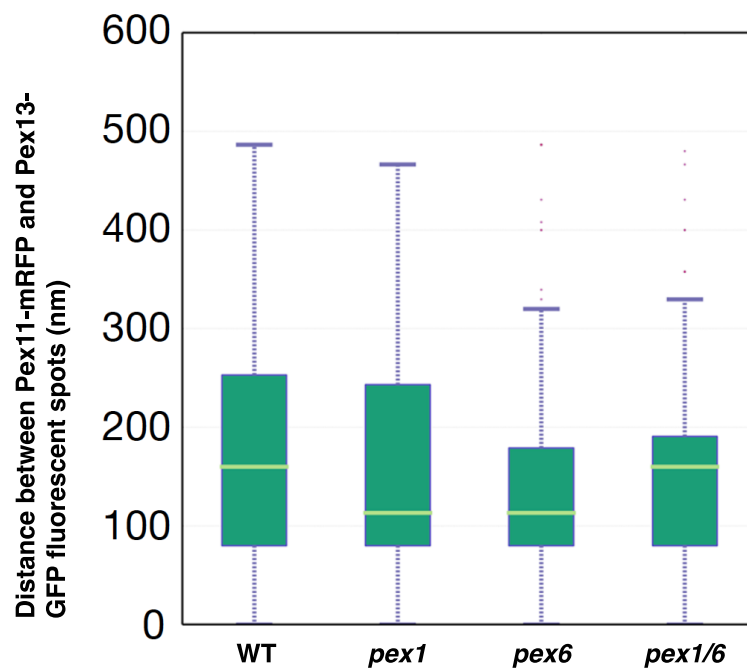


Figure 3.3. Box plot representing the measured distances between the centre of each fluorescent Pex11-RFP and the nearest neighbouring Pex13-GFP spot for each of the strains. The pale green line across each box indicates the median. Whisker length is 1.5 interquartile ranges (IQR) outside of Q1 and Q3 (i.e. $Q1 - 1.5IQR$ and $Q3 + 1.5IQR$); dots are outliers that do not fit in that range. Number of distances plotted was 259, 88, 90, 180 for WT, *pex1*, *pex6* and *pex1/6* respectively. Figure produced using matplotlib 2D plotting library for Python 2.7. (Figure 6B from Motley et al., 2015).

3.3 Fission of Peroxisomes in Absence of Dynamin-Related Proteins Vps1 and Dnm1

According to the vesicle fusion model, the DRPs Vps1 and Dnm1 perform fission on pre-peroxisomal vesicles to give rise to multiple mature peroxisomes (van der Zand et al., 2012)(Figure 3.1c). In the growth and division model, Vps1 and Dnm1 perform fission on mature peroxisomes only (Motley and Hettema, 2007).

Previous observations of *vps1/dnm1* mutants show that most cells only contain a single, enlarged peroxisome (Motley and Hettema, 2007). As the vesicle fusion model states that the synthesis of peroxisomes is occurring continuously it is difficult to explain this observation unless only one enlarged peroxisome per cell is formed that does not segregate to daughter cells in the absence of DRPs (this scenario is outlined in Figure 3.4). By forcing *vps1/dnm1* mutant cells that lack peroxisomes to make them *de novo*, this could be investigated. The experiment and expected results are summarised in Table 3.3.

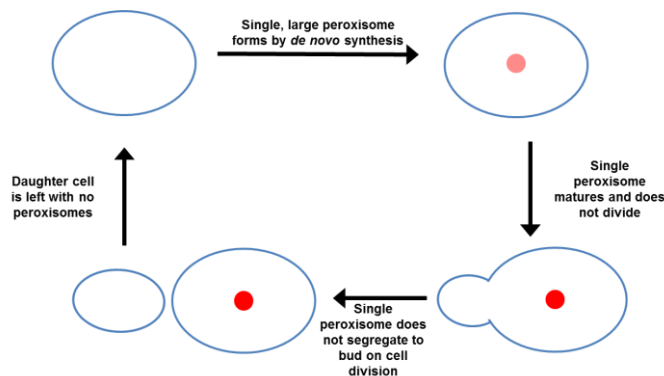


Figure 3.4. Possible course of events of *de novo* synthesis in *vps1/dnm1* cells according to the vesicle fusion model. Cells devoid of peroxisomes (top left) form a single large peroxisome by *de novo* synthesis, which subsequently does not divide or segregate to daughter cells upon cytokinesis, leaving them without any peroxisomes.

Table 3.3. Role of Vps1 and Dnm1 in peroxisomal fission in the vesicle fusion model, how this was tested, and the results expected in line with either the vesicle fusion or growth and division model.

Proposal in Vesicle Fusion Model regarding fission of peroxisomes	Experiment	Result expected in line with Vesicle Fusion Model	Result expected in line with Growth and Division Model
Fission occurs via action of Vps1 and Dnm1 on pre-peroxisomes to give rise to multiple mature peroxisomes.	Use time-lapse live-cell imaging to investigate the number of peroxisomes formed by <i>de novo</i> synthesis in <i>vps1/dnm1</i> mutant cells lacking pre-existing peroxisomes by using a conditional Pex19 promoter.	Only one large peroxisome per cell will form by <i>de novo</i> synthesis that does not divide or segregate to daughter cells upon cytokinesis (as Figure 3.4).	Multiple peroxisomes will initially form by <i>de novo</i> synthesis that will segregate out over several cell divisions eventually resulting in one large peroxisome per cell.

Mutant *pex19* cells are devoid of peroxisomes and peroxisomal membranes (see Chapter 1.3.1). By swapping the PEX19 promoter with the GAL1 promoter, the expression of the Pex19 protein can be made conditional. A *vps1/dnm1* mutant strain was produced with its Pex19 expression under control of the galactose promoter. In the absence of galactose the promoter is inactive and therefore cells lack peroxisomes.

These *vps1/dnm1* cells with conditional Pex19 expression were transformed with a plasmid expressing HcRed-PTS1 (via one-step transformation, see Chapter 2.7.3). These cells were grown on raffinose prior to switching cells to galactose, as growth on raffinose does not actively suppress the GAL1 promoter unlike growth on glucose. This reduces the time one must wait to see results of the expression from the GAL1 promoter.

The cells were grown on raffinose to exponential phase prior to switching to galactose medium and loaded into the flow cell for live-cell imaging (see Chapter 2.9.4). As the minimum length of time required to see peroxisomes form *de novo* is 3.5 hours (Hoepfner et al., 2005; Motley and Hettema, 2007; Tam et al., 2005), the imaging only commenced 4.5 hours after first exposure to galactose. Eleven slices in Z spaced 0.5µm apart were taken every 10 minutes after imaging commenced in both transmitted light (brightfield) and red fluorescence channels. Selected frames from this live-cell imaging video are displayed in Figure 3.5. Time in minutes is after commencement of imaging, not of exposure to galactose.

In the first frame shown, at 0 minutes, there are no peroxisomes (although perhaps a hint of

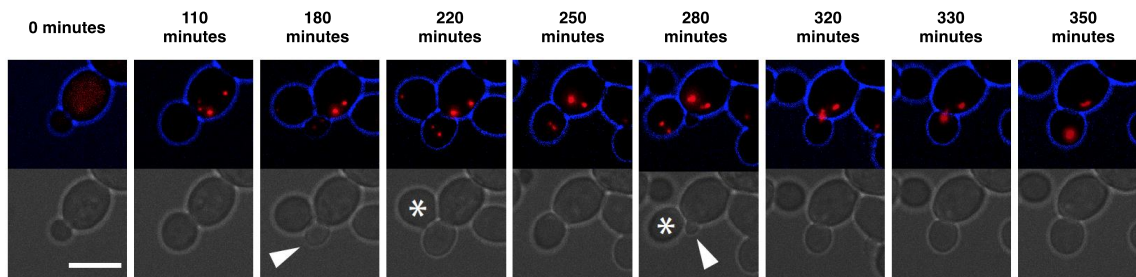


Figure 3.5. Stills of a time-lapse video of *vps1/dnm1* cells with galactose-inducible Pex19 expressing HcRed-PTS1 from a plasmid. Images were taken every 10 minutes. Top panel is red channel with cell outlines in blue; bottom panel is brightfield image. Peroxisomes that are formed *de novo* in these cells segregated upon cell division, until a single enlarged peroxisome remained. Asterisks indicate cells that move away during video capture due to the action of the flow cell. Arrows indicate where new buds are forming. Cells grown on galactose to induce expression of Pex19. Scale bar indicates 5 µm. (Figure 2C from Motley et al., 2015).

one can be seen in the 6 o'clock position of the cell), along with a haze of HcRed-PTS1 still scattered in the cytosol. According to the vesicle fusion model after this stage only one large peroxisome should form *de novo* in this cell.

Instead, as can be seen from the frame at 110 minutes, multiple peroxisomes form by *de novo* synthesis. Over several cell divisions the number of peroxisomes decreases in this mother cell and their size increases as they segregate between mother and daughter cells. In the frame at 220 minutes four peroxisomes are equally segregated between mother and bud. This leaves two peroxisomes remaining in the mother cell. By 320 minutes a new bud has formed and the remaining two peroxisomes are shared between the two cells so that by 350 minutes only one peroxisome remains in the mother cell. This lone peroxisome is split upon cytokinesis between mother and daughter (Figure 3.6).

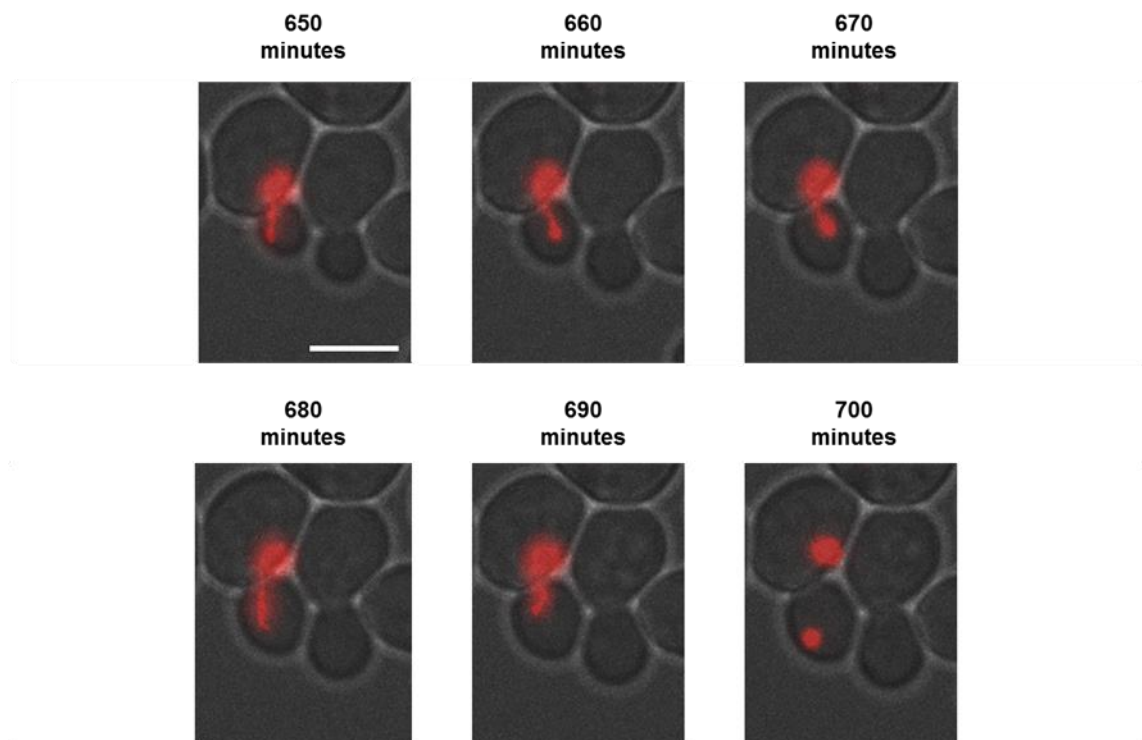


Figure 3.6. Stills of a time-lapse video of *vps1/dnm1* cells with galactose-inducible Pex19 (same as Figure 3.5) showing division of single large peroxisome upon cytokinesis. The cell containing the enlarged single peroxisome is the same cell from the previous figure. The peroxisome is pulled between mother and bud between 650-690 minutes, before splitting into two by cytokinesis at 700 minutes. Images were taken every 10 minutes. Cells expressing HcRed-PTS1 (red). Brightfield in grey. Images are maximum intensity projections. Scale bar indicates 5 μ m.

This experiment demonstrates that the single, large peroxisome seen in *vps1/dnm1* cells is not produced in that form by *de novo* synthesis as predicted by the proposals of the vesicle fusion model (see Table 3.3). Instead it resulted from the multiple peroxisomes originally present being inherited over several cell divisions, leaving the lone peroxisome per cell. The absence of DRPs does not affect the initial formation of multiple peroxisomes. This, along with that observation that after the initial set of peroxisomes is formed by *de novo* synthesis, no further *de novo* synthesis can be seen, is in line with the expectation of the growth and division model

whereby peroxisomes do not form *de novo* in the presence of pre-existing peroxisomes, and that the DRPs Vps1 and Dnm1 are involved in the fission of mature peroxisomes (Motley and Hettema, 2007).

Further evidence to support this conclusion could be performed by counting the number of peroxisomes over time per *vps1/dnm1* cell utilising image quantification techniques: this would show that the average number of peroxisomes per cell starts high but decreases over time until only one per cell remains over the course of a time-lapse live-cell imaging experiment.

3.4 Asymmetric Division of BiFC Marker and Peroxisomal Matrix Marker

In order to demonstrate that there are two distinct vesicles that bud off from the ER, van der Zand et al., 2012 used bi-molecular fluorescent complementation (BiFC) markers. The BiFC technique utilises the green fluorescent protein Venus, which is split into N and C terminal halves (VN and VC). Each half on its own is non-fluorescent, so fluorescence only occurs when the two halves are brought together. Fusing the two halves to two different proteins can be used as an indicator that the two proteins interact, or are at least present in the same compartment within the cell.

In van der Zand et al., 2012, WT haploid *S. cerevisiae* cells expressing Pex2-VN or Pex13-VN with a galactose-inducible CFP-PTS1 were grown on galactose media before switching to glucose. These cells contained a pool of peroxisomes that were pre-labelled with CFP-PTS1. These cells were then mated with cells expressing the other half of Venus fluorescent protein (Pex10-VC/Pex14-VC). All combinations of Venus fluorescent protein halves (Pex2 with Pex10/14, and Pex13 with Pex10/14) produced green fluorescent complexes. However, none of these puncta colocalised with the CFP-containing peroxisomes. The conclusion of van der Zand et al., 2012 was that any peroxisomes formed by fission during this experiment would contain CFP as they would be derived from the pool of pre-existing peroxisomes; therefore the green-only peroxisomes were part of a newly formed pool of peroxisomes that arose *de novo* after mating the cells.

This conclusion is not in line with the more long-standing growth and division model where peroxisomes do not form *de novo* in the presence of pre-existing peroxisomes (Hettema and Motley, 2009; Motley and Hettema, 2007; Nuttall et al., 2011). For Motley et al., 2015, this conclusion of van der Zand et al., 2012 was explored by first repeating their experiments before expressing the BiFC in other configurations. Initially, repeating the same mating experiments between WT strains expressing VN- and VC- tagged proteins and HcRed-PTS1 showed results in agreement with van der Zand et al., 2012, whereby some peroxisomes did not contain both green and red fluorescent proteins (Figure 9A, Motley et al., 2015).

However, the same effect was also noticed in haploid WT cells expressing both Pex2-VN and Pex14-VC halves in addition to HcRed-PTS1. These cells occasionally contained just HcRed-labelled peroxisomes (Figure 3.7). This is unusual as it has been demonstrated

previously that newly synthesised PMPs are received by pre-existing peroxisomes (Fakieh et al., 2013; Motley and Hettema, 2007). Given this, and the evidence in the previous section demonstrating a lack of *de novo* synthesis in the presence of pre-existing peroxisomes, it was hypothesised that BiFC complexes were perhaps instead not distributing equally over peroxisomes as one would expect and consequently not dividing evenly between peroxisomes upon peroxisomal fission.

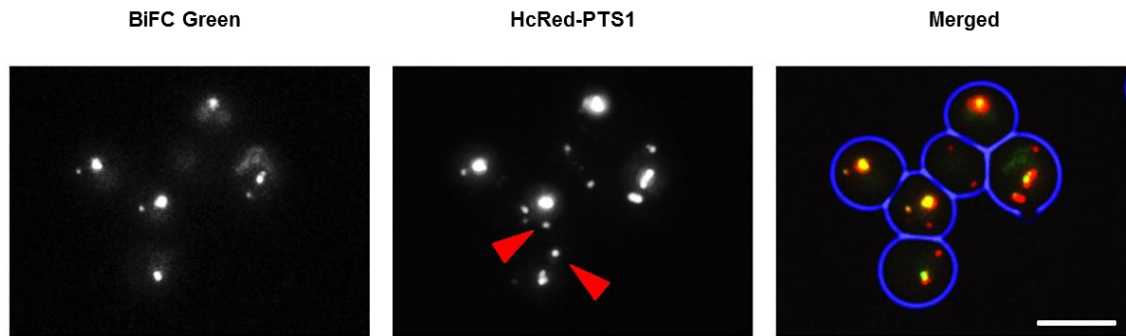


Figure 3.7. Images of haploid WT cells expressing Pex2-VN, Pex14-VC, and HcRed-PTS1 from a plasmid. Red arrowheads indicate where a peroxisome in a cell displaying both HcRed-PTS1 and Venus expression does not contain any BiFC green signal. Scale bar indicates 5 μm . (Figure 9B from Motley et al., 2015)

This was investigated utilising *vps1* cells. The peroxisomes in these cells are phenotypically similar to those in the double mutant *vps1/dnm1* cells: elongated, with generally only one per cell. If the complex producing the BiFC signal was not segregating correctly along with the rest of the peroxisome, it should be more evident in the elongated structures of *vps1* cells. Images were acquired of diploid *vps1* cells expressing Pex13-VN and Pex14-VC fluorescent halves and HcRed-PTS1, and this unequal distribution was indeed seen: BiFC signal was in punctate structures on an elongated peroxisome (Figure 3.8).

One can understand what might happen when the elongated peroxisomes in Figure 3.8 are divided between the mother and bud cells based on the frames at 690 and 700 minutes in Figure 3.6; the peroxisome will split upon cytokinesis, leaving the two buds in the frame with a HcRed-only labelled peroxisome, while the mother cells would have a peroxisome that was labelled both with HcRed and the BiFC green signal.

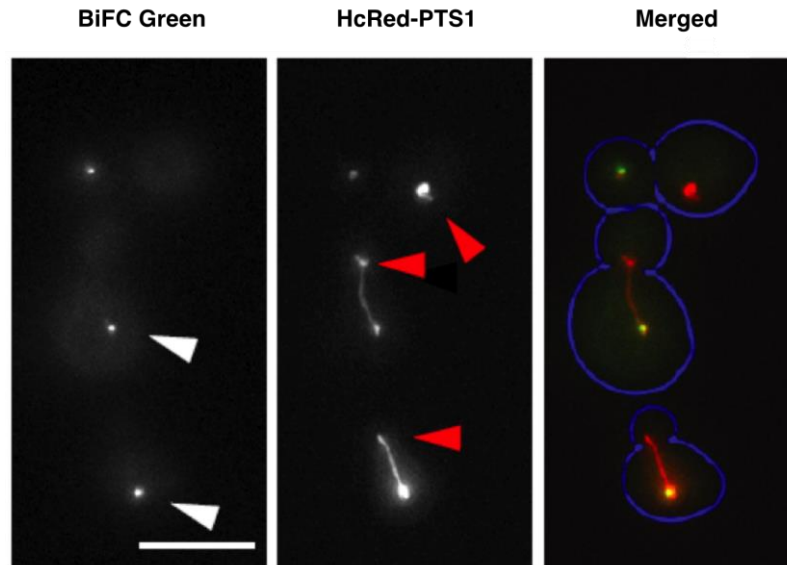


Figure 3.8. Images of diploid *vps1* cells expressing Pex13-VN, Pex14-VC and HcRed-PTS1. Red arrowheads indicate where part of a peroxisome with HcRed-PTS1 does not contain any BiFC green signal. White arrowhead indicates where the BiFC signal co-localises with part of an elongated peroxisome. Scale bar indicates 5 μm . (Figure 9E from Motley et al., 2015).

Utilising live-cell imaging showed that this was indeed the case. The same diploid *vps1* mutant cells expressing Pex13-VN and Pex14-VC fluorescent halves and HcRed-PTS1 were grown on glucose to log phase. They were then loaded into the flow cell for live-cell imaging (see Chapter 2.9.4 for technique). Eleven slices in Z spaced 0.5 μm apart were taken every 20 minutes after imaging commenced in brightfield, green, and red fluorescence channels (microscopy setup is described in Chapter 2.9.1). Several cell divisions demonstrated that on multiple occasions the BiFC-labelled punctate structures failed to segregate with the rest of the peroxisome on division via cytokinesis, resulting in some HcRed-only labelled peroxisomes (Figure 3.9).

In conclusion, the evidence above presents a convincing case that the peroxisomes labelled exclusively with BiFC green signal as seen by van der Zand et al., 2012 in their experiments are likely to have arisen by asymmetric division of the CFP-PTS1 matrix content and the BiFC-labelled structure, and not by *de novo* synthesis.

Further quantitative evidence could be provided by measuring the total overlapping percentage of the two fluorescent protein markers over many *vps1* mutant cells: this would demonstrate that the green BiFC complex signal does not overlap with a majority of the HcRed-PTS1 signal, and is not distributed over the whole peroxisome, as predicted by the vesicle fusion model.

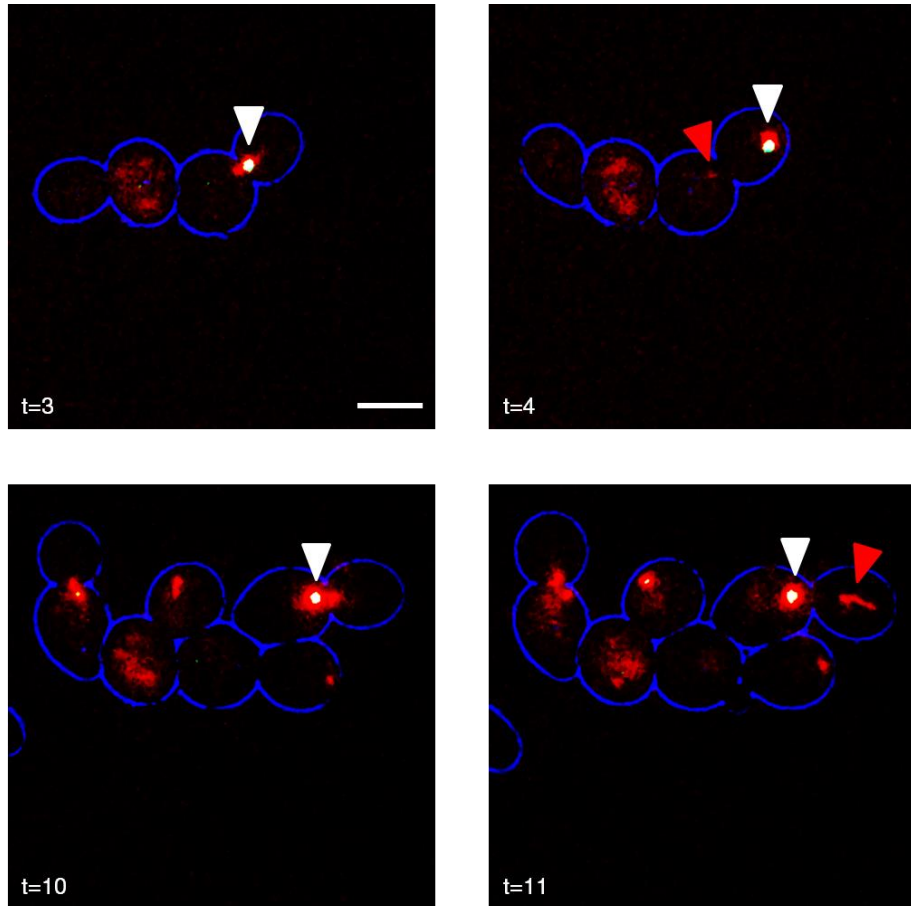


Figure 3.9. Video stills taken from a video of *vps1* diploid cells expressing Pex13-VN, Pex14-VC and HcRed-PTS1. White arrowheads show colocalisation of the green and red signals. Red arrowheads indicate where a peroxisome without green signal has split from the white arrowhead. Scale bar indicates 5 μm . T (time) is in 20 minute intervals; t=3 is 60 minutes after experiment has started.

3.5 Re-examination of the Vesicle Fusion Model

Three of the key aspects of the vesicle fusion model as proposed by van der Zand et al., 2012 have been addressed in the preceding section and it has been shown that they do not reconcile with the evidence gathered during this study. All the above evidence backs up previous studies and other evidence that peroxisomes multiply by growth and division under wild-type conditions (Motley and Hettema, 2007). This section illustrated the usefulness of live cell imaging and computational image analysis for examining questions related to peroxisomes.

Addressing the KPPC model was a more challenging application of these techniques. The next chapter will outline the further improvements to the live cell imaging system and developments in image analysis necessary to acquire and examine data to evaluate the KPPC model.

Chapter 4: Development of Live Cell Imaging and Image Analysis

4.1. Introduction

As set out in Chapter 1.6.2, the main aim of this thesis was to observe and analyse cells and their peroxisomes over time in order to address the points raised in the KPPC model. Like addressing the vesicle fusion model, this required imaging cells across multiple generations.

When addressing the vesicle fusion model, the sampling frequency was 10 minutes and 20 minutes respectively for the experiments in Chapter 3.3 and Chapter 3.4. This was adequate for the purposes of watching peroxisomes segregate over several cell divisions and observing the asymmetric separation of the BiFC complex with the rest of a peroxisome upon cell division, as those events occurred over long periods of time. To follow and hopefully track individual peroxisomes in cells required a different set of experimental conditions (section 4.2), which necessitated a series of improvements (sections 4.3 and 4.4). Discussed at the end of this chapter are the methods used to analyse this live-cell imaging data (section 4.5).

4.2 Experimental Requirements

To follow peroxisomes over time required an increase in sampling frequency to one image every few minutes, but the desired target was under one minute. There were also desired requirements for the other experimental factors (see Figure 1.14 for a reminder):

- Resolution in Z – peroxisomes in *S. cerevisiae* are small objects ($0.1\mu\text{m}$ - $0.2\mu\text{m}$ (Sibirny, 2016)) and in order to track individual ones a high spatial resolution is needed to distinguish between them throughout a cell. As the limit of resolution in Z on a widefield microscope is roughly $0.5\mu\text{m}$ (explained in Appendix E), there is no point sampling more often than this. *S. cerevisiae* cells are roughly $5\mu\text{m}$ in diameter and therefore sampling every $0.5\mu\text{m}$ for $7\mu\text{m}$ (fifteen steps in Z in total) was thought to be necessary to see all the peroxisomes throughout the cell and get a much 3D resolution as possible.
- Experimental Duration – the experiment needed to last at least long enough for several cell divisions at one division every roughly every 1.5-2 hours to have taken place (around 6-8 hours in total).

- Signal Strength – Ideally in live-cell imaging one wants the strength of the signal to be as low as it possibly can be whilst still being able to see and distinguish between objects. However, due to the variable intensities of signal that come from peroxisomes, setting a robust lower limit is problematic as one still wishes to detect even the weakest intensity peroxisomes. The light intensity for each imaging experiment was based on taking a few sample pictures, starting at the lowest light intensity and working upward, until it was decided that all the peroxisomes in cells were visible.

The final experimental setup might have to be some compromise between all the factors. Trials were run to see what would happen when the sampling frequency was increased.

These early forays in attempting to reach the desired parameters resulted in image sets containing many dying or dead cells. This was certainly because of phototoxicity (explained in Chapter 1.5.1) on the cells. Therefore, to acquire data closer to the parameters desired it was patently necessary that further improvements to the live-cell imaging setup should be sought to better facilitate the growth and longevity of cells in the experiments. Improving the viability of cells was the major obstacle in terms of improving the quality of the live cell imaging data. In order to increase the cell viability, there needed to be a decrease in the total light exposure. Section 4.3 discusses the strategies that were used to achieve this. A smaller but nevertheless important issue that arose during optimisation of the live-cell imaging was the tendency of *S. cerevisiae* cells not to express proteins when they are encoded on a plasmid. This also affected the quality of the image data. This is addressed in section 4.4.

4.3 Decreasing Total Light Exposure

Decreasing total light exposure is the predominant way to reduce phototoxicity and therefore increase cell viability. To decrease total light exposure, one must alter one or more of the four factors governing it: imaging frequency, total duration, number of images in Z and signal strength from the fluorophore.

As outlined in 4.2, there were targets to reach for the number of Z slices, imaging frequency and experimental duration. Therefore the only remaining factor that could be optimised to decrease the total light exposure was to change the strength of the signal from the fluorescent protein. There is a still a lower limit on the strength of the signal – it must be at least strong enough to distinguish peroxisomes from each other and from the background. How can the signal strength be maintained at the minimum amount necessary whilst decreasing the total light exposure? Signal strength is governed through three aspects: the intensity of the excitation light from the light source; the exposure time (the length of time that the sample is illuminated with light – usually between a dozen and a hundred milliseconds); and the changes to the fluorophore itself (Figure 4.1).

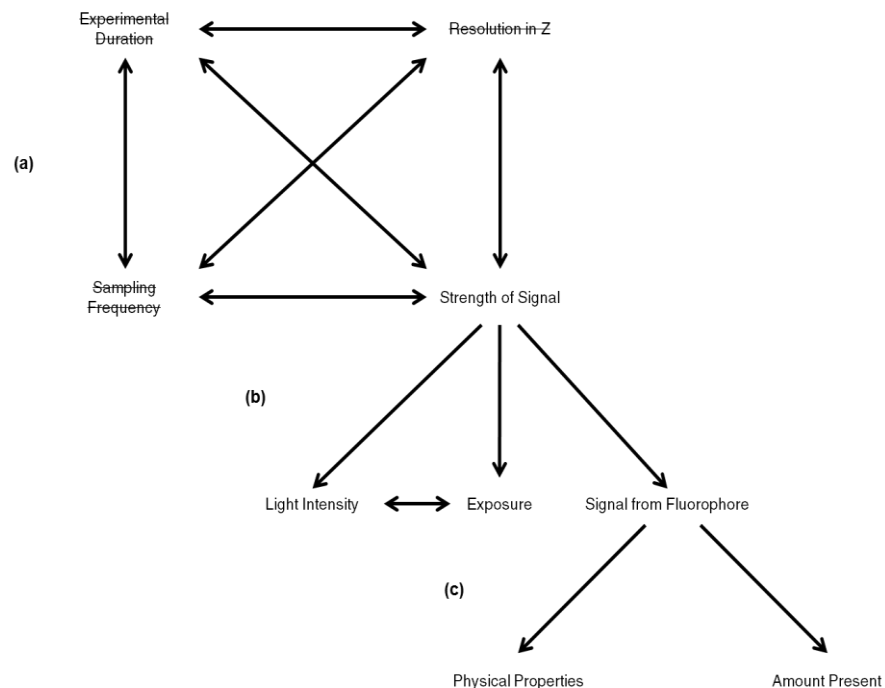


Figure 4.1. Signal strength as the only remaining aspect to optimise. Refer to Figure 1.14 for the original image displaying factors of a live-cell imaging experiment. (a) As there were targets to reach for experimental duration, Z resolution and sampling frequency, the only factor that could be altered was signal strength. (b) The signal strength is affected by light intensity, exposure time and the signal from the fluorophore. (c) Signal from the fluorophore is influenced by the physical properties of the fluorophore, and how much fluorophore is present when imaged.

The intensity of the excitation light and exposure time are two linked factors. In general, one can achieve the same amount of signal by increasing the intensity of light and decreasing the exposure time or vice-versa. Different tissues and cells react to this in different ways however, and with practice it has become evident that *S. cerevisiae* cells are much more tolerant to a low light intensity and a longer exposure time. Again, there is a lower bound as to what extent these factors can be pushed. There is an actual physical limit to the minimum amount of power that a fluorescence light source can put out; and the longer the exposure time, the more confusion there becomes between objects if they are motile in different planes in Z.

4.3.1 Locating a New Fluorescent Protein

The signal from a fluorescent protein is dependent on its inherent physical characteristics and the number of fluorescent protein molecules localised to a particular area. HcRed was the fluorescent protein that was used in the live-cell imaging experiments in sections 3.3 and 3.4. This fluorescent protein was quickly abandoned for the much brighter protein EGFP (Table 2.6 compares their properties, what these properties mean is explained in the next section).

EGFP (enhanced green fluorescent protein) was the brightest fluorescent protein available at the start of this study. EGFP is already a well-optimised protein for fluorescence imaging. It was produced from the original GFP by a series of point mutations; a notable change being the amino acid change at position 65 from Ser to Thr (Cormack et al., 1996) which had the effect of moving its peak excitation wavelength from 395nm (near ultra-violet) to 488nm (cyan), which is less phototoxic to cells (Tsien, 1998; Yang et al., 1996).

Many new fluorescent proteins have become available since EGFP was first produced. One of these newer fluorescent proteins was sought that was superior in its inherent physical characteristics. The characteristics being searched for here but also generally desirable for any fluorescent protein are: 1) resistance to photobleaching; 2) low maturation time; 3) high extinction coefficient and 4) high quantum yield. These are explained below:

- 1) Resistance to photobleaching. A fluorescent protein will become damaged over the course of the experiment to the point that it will no longer be fluorescent. Photobleaching is believed to be due to the interactions between fluorophores in their excited states and molecular oxygen (O_2) within the cell, along with the formation of errant covalent bonds within the protein itself (Diaspro et al., 2006). Resisting this damage is clearly a desirable property.

- 2) Low maturation time. After being released by a ribosome and folding, a fluorescent protein undergoes a series of stages of maturation (including torsional rearrangements, oxidation etc.) to become fluorescent (Remington, 2006). Depending on the fluorescent protein, this maturation time can vary. Having a low maturation time means that a fluorescent protein becomes visible closer to the time it actually started being transcribed, which is useful if one wishes to observe the movement of a fluorescent protein through stages in a cellular process, for example. Lower maturation time also affects the signal strength coming from the sample as any photobleaching that is occurring is being counteracted by the addition of freshly matured protein.
- 3) High extinction coefficient. The extinction coefficient (EC) is how strongly an object absorbs photons at a given wavelength; ergo a high extinction coefficient means that a fluorescent protein is more efficient. A representative high EC is 75000-170000.
- 4) High quantum yield. Quantum yield (QY) is a measure of the efficiency of photon emission of a fluorescent protein. It is the probability of one photon being emitted from a fluorescent protein for each photon absorbed, and is expressed as a ratio between 0 and 1 (Lakowicz, 2006). A high quantum yield is generally a desirable property of a fluorescent protein across all imaging applications. Values generally range between 0.2 – 0.7, although there are several examples of fluorescent proteins both below and above those bounds.

EGFP already has a reasonably high quantum yield, extinction coefficient and resistance to photobleaching. However, it should be noted here that photobleaching never really appeared to be a major issue with these experiments, and cells death via phototoxicity often occurred before there was loss of signal.

Bearing these factors in mind, the literature was searched for another fluorescent protein that could better EGFP in some of the above factors. The results of this were that a new yellow-green fluorescent protein called mNeonGreen was located (Shaner et al., 2013). In comparison to EGFP, mNeonGreen has a higher QY, EC, a lower folding time and similarly high resistance to photobleaching. A comparison between the two proteins is detailed in Table 4.1.

Table 4.1. Comparison of EGFP and mNeonGreen fluorescent proteins. Maturation speed is half-maximal value after exposure to oxygen at 37°C. Brightness is the product of EC and QY.

Protein	λ_{ex} (nm)	λ_{em} (nm)	EC	QY	Brightness	Maturation Speed(mins)	Time to Photobleach(s)	References
mNeonGreen	506	517	116000	0.8	92.8	10	158	(Shaner et al., 2013)
EGFP	488	507	56000	0.6	33.6	25	174	(Cormack et al., 1996; Lam et al., 2012)

4.3.1.1 Creating a New Plasmid with mNeonGreen

An mNeonGreen-expressing plasmid was obtained from a commercial vendor (Allele Biotechnology). The first step was to clone the sequence into a plasmid that could express in *S. cerevisiae* (see Chapter 2.10.1).

With its higher QY and EC, mNeonGreen did provide a stronger signal than EGFP under the same imaging conditions. This meant that the intensity of the light could be reduced when imaging this new fluorescent protein over EGFP, and therefore decreasing the total light exposure.

4.3.2 Increasing the Amount of Fluorescent Protein

In addition to changing the fluorescent protein itself, the strength of the signal can also be upped by increasing the amount of fluorescent protein present. The number of fluorescent protein molecules depends predominantly on how much is being translated at any given time. This in turn depends on how much of that specific mRNA present in the cell, which in turn depends on how often the gene in question is being transcribed. The transcription of genes is based on the activity of promoters. The GAL1 promoter has been mentioned previously in Chapter 3.4. This promoter is only active in the presence of galactose, which is an unusual case. Many promoters are always ‘on’ (their expression is ‘constitutive’) but some promoters are ‘stronger’ than others; they cause the downstream gene to be transcribed more often over a particular time frame than others. In this study, the promoter first used on most of the plasmids to express mNeonGreen was the HIS3 promoter.

The HIS3 promoter shows moderate constitutive expression, and is normally the promoter for the enzyme involved in the sixth step of histidine biosynthesis. Using a promoter that was stronger would produce more fluorescent protein and in turn this would provide more

signal. The generally used high-expressing promoters for *S. cerevisiae* molecular biology are the TEF1 promoter or the TPI1 promoter. In their natural genomic function these are promoters for the highly expressed constitutive proteins Translation Elongation Factor 1 and glycolysis enzyme Triose-Phosphate Isomerase respectively. TPI1 was utilised in this study as it was readily available to be cloned from other plasmids in the lab. The steps taken to do this are outlined in Chapter 2.10.2.

The increased activity of the TPI promoter compared to the HIS3 promoter means that there is more fluorescent protein present (Figure 4.2). This in turn allows for a decrease in the total light exposure whilst maintaining the same signal strength.

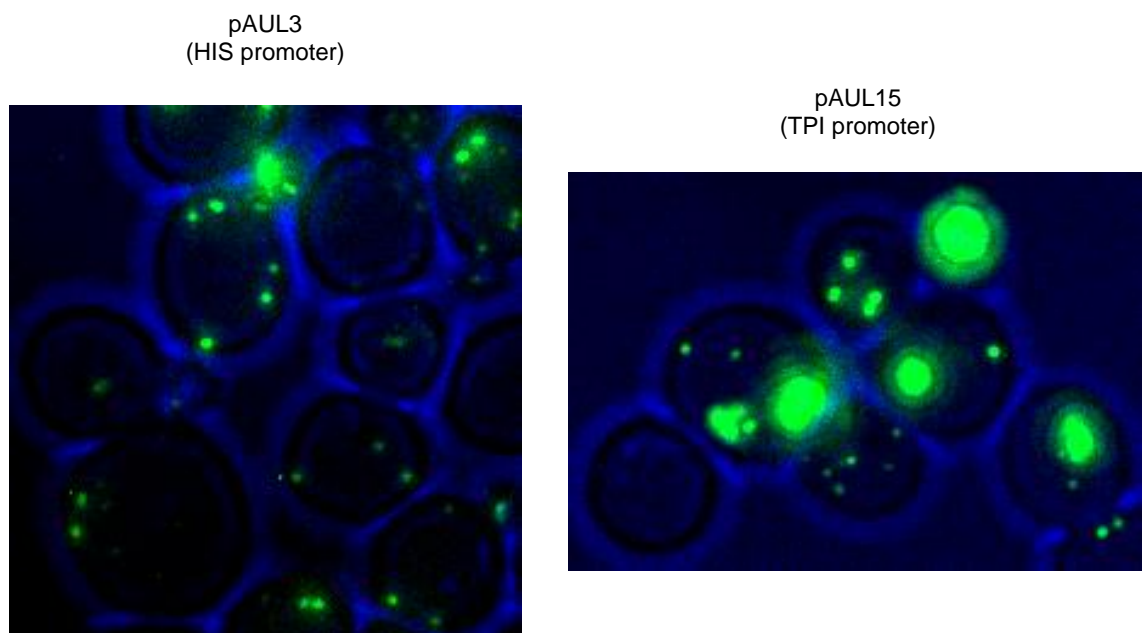


Figure 4.2. Comparison between pAUL3 plasmid (HIS promoter) and the pAUL15 plasmid (TPI promoter). Both plasmids are expressing mNeonGreen-PTS1, and imaged with the same exposure time and light intensity; brightfield image in blue. Although it does not appear that the image on cells with the TPI-containing plasmid (right) is that much brighter than the HIS-containing plasmid (left), the brightness of the green channel on left image had to be adjusted so that the peroxisomes are visible. If the two images used the same brightness scale then the peroxisomes in the left image would not be visible. The absolute intensity values of the pixels in the peroxisomes in the right image are roughly 4x as large as the ones in the left image. Moreover, one can see how large the peroxisomes appear in the right image, suggesting they are much brighter (and saturating the pixels in the camera) than the ones on the left.

4.3.3 Summary

To summarise the above section, the result was a brighter fluorescent protein than the one that was used originally, expressed downstream of a more powerful promoter. Both these factors allowed for a decrease in the total light exposure whilst maintaining the amount of signal needed to distinguish peroxisomes from each other and the background.

4.4 Fluorescent Protein Expression

Although not directly related to achieving any of the parameters described earlier, ensuring a uniform expression of the fluorescent protein across the yeast population was a small but significant part in the development of a robust system for live cell imaging.

When working with *S. cerevisiae*, the predominant way of expressing a gene of interest is to transform the yeast with a plasmid containing the gene. If it is a fluorescent protein checking the expression of the gene simply requires one to look at the yeast population using fluorescence microscopy. However, when imaging a population of yeast containing a plasmid, it is clear that not all yeast will be expressing the gene equally. Some of the yeast will not be expressing at all, and some will be expressing to a much higher level than others (Figure 4.3).

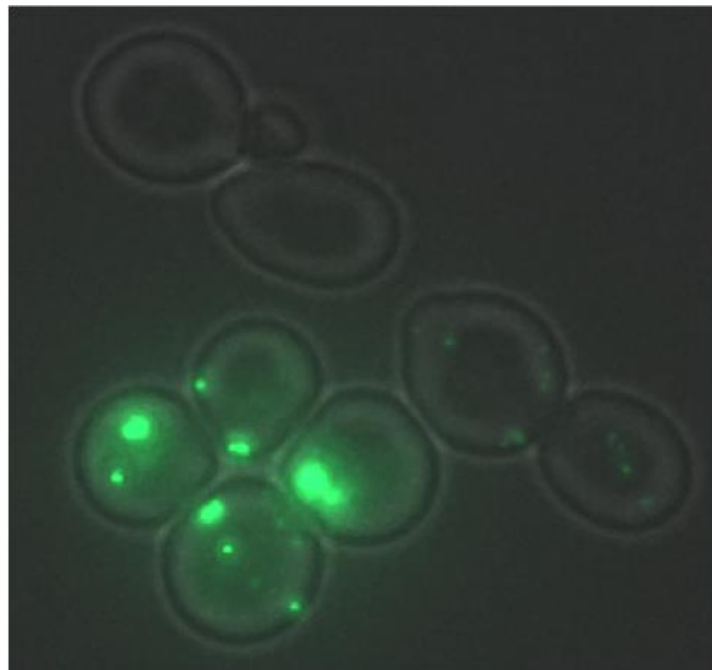


Figure 4.3. Variable levels of mNeonGreen-PTS1 expressed (from plasmid pAUL15) in diploid WT cells grown on glucose for 4 hours. The cells in the top left of the image are not expressing at all, whereas the cells in the bottom left of the image are expressing at a stronger level than those on the right (as they are brighter). Image is maximum intensity projection. Scale bar indicates 5 μ m.

A complete lack of expression is usually due to the plasmid being lost upon cell division (about 1 in every 100 cell divisions (Heslot and Gaillardin, 1991)). Higher levels of expression can be due to yeast having multiple copies of the plasmid. This varying expression is a problem when processing images, as it affects the thresholding and segmentation steps of image processing (see Chapter 1.5.2). Another practical consideration for imaging is that any

cells not expressing the protein provide no information; acquiring images of them is a fruitless exercise. Additionally, the growth and proliferation of these non-expressing cells can push cells which are expressing the fluorescent protein out of the frame of image capture, which further reduces the amount of information one is receiving from an imaging experiment.

4.4.1 Ensuring Uniform Expression

Instead of expressing from a plasmid, genes can be integrated into the *S. cerevisiae* genome, and be expressed from there. The prime candidate for genomic integration was the plasmid expressing mNeonGreen-PTS1 behind the TPI promoter (pAUL15).

To integrate the fluorescent protein into the genome, the sequence of interest should contain a selectable marker. To preserve the already existing selectable markers and make the process more efficient (i.e. so there is less background when screening for successful integration), selectable markers for genomic integration are usually antibiotic resistance markers.

The antibiotic used for selection of *S. cerevisiae* was clonNAT. clonNAT, the trade name of the antibiotic nourseothricin, is used in the selection of both bacteria and eukaryotic cells; it induces the miscoding of mRNA and therefore leads to the inhibition of protein synthesis (Kochupurakkal and Iglehart, 2013). The clonNAT resistance gene (natMX) is derived from the original bacterial species that produces the nourseothricin (*Streptomyces noursei*) (Krügel et al., 1993). natMX codes for nourseothricin N-acetyl transferase (NAT), which acetylates one of the groups of the nourseothricin molecule, rendering it inactive. Cells cannot grow on clonNAT-containing media without also possessing the natMX gene. The steps taken to integrate the TPI-mNeonGreen-PTS1-clonNAT sequence into the genome are explained in Chapter 2.10.3.

The resultant *S. cerevisiae* cells with the mNeonGreen expressing from the genome were much more useful for imaging and automated processing, and there were no concerns regarding imaging yeast that were not expressing any fluorescent protein. The cells had a much more uniform level of expression (as there was only one copy of the gene being transcribed), and all were expressing (as cells lacking the clonNAT resistance gene cannot grow in the presence of clonNAT)(Figure 4.4).

However, it was noted that due to the integration the overall intensity of light used to image the *S. cerevisiae* had to increase slightly, from 1% intensity to 7% intensity, because the overall

expression level of the mNeonGreen protein was lower compared with the cells transformed with the pAUL15 plasmid. Again, this situation highlights the trade-offs and compromises that must be sought when doing prolonged time-lapse live cell imaging.

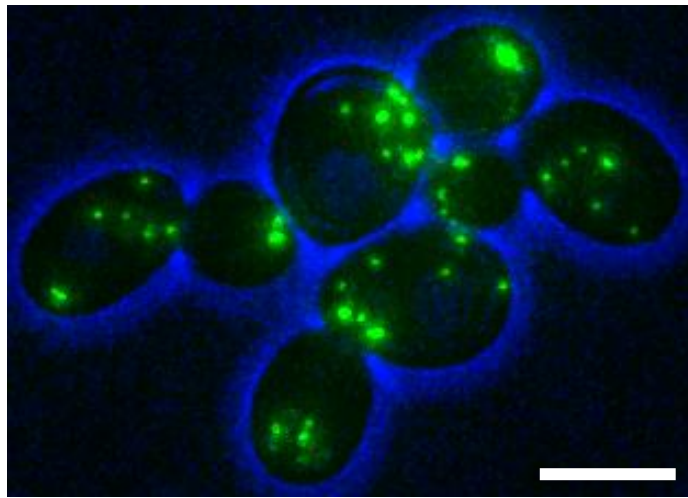


Figure 4.4. Example of WT *S. cerevisiae* cells expressing mNeonGreen-PTS1 (green) from the **genome**. Note how all cells are expressing at a relatively uniform level (compare with Figure 4.3). Brightfield in blue. Image is maximum intensity projection. Scale bar indicates 5 μ m.

4.5 Computational Analysis of Live Cell Images

4.5.1 Introduction

Once the parameters and techniques required to keep the cells alive and their peroxisomes visible over many generations were developed, a computational method of tracking peroxisomes over a time-lapse experiment was required to describe their behaviour over these multiple generations.

Instead of writing a program in Python to perform this, one of the plugins included with FIJI was sought for this task. Although user-written scripts such as those described in Chapter 2 are useful as they provide complete control over the analysis and can be adapted for specific needs and circumstances, it seemed more sensible to use a program that was already available and adapting it if necessary rather than building a script from the ground up to track peroxisomes.

4.5.2 TrackMate

There exist multiple plugins for FIJI that seek to perform tracking of objects in time-lapse images. As with previous descriptions of image analysis (Chapter 2), one tracking program does not suit all purposes. Different ones use different methods of detecting objects and then linking these objects together over several frames to form tracks. A few were trialled based on an evaluation in the literature (Chenouard et al., 2014), including one called MOSIAC (Sbalzarini and Koumoutsakos, 2005), which showed some promise. In the end, the one that was used in this study was TrackMate (Tinevez et al., 2016), as it was the most user-friendly and provided the best numerical output for subsequent analysis.

In FIJI, TrackMate can be accessed via Plugins > Tracking > TrackMate. Analysis of images in TrackMate is performed in two stages before data can then be extracted (Figure 4.5). First, objects (in this case, peroxisomes) are detected after a small amount of pre-processing. Second, these objects are linked together to form tracks. Then the data can be extracted.

Object Detection

No previous pre-processing of an image is required before starting the plugin, as conveniently one of its methods to segment an image is a difference of Gaussians filter. This has already been shown to be a reliable method of segmenting peroxisomal images (Chapter

2.12). The user can then provide an estimate of the diameter of the objects that TrackMate should seek to extract, along with a threshold value. After this, objects are detected and extracted.

Object Linking into Tracks

The plugin then attempts to link the objects it has detected in each frame of the time-lapse imaging into tracks (Figure 4.6). There are multiple ‘trackers’ to choose from within the TrackMate plugin that execute different algorithms. In this study, the LAP tracker of TrackMate was used. This is based on the Linear Assignment Problem mathematical framework adapted from Jaqaman et al., 2008.

The LAP tracker has functionality for frame-to-frame linking, gap closing and track merging/splitting. Only the first two options were utilised in this study, as the track merging/splitting led to a massive increase in the number of erroneous tracks that the algorithm detected. Frame-to-frame linking attempts to find an association between an object in frame N with another object in frame $N+1$ based on a user-defined maximum distance between the two objects, and also any other restricting criteria the user has selected. These criteria can make this process more robust by adding weight to parameters that should be similar between the two objects; the parameters used in this study were a peroxisome’s intensity and its position in the Z dimension.

The gap closing part of the algorithm allows for ‘skipping’ of a certain number of (user-defined) frames; if an object in frame N cannot be linked to one in frame $N+1$, the algorithm will attempt to link it to an object in frame $N+2$, etc. up until frame $N+X$ (where

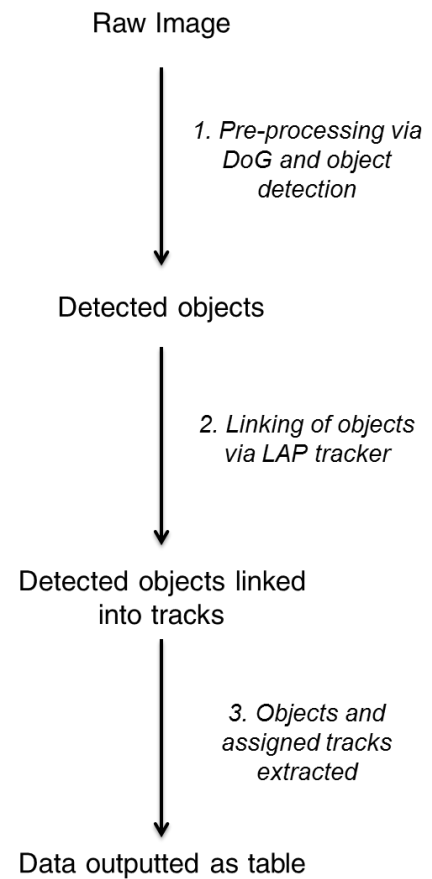


Figure 4.5. Schematic of TrackMate workflow. Raw image is pre-processed using Difference of Gaussians filter, followed by object detection (1). The LAP tracker then attempts to link objects into tracks (2). Then data concerning object positions and tracks can be extracted (3). Figure 4.7 shows an example of the results table.

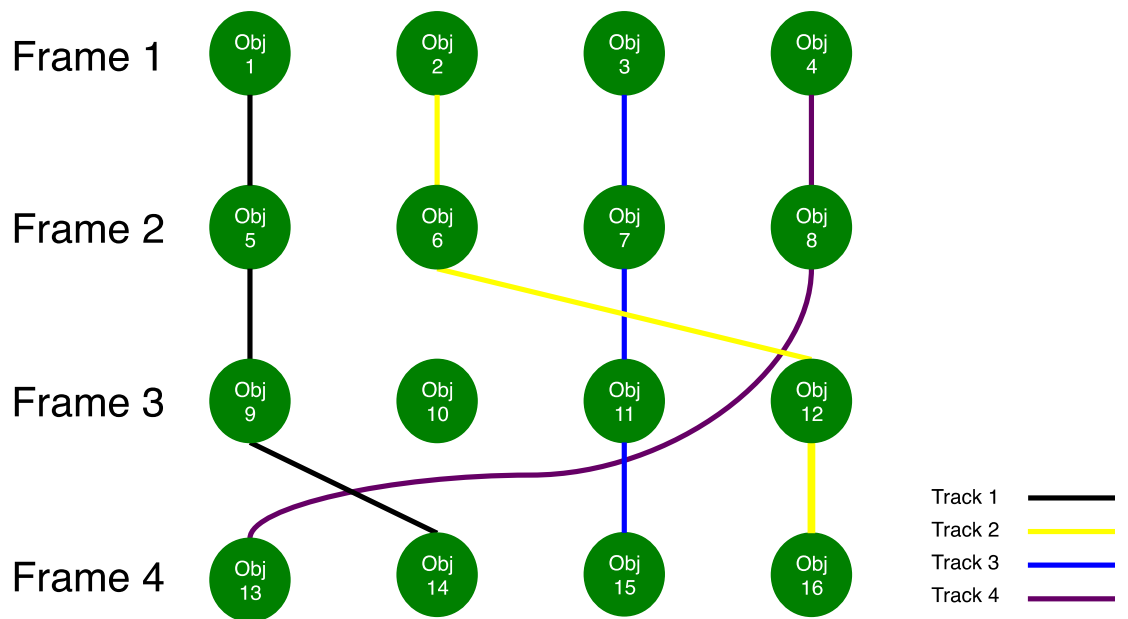


Figure 4.6. A schematic diagram of the linking of objects together to make tracks. Objects that are similar from one frame to the next will be joined into a track. Object 8 was not considered to be similar enough to any of the objects in frame 3 to link them, but was found to be similar to Object 13 in frame 4, so they are joined. This is an example of ‘gap closing’ – if this option is disabled then this sort of linking does not occur. This has left Object 10 without any links. However, the way TrackMate records data means that every object has to be placed into a track, even though the track might only contains one object. Technically therefore, Object 10 is part of ‘Track 5’, which begins and ends at frame 3.

X is the user-defined limit on the number of frames the tracking can skip).

The end point of this is a table containing parameters about every object (i.e. peroxisome) that the program has identified and its characteristics (position, intensity, etc.) and the track that the algorithm had placed it in to (Figure 4.7). It rapidly became clear that the tracking of the peroxisomes would be a much more difficult task than first appreciated at the outset of this study due to the restrictions placed on the temporal resolution of the data and behaviour of peroxisomes themselves. The problems encountered surrounding tracking peroxisomes and the description of the behaviour of the peroxisomes is explored in the next chapter.

	Label	ID	TRACK_IDUALITY	X	Y	Z	T	FRAME	RADIUS	VIS	MANUAL_COLOR	MEAN_INT	MED_INT	MIN_INT	MAX_INT	TTL_INT	STD_DEV	EST_D	CONTRAST	SNR	
1	ID13525	13525	0	215.691	14.282	6.105	3.902	0.000	0	0.325	1	-10921639	2556.193	2471	1361	4466	345086	835.306	1.150	0.066	0.380
2	ID13549	13549	0	394.210	15.473	6.372	3.972	300.038	1	0.325	1	-10921639	2586.867	2635	595	5471	349227	1073.605	1.083	0.024	0.115
3	ID13500	13500	0	346.848	14.561	6.571	2.405	600.076	2	0.325	1	-10921639	2152.163	1879	959	6126	290542	922.697	1.235	0.064	0.282
4	ID13607	13607	0	421.090	14.874	6.907	2.355	900.114	3	0.325	1	-10921639	2115.067	1797	0	6458	285534	1150.753	1.053	0.184	0.347
5	ID13627	13627	0	350.085	15.358	6.662	3.406	1200.152	4	0.325	1	-10921639	1810.844	1497	771	4797	244464	851.390	1.084	0.048	0.194
6	ID13576	13576	0	253.048	14.670	5.151	2.597	1500.190	5	0.325	1	-10921639	2031.244	1818	759	5394	274218	756.019	1.104	-0.003	-0.015
7	ID13593	13593	0	311.230	14.769	5.004	2.749	1800.228	6	0.325	1	-10921639	1883.215	1656	0	5456	254234	940.687	1.074	-0.002	-0.008
8	ID13560	13560	0	331.579	14.443	4.317	2.186	2100.266	7	0.325	1	-10921639	1931.844	1804	590	5340	268839	885.323	1.124	0.019	0.085
9	ID13649	13649	0	165.270	13.304	4.590	5.481	2400.304	8	0.325	1	-10921639	1854.556	1833	656	4271	250865	681.674	1.072	0.002	0.008

Figure 4.7. Example of output from the TrackMate algorithm. Columns with important information are; ID of the detected object; Track ID, the track the object has been assigned to; position in X; position in Y; position in Z; Frame number; Mean intensity; and Total intensity.

4.5.3 Manual Cell Segmentation

In order to follow the lineages of the peroxisomes over multiple cell generations, the lineages of the cells also had to be identified. This meant defining the cells and tracking which cell was which from frame to frame, something that was done semi-manually. The reasoning behind doing this semi-manually was two-fold. Firstly, these images were not of cells that were expressing a cytosolic label and therefore computational segmentation would have been problematic. The reason behind not using a cytosolic label was to keep the amount of light to which the cells were exposed to an absolute minimum.

Secondly, a really accurate outline of each cell was required, especially when new buds were forming. This is not always obvious, even to the eye. Automated segmentation of cells that have buds forming does not often segment the mother and bud cell as two separate objects, something that was needed here with some accuracy.

To segment the cells using FIJI, the central Z-slice of the bright-field image of the cells was first extracted using Image > Duplicate, and selecting the correct channel and Z position. The central Z slice is where the cell wall of the yeast cell is the most well defined, and is used as a guide to outline the cell. The outlining of the cell was performed using the segmented line tool, which can be accessed on the FIJI menu bar. With the tool selected, clicking on the screen will put down a point. One can then click a number of points around the perimeter of the cell, and clicking on the starting point again will finish the line. This object can then be added to the ROI Manager (Tools > ROI Manager). After outlining the same cell across all frames, the ROIs are first renamed to denote that they all belong to 'Cell A' etc. and are then saved to a file to be accessed later (Figure 4.8). The main downside of this semi-manual approach was that it took several hours to outline a group of a dozen or so cells correctly. A few useful bits of information that would have been useful to know beforehand regarding segmenting cells semi-manually are documented in Appendix B.3.

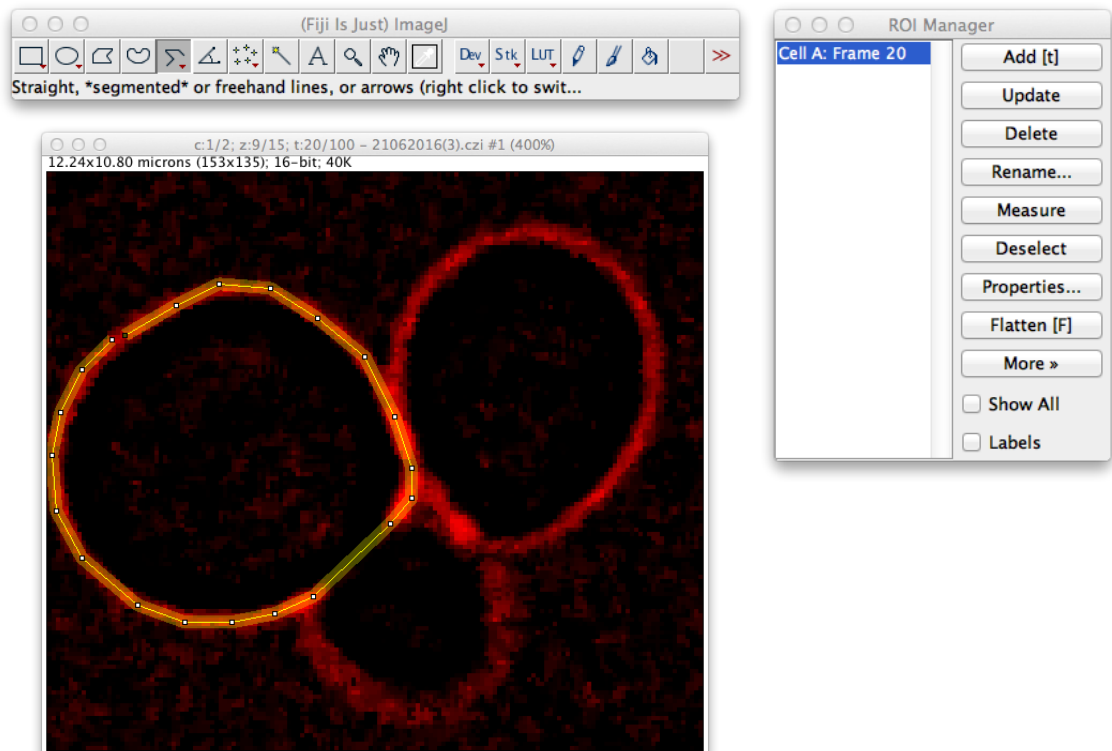


Figure 4.8. Manual cell outlining in FIJI. The segmented line tool (FIJI menu bar, top) is used to trace the outline of a yeast cell. Clicking once on the screen will place the first point, and subsequent clicking will continue the line. Clicking back on the starting point will finish the line. This can be added to the ROI manager (right). Then one can move onto the next frame and continue outlining the same cell.

4.5.4 Matching Peroxisomes to Cells

After outlining all the cells in an image, the peroxisomes detected by TrackMate needed to be matched to the individual cells. This was done using a small Python program. It first read in the XY positional information of the peroxisomes from the TrackMate results table into a Python dictionary. It then opened the set of ROIs describing the positions of the segmented cells and matched the XY co-ordinates of the peroxisomes to the cells. This program outputted the original results table of the TrackMate program describing the properties of the peroxisomes, but with the addition of another column describing which cell that peroxisome is in (Figure 4.7, but with the addition of an extra column containing a cell letter that the peroxisome has been assigned to). The code for this Python program is included below.

```
import glob, string, time, sys, os, fnmatch, math
from ij import IJ, ImagePlus, WindowManager, ImageStack
from ij.plugin import ImageCalculator, Duplicator, ChannelSplitter
import ij.plugin.frame
from ij.plugin.frame import RoiManager
from ij.plugin.filter import ParticleAnalyzer, MaximumFinder
from ij.measure import Measurements, ResultsTable
from java.lang import Double
from ij.gui import PolygonRoi
from ij.process import ImageProcessor
from loci.plugins import BF
```

```

# Program to match peroxisomes from TrackMate output to cells

def get_perox_info(spot_filename): # get peroxisome information e.g. co-ordinates

    ppoints = []

    for line in open("%s"%(spot_filename)).readlines()[1:]:
        f = line.split()
        traj_id = int(f[3])#
        perox_id = str(f[1])
        i_frame = int(f[9])
        x = int(round(float(f[5])*12.5))
        y = int(round(float(f[6])*12.5))
        ppoints.append([perox_id,x,y,i_frame,line])

    return ppoints # return list of peroxisome points

def roi_bit(spot_filename, cell_filename, ROI_filename, results_filename):

    ppoints = get_perox_info(spot_filename)

    filename = (cell_filename)
    IJ.run("Bio-Formats Importer", " open=[%s] autoscale split_channels color_mode=Composite view=Hyperstack
stack_order=XYCZT" %(filename))

    imp = WindowManager.getCurrentImage()
    roiP=imp.getProcessor()
    IJ.run("ROI Manager...")

    rm = RoiManager.getInstance()
    if (rm==None):
        rm = RoiManager()
    rm.runCommand('Open',ROI_filename) #open list of ROIs and associated data regarding cell co-ordinates
    rois = rm.getCount()

    # Extract Rois

    cell_path = (results_filename)
    cell_file = open(cell_path,'w')

    for roin in range(0,rois): # for each cell in image, see if any peroxisomes match to it
        rm.select(roin)
        roi = rm.getRoi(roin)
        frame = imp.getFrame()
        roi.setPosition(1,1,frame) #channel, slice, frame

        # Iterate over cell X,Y co-ordinates and if peroxisome matches,
        # mark that peroxisome as belonging to that cell and then delete so it can't be matched to another cell

        poly_roi = roi.getPolygon()
        x_points = (str(roi.getPolygon().xpoints)[12:-2]).split(',')
        y_points = (str(roi.getPolygon().ypoints)[12:-2]).split(',')
        roiFrame = roi.getTPosition()
        name = roi.getName().split()

        for y in range(int(min(y_points, key=lambda x:int(x))), int(max(y_points, key=lambda x:int(x)))):
            for x in range(int(min(x_points, key=lambda x:int(x))), int(max(x_points, key=lambda x:int(x)))):
                if poly_roi.contains(x,y):
                    for point in ppoints:
                        if point[1] == int(x) and point[2] == int(y) and point[3] == int(roiFrame):
                            print>>cell_file, point[4][:-1], name[1]
                            ppoints.remove(point)

    rm.runCommand('Delete')
    print len(ppoints)

    ppoints = []

    print 'Done'
    IJ.run("Close All", "") # Close all FIJI windows
    rm.reset()

# roi_bit(spot_filename, cell_filename, ROI_filename, results_filename)

roi_bit()

```

Chapter 5: Evaluating the KPPC Model

Using One Cell

5.1 Introduction

Evaluating the KPPC model required a system of live-cell imaging to follow peroxisomes over multiple generations and then analyse these images as described in Chapter 4. This introduction and the following section (5.2) describe the data that was gathered for this purpose. Due to the overwhelming amount of data to be dealt with here, the analysis and presentation of the data will be split across two chapters. The remainder of this chapter after 5.2 will examine the behaviour of peroxisomes in just one cell, and Chapter 6 will move to looking at whole cell clusters.

Chapter 4.2 outlined the ideal parameters of the live-cell imaging for investigating the KPPC model. Emphasis was placed on the need to increase the sampling frequency preferably to under one image every minute, whilst keeping good Z resolution (every $0.5\mu\text{m}$ for $7\mu\text{m}$) and imaging for at least 8 hours to allow for multiple cell divisions at one division/1.5-2 hours.

It transpired that not all of these parameters were achievable due to the effects of phototoxicity. Attempts were made to image cells every 30 seconds, every minute and every 2.5 minutes. In all these scenarios, the cells were clearly not growing and dividing as much as they should be over the course of an 8-hour experiment (examples of imaging every 30 seconds and 2.5 minutes are shown in Figure 5.1). Over an 8-hour experiment one should expect to see roughly four cell divisions at one division/1.5-2 hours. Even at 2.5-minute intervals between frames, cells would manage to complete one or two cell divisions at most, before growth stopped and signals from the peroxisomes would become dimmer and dimmer. As there was no further optimisation possible with the fluorescent protein, a choice had to be made here to increase the cell viability and get images of dividing and growing cells over 8 hours: either the number of Z slices had to be decreased or the time between frames had to be increased (i.e. a decrease in the sampling frequency).

It was decided that to ensure that all peroxisomes throughout the cells were being detected, the number of Z slices should be maintained to keep the resolution in Z, and therefore the time between frames was increased. As at least four cell divisions were expected over an 8-hour period, and only one or two cell divisions were occurring at 2.5-minute sampling

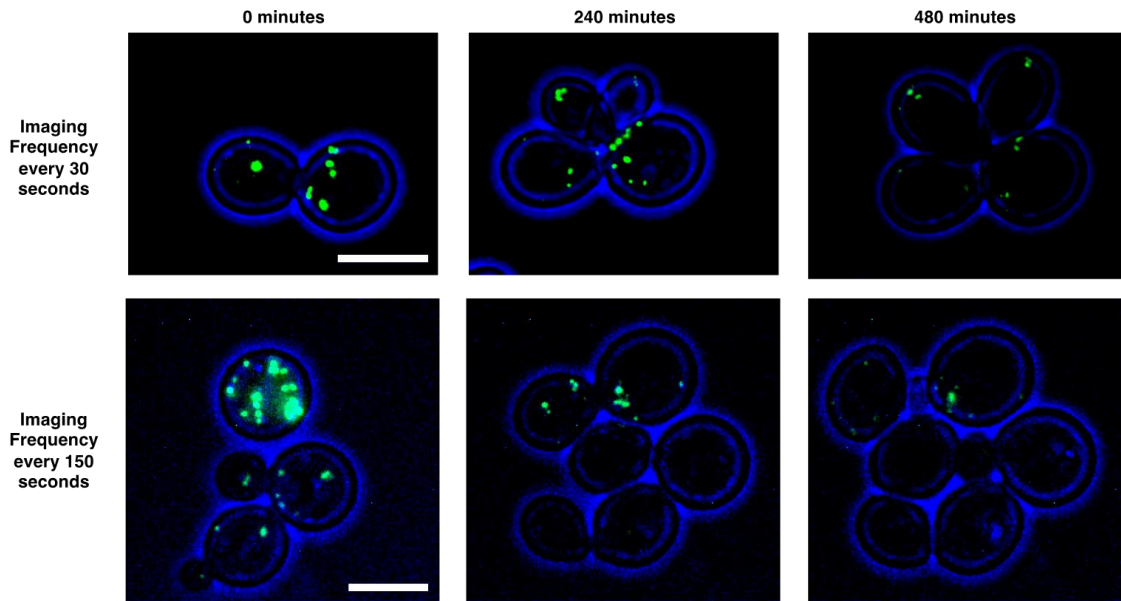


Figure 5.1. Examples of cells growing sub-optimally due to the effects of phototoxicity when imaged at 30 or 150 second intervals for 8 hours. One would expect roughly four cell divisions over an 8-hour period, given roughly one cell division/2 hours. However, when growing under conditions when cells are imaged every 30 seconds only one cell division is observed, and cells growing under conditions when imaged every 150 seconds manage to complete one full cell division and have just started another. Note how the intensity of the fluorescent signal has dropped significantly in both experiments by 480 minutes. Cells are expressing mNeonGreen-PTS1 (green), brightfield in blue, and are grown in the cell culture chamber. All images are maximum intensity projections of 15 slices, taken every 0.5 μ m. Scale bar indicates 5 μ m.

intervals, halving the sampling frequency to every 5 minutes seemed a sensible assumption to make. This enabled the capturing of data sets containing multiple cell divisions, five in some cases, which is close to what is optimally expected in liquid culture (90 min per division in liquid culture vs. 100 min in the cell culture chamber).

The final parameters for imaging were thus:

- 15 Z slices (every 0.5 μ m for 7 μ m)
- Sampling Frequency of every 5 minutes
- Total Experimental Duration of 8hours 15mins (100 frames)

Data sets were gathered of wild-type yeast with genomically integrated mNeonGreen-PTS1 expressing downstream of the TPI promoter in both green and brightfield channels at 100x magnification.

5.2 Data Acquisition and Handling

S. cerevisiae cells expressing genomically integrated mNeonGreen-PTS1 were imaged in the chamber within the flow cell (Chapter 2.9.4) using the parameters described in the previous section. A function of the microscope called ‘Positions’ allowed for the imaging of several different places in the cell chamber in one experiment. Nine positions were assigned and imaged. The images of each of these positions were then examined for groups of cells whose lineage could be traced back to one or two cells in the first few frames. This was so that their peroxisomes could be followed more easily using the TrackMate plugin. The parts of the images containing these clusters were excised from the larger images so that they were easier to work with (Figure 5.2). Table 5.1 shows the five clusters that will be analysed in Chapter 6 and which position they originated from. It also gives the filename of the time-lapse video which can be accessed in the external media for reference. Later

Table 5.1. Image data acquired, assigned name in analysis and filename in external media.

Position in Acquisition	Cluster Name in Analysis	Filename in External Media
Position 1	Cluster 3	Cluster3.avi
Position 2	Cluster 2	Cluster2.avi
Position 3	Cluster 1	Cluster1.avi
Position 4		
Position 5	Cluster 4	Cluster4.avi
Position 6		
Position 7		
Position 8		
Position 9	Cluster 5	Cluster5.avi

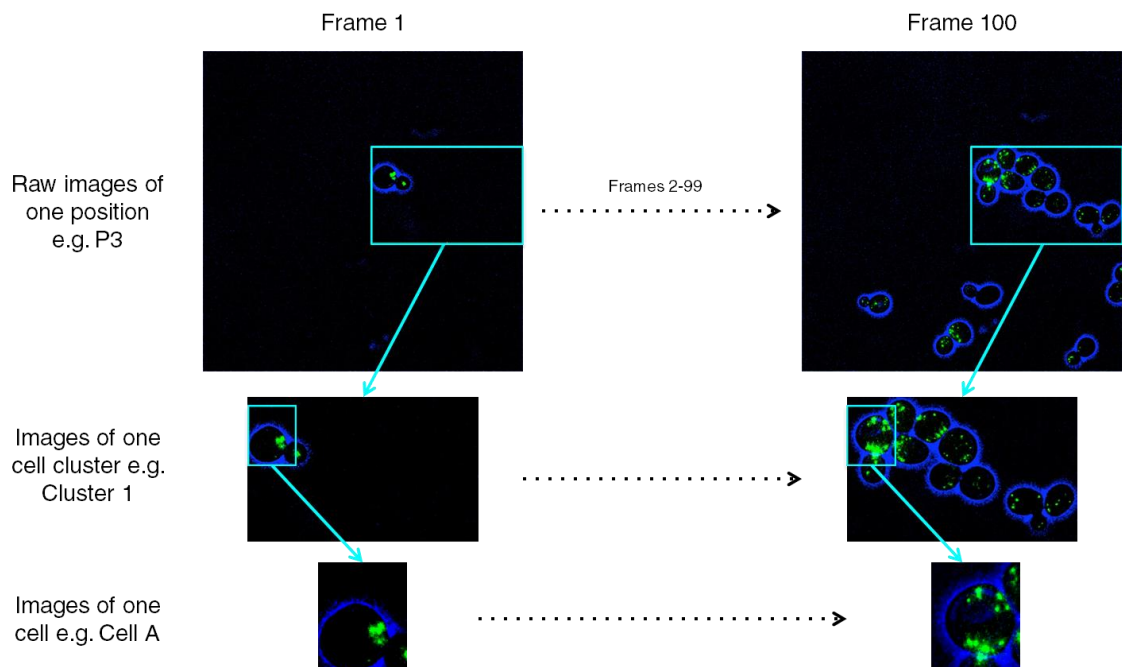


Figure 5.2. Acquisition and cropping of data. Nine positions were assigned and imaged. The images from each of these positions were examined for clusters of cells whose lineage could be easily followed. This example shows image data from position 3. These clusters were then cropped from the original raw images, and assigned names e.g. Cluster 1. In the following sections of this chapter, a cropped area of Cluster 1 containing only one cell, Cell A, the original mother cell present in frame 1, will be used to evaluate the TrackMate algorithm and peroxisomal behaviour.

in this chapter, Cell A from Cluster 1 is excised from those images so that the behaviour of the peroxisomes could be examined in detail.

Not every position had suitable clusters of cells that could be followed relatively easily over the whole course of the experiment. The names of the clusters were assigned based on the order in which they were analysed.

5.3 Analysis of the Images

The computational analysis of these cell clusters was done using the TrackMate plugin in FIJI for peroxisomes and cell definition was performed separately by manually outlining cells (described in Chapter 4.5).

Peroxisome Detection in TrackMate

The parameters set for the detection stage of the TrackMate algorithm (see 4.5.2, Object Detection) varied slightly on the cell cluster being analysed to account for the relative intensities of the peroxisomes in each cluster. Although the purpose of the genomic integration of the mNeonGreen-PTS1 was to give a more uniform level of expression, which it does, variability in peroxisomal intensity still exists, especially between the peroxisomes in the older and younger cells in a population (as peroxisomes accrue fluorescent protein over time). Therefore, the threshold of detection was set on a case-by-case basis. The maximum radius was set at between 0.5 μ m and 0.65 μ m, again to allow for differences in peroxisomal intensity. Judging whether the parameters were correct was an empirical undertaking and was based on whether all the peroxisomes in a few frames were being detected correctly, without the algorithm identifying areas of noise as peroxisomes. An assessment of detection of peroxisomes by TrackMate is performed in section 5.6.

Peroxisome Linking into Tracks in TrackMate

For the tracking stage of the TrackMate algorithm (see 4.5.2, Object Linking), the maximum distance the algorithm could link two objects was set at 5 μ m. This is based on the observations in Knoblach et al., 2013 regarding movement speed of peroxisomes; in their Figure 7D, peroxisomes are documented as having movement speeds from 0nm/s to in excess of 30nm/s. Therefore, with the 5-minute sampling frequency used here, a peroxisome could feasibly move over 10000nm (10 μ m). This is much larger than the average diameter of a fully-grown yeast cell of around 5 μ m. Given that a peroxisome could theoretically move the entire diameter in between frames, setting the maximum distance as the average *S. cerevisiae* cell diameter seemed reasonable. This accommodated for the (probably rare) possibility of a peroxisome moving from the far side of a mother cell into a newly forming bud.

The maximum number of frames that the algorithm could search over (for the ‘gap closing’) was set at 5. The reasoning behind this was to give provision for when peroxisomes are

initially moved into a newly forming bud cell where they cannot be distinguished against each other. Within the tracking, the algorithm was directed to give greater weight to creating linkages between peroxisomes that had similar total intensity or position in Z.

Cell Outlining

The cells in each cluster were manually outlined to give good definition between cells and newly forming buds and allow for analysis of peroxisomal number and distribution on a cell-by-cell basis (4.5.3). Peroxisomes were matched to cells using a Python program written for that purpose (4.5.4).

The remainder of this chapter documents in detail the behaviour of peroxisomes in one budding cell (Cell A) in Cluster 1. This is to examine the accuracy of the detection and then linking of peroxisomes into tracks by the algorithm over the course of what should be a particularly active part of the cell cycle as the peroxisomes are divided and moved into the daughter cells. It is also an exercise to see what kind of descriptions can be placed on the movement of peroxisomes when they are scrutinised in much detail. Section 5.9 outlines the conclusions from the analysis of this data with respect to the claims put forward in the KPPC model.

5.4 In-depth Analysis of One Cell

One cell in Cluster 1 was selected for an in-depth analysis. This cell, Cell A, is the original mother cell from which the rest of the cells in the cluster derive (bottom panel, Figure 5.2, Figure 5.3). Cell A budded a total of 6 times over the course of the experiment. Another 6 buddings occur between the daughter cells, and 3 cells move away from the cluster due to the action of the flow, so there are 10 cells in total in the final grouping (Figure 5.3).

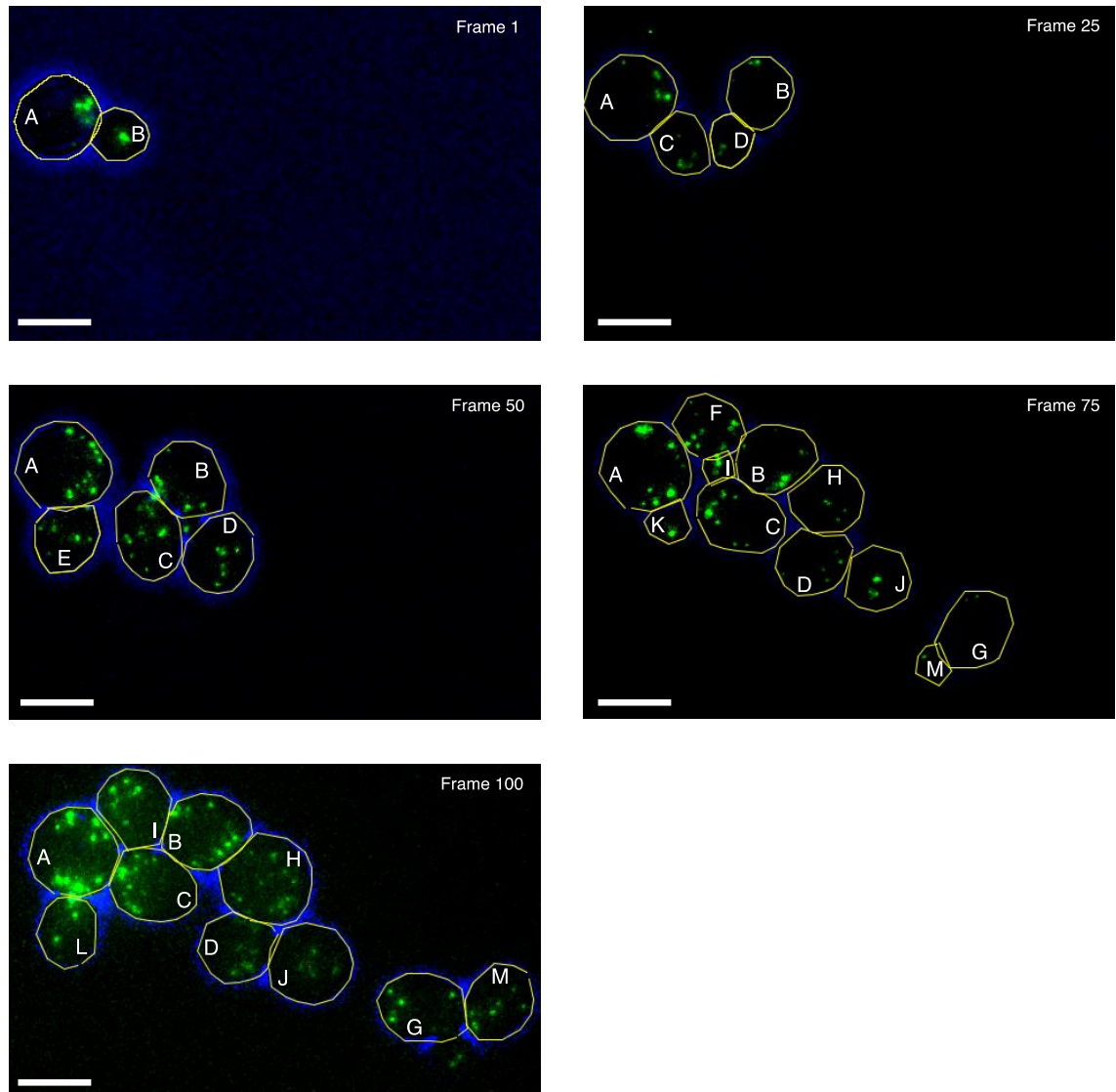


Figure 5.3. Progression of the growth of Cluster 1 from the original mother cell (“Cell A”). Total experimental duration is 8 hours 15 minutes. All cells are derived from Cell A (lineage is shown in Table 6.1). Letter labelling is based generally on when cells originally appeared. Notice that Cell E is absent in frame 75 and 100, and Cell F and K are absent in frame 100. They were moved away due to the action of flow in the flow cell after separating from their respective mother cells.

Peroxisomal channel is green and is a maximum intensity projection. Brightfield image has been coloured blue and is the central slice from the Z stack of images. Manual cell outlines are in yellow. Per channel, the brightness and contrast of the images has been adjusted manually. No other processing has been performed on these images. Scale bar indicates 5 μ m.

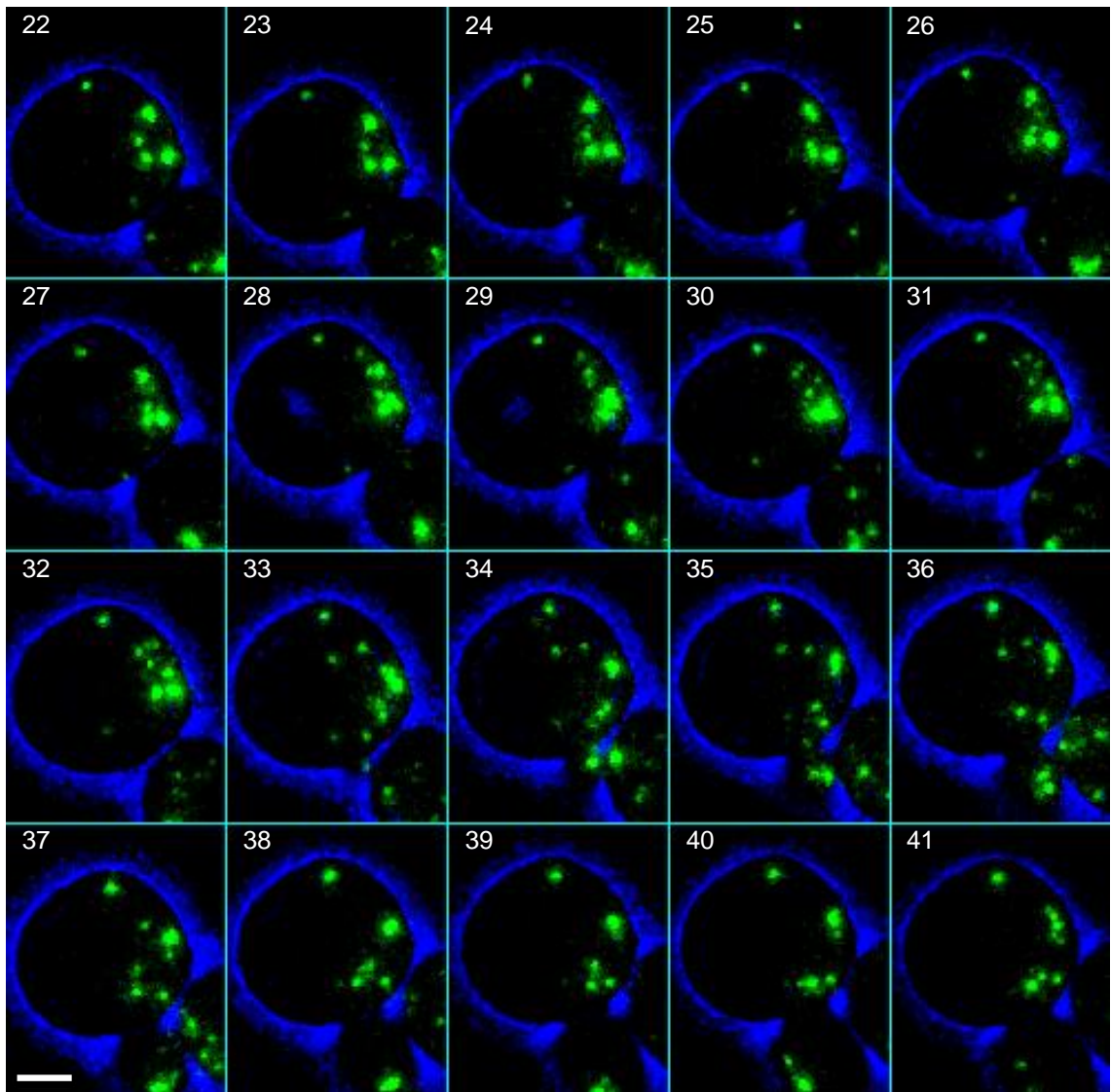


Figure 5.4. Montage of Cell A between frames 22 and 41. During this period the cell is finishing one budding event and starting another. The peroxisomes are mobile over this duration and the number in Cell A fluctuates between six in frame 22 and nine in frame 31. Processing and display of this montage is the same as for Figure 5.3. All 100 frames of this montage are included as Appendix G.

Instead of trying to comprehend all the peroxisomes across the 100 frames for this cell and its buds, an in-depth analysis was performed of the movement of peroxisomes in Cell A over only a small section (frames 22-41) of the entire experimental duration. This was chosen due to the marked difference in the peroxisomal arrangement over the course of the twenty frames, and covers the end of a budding and the start of another (Figure 5.4). During this period, Cell C is just finishing budding off from Cell A, and the bud Cell E starts forming about halfway through.

5.4.1 Evaluation of Peroxisome Detection and Tracking in One Cell

By overlaying the detected TrackMate objects on to the peroxisomal data, one can start to get a sense of how accurate or otherwise the plugin was at a) detecting peroxisomes and b) linking peroxisomes into tracks. Understanding this is key to evaluating to what extent the KPPC model can be addressed using these methods. This evaluation is done with reference to Figure 5.8 that shows a five-page frame-by-frame breakdown of frames 22-41. An example of one of these frame-by-frame breakdowns is shown in Figure 5.5.

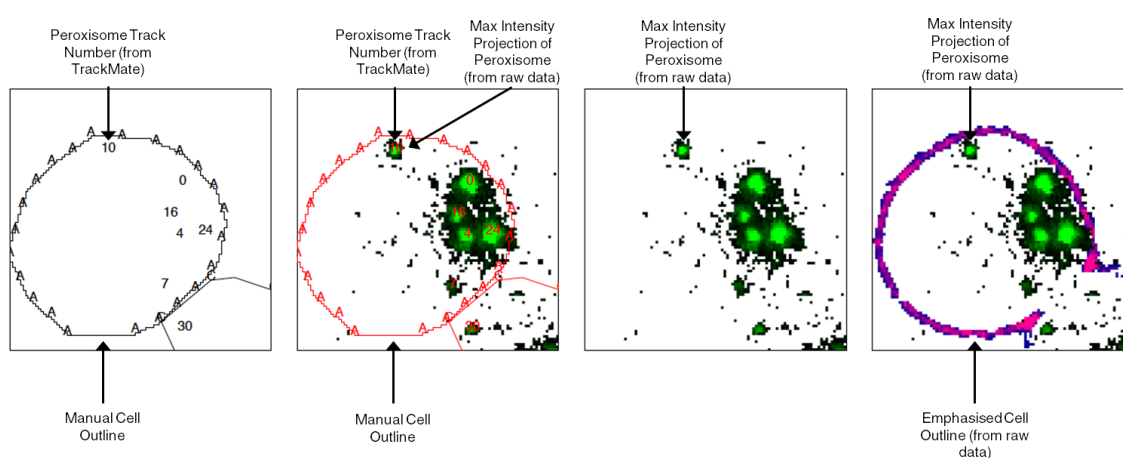


Figure 5.5. Example of frame-by-frame breakdown used to evaluate peroxisome tracking ability of the TrackMate algorithm. Left) Manual cell outlines, with cell identifier around the edge, and the track identifier that peroxisome has been assigned in TrackMate. Centre Left) Same as previous panel but with the overlay of a maximum intensity projection of peroxisomes. Centre Right) Maximum intensity projection of peroxisomes. Right) Brightfield image with cell outline emphasised in red, overlaid with the maximum intensity projection of the peroxisomes.

The track identifier used in these images is the track number that a particular peroxisome has been assigned to in that particular frame, and is referred to in the text below to distinguish individual peroxisomes in frames. It is important to realise that the track ID does not consistently identify the same peroxisome from frame to frame (although that is clearly one of the aims of this exercise) – a peroxisome labelled ‘50’ in frame X may not actually be the same peroxisome as the one labelled ‘50’ in frame Y. The reasons for this will be discussed in section 5.6.

5.5 Peroxisome Detection

Evaluating to what extent any algorithm detects all the objects that one wishes it to is either done by a comparison to a manual examination of the data (i.e. computer attempt vs. human attempt) or by creating simulated data when one already knows the number of objects that the algorithm should detect. When evaluating the ability of the TrackMate algorithm to detect peroxisomes in this data, it is done by comparison with a manual examination.

Across the twenty frames analysed in detail here, the TrackMate plugin had detected 151 objects in Cell A and its bud, Cell E. The following section describes instances when peroxisomes identified by eye were missed by the algorithm; instances when the algorithm had erroneously detected peroxisomes; and cases when the situation was ambiguous.

Missed Peroxisomes Identifiable by Eye

After examination by eye, there were eight peroxisomes that were readily visible yet not picked up by the TrackMate plugin: one in each of frames 26 and 33, and two in each of 34, 35 and 41; these are highlighted with magenta circles on the peroxisomal only image of the relevant frame in Figure 5.8.

The peroxisome in frame 26 that TrackMate failed to detect is clearly the same peroxisome labelled '10' in the preceding and succeeding frame, it does not appear to have become smaller or reduced in intensity; it is therefore not clear why TrackMate has failed to pick this up. In frame 33, the peroxisome not detected by TrackMate is on the boundary between Cell A and its bud Cell E, its appearance is similar to the peroxisome labelled '39' in the same frame; it is therefore unclear why this peroxisome is detected and the other peroxisome is not.

In both frames 34 and 35, a peroxisome can be seen in the 6 o'clock position of Cell A and is likely the same peroxisome as the lone one detected in the area in the previous frame ('39' in frame 33), but has now fallen below the threshold level for detection. A different peroxisome can be seen straddling the Cell A/Cell E border in frame 34 (directly above peroxisome '30'), and another is to the left of peroxisome '42' in frame 35. These are likely the same peroxisome, and also presumably the same one as the one not detected by TrackMate in frame 33 that has progressed from the edge of Cell A and into Cell E. In both instances it might be too faint to be detected against the other larger peroxisome in its vicinity, or has been counted as part of that peroxisome.

Lastly, in frame 41 there are two peroxisomes that are visible to the eye that are not detected by TrackMate. One is at the 1 o'clock position of the peroxisome labelled '7'; the other is in Cell E above the peroxisome labelled 42. It is unclear why the algorithm has not picked up the peroxisome next to '7'. The other peroxisome is very faint to the eye.

Erroneous Detection

There is one instance where the TrackMate algorithm has detected an object that is not visible to the eye – the '16' in frame 31. On close inspection there is not a definitive peroxisome present there, or at least something resembling a peroxisome that is distinct enough from the other three peroxisomes in close proximity.

Ambiguous Peroxisomes Identifiable by Eye

A distinction has been made here between peroxisomes that are 'missing' with respect to their detection by the algorithm, and those that are ambiguous. These instances of 'ambiguous' peroxisomes are situations where the algorithm detected no peroxisome but there is some suspicion that perhaps there are more peroxisomes present. These are not as clear-cut as the 'missing' peroxisomes however, and are indistinct to the eye as well. Instances of this can be seen in frames 29, 30, and 33; there are areas of intense signal that actually consist of more individual peroxisomes than TrackMate has detected. Blue filled circles have been added to the peroxisomal only images in these frames in Figure 5.8 to show how the larger objects could possibly be broken down into other peroxisomes.

Using the 3D projection feature of FIJI allows one to view the stack of images from different angles. Viewing these frames in the YZ direction can allow for more detailed dissection of the images. This has been performed for frames 28-30 (Figure 5.6), and frames 32 and 33 (Figure 5.7).

In frames 29 and 30, TrackMate has identified two peroxisomes as part of a particularly intense area of signal. Examination of an YZ projection of these frames shows that this area of high intensity can be broken down further. In the previous frame, 28, there are five peroxisomes in the same area, and they can be distinguished in the maximum intensity projection and in the YZ direction (see Figure 5.6). In frame 29, looking at the maximum intensity projection both '0' and '16' have disappeared. Looking in the YZ direction, it appears that the peroxisome that was labelled '0' has moved into close proximity to peroxisome '24' and therefore become indistinguishable to the TrackMate algorithm and by

eye using a maximum intensity projection (central panel Figure 5.6). This situation continues in frame 30. It is very difficult to see another peroxisome in this high intensity area. It is possible that the peroxisome ‘16’ is also part of this high intensity area, or it may have moved into the bud (it is possibly peroxisome ‘30’ in frames 29 and 30). It is impossible to give a definitive answer in this instance.

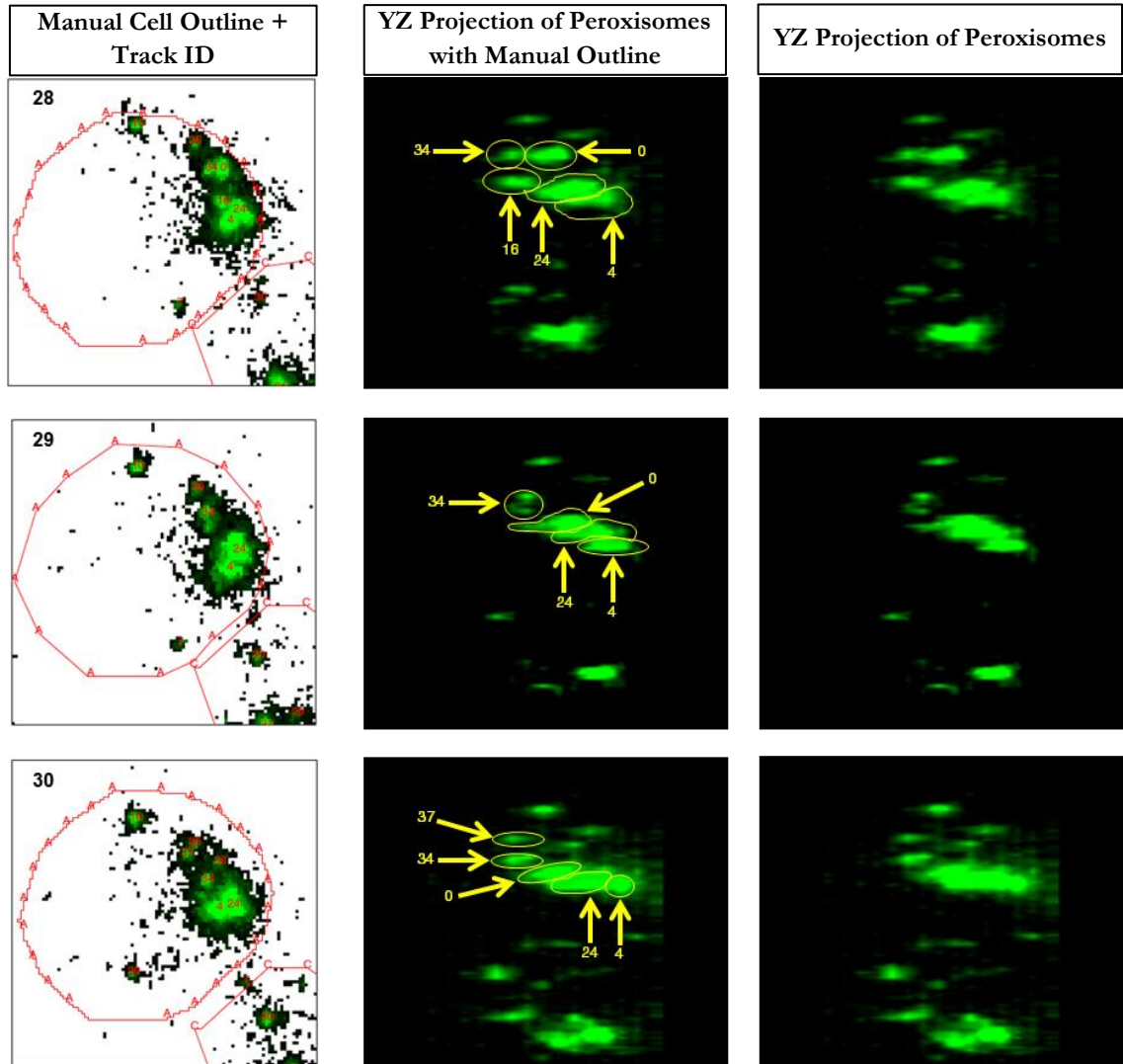


Figure 5.6. YZ projection of frame 28-30. The images on the left are the maximum intensity projections of the peroxisomes overlaid with the manually defined cell outline. The central image is an YZ projection of the peroxisomal images across the 15 slices with manually outlined peroxisomes. The original Z direction is on the X-axis, going from the 1st slice on the left to the 15th slice on the right; the Y-axis is the same (we are looking down the X-axis). FIJI has interpolated the images to fill in the gaps between the slices to make the image appear 3D. Image on the right is the same as the middle without manual outlines overlaid. Note how elongated peroxisomes appear in Z – this is due to the signal from peroxisomes being spread over several Z slices.

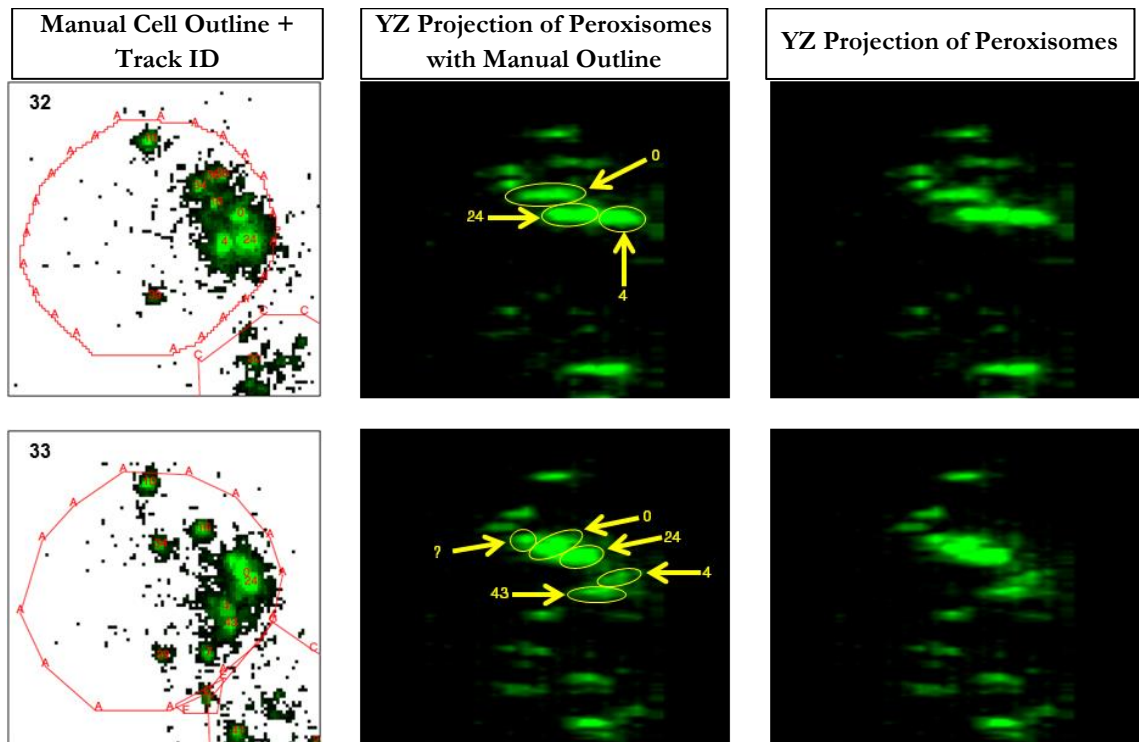


Figure 5.7. YZ projection of frames 32 and 33. The order of the images is the same as Figure 5.6. The putative peroxisome labelled ‘?’ in frame 33 is not seen in previous or subsequent frames so it is unclear whether it is a bona fide peroxisome or not.

In frame 33, the area of high intensity could also contain another peroxisome that TrackMate has not accounted for (Figure 5.7). This could be a peroxisome forming off from ‘0’, as the other peroxisomes present in frame 32 are accounted for. It is possible that the object in frame 33 is the peroxisome ‘16’ from frame 32 that has moved closer to ‘0’, and that the peroxisome labelled is ‘16’ in frame 33 is not the same one as in frame 32. However, as most of the peroxisomes have moved a great deal in between frames 32 and 33, and the fact that this putative peroxisome cannot be seen in a YZ projection of frame 34 (not shown), its status remains unresolved.

Summary of Peroxisome Detection

On the whole, the detection of the TrackMate plugin is nearly as good as a manual inspection - the few peroxisomes it failed to detect were faint or in close proximity to other more intense peroxisomes; the other cases that were ambiguous were also difficult to distinguish by eye. It detected 151 particles in total in Cells A and E, of which one was erroneous, and missed eight others. This information is summarised in Table 5.2.

One thing to take away from this table is that the total number of peroxisomes detected for Cells A and E together is not consistent – even taking into account peroxisomes that the

algorithm missed and cases of ambiguous peroxisomes. This can partially be explained by peroxisomes in the bud not being visible against each other due to the smaller volume, at least at first. Otherwise, it indicates that peroxisomes often move close enough to each other that they can no longer to distinguished either by the computer or by eye.

	Frame																			
	22	23	24	25	26	27	28	29	30	31	32	33	34	35	36	37	38	39	40	41
Total Number of Peroxisomes Detected By TrackMate in Cell A	6	6	6	6	6	7	8	6	8	10	9	9	7	8	7	7	5	6	5	6
Total Number of Peroxisomes Detected By TrackMate in Cell E													1	1	2	2	1	2	2	2
Additional Peroxisomes Visible By Eye					1							1	2	2						2
Erroneous Peroxisomes										-1										
Ambiguous Peroxisomes								1	1			1								
Total Number of Peroxisomes in Cell A and Cell E	6	6	6	6	7	7	8	6-7	8-9	9	9	10-11	10	11	9	9	6	8	7	10

Table 5.2. Summary of TrackMate’s detection of peroxisomes in Cells A and E across the twenty frames examined in detail (Figure 5.8). Included are any peroxisomes that are visible to the eye that TrackMate has not detected, one case of a peroxisome being identified where there is none, and cases of ambiguous peroxisomes. Then there is an estimate based of the total number of peroxisomes existing in both of the cells based on those numbers. Cases of missing peroxisomes, the erroneous peroxisome and ambiguous peroxisomes are discussed in the text.

Figure 5.8. (following 5 pages). Frames 22-41 of Cell A in Cluster 1. Figure 5.5 describes what each panel from left to right is displaying. Hollow magenta circles on peroxisomes-only images show peroxisomes that the TrackMate Plugin has missed but are visible to the eye (frames 26, 33, 34, 35 and 41). Blue circles on peroxisomes-only images show instances when the number of peroxisomes is ambiguous (frames 29, 30 and 33).

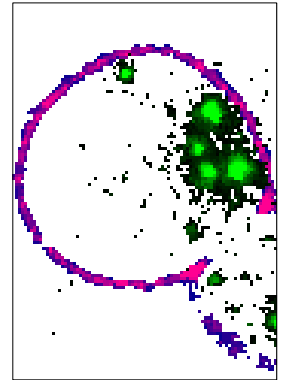
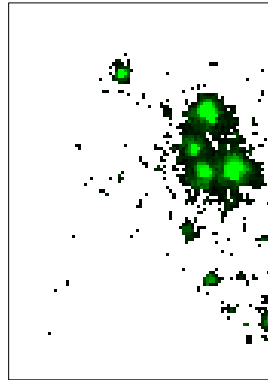
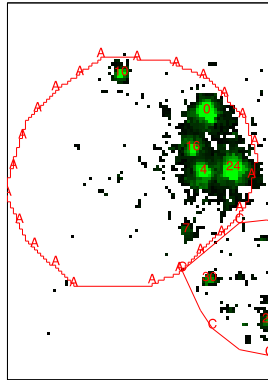
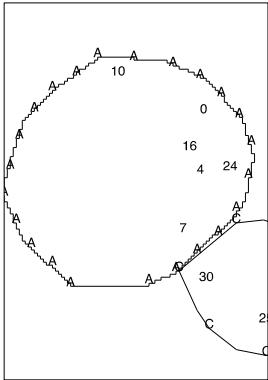
Manual Cell Outline +
Track ID

Cell Outline + Track
ID + Peroxisomes

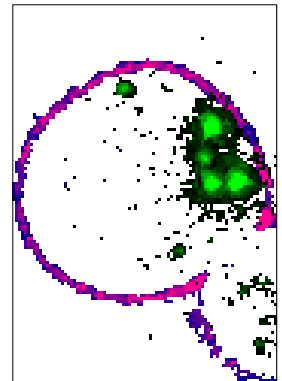
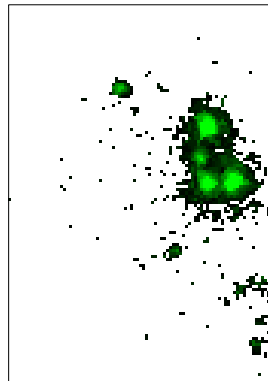
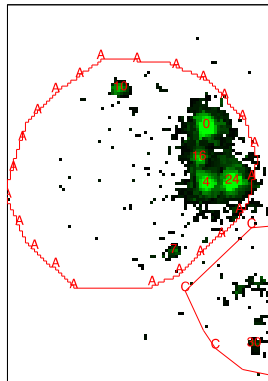
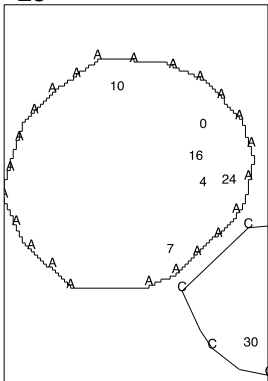
Peroxisomes Only

Brightfield Cell
Outline + Peroxisomes

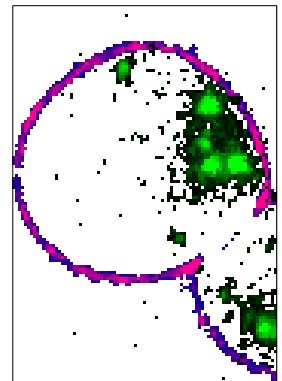
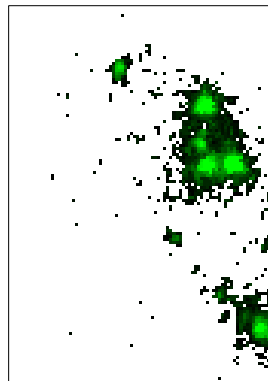
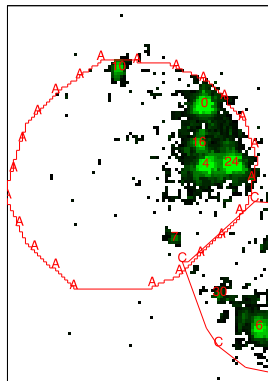
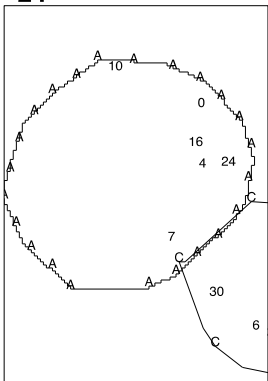
22



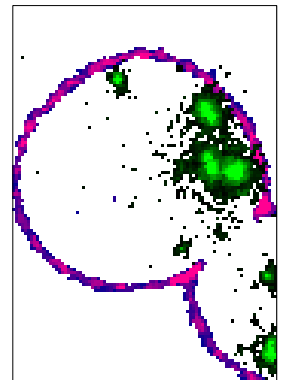
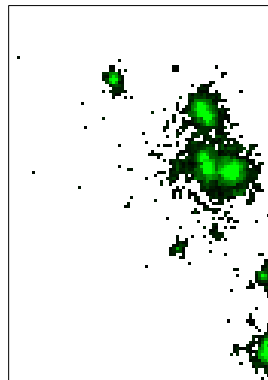
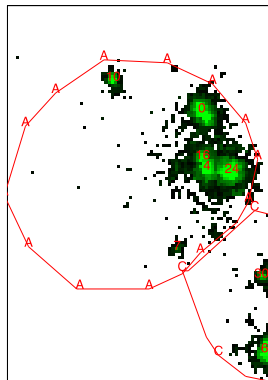
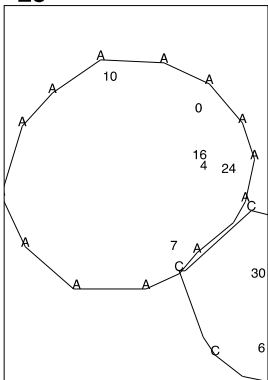
23

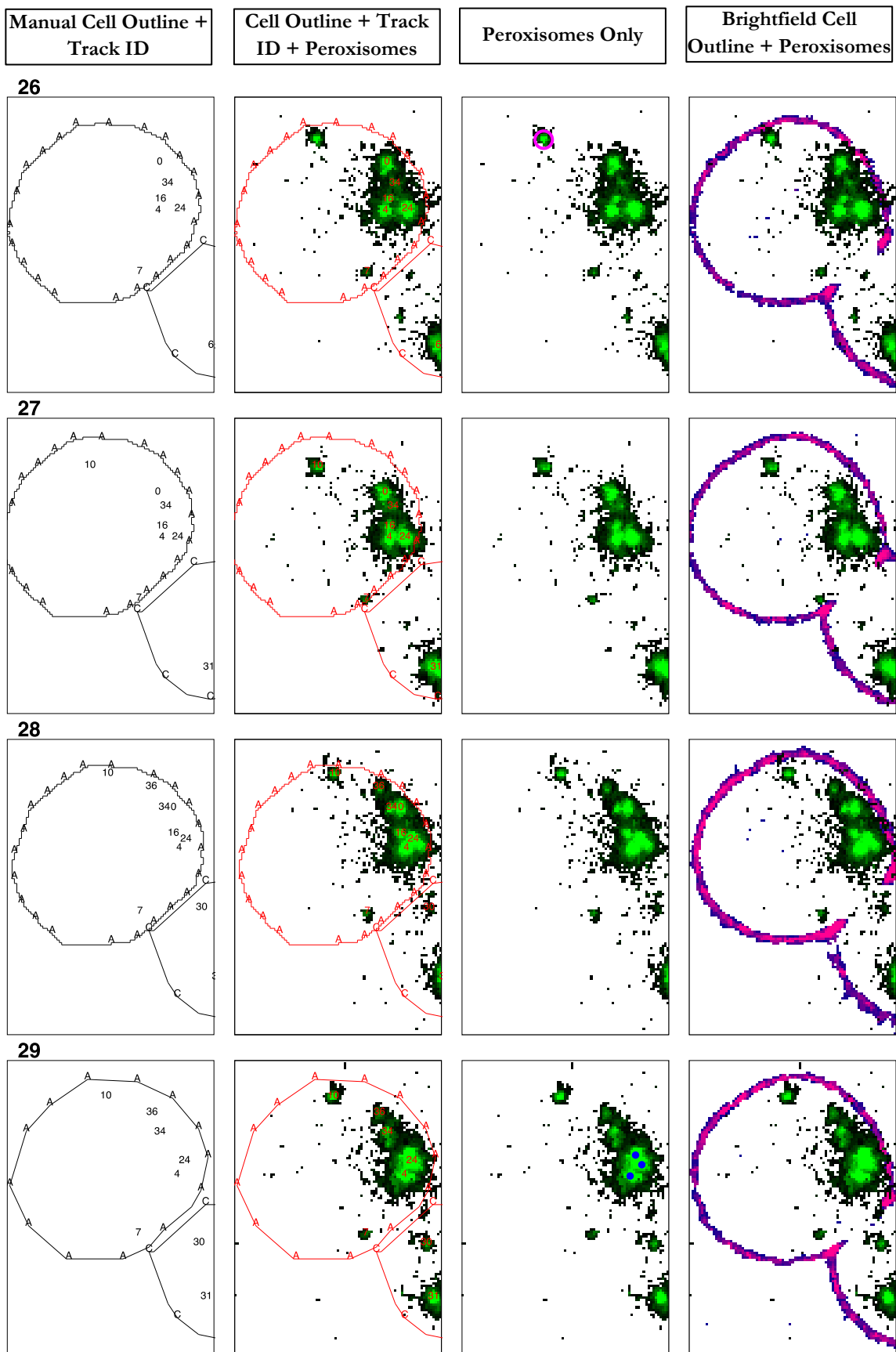


24



25





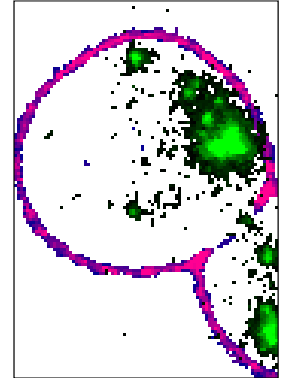
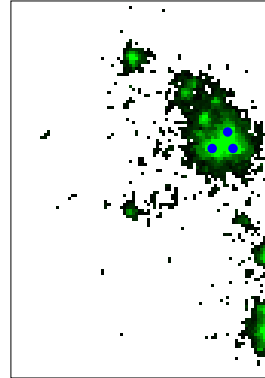
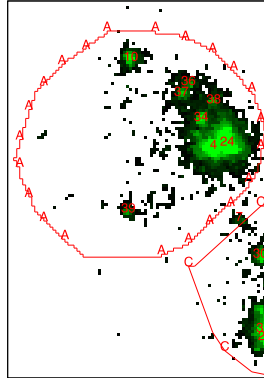
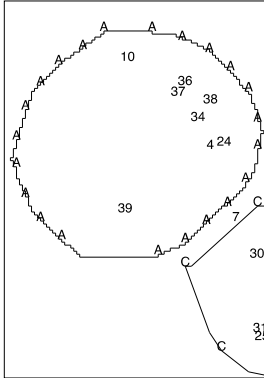
Manual Cell Outline +
Track ID

Cell Outline + Track
ID + Peroxisomes

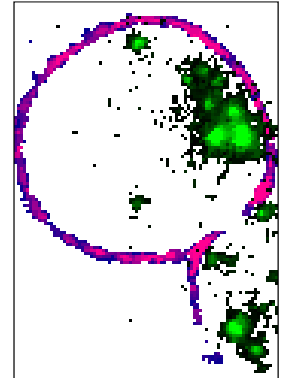
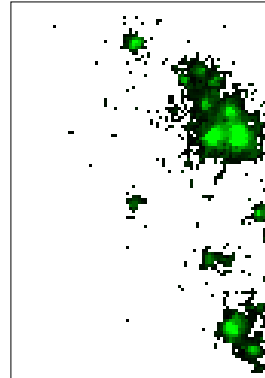
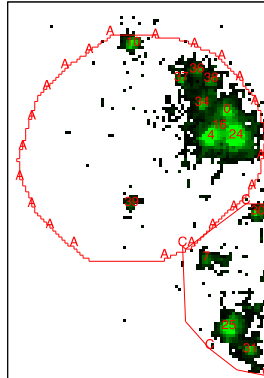
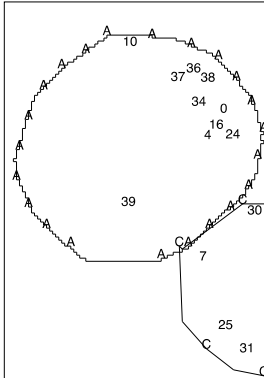
Peroxisomes Only

Brightfield Cell
Outline + Peroxisomes

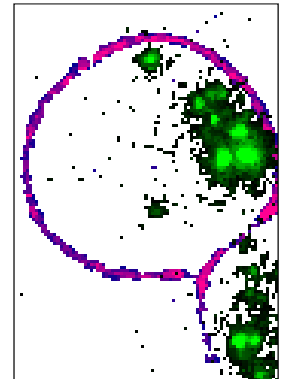
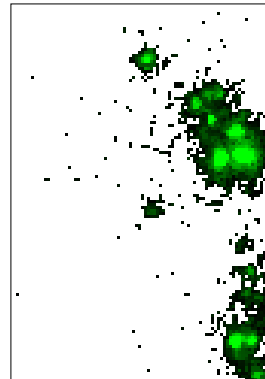
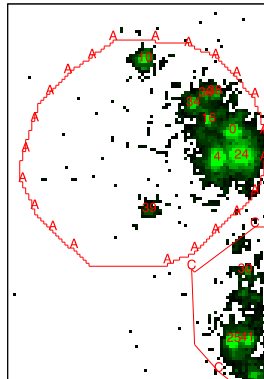
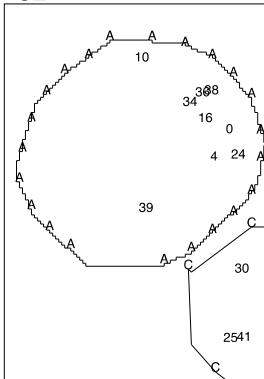
30



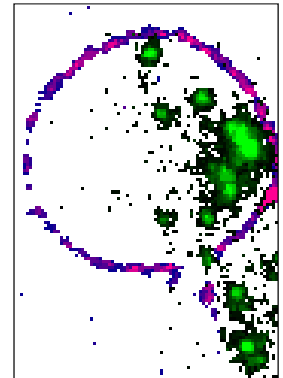
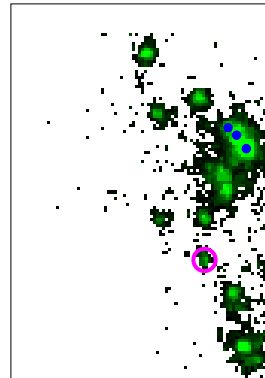
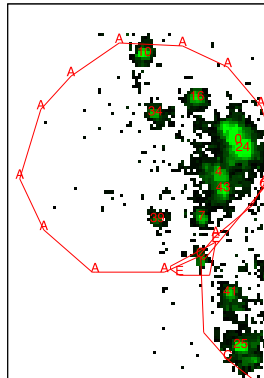
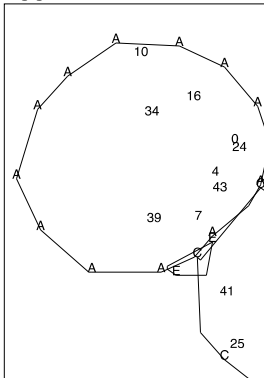
31



32



33



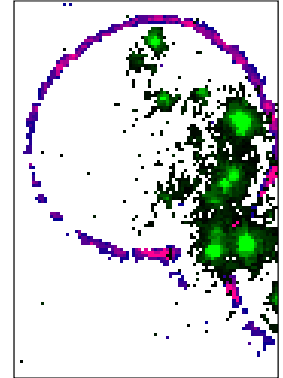
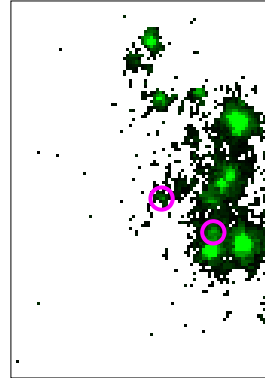
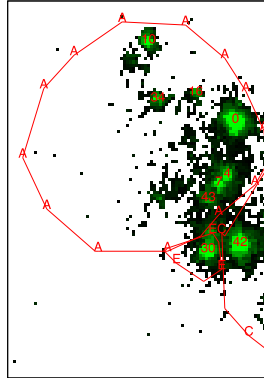
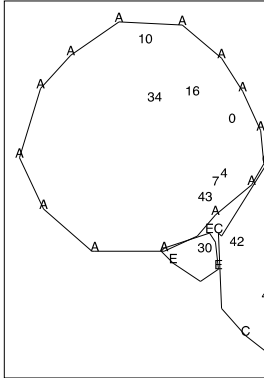
Manual Cell Outline +
Track ID

Cell Outline + Track
ID + Peroxisomes

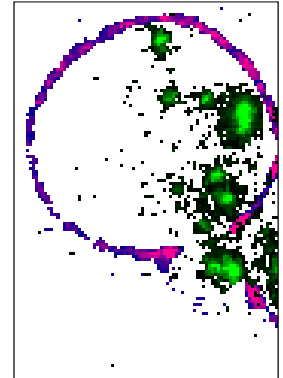
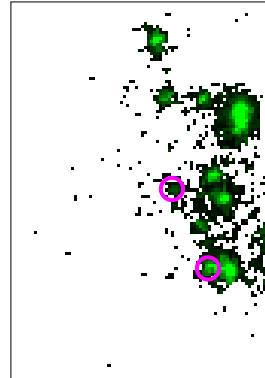
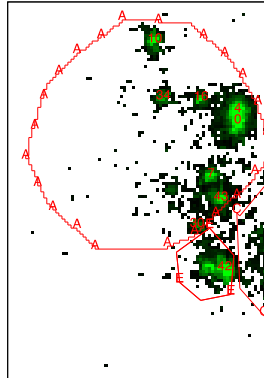
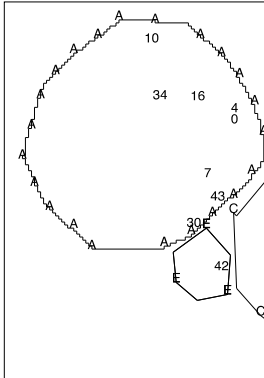
Peroxisomes Only

Brightfield Cell
Outline + Peroxisomes

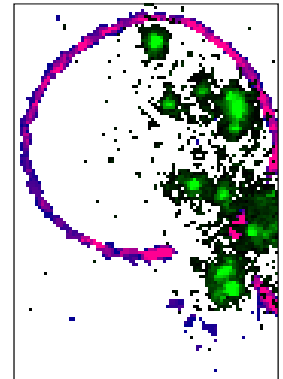
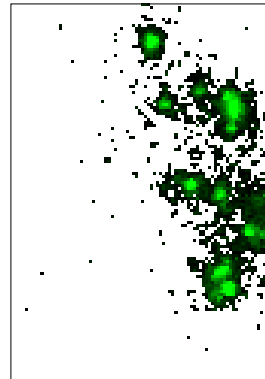
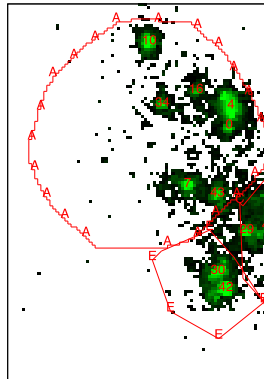
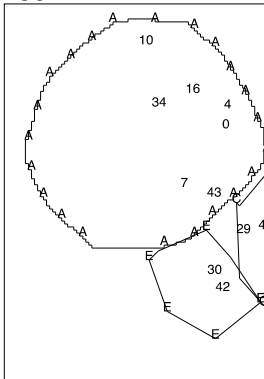
34



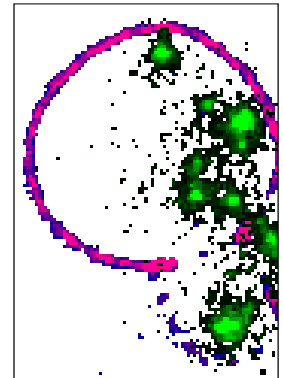
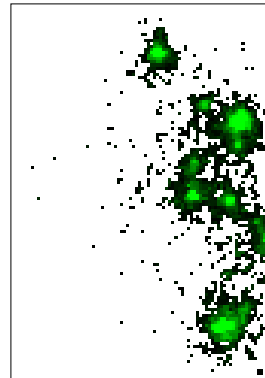
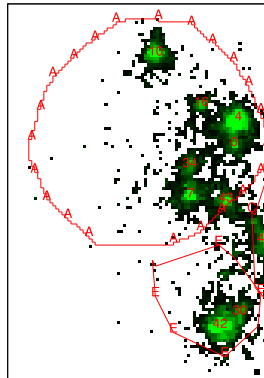
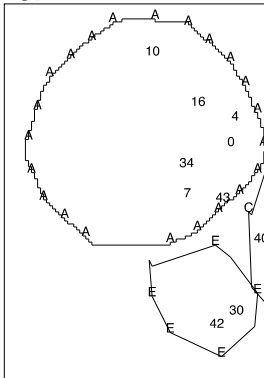
35

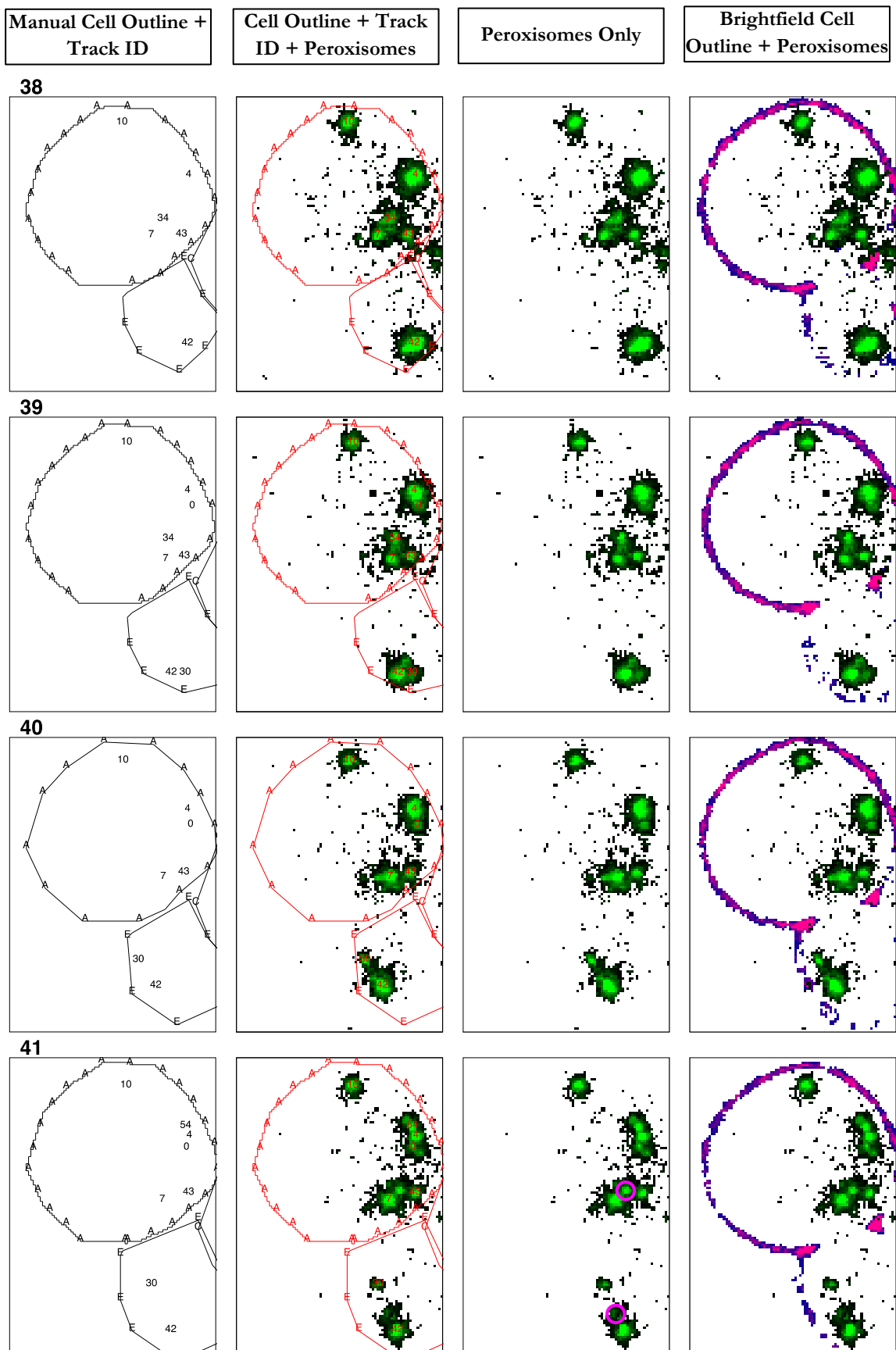


36



37





5.6 Peroxisome Tracking

The tracking via the TrackMate plugin assigned the 151 detected objects to 14 different tracks in Cell A and its bud Cell E over the twenty frames analysed in detail here. Evaluating the tracking requires a very focused frame-by-frame scrutiny of Figure 5.8. Examining where the tracking algorithm got it correct or incorrect also gives some insight into peroxisomal behaviour and the challenges of following peroxisomes using this data.

Recording the information from such an evaluation is a challenge and as such the following section is a dense, written account of the tracking from frame to frame. It is written in the style of a ‘field notebook’ and as such is not structured to be ‘read through’ like the remainder of this study. Tables 5.3 and 5.4 highlight the comparison between the tracks produced by TrackMate (Table 5.3) and a manual attempt to follow each peroxisome using the TrackMate track numbers (Table 5.4). All the findings of the section are summarised at the end in section 5.6.2. A video of this can also be accessed in the external media with the filename “Cluster1_CellA.avi”.

In the following section, each peroxisome is referred to by its track identifier. If a manual interpretation suspects that there have been some changes of the track identifier for the same peroxisome from frame to frame, this is documented. Also described is when a peroxisome has been detected in one frame and is no longer detected or distinguishable in a subsequent frame. Reasons are given in the text for when the author believes that the tracking has got the situation incorrect from one frame to the next, and also reasons for when peroxisomes can no longer be distinguished. It may be useful to refer to Table 5.4 if reading through the following section, as it summarises the events.

5.6.1 “The Private Life of Peroxisomes” - Tracking Peroxisomes in Cells A and E over Twenty Frames

Frames 22-27

For the first couple of frames of this analysis, there is not much movement of peroxisomes or any peroxisome proliferation until the appearance of the new peroxisome labelled as ‘34’ in frame 26, which appears to have split from the peroxisome ‘0’. The same peroxisomes appear to be consistently tracked over the course of these frames.

Frame 28

In this frame a new track is started by the presence of another new peroxisome ('36'). However, it is unclear whether this peroxisome '36' is actually the peroxisome labelled '34' from frame 27 that has shifted position, or whether it is another new peroxisome that has split off from '0'. If peroxisome '36' is actually the '34' from the previous frame then the '34' in this frame appears to be another new peroxisome.

Frame 29

There has been some activity between this frame and the last. The peroxisome that was '0' in frame 28 has moved closer toward '24'; it was not identified by TrackMate and is not readily visible to the eye but can just about be made out in XZ projections (as discussed above; see Figure 5.6). In addition, the peroxisome labelled '16' in the same area from frame 28 is absent in frame 29; it cannot really be distinguished separately from the other peroxisomes in the area of high intensity which appears to contain the peroxisome '0', as discussed earlier. It may have moved into Cell C; it could conceivably be the peroxisome '30' visible in the bottom right corner of the frame. That peroxisome labelled '30' is very faint in frame 28, and is twice as intense in frame 29. As said earlier, this situation proved impossible to untangle.

This highlights a major issue in that sometimes both the tracking and some manual intervention in this case could not unpick the complexity of the situation. The tracking for peroxisomes '4', '24', '34' and '36' remains consistent with the previous frame.

Frame 30

In frame 30, there are three new track identifiers: '37', '38', and '39'. Two of these are labelling new peroxisomes that have formed since the last frame was taken.

What are the origins of these two peroxisomes? At first glance on the maximum intensity projection image, it appears that the peroxisome labelled as '37' is a new peroxisome formed via fission of peroxisome '36' given their proximity in XY. However, when looking in the XZ direction (bottom set of panels, Figure 5.6), it makes much more sense that the peroxisome '37' has split from peroxisome '34' as they are both in the same plane in Z. This implies that peroxisome '38' therefore has split from peroxisome '36'; this is supported by the fact that they are also alike in terms of position in Z.

Elsewhere in the frame, the algorithm believes that the peroxisome '7' has now moved into Cell C in the bottom-right corner of frame 30. The new identifier '39' has been added to frame, labelling a peroxisome that is in the same location as the peroxisome labelled as '7' in frame 29. This interpretation by the computer seems highly unlikely to be true. It seems more probable that the peroxisome labelled as '39' is the same one as the peroxisome labelled as '7' in the previous frame, rather than it being a new peroxisome that has moved to occupy the same space.

As for the peroxisome that has been labelled '7' in Cell C in this frame it is unclear where it comes from; it is either the product of another fission event in Cell A that has occurred between frames and has just been moved into the bud, or it could also just be a peroxisome already present in the bud becoming distinguishable. The former scenario is unverifiable at this temporal resolution; the latter is a reasonable assumption but not one investigated as part of this analysis.

This confusion with the tracking arises due to the TrackMate algorithm attempting to link objects over a relatively long distance; as already mentioned in section 5.3, the possibility exists that peroxisomes can move fairly far between frames. However, the consequence of this is that the number of objects that the algorithm is comparing in frame N+1 to find the best match with the original in frame N is drawn from a larger pool. Complicating matters is the fact that the algorithm knows not of where the cells are placed – as far as the tracking is concerned the peroxisomes are objects that could move around freely anywhere in 3D space within the user-defined distance.

Frame 31

In frame 31, the old track identifiers '0' and '16' have reappeared, but as has already been described in 5.5, there does not appear to be a peroxisome where the algorithm has identified the peroxisome '16'. The peroxisome labelled '0' is the same one that was labelled '0' back in frame 28 and has now moved away from peroxisome '24'. This is a good example of a difficult situation when a peroxisome could not be identified for several frames but nonetheless the tracking algorithm correctly acknowledged that they were the same object and linked them. The tracking of the other peroxisomes appears consistent with the previous frame. Cell C finishes budding from Cell A sometime between the end of this frame and the start of frame 32.

Frame 32

In frame 32, manual inspection reveals that the tracking algorithm has confused some of the peroxisomes. Presuming that the peroxisomes have maintained roughly the same relative XY position to each other between the frames, the tracking algorithm has relabelled the peroxisome '37' from frame 31 as '34' and the peroxisome that was identified as '34' in frame 31 is now '16'.

This is an example of peroxisomes of that have similar intensity being confused for one another. It also highlights a sort of 'compound' error that can occur; the previous object labelled as '16' (in frame 31) was not really a peroxisome, yet it is included in the objects that the algorithm is trying to find a corresponding link for in this frame. The cumulative effect of this is to cause the algorithm to misidentify two objects in this frame.

Frame 33

The tracking situation from frame to frame becomes increasingly harder to interpret. This is due to the large amount of movement of peroxisomes between frames 32 and 33; this activity coincides with the formation of a new bud ('Cell E').

The new track '43' has been added to show a peroxisome that has split off from '4', which itself has moved slightly. The group of four smaller peroxisomes in the 2 o'clock position of Cell A from frame 32 have since scattered. In this frame, the algorithm maintains that the peroxisomes that are marked '16' and '34' are the two to have remained in the top half of Cell A. To investigate whether these were the same peroxisomes as the '16' and '34' in the previous frame, and not either '34' or '39', some manual inspection of 3D projections of frames 32 and 33 was carried out. Based on their Z position, it did appear likely that the two peroxisomes labelled as '16' and '34' in this frame were the same two as in frame 32. However, it is harder to discern whether the algorithm has labelled them the correct way around. It is perhaps more likely that one of the peroxisomes remained stationary ('34' in frame 32; '16' in frame 33) and the other one moved, rather than both peroxisomes moving and '16' in frame 33 ending up where '34' was in frame 32. If this is indeed the case, then the peroxisome '34' in this frame is likely to be the peroxisome labelled as '16' from frame 32, and the peroxisome now labelled as '16' is actually the peroxisome '34' from the previous frame (because it has remained stationary). This is the accepted situation for Table 5.4.

The peroxisomes labelled '36' and '38' from frame 32 are unaccounted for in this frame. However, the track identifier '7' has reappeared; it is evidently not the same peroxisome that was originally characterised as '7' from frames 22 to 29. That peroxisome was relabelled by the algorithm as '39' in frame 30; therefore this '7' peroxisome in frame 33 is one of either '36' or '38' from frame 32. There is also a peroxisome that was not detected by TrackMate in this frame on the cell boundary between Cell A and Cell E. Either '7' or this undetected peroxisome could be one of peroxisome '36' or '38' from frame 32. There is insufficient evidence to place it one way or another, as the intensity of the two peroxisomes is very similar. This ambiguity is reflected in the description of these peroxisomes in Table 5.4.

Frame 34

Extensive movement of peroxisomes continues between frames 33 and 34, as some of the peroxisomes are shifted towards the budding site.

In the growing Cell E there is now a peroxisome, which is labelled as '30'. However, this track identifier was previously used for a peroxisome located in Cell C in frame 32 so it clearly cannot be the same peroxisome; again this highlights that the tracking algorithm attempts to link any of the objects it finds within the maximum distance and has no knowledge of cell boundaries. This peroxisome '30' looks very likely to actually be a relabelling of the peroxisome '24' from frame 33 based on its size and intensity (additionally, the '24' track identifier is now missing). This is interesting as that peroxisome had been static until now.

The group of three peroxisomes labelled as '4', '7' and '43' in frame 33 are all still labelled one of '4', '7' or '43'. At first glance using the maximum intensity projection image it looks probable that the algorithm has swapped around the labels of peroxisomes '7' and '43'. This is presuming that they maintained their positions relative to each other in XY. However, when viewing in 3D, the peroxisome '7' is lower in Z than the peroxisomes '4' and '43' in frame 33. Presuming instead that the peroxisomes have maintained the same Z position between frames 32 and 33, the algorithm's version of events and therefore the tracking is actually consistent.

Remember that the peroxisome '7' is one of the two peroxisomes '36' or '38' from back in frame 32. The other one is presumably the peroxisome that is visible at the 12 o'clock position of the peroxisome labelled '30' in Cell E but that has not been detected by TrackMate in this frame, and it is also probably the same one as the peroxisome that was not detected in the previous frame.

The peroxisome that was labelled '39' in frame 33 has failed to be detected by TrackMate in this frame, although it is visible at roughly the same position as in frame 33 to the eye. Tracking of the peroxisomes labelled as '0', '10', '16' and '34' in the top centre of Cell A remains consistent from frame 33.

Frame 35

There is more movement of peroxisomes from Cell A toward Cell E in this frame. The tracking of peroxisomes '10', '16' and '34' in the top centre of Cell A again appears consistent from the previous frame, as they show no movement. Once more the peroxisome that was labelled '39' in frame 33 is not detected although it is visible to the eye and in the same position.

On manual inspection it appears that several peroxisomes are misidentified in this frame. The peroxisome in Cell E that was labelled '30' in frame 34 is now labelled '42'; this is another error of the tracking algorithm not knowing the boundaries of cells as there is a peroxisome labelled '42' in Cell C in frame 34 and therefore cannot be the same peroxisome.

Of the group of three peroxisomes in the 5 o'clock position of Cell A, only '7' remains consistently labelled from frame 34, based on a manual inspection of its Z position in a 3D projection. The peroxisome that was labelled '43' in frame 34 is now '30' and the peroxisome that was labelled as '4' in frame 34 is now '43' in frame 35. The label '4' is now attached to what was labelled '0' in frame 34, and '0' is labelling what appears to be an elongated part of the same peroxisome, though it is impossible to tell whether it is actually a separate peroxisome, even in 3D (data not shown).

There is a peroxisome in Cell E to the left of the peroxisome labelled as '42' that is undetected by TrackMate. This is presumably the same one that was also not detected in frames 33 and 34; it is one of either peroxisome '36' or '38' from back in frame 32.

Frame 36

All the tracking of peroxisomes detected from 35 to frame 36 appears to be consistent. Peroxisome '30' from the previous frame has now moved into Cell E. There are no ambiguous peroxisomal structures or undetected peroxisomes visible to the eye in this frame so one of '36' or '38' from frame 32 is now indistinguishable from any other peroxisome; the same is true of the small peroxisome that is visible by eye in Cell A in frames 34 and 35, and

was labelled as '39' in frame 33. The peroxisomal structure that is labelled as '0' and '4' looks more elongated at the '0' end but it is still unclear whether it is two peroxisomes or one.

Frame 37

Again all the tracking appears consistent with the previous frame. There is not much movement of peroxisomes save for peroxisome '34' that has moved in the direction of the bud neck, and the peroxisomes in Cell E are now focused at the tip opposite the bud neck. It is still unclear if '0' represents a new, separate peroxisome from '4'.

Frame 38

There are several peroxisomes that are missing in this frame and cannot be distinguished against other peroxisomes: '0', '16' and '30'. The putative peroxisome '0' from frame 37 has moved too close to peroxisome '4' and cannot be distinguished by eye. The same situation seems to have occurred with peroxisome '30' from frame 37 moving too close to peroxisome '42'. This is due to all peroxisomes in the bud concentrating at the bud tip.

As for the peroxisome '16' from frame 37, the situation is more ambiguous. It is possible that it has moved close to peroxisome '34'. It could also have moved into the bud. The other peroxisomes that have been detected have tracks consistent with frame 37.

Frame 39

In this frame, another peroxisome can again be distinguished separately from the peroxisome '42' at the bud tip and is labelled as '30' by the tracking, maintaining the consistent label even with a gap in detection. The putative peroxisome '0' has also reappeared next to peroxisome '4'; it is still unclear if it is a new, separate peroxisome.

The peroxisome '16' from back in frame 37 is still unaccounted for. It is either still near peroxisome '34' or it has been moved into the bud and is indistinguishable from the peroxisomes there.

All the other tracking of peroxisomes looks consistent from frame 38.

Frame 40

The peroxisome labelled as '34' in the previous frame is not detected in this frame. It is possible that it has moved close to the peroxisome '7' and now can no longer be

differentiated. This is due to the slightly ‘smeared’ appearance of peroxisome ‘7’ now compared with the previous frame.

The peroxisome ‘0’ now appears to be a separate object, given the space between it and the peroxisome ‘4’. Tracking of the other peroxisomes is consistent with frame 39.

Frame 41

There are two peroxisomes that are visible to the eye in this frame that TrackMate has not detected; one in the 2 o’clock position above peroxisome ‘7’, and another, fainter peroxisome above peroxisome ‘42’ in the bud. The peroxisome in proximity to ‘7’ is presumably the peroxisome ‘34’ from frame 39, though this cannot be stated for certain; it may be a new peroxisome splitting from ‘7’ and ‘34’ could have been moved into the bud. The other peroxisome next to peroxisome ‘42’ in Cell E could either be any of the aforementioned peroxisomes that could no longer be detected in the course of this analysis: ‘16’, ‘34’, ‘36’/‘38’, or ‘39’ or could be a new peroxisome forming in the bud.

In Cell A there is a new peroxisome that has been labelled as ‘54’, it appears to have formed from peroxisome ‘4’. Other tracking of the peroxisomes is consistent from the previous frame.

5.6.2 Summary of Peroxisome Tracking

Using all of the above notes, and a comparison of Tables 5.3 and 5.4, it can be seen that the tracking algorithm does run into difficulty when attempting to track peroxisomes. For example, it switches the tracking for the same object several times over the course of just twenty frames (Table 5.4) and the tracks can be fragmentary, coming into and out of existence, or ending abruptly (Table 5.3).

The tracking does often interpret the situation correctly with peroxisomes that do not move greatly between frames, such as the peroxisome ‘10’. This was followed correctly over the course of the twenty frames, even when there was a gap in the peroxisome not being detected in frame 26. The same can be said of the peroxisome labelled ‘24’ until frame 33, which it successfully tracked until it moved a large distance into the budding cell.

	Frame																			
	22	23	24	25	26	27	28	29	30	31	32	33	34	35	36	37	38	39	40	41
Track Present in Each Frame in Cells A and E	0	0	0	0	0	0	0			0	0	0	0	0	0	0		0	0	0
	4	4	4	4	4	4	4	4	4	4	4	4	4	4	4	4	4	4	4	4
	7	7	7	7	7	7	7	7				7	7	7	7	7	7	7	7	7
	10	10	10	10		10	10	10	10	10	10	10	10	10	10	10	10	10	10	10
	16	16	16	16	16	16	16			16	16	16	16	16	16	16				
	24	24	24	24	24	24	24	24	24	24	24	24								
													30	30	30	30		30	30	30
							34	34	34	34	34	34	34	34	34	34	34	34		
								36	36	36	36	36								
									38	38	38									
										39	39	39	39							
													42	42	42	42	42	42	42	
													43	43	43	43	43	43	43	
																			54	

Table 5.3. Tracks assigned to peroxisomes in Cells A and E over the course of the twenty frames by the TrackMate algorithm. Some tracks are assigned to peroxisomes in Cell A and Cell E that were previously used for peroxisomes in Cell C after it has budded off. As peroxisomes are not transferred between cells that are now separated, this is clearly not a true reflection of what is going on in reality e.g. track 42. Several tracks end abruptly as peroxisomes can no longer be distinguished against each other. The colouration of the different tracks is arbitrary to aid the eye. This table should be compared with Table 5.4, which is manual interpretation of which tracks the same peroxisome is assigned to over time.

Table 5.4 (next page). Manual interpretation of tracks that each peroxisome is assigned to over time. Following each individual peroxisome across each of the frames and then mapping the tracks that TrackMate has assigned to them gives this table. As can be seen, the tracks for most of the peroxisomes change over the course of the fifteen frames. Cell E emerges at frame 32. The colouration of the different tracks is arbitrary to aid the eye.

Note:

- The missing peroxisome from frame 29 onwards (originally '16' from frames 22-28) might be the peroxisome in Cell C that is labelled '30' in frame 29. The identifier '30' is used again in subsequent frames by TrackMate to label peroxisomes in Cells A and E but these cannot be the same peroxisome as Cell C has budded off by this point.
- Either of '36' and '38' in frame 32 might be '7' thereafter, whilst the other one is visible for a few frames, and then no longer distinguishable.
- Identifiers for peroxisomes '34' and '36' in frame 28 may be the other way around.
- Identifiers for peroxisomes '16' and '34' in frames 33-36 might be the other way around.
- Many peroxisomes that cannot be seen for a frame have just moved next to another peroxisome so that they can no longer be distinguished.

Manual Interpretation of Tracks Peroxisomes Belong to Over Time in Cells A and E

		Frame																				
		22	23	24	25	26	27	28	29	30	31	32	33	34	35	36	37	38	39	40	41	
	0	0	0	0	0	0	0	0	⊙	⊙	0	0	0	4	4	4	4	4	4	4	4	
	4	4	4	4	4	4	4	4	4	4	4	4	4	4	43	43	43	43	43	43	43	
	7	7	7	7	7	7	7	7	7	39	39	39	39	⊙	⊙	⊙	⊙	⊙	⊙	⊙	⊙	
	10	10	10	10	10	⊙	10	10	10	10	10	10	10	10	10	10	10	10	10	10	10	
	16	16	16	16	16	16	16	16	⊘	⊘	⊘	⊘	⊘	⊘	⊘	⊘	⊘	⊘	⊘	⊘	⊘	
	24	24	24	24	24	24	24	24	24	24	24	24	24	30	42	42	42	42	42	42	42	
							34	34	34	34	16	16	34	34	34	34	34	34	⊙	⊙	⊙	
								36	36	36	36	36	7/⊙	7/⊙	7/⊙	7/⊙	7/⊙	7/⊙	7/⊙	7/⊙	7/⊙	
										37	37	34	16	16	16	16	16	⊙	⊙	⊙	⊙	
										38	38	38	7/⊙	7/⊙	7/⊙	7/⊙	7/⊙	7/⊙	7/⊙	7/⊙	7/⊙	
												43	43	30	30	30	⊙	⊙	⊙	⊙	⊙	
																						54

Key	
Peroxisome visible to eye but not detected by TrackMate	⊙
Peroxisome cannot be distinguished by eye	⊘

So for what reasons did the tracking go wrong? The following explanations have been discussed above but will be reiterated together here (refer to Figure 5.8 for the examples discussed):

- Peroxisomes ‘clump’ or ‘stick’ together and become so close to one another they can no longer be distinguished as separate objects (‘0’ in frame 29, reappearing frame 31; several peroxisomes in frame 38; most peroxisomes in bud).
- Peroxisomes that are the same intensity and in roughly the same area of the cell will appear similar to the algorithm. This causes them to be confused with each other and therefore misidentified (frame 32; frame 35 especially).
- Peroxisomes can move far in 3D space in the 5 minutes between each frame being acquired. This is especially evident by the movement of the peroxisome labelled ‘24’ in frame 33, between frames it has moved to the bud and becomes labelled as ‘30’ in frame 34.
- The algorithm does not know where the boundaries of the cells are, and therefore compares the positions of all peroxisomes as objects in 3D space between frames. In reality, peroxisomes do not flit between mature cells that no longer share any cytoplasm (‘7’ in frame 33 and ‘42’ in frame 35; both these track identifiers previously labelled peroxisomes in Cell C, which had finished budding off from Cell A in around frame 31 and therefore cannot be tracking the same peroxisome).

The last problem highlighted is a software issue, which although beyond the scope of this study is something that could be rectified with the aid of the plugin’s developers or more complicated FIJI scripting to exclude objects not in the cell or its current bud. All the other issues above would require an increase in both spatial (not possible with current techniques) and temporal resolution. This would make peroxisomes easier to distinguish between when they are close together, and also make the parameters used for the tracking more accurate. In addition, as a consequence of decreasing the time between frames the maximum distance parameter for the TrackMate tracking could be reduced. Therefore the algorithm would have a smaller pool of potential objects to choose from.

Although the above shows that the tracking has limited usefulness, it also indicates that the behaviour of peroxisomes is complex and that there is a high degree of ambiguity. The failure of the tracking algorithm to accurately link together correctly many of the peroxisomes over time reinforces the intricacy of the situation trying to be comprehended here.

5.7 Peroxisomal Fission and *De novo* Synthesis

In the frames analysed there is clearly a proliferation of peroxisomes. There are a few instances where a new peroxisome appears in proximity to a pre-existing peroxisome. These are often (but not always) accompanied by a drop in intensity of the pre-existing peroxisome (Figure 5.9). These are taken to be fission events. Putative fission events that can be discerned in the above analysis are:

- '34' from '0' in frame 26
- '36' from '0' in frame 28
- '37' from '34' in frame 30
- '38' from '36' in frame 30
- '43' from '4' in frame 33
- '0' from '4' in frame 40*
- '54' from '4' in frame 41

Note that the track identification here is not that useful as '0' is referencing different peroxisomes over time (Table 5.4). Something of interest is that there is a lot of peroxisomal fission toward the end of the budding of Cell C (which has separated from Cell A at around frames 30-31, Figure 5.8). Save for the peroxisomal division at frame 33, there is a long gap before some more peroxisomal division occurs at frames 40 (*presuming they were not separate objects previously) and 41.

Although it has been demonstrated previously that peroxisomes only form *de novo* in cells that previously lack them both in the literature (Motley and Hettema, 2007), and in Chapter 4 of this study, the possibility was nevertheless probed as part of the analysis of Figure 5.8. Deciding if any *de novo* synthesis has occurred is trickier than looking for the signs of fission – what would *de novo* synthesis look like? Would one be able to detect these *de novo* formed peroxisomes against other brighter, pre-existing peroxisomes?

Inference can be made using previous known examples from *S. cerevisiae* mutants that at one stage or another lack peroxisomes and then form them by *de novo* synthesis, such as *imp1*, *imp2*, or the *vps1/dnm1* mutant that has conditional Pex19 expression used in Chapter 3. If a fluorescent protein with PTS1 is used to visualise the peroxisomes in these cells then it is localised in the cytosol in the absence of peroxisomes. When the peroxisomes are formed by *de novo* synthesis, the fluorescent signal in the cytosol tends to decrease, whilst punctate

structures (i.e. the peroxisomes) appear slowly out of the background. These peroxisomes gain in intensity over time as more fluorescent protein is imported (Figure 5.10). This was something to look for in the wild-type cells. However, it is highly likely that any *de novo* formed peroxisomes would not be distinct against any pre-existing peroxisomes in its vicinity, at least at first. As a *de novo* formed peroxisome gained intensity, it would probably look akin to a peroxisome formed by fission of a pre-existing peroxisome in the neighbourhood. Therefore, to say with some confidence that a peroxisome was *de novo* formed it would have to appear out of the background in an area of the cell that did not contain any pre-existing peroxisomes. Perhaps not surprisingly, there were no candidate peroxisomes that fitted these stringent criteria. All peroxisomes that appeared could be explained as the fission of a pre-peroxisome

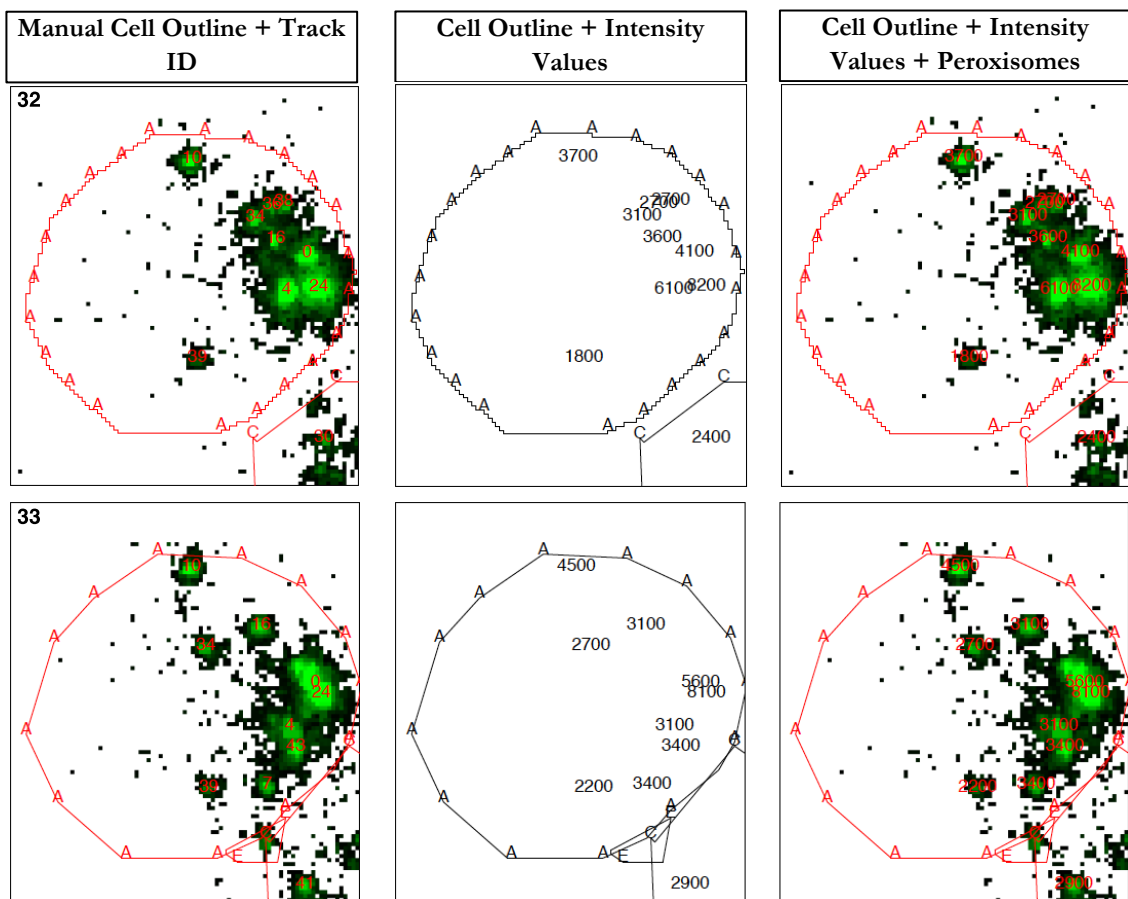


Figure 5.9. Frames 32 and 33 showing splitting of peroxisome ‘4’ into ‘4’ and ‘43’ and corresponding intensity values. In frame 32 the peroxisome ‘4’ has an intensity of 6100 units; the frame later fission has occurred, splitting it into two peroxisomes of 3100 and 3400 units. This is a rough halving of intensity after the split, and neatly demonstrates peroxisomal fission in action. The ‘extra’ intensity in the two resultant peroxisomes compared with the original can be explained by the peroxisomes having imported some fluorescent protein between frames and also that the background intensity is now being counted twice e.g. if the background intensity on the camera is 200 units (the intensity level of pixels in empty space without fluorescence), then the ‘true’ value of the peroxisome in frame 32 is 5900, and the ‘true’ intensity of the two peroxisomes in frame 33 are 2900 and 3200 – bringing the original peroxisome and daughter peroxisomes closer together in intensity. Intensity values have been rounded to 2 significant figures.

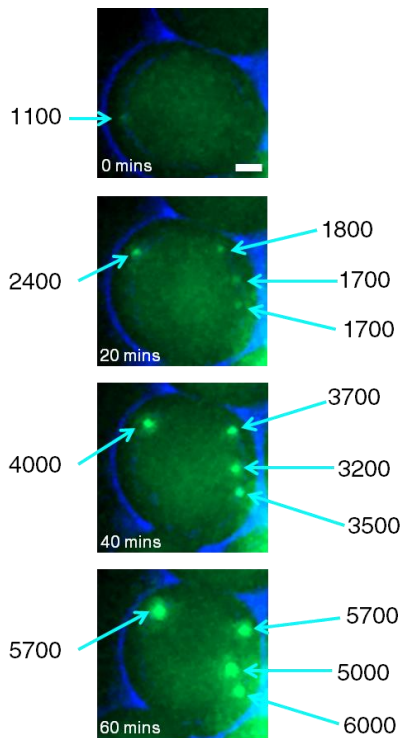


Figure 5.10. *inp2* cell showing *de novo* synthesis of peroxisomes and corresponding increases in intensity values. At 0 minutes, most of the fluorescent protein is in the cytosol. A peroxisome can just be seen above the background (cyan arrow). The intensity value of this peroxisome is listed next to the image. 20 minutes later several peroxisomes have formed by *de novo* synthesis. Note the increase in intensity of the peroxisome on the left of the image. The intensity values of all the peroxisomes increase over the next 40 minutes. Intensity values have been rounded to 2 significant figures. Fluorescent protein is mNeonGreen-PTS1. Brightfield in blue. Images are maximum intensity projections. Scale bar indicates 1 μm .

in their proximity. This absence of evidence is in line with previous expectations of *de novo* synthesis in cells already containing pre-existing peroxisomes in this study and elsewhere (Knoblach et al., 2013; Motley and Hettema, 2007). This is not necessarily evidence of absence however; greater spatial and temporal resolution may be needed to unravel the situation and not detecting *de novo* synthesis may be a larger reflection on the current constraints of this experimental setup, rather than what is occurring in reality. As it stands, this data agrees with most of the literature and Chapter 3 of this study on yeast peroxisomal formation with regards to *de novo* synthesis.

5.8 Insights into Peroxisomal Behaviour from Cells A and E in Cluster 1

Some observations about peroxisomal behaviour can be made from the detailed frame-by-frame analysis of Cell A and Cell E. Refer to Figure 5.8 for examples of behaviours discussed below.

Peroxisomes Have a Tendency to Clump Together

Peroxisomes tend to clump into groups in certain parts of the cell. This is particularly obvious in the first half of the frames analysed (frames 22-32), when 4 of the peroxisomes exist in the same region, and there is much space in Cell A that does not contain any peroxisomes. They also appear to stick to each other, making it unclear if peroxisomes have separated or not, e.g. the peroxisomes '0' and '4' over frames 35-40. As peroxisomes do not fuse (Motley and Hettema, 2007), this means that we have to be careful when deciding if a particular peroxisome has split via fission, was in fact two separate peroxisomes the whole time or indeed if any division has taken place at all. With greater spatial (if or when possible) and temporal resolution, more certainty could be placed as to when fission events have actually occurred.

Peroxisomes are Very Static Over Long Periods

For example, the peroxisome labelled '10' consistently across all the frames does not move from its 12 o'clock position within Cell A for the whole 100 minutes. The peroxisome originally labelled '0' in frame 22 (1st row Table 5.4) does also not move very much from the 3 o'clock position across all the frames.

Peroxisomal Movement Occurs at the Start of a Bud Formation

This is particularly evident in the difference between frame 32 and frame 33, when Cell E first appears.

Heterogeneity of Peroxisomes Division and Inheritance Behaviour

Peroxisomes can be split multiple times, the division of a peroxisome does not always destine that peroxisome for inheritance, and peroxisomes can be inherited without division. For example, the peroxisomes labelled '36' and '38' in frame 30 are products of a peroxisomal

division, but '36' was itself already a product of a division from '0' in frame 28. Both of these peroxisomes are moved towards the bud over the next few frames, with one going into the bud and one remaining (labelled '7' at this point). Neither peroxisome is static at any point, which indicates that they are not anchored via Inp1. Peroxisome '24' in frames 22-33 is an interesting case where no peroxisomal division seems to occur within the time frame and yet it is moved into the bud.

Peroxisomal Division Occurs Around Bud Formation

Most of the peroxisomal division occurs around the time when the bud appears and is flanked either side by periods of relative inactivity. For example, frames 22-25 show barely any activity, before some peroxisomal division in frames 26, 28, 30 and 33, followed by another period of inactivity, and then some division in frames 40 and 41. In terms of cell growth, these twenty frames roughly constitute the second half of the budding of Cell C (finishing roughly frames 30-31), and the appearance and first half of the budding of Cell E (starting roughly frame 33).

5.9 Regarding the KPPC Model Using Cell A from Cluster 1

Is it possible to say anything about the questions raised in Chapter 1.6.2 concerning the KPPC model at this point?

First, could a ‘steady state’ number of peroxisomes be identified in the relationship between the number of peroxisomes in the mother at the start of bud formation and the number of peroxisomes in the daughter following cell division?

If we examine beyond the analysis of Figure 5.8 for a moment and look at the number of peroxisomes in Cell A before it has started to produce Cell C, which is at roughly frame 13, it contains 12 peroxisomes (Table 5.5). After the budding of Cell C has finished, roughly frame 31, Cell C only contains 8

Budding	Number of Peroxisomes in Cell A at Start of Budding	Number of Peroxisomes in Bud After Splitting from Cell A
Cell C Budding	12 (Frame 13)	8 (Frame 31)
Cell E Budding	9 (Frame 32)	6 (Frame 51)

Table 5.5. Peroxisome numbers in Cell A, and Cells C and E at the start and end of their respective buddings.

peroxisomes. At the start of budding Cell E, Cell A contains 9 peroxisomes and at the end of the budding Cell E contains 6 peroxisomes (Table 5.5). Therefore directly following a cell division there is not parity in peroxisomal number between the number the mother had and the final number of peroxisomes in the daughter. This indicates that a ‘steady state’ number is not reset at the start of a budding event but instead at some other point. However, several peroxisomal divisions occur at the end of the Cell C budding and prior to the budding of Cell E, and several peroxisomes are moved into Cell E right at the start of the budding. Perhaps at the start of a budding is too late to define as the ‘steady state’ point – maybe it is instead established during the periods between the buddings? This requires a more ‘zoomed out’ approach and is discussed further when looking at the number of peroxisomes across all the cells in the cluster (Chapter 6.3).

The second question concerned whether peroxisome proliferation could be seen. This has been accomplished, and as mentioned much of it appears to occur around the end of a budding and the start of the next one. Whether this is true for all cells is discussed in Chapter 6. Does this proliferation represent a doubling of peroxisomal number in Cell A? From a low of 6 peroxisomes in frame 22, the number of peroxisomes in Cell A reaches a peak at 10

or 11 in frame 33. There is some more peroxisomal division that takes place after the inheritance of some of the peroxisomes into Cell E has started. Therefore it is possible that there was a net doubling of peroxisomes in Cell A overall.

As one is looking in detail at this stage in the analysis, a further question can be asked. According to the KPPC model, each individual peroxisome should be split, with one half being retained through anchoring to Inp1 in the mother and the other half inherited via Inp2-Myo2 into the bud. Could this actually be seen in the above analysis?

The actual situation appears more complicated than the above proposition. Some of the inconsistencies between what is seen in this set of images and the propositions of the model are mentioned at the bottom of section 5.8. For example, the aforementioned peroxisome '24' in frame 33 appears to be a straight transfer from the mother cell to the bud with no fission occurring in the frames analysed (Figure 5.8). This kind of observation is accounted for in the caption to Figure 9 in Knoblach et al., 2013, where the authors assert that peroxisomal division process is asymmetric and may result in different sized fragments. However, if no fluorescent signal can be seen after such an event, indicating that there is no matrix content remaining, can it be affirmed whether the division is asymmetric or whether there was actually any division at all (i.e. as appears to be the case with peroxisome '24')? It is probably not possible to definitively conclude this without the use of microscope techniques with much higher spatial resolution, sensitivity and/or different (non-matrix) labels for the peroxisome. Additionally, some peroxisomes in the mother move from frame to frame and do not appear 'anchored', yet are divided anyway ('36' and '38', frame 32, Figure 5.8). According to KPPC model, peroxisomes lacking Inp1 should be moved through to the bud, so it is unclear how this example could reconcile with that model. Moreover, there is an example of a peroxisomal division where both peroxisomes stay in the mother cell (peroxisomes '34/16' and '37/16/34', 7th and 9th rows Table 5.4), indicating that division does not mean that one of the resultant peroxisomes is destined to be inherited.

5.10 Summary

In summary, this frame-by-frame analysis has demonstrated the usefulness of the TrackMate plugin for detecting peroxisomes. Across the frame-by-frame analysis there was roughly a 5% error rate in the detection of peroxisomes, and Figures 5.6 and 5.7 demonstrate the ability of the TrackMate plugin to dissect several overlapping peroxisomes in 3D. However, the difficulty of actually linking these detected peroxisomes into coherent tracks was established.

The issues and possible improvements have already been outlined above. As it stands, automated tracking via the TrackMate algorithm has limited usefulness given the high rate of mislabelling and changes of peroxisomal identity. However, even close manual examination was unable to unpick the reality of the situation in some cases, given the level of ambiguity. This demonstrates that a failure to accurately track many of the peroxisomes over time is not wholly related to shortcomings with the program but is also a reflection of the complexity of the data, and that tracking is a tricky endeavour.

The next chapter will continue the evaluation of the KPPC model by moving onto a multiple cell approach and will assess the data gathered regarding all the peroxisomes in the cluster containing Cell A (Cluster 1) and the other four clusters (Clusters 2-5). Due to the difficulties encountered with attempting to track peroxisomes, only peroxisomal number over time will be considered.

Chapter 6: Analysis of Cell Cluster and Clusters

This chapter will evaluate the KPPC model by examining first the remaining cells in the cluster from the previous section (Cluster 1), followed by the other clusters (Clusters 2-5). Videos of these clusters are available in the external media (see Table 5.1 for filenames). This analysis will only deal with an examination of the number of peroxisomes in each cell across all the frames in a cluster. By examining this, the division and subsequent movement of peroxisomes to the bud should be able to be seen, even though the fate of individual peroxisomes themselves is not unambiguously known.

However, just using the number of peroxisomes in each cell presents its own set of problems. When performing the analysis of Figure 5.8, distinguishing between the peroxisomes in the newly growing Cell E bud was difficult; at first due to its small volume and later because peroxisomes are concentrated at the bud tip during growth (particularly evident from frame 37 in Figure 5.8). This meant that peroxisomes were overlapping and therefore unable to be separated by eye or by the TrackMate plugin. The same will be true of all other buds examined here. Therefore the initial number of peroxisomes in the cells just after they appear as buds is likely to be incorrect. As the buds grow and become larger, this is much less of an issue.

Section 5.9 started examining the assertions of the KPPC model, and this section will do so in a more quantitative fashion. Table 6.1 gives the proposals from the KPPC model and the expected observations for this section. Whether a signature of peroxisomal proliferation could be seen was also examined. Sections 6.1 and 6.2 discuss and analyse the data, and the findings of this analysis and conclusions are found in section 6.3.

Table 6.1. Proposal of KPPC model and expected observations.

Proposal in KPPC Model	Expected Observation
Establishment of 'steady state' number of peroxisomes.	Number of peroxisomes in mother cells at bud formation should equal number of peroxisomes in bud after cell division
Every peroxisome in mother is split, with one being retained by the mother and the other being moved through to the bud.	The number of peroxisomes in mother cells should double as they are divided and then halve as peroxisomes are subsequently inherited.

6.1 Cluster 1

First, Cluster 1 will be examined in detail. It contains the Cells A, C and E discussed in Chapter 5 and ten other cells by the end of the 100-frame experiment, giving 13 cells in total by frame 100 (see Figure 5.3 for a reminder). Table 6.2 lists when buds first appear, and Figure 6.1 shows the lineage of cells within the cell cluster. All the cells in this cluster as derived from the original mother cell, Cell A. Figures 6.2 and 6.3a-e are graphs showing the number of peroxisomes in each cell over the course of the 100 frames. Figure 6.2 shows the number of peroxisomes in every cell for all the frames. Figures 6.3a-e are individual graphs for cells that have produced at least one bud (Cells A, B, C, D, and G). All the information in Figures 6.3a-e is contained within Figure 6.2 but trends of peroxisomes for individual cells are more obvious. Versions of these figures without annotations on and beneath the graphs are contained within Appendix H.

Cell	Frames	Buds
A	1-100	B,C,E,G,K,L
B	1-100	D, H
C	13-100	F, I
D	20-100	J
E	32-51	
F	51-76	
G	52-100	M
H	51-100	
I	72-100	
J	55-100	
K	73-94	
L	88-100	
M	73-100	

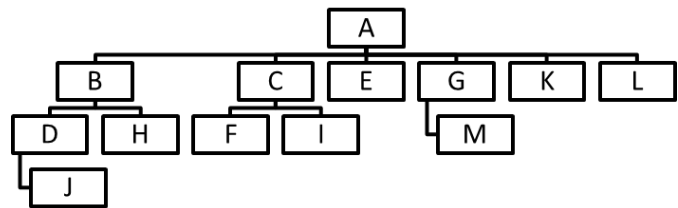


Table 6.2 (left). Frame when each cell is present, along with any buds they produce. Cells E, F and K moved after they separated from their mother cell by the action of the flow in the cell chamber. **Figure 6.1 (right).** Representation of the lineage for all the cells that are present in this cluster. This hierarchy shows how the cells are descended from one another, and that they are all derived from Cell A. Small numbers in bottom left of each box are when each cell is first visible. Cells A and B are present in frame 1 (as seen in Figure 5.3).

It should be noted here that cells are only marked onto a graph when the TrackMate plugin has detected that they contain at least 1 peroxisome. Therefore, buds often appear several frames prior to their first data point on the graph. Exact frame numbers are listed in Table 6.2, and are shown in Figures 6.2 and 6.3a-e with arrows underneath the x-axis.

6.1.1 General Trends

Using the data from Figure 6.2, there are two general trends to observe about the number of peroxisomes.

First, it is evident that the original mother cell, Cell A, consistently has more peroxisomes than any of its daughter cells except for a brief period between frames 63-68 when Cell C has more. This indicates that perhaps older cells accumulate more peroxisomes, as Cell A has existed for the greatest length of time. Also one can see that the number of peroxisomes in a particular cell does not give an indication of the number of peroxisomes one should expect to see in another cell; the number of peroxisomes in a mother cell does not give an indication of how many peroxisomes a bud will end up with even though the two are genetically identical.

Second, there is a general trend towards cells containing more peroxisomes over the course of the 100 frames. Cells B and C appear to be rising towards a similar number that Cell A has, but even after nearly 8 hours (Cell B) and 7 hours (Cell C), they have not quite reached the number of peroxisomes Cell A has. This again may indicate that cells steadily accumulate peroxisomes over time. This accumulation indicates that buds do not quite inherit half of the peroxisomal content of the mother, or that the division and inheritance process is not as tightly coupled as proposed by the KPPC model, with some divisions not leading to inheritance (as shown in examples in the previous chapter).

6.1.2 Cell A and Buds

Focus now turns to peroxisomal number in individual cells and their buds. Figure 6.3a shows Cell A and buds. First consider the graph describing the number of peroxisomes in Cell A (blue diamonds).

There appear to be five or six peaks (the final peak is less well defined) in the number of peroxisomes in Cell A over the course of the experiment. These peaks occur in frames 13, 31, 52, 71-72, 84 and 89, although the peak at 89 could be a continuation of the peak at 84.

These peaks in the number of peroxisomes roughly correspond to when a new bud is formed (frames 13, 32, 52, 73 and 83; see Table 6.2), with the lows of the number of peroxisomes in Cell A corresponding to some time into the first half of the budding. This corresponds in Figure 5.8 with the period of peroxisomal division activity occurring around frames 28-33, followed by a period of movement of peroxisomes into the bud. These trends show that much peroxisomal division occurs prior to a bud's first appearance; and also that, for example, peroxisomes destined for Cell E are formed when Cell C is still attached to Cell A.

A second observation from this graph is that the number of peroxisomes lost by the mother to the bud is not always a clean half of the number of peroxisomes it had at the peak. This may be due to ongoing coupled division and inheritance activity during the middle of the cell cycle. It does sometimes appear true that the number of peroxisomes inherited by the bud is indeed half of the peroxisomal content of the mother, for example in the buddings of Cells C and E. The number of peroxisomes inherited by buds described

here (and in the rest of this analysis) is the amount that the total number of peroxisomes in a mother cell drops from a peak prior to the bud appearing to a low point just after the bud has appeared e.g. in Cell A there is a peak in the number of peroxisomes at 12 in frame 13, and low of 6 at frame 22, so Cell C is taken to have inherited 6 peroxisomes (Figure 6.3a). For the Cell E budding, the peak is of 10 peroxisomes at frame 31, and this number drops to a low at frame 38 of 5 peroxisomes, so it is taken that Cell E has inherited 5 peroxisomes.

Later buddings of Cells G, K and L do not quite have a drop to half the number of peroxisomes at the peak. For these buddings the peaks are at 12, 11 and 14 peroxisomes, and are followed by lows of 7, 7, and 9 peroxisomes respectively. As mentioned in the introduction to this section, it should be noted that the number of peroxisomes in the buds do often not rise in proportion to the decrease of the number of peroxisomes in the mother cell at first.

The number of peroxisomes in Cell A dropping to exactly half from its peak during the buddings of Cells C and E is in line with a prediction of 1:1 inheritance of peroxisomes between mother and bud, as suggested by the KPPC model. However, it is uncertain whether the peroxisomes inherited are all products of a 1:1 division of each of the peroxisomes in the mother; as was seen in Figure 5.8 of peroxisomes being inherited by Cell E, this is not necessarily true. For the buddings of Cells G, K and L the number of peroxisomes in Cell A drops instead by roughly one third, before rising again. This does not show a straight 1:1 division of peroxisomes between the mother and bud but a more imprecise inheritance situation.

A third point of interest for these buddings is that the number of peroxisomes in each of the buds does not increase past the number initially inherited from Cell A until the bud has detached, as shown in Table 6.3. This indicates that there is an initial period as the bud forms when some of the peroxisomes that are already present in the mother are transferred.

Peroxisomes in the mother are then multiplied in preparation for next budding event, with their number peaking just before the next budding starts.

Bud	Peroxisomes Inherited From Cell A	Frame Bud Detaches From Cell A	Frame When Bud Has More Peroxisomes Than Inherited from Cell A
C	6	30	38
E	5	50	Never (cell moves out of frame)
G	5	72	89
K	4	84	89
L	5	N/A	Never (cell still attached)

Table 6.3. Buds of Cell A do not make more peroxisomes until after they have finished budding. The number of peroxisomes inherited by a bud is taken to be amount that the total number of peroxisomes in Cell A drops from its peak to a low point e.g. peak of 12 at frame 13, and low of 6 at frame 22. The number of peroxisomes in each of the budding cells never exceeds this number until after they have finished budding.

6.1.3 Cell B and Buds

Looking at the graph of Cell B and buds (Figure 6.3b), any trends are not as obvious as for Cell A. There are slight peaks in the number of peroxisomes at frames 10, 15-16 (probably a continuation of the first peak), and 51; with a gradual rise toward 10 peroxisomes at the end of the experiment. Cell B produces two buds, Cells D and H, starting at roughly frames 20 and 51. Like Cell A, these peaks correspond roughly with the appearance of the two buds.

However, prior to the Cell D budding, the peak number of peroxisomes occurs in Cell B as it still attached to Cell A at frame 10 (5 peroxisomes). The number of peroxisomes does not rise above 5 until just before the budding of Cell H starts. This implies that none of the peroxisomes in Cell B were divided before the cell started the budding to produce Cell D. Therefore this indicates that the peroxisomes inherited by Cell D from Cell B are the same ones directly inherited from Cell A by Cell B. This unusual behaviour is not seen again, but demonstrates a strange situation and certainly not one predicted by the KPPC model.

The budding of Cell H from Cell B is also different to anything else described thus far. Initially Cell H inherits a couple, but not quite half of the peroxisomes in Cell B, in a similar fashion to the buddings of G, K and L from Cell A. However, as the experiment continues, the number of peroxisomes in Cell B first slightly increases and then remains flat. The intriguing aspect is that the number of peroxisomes in Cell H increases steadily over the same

period. Notably, this increase is by much more than the initial drop from 6 to 4 peroxisomes in Cell B just as the budding started.

The increase in the number of peroxisomes in Cell H could suggest that peroxisomes are dividing in the bud itself – how does this reconcile if the division of peroxisomes is dependent on being anchored by Inp1 and pulled apart by Inp2-Myo2? Inp1 is known to be recruited to bud localised peroxisomes between 60-90 minutes after budding starts (Knoblach et al., 2013), so perhaps there is Inp1-Inp2 mediated peroxisomal fission in the bud during this time (12 frames after budding starts at 5 minutes/frame). Another explanation is that this increase in peroxisomes in the bud could also indicate that there is coupled peroxisomal division and inheritance occurring from the mother to bud. Which peroxisomes are chosen to be divided and moved across? Does it depend on whether they had been split previously? In Figure 5.8 the same peroxisome is divided twice ('0', frames 26 and 28), and one of the resultant halves is also divided again ('36', frame 30), indicating that this is not the case. Perhaps both processes could be occurring. Nevertheless, one can infer that there is more going on than a simple transfer of the split half of a peroxisome from the mother being moved through into the bud.

6.1.4 Cell C and Buds

Cell C produces two buds, Cell F and Cell I, at roughly frames 51 and 72 respectively (Figure 6.3c). There are peaks in the number of peroxisomes in Cell C at frames 50 and 67, which are again prior to the start of the buddings.

Cell F proceeds to inherit exactly half of the peroxisomes in Cell C. Akin to the Cell B/Cell H budding, some frames later there is a large increase in the number of peroxisomes in both Cell C and Cell F. The increase in peroxisomal number in Cell F is larger than the initial inheritance of 4 peroxisomes. Again, this indicates that there is either some peroxisome proliferation occurring in the mother, with some transfer into the bud, or peroxisomal fission in the bud, or both. Again, this is a more complex situation than outlined in the KPPC model.

The budding of Cell I from Cell C is similar to the buddings of Cells G, K and L from Cell A. Not quite half (5/12) of the peroxisomes are inherited by Cell I. The number of peroxisomes in Cell I increases steadily towards the end of the experiment, but not by more than the initial inheritance of 5 peroxisomes until nearly frame 100. There is a slight drop in the number of peroxisomes in Cell C toward the end of the experiment; it is unclear if this is evidence of further inheritance from the mother to the bud.

6.1.5 Cell D and Bud

Cell D produces one bud, Cell J, at roughly frame 55 (Figure 6.3d). There is a peak in the number of peroxisomes Cell D has at frames 50-52, just prior to the start of the budding. The number of peroxisomes in both cells then rises, and in Cell J rises above the initial inheritance of 3 peroxisomes. This indicates a similar situation to the buddings of Cells F and H from their respective mother cells; sporadic fission in the mother cell, with some inheritance of peroxisomes, or fission in the bud, or both.

6.1.6 Cell G and Bud

Cell G also produces just one bud, Cell M, which initially appears at frame 73 (Figure 6.3e). There is a peak in the number of peroxisomes in the mother at frame 72, coinciding with the arrival of the bud a frame later. The initial inheritance of Cell M appears to be 5 peroxisomes given the drop from the peak down to 1 peroxisome at frame later. Cell M does not rise above 5 peroxisomes before the end of the experiment, suggesting a scenario like the buds produced by Cell A.

6.1.7 Summary of Behaviour

The above section shows the presence of a few different behaviours of peroxisomal division and inheritance within the same group of cells all related to each other, growing under the same conditions and imaged in the same way.

Most of the buddings show that there is peroxisome proliferation in the mother before the arrival of a bud, with the peak number of peroxisomes occurring a few frames before the bud is seen. This is in line with what was seen in Figure 5.8 before the arrival of Cell E (also seen in Table 5.2.). One may question why the number of peroxisomes often drops just prior to the bud arriving and not immediately after. This is probably due to the peroxisomes clustering around the bud neck just as the bud is forming and therefore being unable to be distinguished from one another.

Buds then inherit some peroxisomes from the mother within the first few frames of being seen. This is in line with previous observations that peroxisomes are segregated within 10-40mins of bud arrival (Knoblach et al., 2013). The number of peroxisomes inherited is not necessarily half of the peak number of peroxisomes the mother had however.

Some buds have an increase in their peroxisomal number past their initial inheritance whilst they are still attached to the mother, and others do not. All the buds that are produced by Cell A, Cell M budding from Cell G, and Cell I budding from Cell C fit the latter description. The former can be seen with the Cell H budding from Cell B, Cell F from Cell C, and Cell J from Cell G. This situation indicates that either a) there is peroxisomal fission in the mother that occasionally results in some inheritance or b) that there is division of peroxisomes in the budding cell, or c) both processes. If the peroxisomes are arising due to proliferation in the buds, does Inp1 anchor these peroxisomes at this point? If not, how does the division occur in accordance with the KPPC model? This question is beyond the scope of this study to answer but would be an interesting area for further development.

The only budding that does not fit with the above set of events is that of Cell D budding from Cell B, where there is not really a peak in the number of peroxisomes in the mother cell prior to bud arrival. As mentioned above, it appears that the peroxisomes inherited by the Cell D had not undergone division in Cell B. This appears to happen infrequently, as it was not witnessed in other buddings.

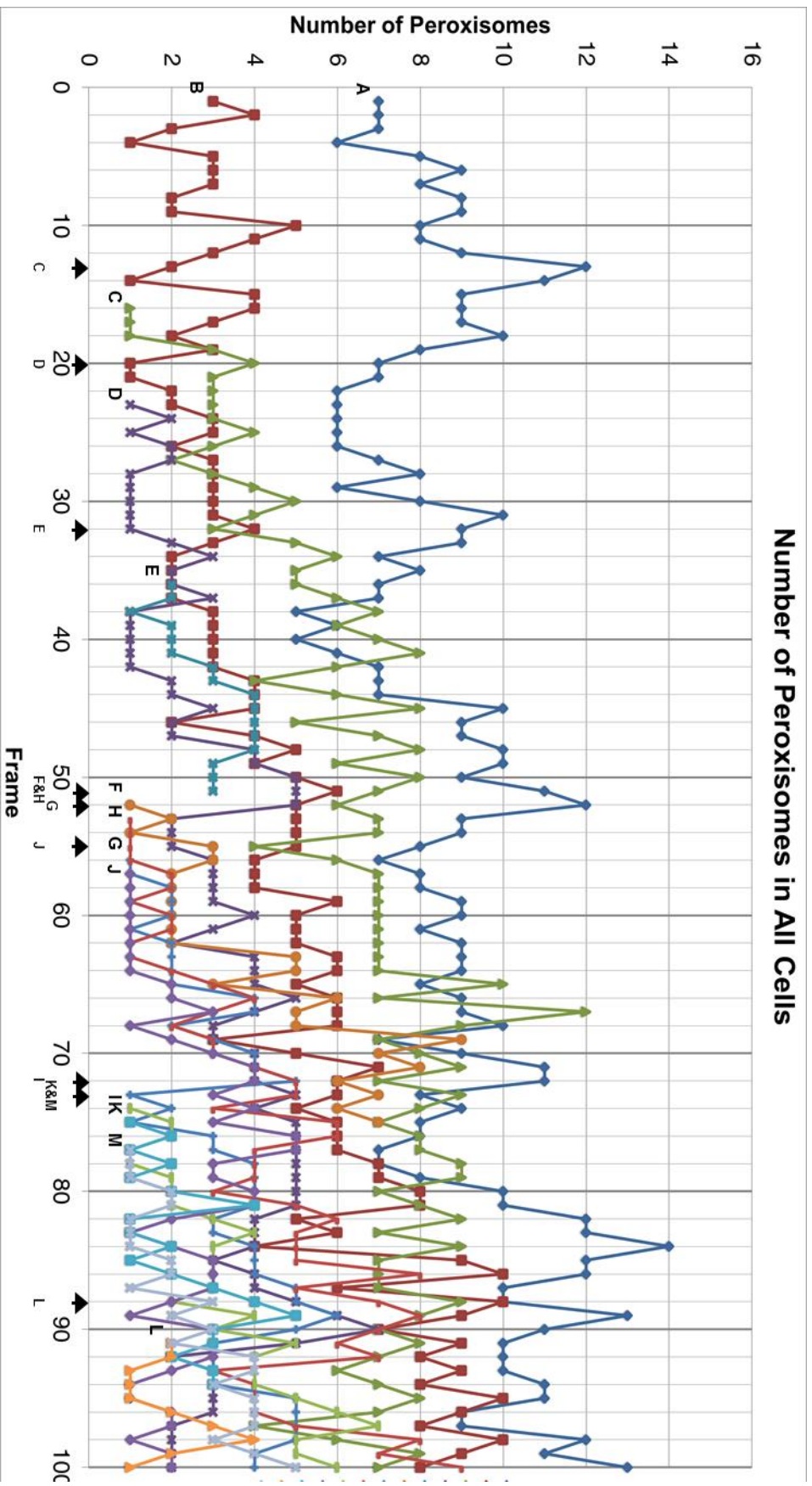
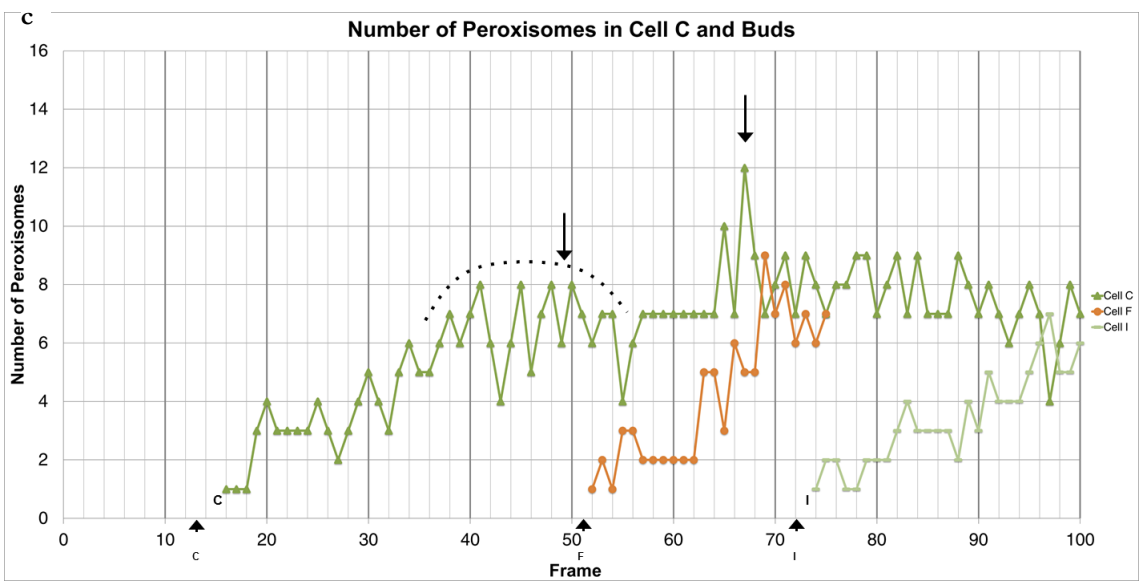
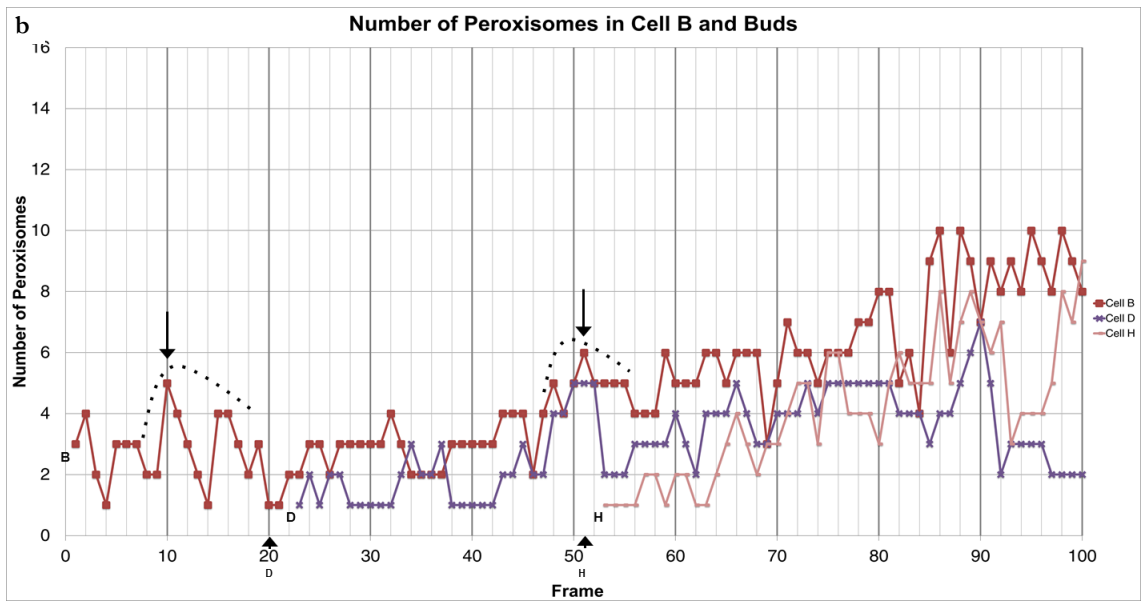
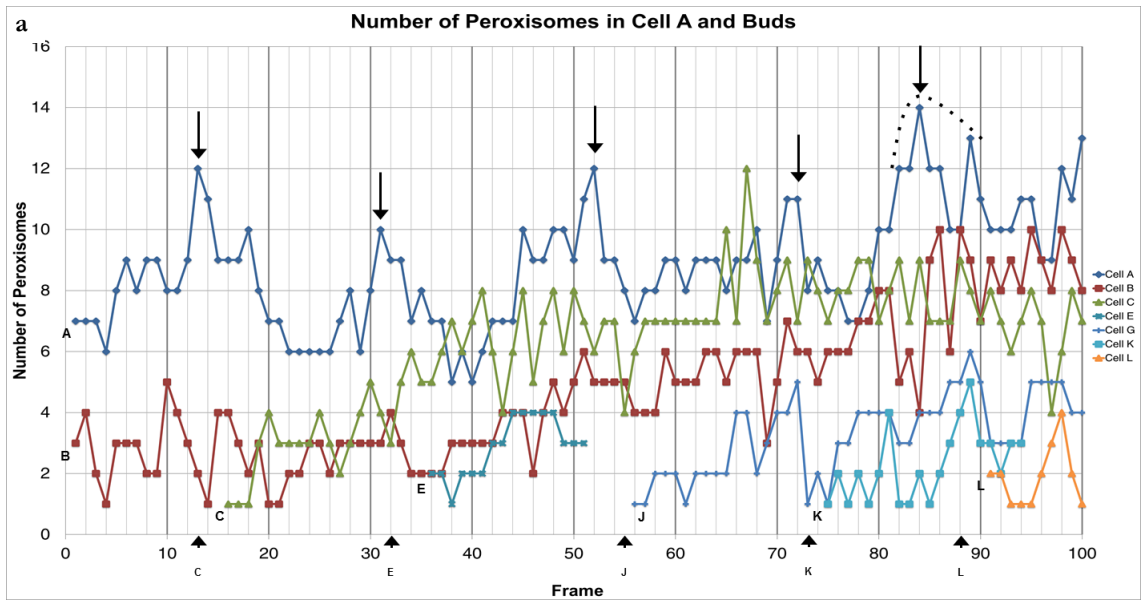


Figure 6.2. Graph of number of peroxisomes per cell for all the cells in Cluster 1. Black arrows underneath the x-axis indicate when that bud can first be seen. This is usually a few frames prior to it getting a point on the graph, as a point is not plotted when 0 peroxisomes are detected in the bud.



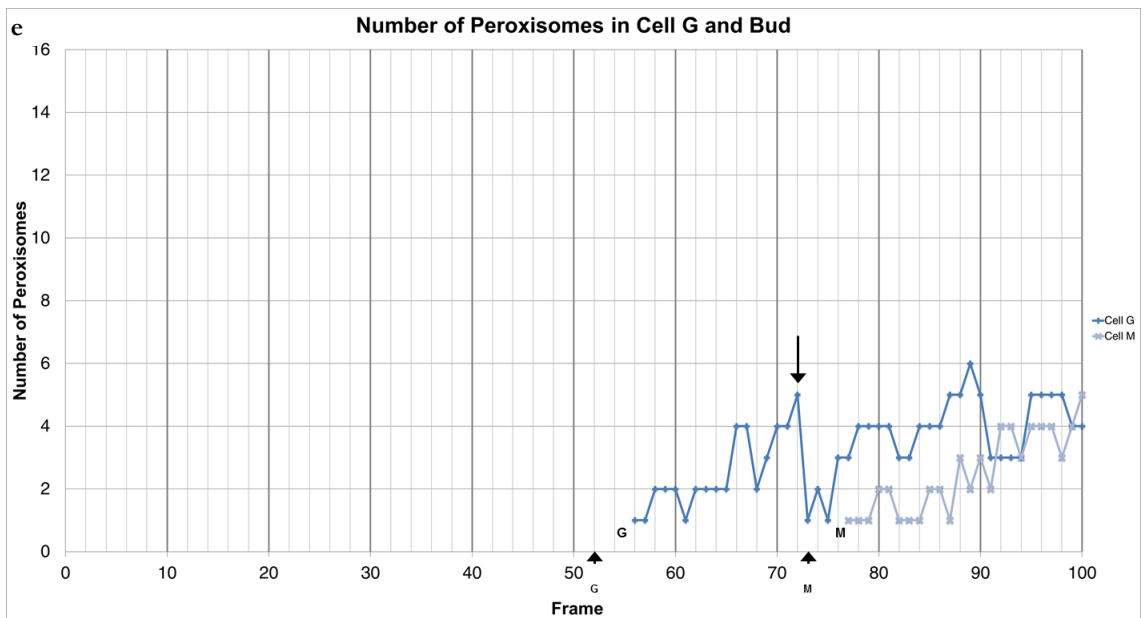
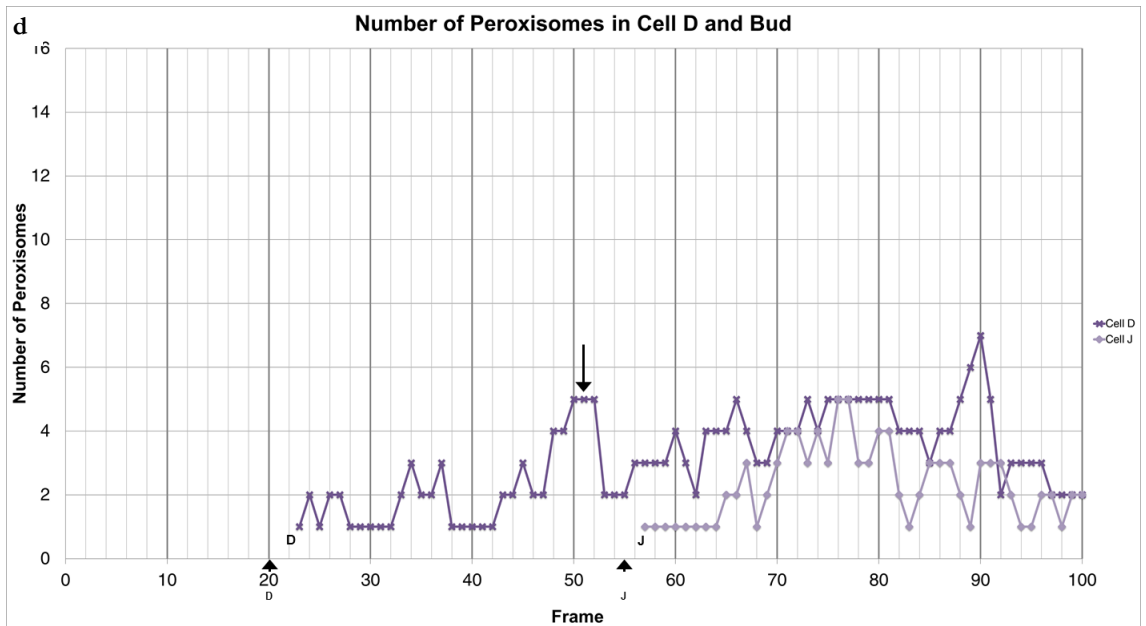


Figure 6.3a-e (above and previous page). Individual graphs of mother cells (A, B, C, D and G) and their bud cells. Short arrows below the x-axis indicate when the buds are first visible, which is usually a few frames prior to the first recorded point on the graph. Longer black arrows on the graph indicate where there are peaks in the peroxisomal number in the mother cells. Dotted curved lines indicate more tentatively identified peaks. Note how the peaks are prior to the appearance of buds a few frames later.

6.2 Peroxisomal Inheritance in Other Cell Clusters

Do other budding events in other clusters support the observations above? These other clusters of cells have been grown, imaged and processed in the same manner as the one previously described. This section will contain the descriptions of four other clusters of cells (Clusters 2-5). Like Cluster 1, they originate with one starting cell (all called 'Cell A') before growing out into a group of cells. The number of cells in these clusters ranges from 10 to 15. In the same fashion as Table 6.2 and Figure 6.1, the lineages of the cells are presented in Appendix I, along with graphs like Figures 6.2 and 6.3a-e showing peroxisomal number over time, first for all the cells in the cluster followed by graphs for mother cells and their buds.

Across these four clusters there are 43 budding events that can be witnessed from start to finish. Having established with Cluster 1 that it appears a majority of peroxisome proliferation is occurring prior to bud appearance, is the same true across many more cell clusters analysed?

This does indeed appear to be the case. Those situations that do not have a peak in peroxisomal number prior to bud arrival are highlighted in Table 6.4. Out of the 43 buddings in Clusters 2-5, only 7 do not have a peak in peroxisomal number in the mother prior to bud first being visible (16%). If one also includes the buddings from Cluster 1, then there are 9/54 buddings that do not have any peak of peroxisomes in the mother just prior to bud arrival (17%).

This can also be demonstrated graphically by observing the change in peroxisomal number before and after a bud first appears (Figure 6.4). This figure takes the average of the difference between the number of peroxisomes in a frame when a bud first appears (0 on the x axis) and 25 frames either side (-25 to +25 on the x axis) across all budding events. For example, if a mother cell has 10 peroxisomes in a frame when a bud first appears, and only 8 peroxisomes ten frames previously, the number at -10 frames would be recorded as -2. The graph shows the average of these differences for all the 53 buddings examined in this body of work (i.e. all of Clusters 1-5).

As can be seen in from Figure 6.4, compared to the frame when the bud first appears, there are on average more peroxisomes in the preceding 4 frames in the mother cell. This demonstrates that the peak in peroxisomal number occurs prior to the instance when the

bud first becomes visible to the eye. The steady rise to this peak indicates that most of the peroxisomal division is occurring in the 10 frames prior to bud arrival, and that on average mother cells have about 1.5-2 more peroxisomes at the peak number than they did at a low point during the middle of the cell cycle (from roughly -1.2 peroxisomes at -10 frames to roughly +0.6 peroxisomes at the peak in -1 frame).

In Cluster 1, the doubling and halving of peroxisomal number in mother cells suggested by the KPPC model could not be seen in most cases. Does this peroxisome proliferation constitute a doubling and halving of peroxisomal number in mother cells when looking across buddings in all the clusters?

After the bud arrival there is a drop in the average difference in the number of peroxisomes as the bud inherits them. On average this difference in the number of peroxisomes prior to a bud being seen and after is not equal, indicating that generally there is a rise in the number of peroxisomes in a mother cell over time. Figure 6.4 demonstrates that this accumulation in mother cells is on average about 0.5 peroxisomes per cell division, as indicated in the difference in average number of peroxisomes relative to the start of the bud formation of ~ -0.9 at -10 frames and ~ -0.4 at +10 frames. This also shows that on average there is not quite a doubling and halving of peroxisomes over the course of the cell cycle; instead mother cells retain relatively more peroxisomes than they give to their buds.

Something noted with Cluster 1 was that after the initial inheritance of peroxisomes from mother to bud, there were instances when the peroxisomal number in the bud increased past this number. Was this seen again?

An assumption is made here regarding when buds have detached from their mother cell, as getting precise information of when each budding event ends would require manual analysis of all the individual images. Buds are assumed to have detached from their mother cells within 20 frames of first appearing (assuming a rough generation time of 100 minutes in the flow cell chamber, which is just slightly less than optimal (90 minutes)). Those buds that have not yet finished budding by the end of the experiment are not included in the following analysis.

As can be seen in Table 6.4, for a majority of buddings in Clusters 2-5 that have completed by the end of the experiment there is an increase of peroxisomes in the bud past the initial inheritance in the mother whilst the bud is still attached (26/34 observations, 76%).

That an increase of peroxisome number in the buds past the number initially inherited from the mother occurred in a majority of cases is different to Cluster 1, when it only occurred for three of the ten buddings that had completed by the end of the experiment (30%); perhaps this indicates that Cluster 1 is an unusual case. A comparison of Figures 6.4 and 6.5 shows that on average the increase of peroxisomes in the bud past the inheritance in the mother is the normal scenario. The average number of peroxisomes given to a bud by a mother cell is ~1.5 (Figure 6.4), indicated by the drop from the peak at -1 frames to the low point at +6 frames. Knoblach et al., 2013 assert that inheritance of peroxisomes from mother to bud is finished by 40 minutes after the bud first appears (8 frames in this analysis), which is in near agreement with Figure 6.4 indicating that inheritance has completed by 6 frames (30 minutes) after bud has first appeared. However, the number of peroxisomes in a bud at this point is already larger on average than 1.5 peroxisomes inherited from mother cells, and continues on an upward trend away from this number over time. This indicates that buds are acquiring additional peroxisomes than they initially inherit from the mother: either there is fission of peroxisomes occurring in the bud or rapid coupled division and inheritance of peroxisomes from mother to bud.

Table 6.4 (next page). The correlation between peaks in the number of peroxisomes in a mother cell and when buds first appear. Instances when this does not occur are highlighted in yellow (9/54 buddings across the five clusters). Also documented in the table are instances when the peroxisomal number in the bud rises past the initial inheritance (29/44 observations when those buds that are not finished by the end of the 100 frames are excluded). As with section 7.1, initial inheritance of peroxisomes is the amount that the total number of peroxisomes in a mother cell drops from its peak to a low point e.g. in Cell A in Cluster 1 there is a peak in the number of peroxisomes at 12 in frame 13, and low of 6 at frame 22, so Cell C is taken to have inherited 6 peroxisomes. 20 frames (100 minutes) after first appearance of the bud is used as the cut off point for when budding will have finished and the buds will no longer be attached to the mother cell.

Cluster	Mother Cell	Bud	Frame Bud First Seen	Peak in Peroxisomal Number Prior to Bud Arrival?	Number of Peroxisomes Initially Inherited	Any Increase Past Initial Inheritance Within 20 Frames?
1	A	C	13	Yes - Frame 13	6	No
		E	32	Yes - Frame 32	5	No
		G	52	Yes - Frame 52	5	No
		K	73	Yes - Frame 73	4	No
		L	88	Yes - Frame 83	5	No - but experiment ends before 20 frames elapsed
	B	D	20	No- Peak very early at Frame 10	3	No
		H	51	Small Peak at Frame 51	2	Yes
	C	F	51	Small Peak at Frame 50	4	Yes
		I	72	Yes - Frame 67	5	No
	D	J	55	Yes - Frames 50-52	3	Yes
G	M	73	Yes - Frame 72	4	No	
2	A	C	7	Yes - Frames 5-7	5	No
		E	30	Yes - Frame 29	3	Yes
		F	47	No - Peak after bud at Frame 51	N/A	Yes
		I	64	Slight Peak at Frame 60	2	Yes
		K	83	Yes - Frame 83	5	No - but experiment ends before 20 frames elapsed
	B	D	19	No - Peak after bud at Frame 24	N/A	Yes
		G	41	No Peak	N/A	Yes
		J	63	Small Peak at Frame 62	1	Yes
	C	L	85	Small Peak at Frame 81-82	1	Yes
		H	49	Yes - Frame 46	3	Yes
I	M	89	Yes - Frame 88	5	No - but experiment ends before 20 frames elapsed	
3	A	C	5	No Peak	N/A	Yes
		D	29	Small Peak at Frames 29-30	1	Yes
		E	68	Yes - Frames 64-69	2	Yes
		I	89	Yes - Frame 89	3	No - but experiment ends before 20 frames elapsed
	D	F	69	Yes - Frame 66	5	Yes
		G	88	Small Peak at Frame 85	2	Yes
	E	J	89	Small Peak at Frame 86	2	No - but experiment ends before 20 frames elapsed
F	H	89	Small Peak at Frame 84	2	Yes	
4	A	C	12	Yes - Frames 8-9	5	Yes
		D	29	No - Peak is at Frame 33	N/A	Yes
		E	48	Yes - Frame 47	5	Yes
		G	72	Yes - Frame 70	6	No
		K	95	No Peak	N/A	No - but experiment ends before 20 frames elapsed
	C	F	44	Yes - Frames 41-43	7	No
		H	67	Yes - Frames 65-67	6	No
E	I	74	Small Peak at Frame 72	2	Yes	
G	J	95	Small Peak at Frame 92	2	No - but experiment ends before 20 frames elapsed	
5	A	C	19	Yes - Frame 16	4	Yes
		E	38	Yes - Frame 37	4	Yes
		H	56	No - Peak is at Frame 59	N/A	Yes
		M	73	Yes - Frame 70	5	No
		P	95	Yes - Frame 94	5	No - but experiment ends before 20 frames elapsed
	B	D	22	Yes - Frame 21	3	Yes
		F	47	Yes - Frame 46	5	No
		J	64	No - Peak is at Frame 67	N/A	Yes
		Q	94	Yes - Frame 90	6	No - but experiment ends before 20 frames elapsed
	C	G	47	Yes - Frames 44-47	3	Yes
		L	71	Yes - Frame 70	5	No
	D	I	57	Yes - Frame 53	4	Yes
	E	K	65	Small Peak at Frames 63-65	2	Yes
		O	88	Yes - Frames 86-87	4	No - but experiment ends before 20 frames elapsed
H	N	78	Yes - Frames 75-76	7	No	

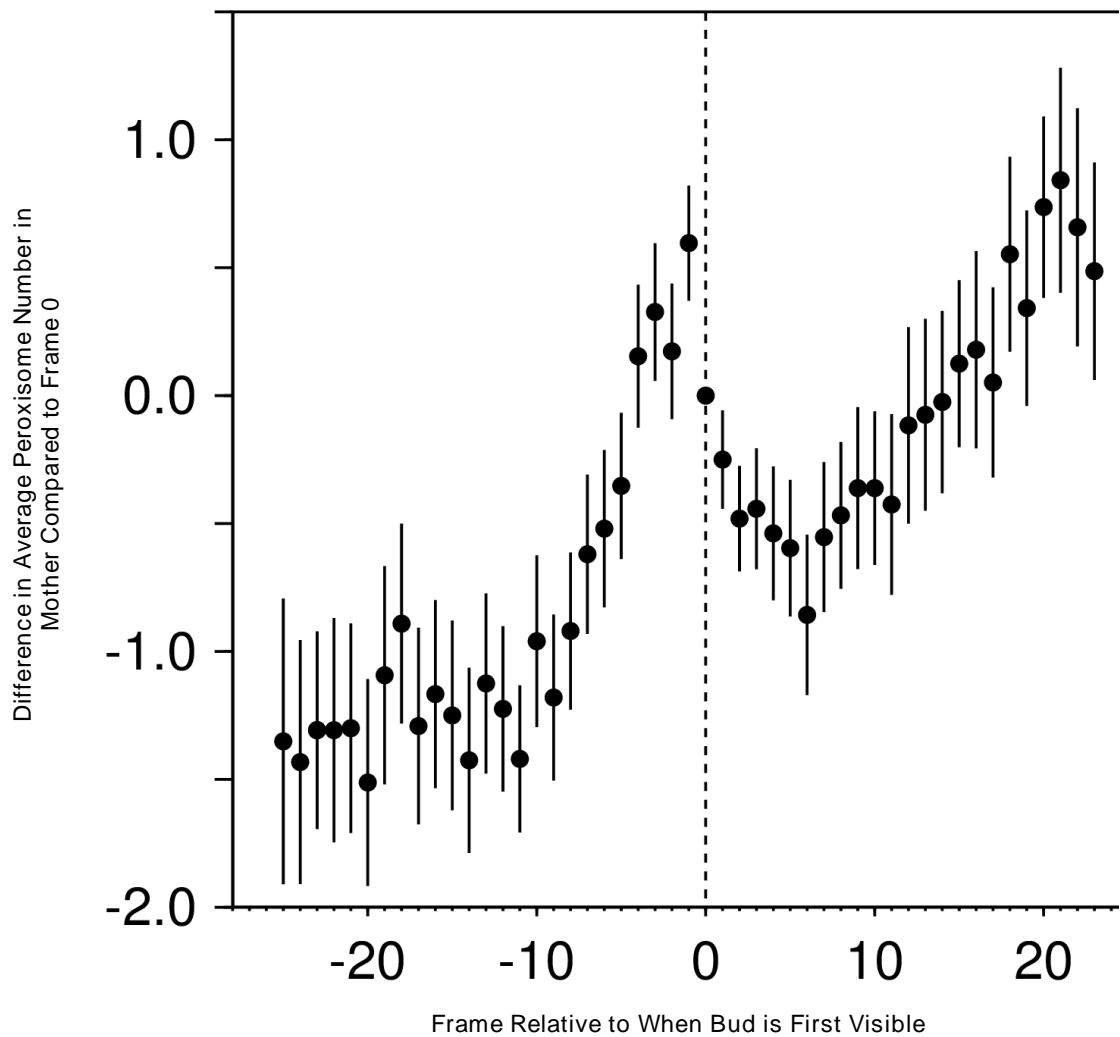


Figure 6.4. Average difference in the number of peroxisomes in mother cells in frames relative to when a bud first becomes visible (0 on x-axis, dotted line). There is an average upward trend in the number of peroxisomes over time, as demonstrated by the higher averages in the positive frames. Graph also demonstrates that mother cells have on average two more peroxisomes at the peak than at the low point before the bud appears. Time between frames is 5 minutes. Error bars are standard error of the mean.

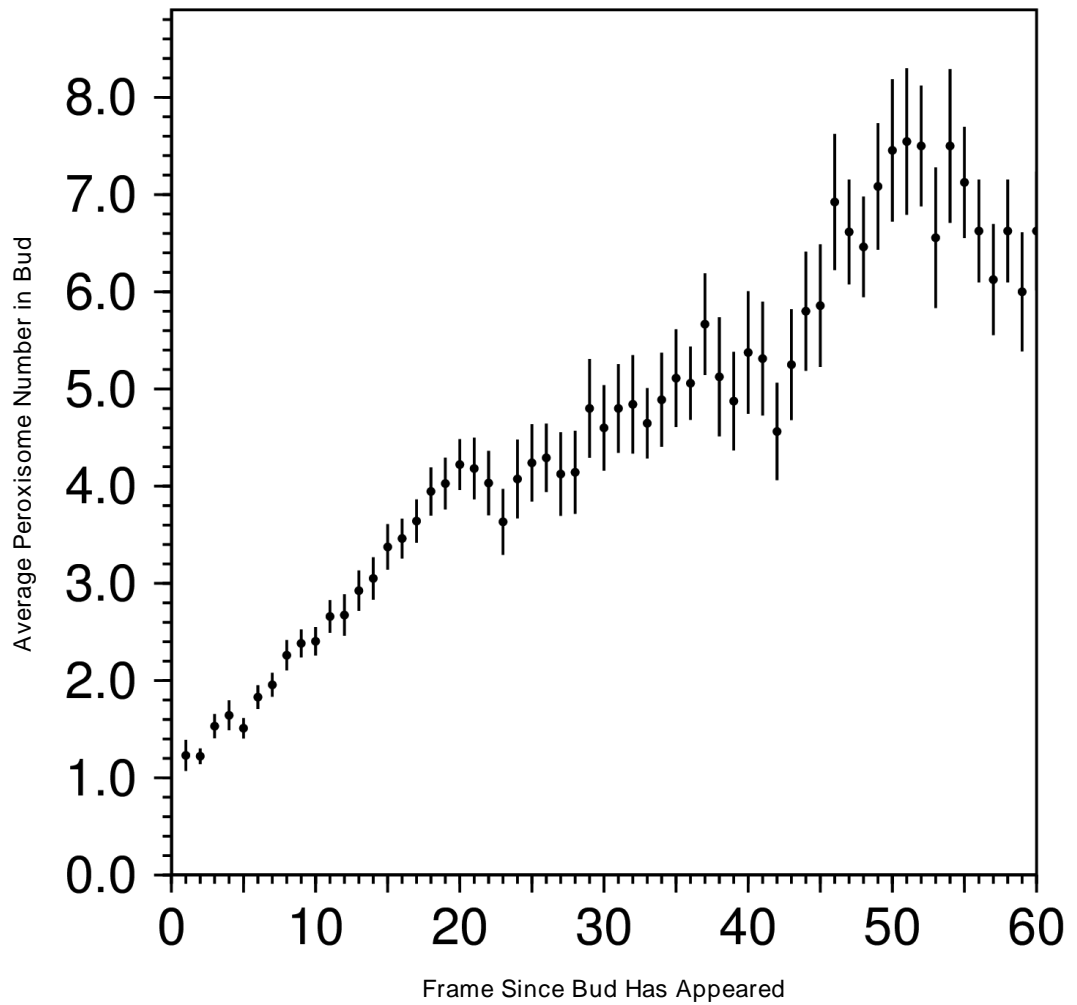


Figure 6.5. Average number of peroxisomes in a bud relative to when the bud first appears. There is clearly an upward trend in the number of peroxisomes that a bud has. Comparison with Figure 6.4 shows that buds quickly have more peroxisomes than given to them by the mother. Time between frames is 5 minutes. Error bars are of the standard error of the mean.

6.3 Evaluation of the KPPC Model from Analysis of All Clusters

How does the analysis of all the clusters of cells feed into the evaluation of the KPPC model raised in Chapter 1.6.2 (and outlined in Table 6.1), and how do the findings here extend what was already seen when looking at just the one cell in the previous chapter?

The first question was whether the establishment of a ‘steady state’ number of peroxisomes could be seen following a cell division. The suspicion from Chapter 5.8 was that the ‘steady state’ number was not set at the end of a budding event. As it has been shown that a majority of peroxisome division occurs just prior to a new bud appearing (Figure 6.4), it is perhaps not surprising that there would not be a relationship between the number of peroxisomes in the mother at the start of a bud formation and the number in the bud at the end. If there is a ‘steady state’ number of peroxisomes presumably it must be established much earlier to the bud’s appearance. There is a period in the middle of the cell cycle when the number of peroxisomes in a mother cell stays relatively flat, indicating that there is little proliferation occurring. This was also seen earlier in the Figure 5.8 analysis of Cell A. Perhaps this is when the ‘steady state’ number of peroxisomes is established?

Figure 6.6 shows the number of peroxisomes in a mother cell 10 frames prior to a bud appearing against the number of peroxisomes in the bud 20 frames after it has appeared. It shows that there is no correlation between the number of peroxisomes in the mother and bud at these points; most of the mother cells have more peroxisomes 10 frames prior to a bud appearing than the buds do when they finish budding, as shown by a majority of the data points being clustered in the bottom-right corner of the graph. If a ‘steady state’ number is established it is not shown by this data. Instead it indicates that there is heterogeneity of behaviour regarding the number of peroxisomes in a mother and the number of peroxisomes in any bud that come off that mother. There are a few instances when the number of peroxisomes in the mother at -10 frames correlates with the number that the bud has by the end, but it does not occur in a majority of instances and does not mean that every peroxisome that existed at that point was split in two; perhaps the same peroxisome was split multiple times and others not at all.

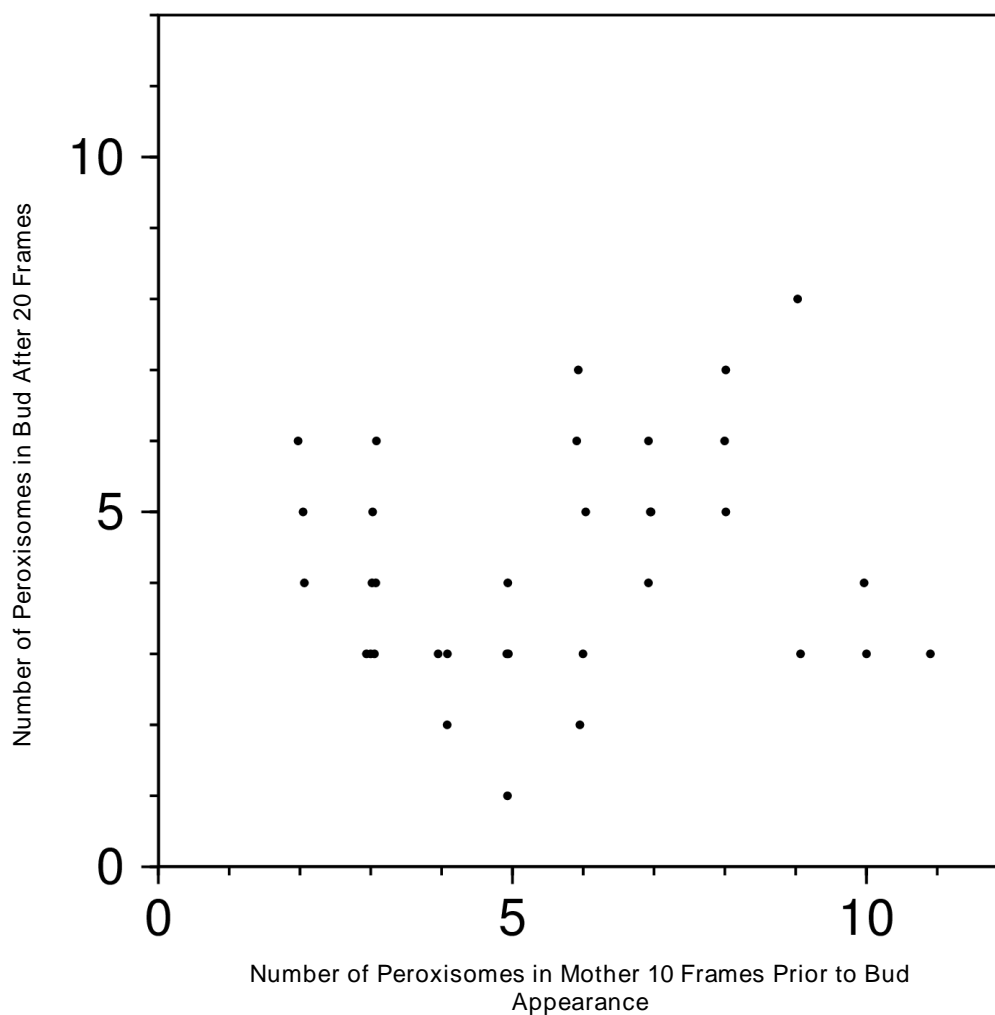


Figure 6.6. Comparison of number of peroxisomes in the mother 10 frames prior to bud appearing and number of peroxisomes in bud 20 frames after it has appeared. At 10 frames prior to a bud appearance the mother cells on average have not started proliferation of peroxisomes, as indicated by Figure 6.4; the 20 frames after bud appearance has been used as a cut off point for buds splitting off from the mother like Table 6.4. As can be seen from the graph, there is no correlation between the number of peroxisomes in the mother at this point and the number of peroxisomes the daughter cells has by the end of the budding. Most points are below the diagonal (bottom right), indicating that mother cells have more peroxisomes prior to a bud appearing than buds do at the end of their budding. There is a slight ‘wiggle’ on the values plotted to allow one to see multiple data points with the same values.

The second question was whether a signature of peroxisome proliferation could be seen. This can be seen as peaks in the number of peroxisomes in mother cells just prior to a bud appearing, as demonstrated in Figure 6.4. This situation is similar to the one proposed in Figure 1.17a, except that peroxisomal number is on a gradual upward trend in most mother cells.

The third question in Chapter 1.6.2 was whether a doubling and halving of peroxisome number over the course of a cell cycle in a mother cell, indicating a 1:1 segregation of peroxisomes between mother and bud could be seen. A doubling and halving appears to be

a good *approximation* of the situation but it is more complicated when one actually looks at the data. As stated in the previous section, mother cells tend to accumulate more peroxisomes over time and this indicates that there is not generally 1:1 segregation of peroxisomes between mother and buds; Figure 6.4 demonstrates that on average mother cells accumulate ~0.5 peroxisome per cell division. Table 6.5 summarises the findings of this analysis.

Table 6.5. Proposal of KPPC model, expected observations for this analysis and actual results.

Proposal in KPPC Model	Expected Observation	Actual Result
Establishment of 'steady state' number of peroxisomes.	Number of peroxisomes in mother cells at bud formation should equal number of peroxisomes in bud after cell division.	Heterogeneity of behaviour witnessed - no clear relationship between number of peroxisomes in a mother and the number of peroxisomes in any bud that come off that mother (Figure 6.6).
Every peroxisome in mother is split, with one being retained by the mother and the other being moved through to the bud, indicating a 1:1 segregation of peroxisomes.	The number of peroxisomes in mother cells should double as they are divided and then halve as peroxisomes are subsequently inherited.	Good approximation of the situation but on average mother cells retain ~0.5 peroxisome per cell division (Figure 6.4).

These findings have also been used to create Figure 6.7, which illustrates a representative portion of one cell cycle and the corresponding changes in peroxisomal number over time. This leads to a few points of discussion regarding the KPPC model.

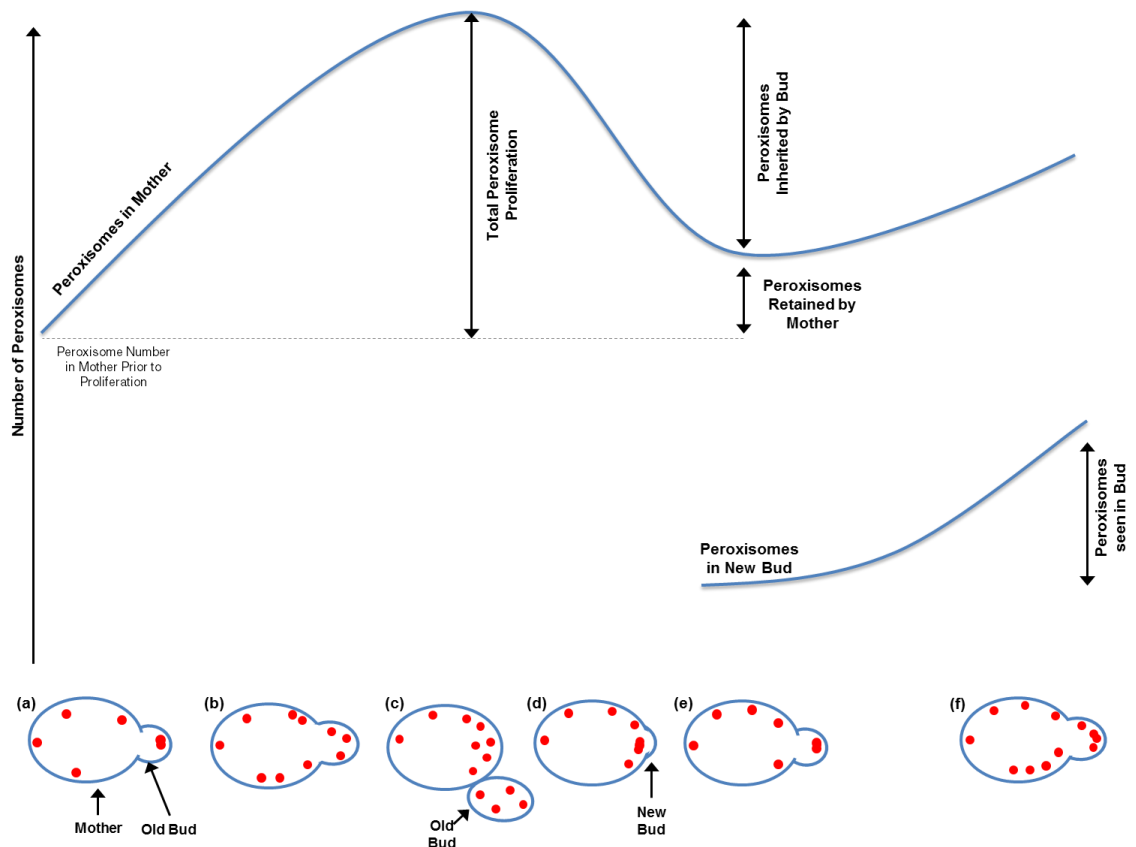


Figure 6.7. Representation of events using the peroxisomal number data. (a) In the middle of the cell cycle there is very little peroxisome proliferation – this represents a low point in the number of peroxisomes in the mother. The old bud has already finished inheriting peroxisomes from the mother. **(b)** Mother cell begins to divide peroxisomes whilst old bud is still attached. These do not get moved across. The old bud now has more peroxisomes than it initially inherited from the mother. **(c)** The old bud has detached and mother cell has completed peroxisome proliferation – represented by peak in peroxisome number. **(d)** New bud begins to be formed, and the peroxisomes cluster around bud neck. This clustering is what gives rise to the initial decrease in peroxisome number seen in mother cells prior to bud formation. **(e)** Bud inherits some peroxisomes from the mother, but not necessarily half of the total peroxisomal content of the mother, and not necessarily all the peroxisomes that the mother produced in this round of peroxisome proliferation. The peroxisomes inherited by the bud are initially clustered at the bud tip and the difference between the number of peroxisomes inherited and the number seen is not equal at first. **(f)** Peroxisomes in the bud separate out and possibly start to divide, and the mother cell starts to divide its peroxisomes again.

6.3.1 Further Discussion Regarding the KPPC Model

Firstly, as this data shows the majority of peroxisome proliferation occurs *prior* to the appearance of a bud, the figure outlining the KPPC model (Figure 9 from Knoblach et al., 2013 and reproduced as Figure 1.9), is somewhat misleading. The bud in a majority of cases is not present when the peroxisomes are divided. This means that peroxisomes are first divided, congregate around the bud neck in most cases (seen in Figure 5.8), before moving across when the bud starts growing. Something to follow up this finding would be to see if there is a relationship between levels of Inp2 and the increases in peroxisomal number in the mother cells. Undoubtedly Inp2 is involved in peroxisomal inheritance (Fagarasanu et al., 2006a), but this line of questioning would investigate to what extent Inp2 is actually involved in peroxisomal division as proposed in the model. Inp2 levels are known to vary with the cell cycle, and have been shown to peak just as peroxisomes are inherited by the bud (Fagarasanu et al., 2009; Knoblach and Rachubinski, 2016); this seems slightly too late to correlate exactly with when most of the peroxisomal division occurs according to this data, so it would be interesting to see what an investigation along these lines uncovers.

Secondly, it is asserted in the KPPC model that peroxisome division is necessary for inheritance (Knoblach et al., 2013). At least in some instances peroxisomes that are divided are not inherited, and also peroxisomes that have been inherited are not divided, at least within 10 frames previously; an example of this is peroxisome '24' in Figure 5.8, which shows no sign of being part of a fission event between frames 22-33 and is moved through to the bud in frame 34. Therefore the assertion in the KPPC model appears not necessarily true in practice. As mentioned in Chapter 5.9, instances like this could be put down to asymmetric or 'non-macroscopic' division of peroxisomes, whereby some portion of the peroxisome remains in the mother but it cannot be visualised – perhaps this is true, but if so little remains of a peroxisome that it cannot be seen, does what remains actually count as a peroxisome? Greater spatial resolution (when or if techniques become available) and a fluorescent protein tagged to a peroxisomal membrane protein would go some way to solving this, as one could observe if there was any peroxisomal membrane content remaining.

Thirdly, in Knoblach and Rachubinski, 2015, the authors 'contend that every peroxisome is split between mother cell and bud, thus guaranteeing that the mother cell keeps, and the daughter cell receives, their fair share of peroxisomes'. The reality appears to be more complicated than this, with peroxisomes in the mother cell undergoing many divisions in the space of a few frames (Chapter 5.7), and the presence of a steadily increasing peroxisomal

number in mother cells indicates that there is much division without inheritance occurring (Figure 6.4).

Lastly there is probably peroxisomal division occurring in buds, as indicated by the average number of peroxisomes in the bud (Figure 6.5) quickly becoming larger than accompanying average drop in the number of peroxisomes seen in the mother cells (Figure 6.4). Peroxisomes dividing on their way to the bud or in the bud itself has been suggested previously (Fagarasanu et al., 2010), so perhaps it is not surprising that it can also be seen here. Coupled peroxisomal division and inheritance in the middle of the cell cycle could also explain this, as the corresponding drop in peroxisomal number in the mother cell would not be seen in this instance. This situation would actually be more akin to the one demonstrated in Figure 1.9; whereby a peroxisome is pulled and split, followed by being moved towards the bud, and finally culminating in the peroxisome being inherited, all happening in rapid succession. The time for all peroxisomes to be inherited from mother to bud has been put at 40 minutes in the literature (Knoblach et al., 2013) and 30 minutes from Figure 6.4, of the bud first appearing. Perhaps this increase in peroxisomal number after the 30-40 minute mark can be attributed solely to fission in the buds, assuming no more inheritance is taking place. However, there is no way of definitively stating that quick coupled division and inheritance of peroxisomes is not occurring in between frames without increased temporal resolution.

The questions set out in Chapter 1.6.2 have been addressed, although only some of them have been answered: a 'steady state' number has not definitively been shown and points instead to heterogeneity of behaviour, a signature of peroxisome proliferation can be seen and looks most similar to the proposal in Figure 1.17a; and lastly there is not a clean doubling and halving of peroxisome number in mother cells.

The overall impression is that the KPPC model is a close *approximation* of what is occurring in wild-type *S. cerevisiae* cells, but is certainly not true in all cases. As demonstrated many times in the above analysis, the KPPC model appears too neat to be a true reflection of reality as there are many caveats and deviations from it. What is clear is that the peroxisomal division and inheritance situation is complex. Returning to the last point, as peroxisomal division appears to be occurring in the bud, then perhaps the purpose of the peroxisomal inheritance machinery is not to ensure that there is tightly regimented inheritance of an exact number of peroxisomes, like the KPPC model suggests, but more to ensure that *some number* of

peroxisomes are retained and *some number* are inherited, regardless of it actually being equitable.

Inp2 levels drop as peroxisomes are moved over to the bud (Fagarasanu et al., 2009), and therefore the presence of a feedback mechanism that regulates this has been speculated about for some time (Fagarasanu et al., 2009; Nuttall et al., 2011), but no such mechanism has yet to be definitively demonstrated. This mechanism, presuming it does exist, might be key to understanding why the data in this study does not suggest such a tightly controlled exact partitioning like in the KPPC model. Perhaps under certain conditions, such as when *S. cerevisiae* are growing on more exotic carbon sources where peroxisomes are required (e.g. oleic acid, methanol, alkanes, etc. (Veenhuis et al., 1983)), this feedback is more tightly regulated, as a system to ensure exact peroxisomal distributions is necessary. Perhaps more loose regulation of peroxisomal distribution between mother and bud is a facet of the yeast growing in conditions where they do not actually require peroxisomes (i.e. on glucose in the lab). Or it may not be, and the buds just compensate for inheriting fewer peroxisomes than they require for growth by dividing them more often on all carbon sources (perhaps regulated via some yet un-described feedback mechanism). This would be an interesting avenue for the future of this work. This may also have some bearing on the relative amounts of *de novo* synthesis of peroxisomes occurring in cells. As has been stated in both Chapters 3 and 5, *de novo* synthesis is not visible in cells that already contain peroxisomes. This additionally may be a case of looking under the wrong conditions; carbon sources requiring more β -oxidation might allow one to witness *de novo* synthesis in action and could be combined with looking into the regulation of peroxisome numbers.

Further possible future work revolves around the question of to what extent the five clusters that were chosen for analysis are representative of the overall population of *S. cerevisiae* cells. The clusters of cells were chosen as they gave a lineage of cells that was easy to follow over time, and also meant that several buddings occurring from the same mother cell could be witnessed. To what extent this biases the analysis from outset remains to be seen.

Perhaps imaging this one area for an extended period causes the cells to behave in a different way than one would observe if one imaged a random area of cells for 2 hours over the course of single budding. One way around this would perhaps be to image large groups of cells only in white light very infrequently (every 20 minutes) as to gather information regarding which cells were mothers and which were buds. This would be followed by an intense period of imaging with a very high sampling frequency with fluorescent light (for example, every 30

seconds) for an extended period to try and catch any peroxisomal division and inheritance events in action. This high sampling rate may allow for accurate tracking of peroxisomes over this period, but may also result in cell death. The current microscopy setup does currently not have the ability to do this in an automated fashion but in principle it could be trialled manually. It would be interesting to see what that data showed regarding which individual peroxisomes are divided and whether they are subsequently inherited, and whether it occurred at the same frequency as seen in Figure 5.8.

Something else to consider is the extent to which any imaging at all is disturbing processes in the cells, and therefore any conclusions that can be made regarding the behaviour of their organelles. Although the Cell As in each of the clusters (i.e. the cell present on commencement of imaging) produced at least 5 buds, the same cannot be said of their progeny. Figure 6.8a demonstrates the time taken for cells to bud, and Figure 6.8b shows the time taken for newly budded cells to produce a bud of their own. A comparison of the two figures reveals none of the first buddings for newly budded cells started before 20 frames after they first appeared. Buds do grow after initially coming off the mother cell so perhaps it is not surprising there is a delay in time taken before they produced their first bud. However, only 14 of the newly budded cells produced over the course of the experiment produced any buds of their own. Of the other buds present at the end of the experiment (i.e. have not been swept away by the action of flow in the flow cell), 10 did not produce any buds even though they existed for longer than 20 frames. The remainder had not yet existed for 20 frames. This demonstrates that ~42% of the newly-budded cells present had not started to produce buds when one would have expected them to – either demonstrating they lack the capacity or are taking a longer time than would be expected to produce a new bud. The extent to which this can be put down to imaging the cells and the extent to which it is heterogeneity of budding behaviour is unclear. It shows that one must always be cautious when making concrete conclusions from live-cell imaging experiments.

Other further work would be to extend this system of live-cell image analysis to a much larger scale. If one were to abandon the rigorous cell outlining and instead aim for a more basic approach, perhaps by utilising a standard circle or oval outline for the cells, then the throughput of the analysis could be increased dramatically. Lineages of cells would still

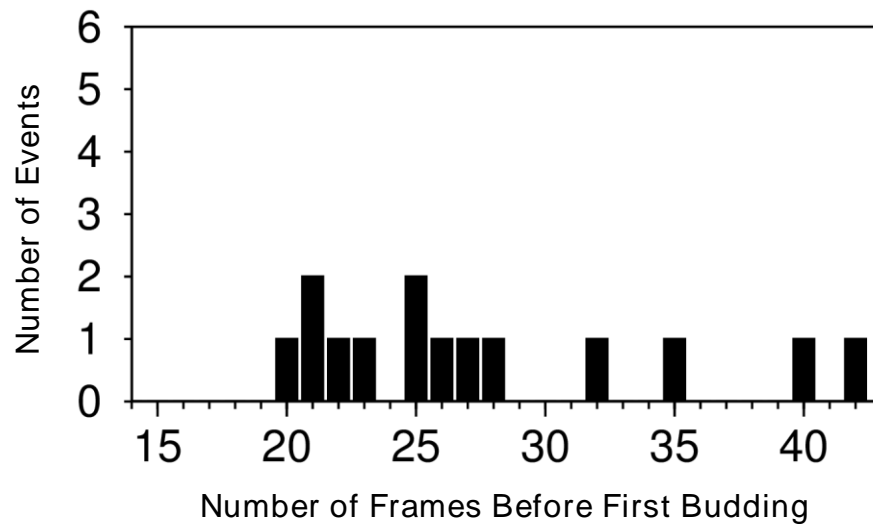
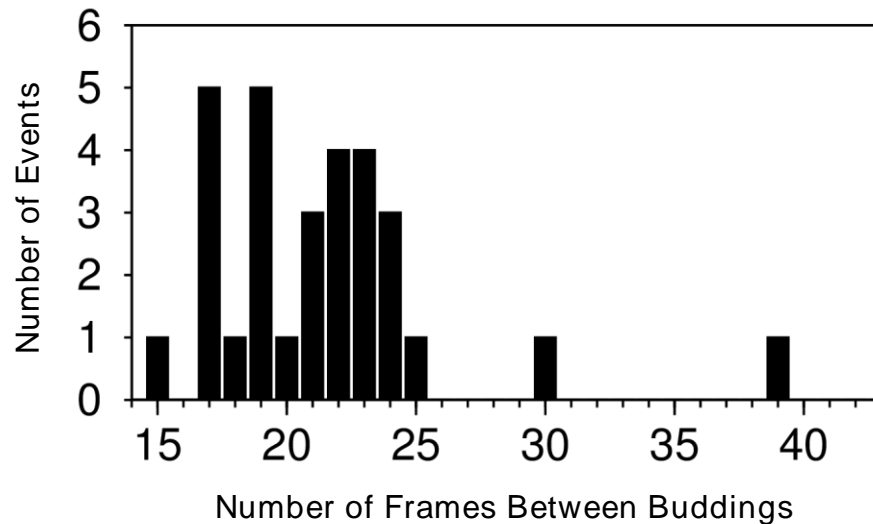


Figure 6.8a and b. a) Number of frames between buddings and b) Number of frames since buds appeared before they start producing buds themselves. As can be seen from a comparison of the two histograms, all newly budded cells (i.e. cells that were not present at the start of the experiment, so this excludes all the Cell As and Bs from the clusters) take in excess of 20 frames in produce their first bud. This means that a vast majority of the buds produced under 20 frame intervals seen in 6.8a are produced by Cell As or Bs. 6b demonstrates that only 14 of the buds that are produced over the course of the 100 frame experiment go on to produce a bud themselves.

have to be discerned, but there would not be emphasis on choosing clusters of cells where the lineage could be traced back through multiple cell divisions. The same quantification technique could be used to analyse the number of peroxisomes over time for a much larger number of cells. Figures like 6.4 and 6.5 could then be produced from this data, and the overall trends would be seen. Once a WT baseline on glucose had been established, the same technique could be used for the WT on different carbon sources or to identify mutants with subtle phenotypes affecting their peroxisomal biogenesis and inheritance.

6.4 Closing Remarks

Taking all into account, the above analysis demonstrates that computational image analysis can be used to see patterns and derive conclusions from complex situations, and adds to the body of work in the literature demonstrating the usefulness of computational image analysis for peroxisomes. Although unfortunately (and frustratingly) tracking the peroxisomes proved too difficult and therefore limited its usefulness for this study, one can imagine how improvements in both the acquired data and image analysis would go far to making the situation tractable. Data acquired with greater spatial (if and when techniques become available) and temporal resolution would enable more accurate localisation of peroxisomes and therefore allow more accurate tracking. This in turn requires advances in keeping cells growing and dividing, which is likely to come from improvements in microscopy hardware setups, such as more sensitive cameras, less damaging light sources, and new ways of imaging samples. Advancements in microscopy are happening quickly, so it is conceivable that one should not have to wait too long until the reality of microscopy techniques has caught up with the imagined uses one has for it.

In collating this body of work, and particularly this ultimate chapter, the impression one gets is that really unravelling what is going on with peroxisomal biogenesis and inheritance is nearly within the grasp of what can be seen in this data. To take an analogy from microscopy, we can see the outline of something, but it is not quite in focus. I am confident that approaches such as those used in this body of work will be key to deciphering the peroxisomal biogenesis and inheritance situation when the necessary image data eventually becomes available.

Appendix A: Data Structures and Terminology in Image Processing

This section describes the data structures and terminology surrounding the handling of images. In image acquisition, one 2D area of a sample in one colour (bright-field, green, red etc.) is taken at one time. Colours are referred to as channels. When acquiring data in multiple channels, for example green and red, one colour is acquired first, then the other. This results in two separate images (one in each channel), which can be stored together.

Acquiring images of the same sample at different focal positions (i.e. to get resolution in Z), results in one image per channel for each focal position (or 'slice') in Z. For example, taking one image every $0.5\mu\text{m}$ for $7\mu\text{m}$ will result in fifteen images, each $0.5\mu\text{m}$ apart in Z. The data structure of a set of images of the same sample at different focal positions is referred to as an image stack (Figure A.1). If acquiring in multiple channels, there will be one stack of images for each channel. This 4D data set is known in FIJI as a hyperstack: a data structure that consists of more than three dimensions. So a 3D Z stack in two channels is a hyperstack because it contains data from four dimensions (X, Y, Z and C (channels)).

Acquiring images over time and in multiple focal planes, such as the live-cell imaging experiments, means acquiring one image for each slice at set intervals. If one continues with the above example, at time = 0, fifteen images will be acquired in each channel, then another fifteen in each channel at time = 1 etc. These images can be stored and opened together as a 5D hyperstack ((X, Y, Z, C and T (time))). As an imaging experiment in two channels, thirteen slices and one hundred time points will consist of 3000 individual images it is easy to see why raw data from the microscope is generally saved in single files as hyperstacks, which can then be dissected down into their individual images at a later point via image processing programs, instead of 3000 individual files.

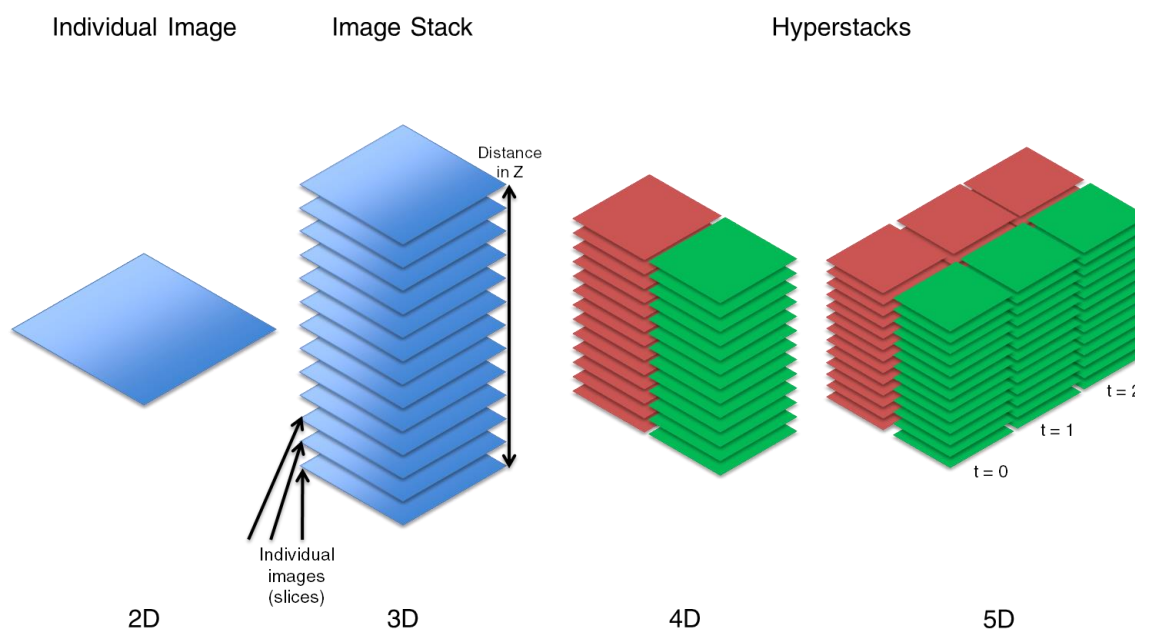


Figure A.1. Examples of different types of image data structure. Taking a picture in one focal plane will result in an individual 2D image. Taking multiple images of the same sample results can be stored as an image stack (with each image called a slice). Taking a stack of images two channels can be stored as a 4D (XYZC) hyperstack. Taking a stack in multiple channels for a set of time points can be stored as a 5D (XYZCT) hyperstack. Stacks and hyperstacks are typically stored as one file but each individual 2D image can be extracted and manipulated using image processing software like FIJI.

Appendix B: FIJI Pointers

ImageJ is a very useful program, and its open source nature means that there is a vast wealth of information out there concerning how best to use its various functions. However, because of the scope of ImageJ, it would have been useful to know a few things about it beforehand. These are outlined below.

B.1 Scripting in FIJI

Writing programs for FIJI can be performed completely external to the program in text editors. Calling FIJI from the command line with reference to the external program will execute the code. However, one can also use FIJI's Macro Editor (Plugins > Macro > New) to write and execute code. Using the Macro Editor in conjunction with the Macro Recorder (Plugins > Macro > Record) allows one to copy recorded commands straight into the editor. If one performs some actions in FIJI with the recorder window open, then the code that is required to execute that command is documented in the recorder. These instructions can then be copied into the editor and adapted as needed. The Macro Recorder can record in the ImageJ Macro language, BeanShell (bash) or Java. However, the Macro language in FIJI is very much self-contained, and does not work in conjunction with Python code. Recording in Java is the easiest way to directly copy the commands from the recorder to the editor when writing in Python, as those commands do not need to be modified extensively.

The ImageJ API is available online (<https://imagej.nih.gov/ij/developer/api/>) and is very useful for troubleshooting. It shows how the classes and objects of FIJI are linked together, what variables and in what order most executable commands require, and normally a brief explanation of what a class or command does. Performing an Internet search of a FIJI command in conjunction with 'ImageJ API' should point one at the correct part of the API.

An important piece of information to know before scripting in FIJI is that the version of Python that currently runs on FIJI is Python 2.5.3. Therefore any functions of Python that exist in the later versions (current release is Python 3.6.0) will not function within FIJI. This is often not a problem, and most of the time anything that can be accomplished in later Python versions can be done so in Python 2.5.3 but with a more verbose code. The website Stack Overflow (<http://stackoverflow.com/>) is highly useful in troubleshooting problems with Python code.

B.2 Tips and Tricks in FIJI

Below are several things that would have been useful to know at the outset of using FIJI:

- CTRL + L can be used to search for commands. As there are many menus in FIJI, it can often be hard to remember which exact menu a particular command is listed under.
- The above trick is highly useful in conjunction with the ‘Close all’ command, and can save much time when a script goes wrong and causes many erroneous windows to open!
- Drawing a line on an image and pressing CTRL + K will display a graph of the intensity values of the pixel that the line passes through.
- Drawing a line or box and pressing CTRL + M will measure various aspects of that line or area. The variables that are being measured can be changed in ‘Set Measurements’ (via Analyze > Set Measurements).

B.3 FIJI Tips for Manual Cell Outlining

- When manipulating ROIs, the arrow keys (↑↓←→) can be used to move the ROI across the image. The inequality symbols (< and >) can be used to move between frames.
- FIJI does not have native support to rename multiple ROIs at the same time. The ‘ROI Manager Tools’ are necessary to perform this function. They can be acquired as part of the BAR suite when updating FIJI (Help > Update FIJI, Manage Update Sites).

Appendix C: Image Processing Techniques

C.1 Rolling Ball Algorithm

Imagine a 3D surface where the intensity of each pixel in 2D is equal to its height on this surface. Rolling a ball over the back of the surface creates the background. This will be subtracted from the original image. This stage of the pre-processing has the effect of levelling out an uneven background, reducing noise and enhancing more intense features of an image. The only parameter that can be specified for this is the radius (in pixels) of the paraboloid. The radius chosen should be appropriate for the size of the object one wants to accentuate. For peroxisomes, which are small, point-like objects, a very small radius was chosen (for peroxisomes this is specified as 1). As cells are much larger objects, a much larger radius of 50 pixels was chosen.

C.2 Z Projection

Projection is way of representing data taken at different focal planes in one 2D image. The appropriate type of Z-projection will vary depending on the original stack of images and how the final 2D image best represents the original set of 3D data. The purpose of Z projection is to provide an extended depth of field view of a sample, bringing objects from across many focal planes together into one 2D image. There are many ways of Z projecting an image. FIJI provides multiple options for a Z-projection to choose from: average intensity, maximum intensity, minimum intensity, sum slices, standard deviation, and median. Performing these different methods of Z projections on the same image stack will produce different outcomes. The maximum intensity projection and the sum slices method were used in this study.

A maximum intensity projection compares all pixels at a particular XY co-ordinate across all Z slices, and selects the one with the highest value to be displayed as the pixel for that co-ordinate in the projected image. A sum slices method of Z projection simply adds up all the values of pixels at a particular XY co-ordinate across all slices and makes that the value of the pixel in the projected image.

For cells, the sum slices method led to a more accurate segmentation of cells compared with a maximum intensity projection. Due to the way fluorescence signal spreads from its source, there is some inevitable smearing of signal into what is really the background surrounding the cells. A maximum intensity projection would give more weighting to this fluorescent

signal, which would be most intense when the sample was most out of focus (i.e. at the extreme of the Z stack), but only slightly above the normal background when the sample was directly in focus (i.e. the central plane of a Z stack). Using a sum slices method of projection corrected for this smearing by making the cells more intense relative to this smearing, and therefore more likely to give a better result from segmentation.

For peroxisomes, the sum slices projection was also used as it corrects for the problem of different intensity peroxisomes in Z. In images with cells containing many peroxisomes, the maximum intensity projection would ‘wash out’ some of the less intense peroxisomes. This is because if there are two peroxisomes that are in the same location in XY, but different planes in Z, then the more intense one will be highlighted over the less intense one, as only the highest value for a particular XY pixel is retained in a maximum intensity projection. By adding all the slices together, more information is retained, as two peroxisomes over one another should be cumulatively brighter than the brightest pixel in the brighter peroxisome. The maximum intensity projection was occasionally used if the signal from the peroxisomes was particularly weak, as to bring it up against the background as much as possible.

C.3 Difference of Gaussians (DoG)

A difference of Gaussians filter is a feature enhancement algorithm that accentuates point-like objects like peroxisomes and suppresses noise. It involves subtracting one blurred version of the image from a less blurred version of the original. The blurring of both images is a convolution with a Gaussian function (a ‘Gaussian blur’). A convolution is where each pixel in an image is assigned a new value set to a weighted average of that pixel's neighbourhood. The weight given to each pixel in a convolution is given by values in a matrix centred on the original pixel. This matrix is called a kernel. In a Gaussian blur, the kernel is a Gaussian function. The original pixel's value receives the heaviest weight (having the highest Gaussian value) and neighbouring pixels receive smaller weights as their distance to the original pixel increases. When performing a Gaussian blur with FIJI, one specifies the sigma (radius) of the blurring. The sigma value is a reference to the radius in pixels of the rate of decay of the Gaussian function to $e^{-0.5}$ i.e. $\sim 61\%$ (the standard deviation of a Gaussian function) (see Figure C.1 for explanation). An important point concerning convolutions in FIJI is that it assumes that pixels that are ‘outside’ of the image are the same value as those on the edge of the image. This gives higher weight to pixels on the edge of the image, especially the corners, so care must be taken when evaluating objects on the edges of the

image.

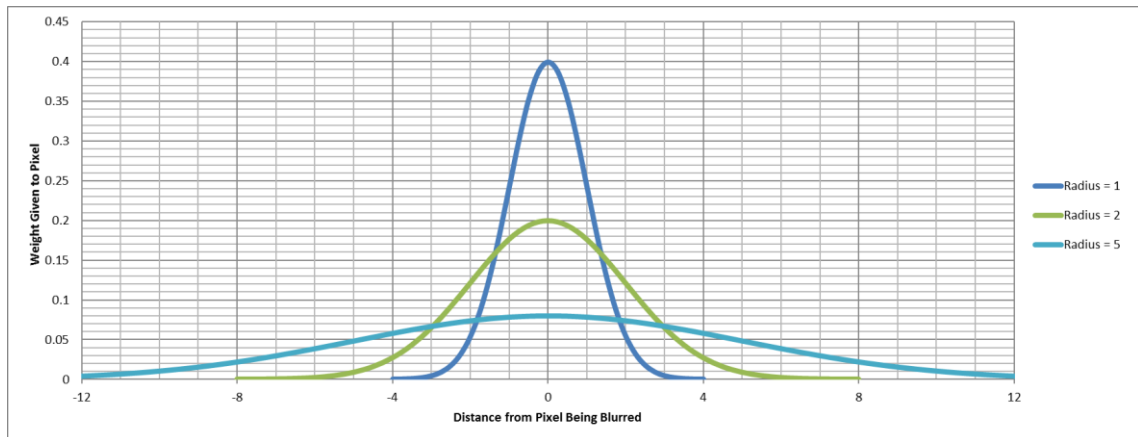


Figure C.1. Example of three Gaussian functions. Three Gaussian functions demonstrating the weights given to pixels when calculating their new intensity on application of a Gaussian blur in one dimension. The original pixel (0 on the x axis) receives the highest weighting. Less weight is given to pixels the further away they are from the original pixel.

The three Gaussian functions have different radii; this is the standard deviation (σ) of the Gaussian function.

As a Gaussian function is given by the equation $e^{-\frac{x^2}{2\sigma^2}}$, the radius is the distance at which the weight given to a pixel decays to $e^{-0.5}$ (~61%) of what it is at the peak (as $x = \sigma$). This can be seen in the Gaussian function with a radius of 1. The weighting decays from ~0.4 at the origin to ~0.24 at -1 and 1 distance ($0.4 \times 0.61 = 0.244$).

So, the larger the input radius for the Gaussian blur, the lower the rate of decay of the Gaussian function. Therefore pixels close to the origin pixel will have a larger weight, and therefore when averaging to complete the convolution the resultant pixel will be more similar to the average of its neighbours. Technically all pixels in an image should be included in the convolution calculation as the Gaussian function never truly decays to 0; however pixels greater than 3x radius away from the origin pixel are considered so small as to be treated as 0. One can see how a larger radius can result in a more blurred image.

Although this graph only represents a one-dimensional Gaussian blur, a two-dimensional Gaussian blur can be achieved by first blurring in one dimension and then the other (i.e. sequentially); this is what the algorithm in FIJI does.

C.4 Conversion to 8-bit

8-bit greyscale images contain pixels with values from 0-255, whereas 16-bit greyscale images (the standard format that images are acquired in) have pixel values ranging from 0-65535. Conversion to 8-bit performs a linear scaling of the values from 16-bit down to 8-bit values. Although this compression of the image should lose information, in reality the information within the microscopy images is contained in the very low end of the 16-bit scale. Conversion to 8-bit makes choosing the thresholding values for the maxima finding algorithm and analyse particles command easier as the range of values to pick from is greatly reduced. Moreover, to perform an automatic thresholding of the image, it must be in 8-bit greyscale anyway.

C.5 Maximum Finder Algorithm

The maxima finder algorithm does the following: it first isolates the local maxima (i.e. the most intense pixels) in an image and ranks them in descending order. Then a flood-fill algorithm is used to determine the boundary of this maximum. The flood-fill algorithm keeps adding pixels to the local maxima until the intensity of any pixels to be added have fallen below the ‘threshold’ value as specified by the user. For example, if the most intense pixel in an image has the value of 150, and the tolerance (the amount the intensity can fall from the maxima) is 30, the flood fill algorithm will keep adding pixels to this maximum that have any value above 120. Once the flood-fill algorithm has drawn the boundary box of one maximum, it moves onto the next. If a maximum falls within the bounding box of a previously defined maximum, then the flood fill algorithm is not performed. If there are several maxima of the same value within one bounding box, then the maximum closest to the geometric centre of the box is chosen.

C.6 Auto Local Threshold

This is different to the automatic thresholding used for the peroxisomal images (‘Auto Threshold’), which thresholds an image on a global scale. The local threshold works by computing the threshold of an individual pixel based on pixels in a user-defined radius r surrounding it. Again, like the global auto threshold method, there are many algorithms that one can use to segment an image. The algorithm that was determined to be the most effective for segmenting images of cells was the ‘Mean’ method; this determines if a pixel is in the foreground based on whether that pixel’s value is greater than the mean value of the other pixels in the radius r surrounding it. This creates a binary image.

Appendix D: Programs Utilising Peroxisomal and Cell Image Analysis Methods

Addressing whether Pex1 and Pex6 were involved in the fusion of heterotypic vesicles required a program that analysed the distance between two fluorescently labelled spots in several different strains of *S. cerevisiae*. This was the only fully automated program used within this thesis for which there are results presented (Chapter 4.2). Nevertheless, this single program alone required good grounding in the techniques of image analysis. The other major programs written during this study are mentioned in this appendix section. They were all written in Python and either ran ‘headlessly’ (i.e. calling an instance of FIJI), or inside FIJI via its scripting interface. Both ways have their merits; programs that call an instance of FIJI can be run in the background or on large computing grids, such as the Iceberg grid in Sheffield. Running scripts from within FIJI itself can take longer, but are much easier to troubleshoot.

D.1 Program to Co-localise Two Different Fluorescent Markers

The raw image data here was of single slices in Z in three channels: brightfield, and green and red fluorescence channels. The brightfield channel did not need to be analysed, as the position of the cells was not relevant. The objects in the fluorescent channels were punctate structures on the images. Therefore the find maxima method of segmenting the image was used to gather the positional information of these puncta in both channels (Chapter 3.8). The version of the program used for acquiring data that was used in Motley et al., 2015 actually used a Fast-Fourier Transform Bandpass filter instead of a Difference of Gaussians, however there is a version of the same program that did use a DoG filter and the results were very similar. Per channel, the positional information of the puncta was saved as a list of XY co-ordinates.

After this, one list of puncta XY co-ordinates was compared against the other. For each XY co-ordinates on the list of co-ordinates from the green channel, the closest corresponding spot in X and Y in the red channel’s list of XY co-ordinates was located using Pythagoras’ Theorem.

The distance in microns between the original green spot and the closest red one was then recorded. This was converted from the distance in pixels that the program had been using until this point at a rate of 0.08 μ m/pixel.

The original spot and its closet match were then removed from their respective lists. After comparing all of the spots, the program recorded the mean, median and standard deviation of the distances between the spots across the different yeast strains. More than 400 fluorescent spots were counted using the program. The Python code for this program is displayed below.

```
# COLOCALISATION OF IMAGES

import glob, string, time, sys, os, math, re
from ij import IJ, measure, ImagePlus, WindowManager
from ij.plugin import ImageCalculator
import ij.plugin.frame
from ij.plugin.frame import RoiManager
from ij.plugin.filter import ParticleAnalyzer, MaximumFinder
from ij.measure import Measurements, ResultsTable
from java.lang import Double
from ij.process import ImageProcessor

#####

def median(x):
    if len(x)%2 != 0:
        return sorted(x)[len(x)/2]
    else:
        midavg = (sorted(x)[len(x)/2] + sorted(x)[len(x)/2-1])/2.0
        return midavg

#####

# Find peroxisomes in green channel

def green_perox(path):

    if not os.path.exists(path):
        return None

    perox = IJ.openImage(path)
    imp_perox = perox.createImagePlus()
    ip_perox_1 = perox.getProcessor().duplicate()

    # -----
    # Image Processing
    # -----

    imp_perox.setProcessor("Perox Copy1", ip_perox_1)

    IJ.run(imp_perox, "Bandpass Filter...", "filter_large=16 filter_small=3 suppress=None tolerance=5 autoscale")
    IJ.run(imp_perox, "Subtract Background...", "rolling=5")
    IJ.run(imp_perox, "8-bit", "")
    IJ.run(imp_perox, "Auto Threshold", "method=Triangle white")

    s = path.split('/')

    img_w_maxi_pth = '/datastore/home1/mba10pcg/Alison/Image_with_perox/'+s[-2]
    if not os.path.exists(img_w_maxi_pth):
        os.makedirs(img_w_maxi_pth)

    img_f = img_w_maxi_pth+'/' +s[-1]
    IJ.saveAs(imp_perox, "Tiff", "%s" %(img_f))

    maxip_perox = IJ.openImage(img_f)
    maximp_perox = maxip_perox.createImagePlus()
    ip_perox_3 = maxip_perox.getProcessor().duplicate()

    maximp_perox.setProcessor("Perox Copy3", ip_perox_3)

    maxi = MaximumFinder().findMaxima(ip_perox_3, 5, ImageProcessor.NO_THRESHOLD, MaximumFinder.SINGLE_POINTS,
False, False)
    imp_perox_m = ImagePlus("Maxima Output", maxi)

    img_f2 = img_w_maxi_pth+'/' + 'g'+s[-1]
    IJ.saveAs(imp_perox_m, "Tiff", "%s" %(img_f2))

    # -----
    # Isolate XY co-ordinates
    # -----

    perox_pixel_path = '/datastore/home1/mba10pcg/Alison/peroxi/'
    perox_file = ''.join(str(perox_pixel_path+s[-1]).split())
    IJ.run(imp_perox_m, "Save XY Coordinates...", "background=0 invert suppress save=%s" %(str(perox_file)))
```

```

perox_path = open(perox_file).readlines()
gpints = []
for line in perox_path:
    f = line.split()
    gpints.append(f[0]+' '+f[1])

return gpints

# -----
# Find peroxisomes in red channel

def red_perox(path):

    if not os.path.exists(path):
        return None

    perox = IJ.openImage(path)
    imp_perox = perox.createImagePlus()
    ip_perox_2 = perox.getProcessor().duplicate()

    imp_perox.setProcessor("Perox Copy2", ip_perox_2)

    # -----
    # Image Processing
    # -----

    IJ.run(imp_perox, "Bandpass Filter...", "filter_large=16 filter_small=3 suppress=None tolerance=5 autoscale")
    IJ.run(imp_perox, "Subtract Background...", "rolling=5")
    IJ.run(imp_perox, "8-bit", "")
    IJ.run(imp_perox, "Auto Threshold", "method=Triangle white")

    s = path.split('/')

    img_w_maxi_pth = '/datastore/homel/mbal0pcg/Alison/Image_with_perox/'+s[-2]
    if not os.path.exists(img_w_maxi_pth):
        os.makedirs(img_w_maxi_pth)

    img_f = img_w_maxi_pth+'/' +s[-1]
    IJ.saveAs(imp_perox, "Tiff", "%s" %(img_f))

    maxip_perox = IJ.openImage(img_f)
    maximp_perox = maxip_perox.createImagePlus()
    ip_perox_4 = maxip_perox.getProcessor().duplicate()

    maximp_perox.setProcessor("Perox Copy4", ip_perox_4)

    maxi = MaximumFinder().findMaxima(ip_perox_4, 1, ImageProcessor.NO_THRESHOLD, MaximumFinder.SINGLE_POINTS,
False, False)
    imp_perox_m = ImagePlus("Maxima Output", maxi)

    img_f2 = img_w_maxi_pth+'/' +r'+s[-1]
    IJ.saveAs(imp_perox_m, "Tiff", "%s" %(img_f2))

    # -----
    # Isolate XY co-ordinates
    # -----

    perox_pixel_path = '/datastore/homel/mbal0pcg/Alison/peroxi/'
    perox_file = ''.join(str(perox_pixel_path+s[-1]).split())
    IJ.run(imp_perox_m, "Save XY Coordinates...", "background=0 invert suppress save=%s" %(perox_file))

    perox_path = open(perox_file).readlines()
    rpints = []
    for line in perox_path:
        f = line.split()
        rpints.append(f[0]+' '+f[1])

    return rpints

#####
#####

the_file = open('/datastore/homel/mbal0pcg/Alison/colocalisation3.txt', 'w')
the_other_file = open('/datastore/homel/mbal0pcg/Alison/colocalisation.txt', 'w')
another_file = open('/datastore/homel/mbal0pcg/Alison/RESULTS.txt', 'w')
onealphalist, sixalphalist, WTlist = [],[],[]
onetttl, sixttl, WTttl, onettlttl, sixttlttl, WTttlttl = 0,0,0,0,0,0
onelttl, sixlttl, WTlttl = 0,0,0

for folder in glob.glob('/datastore/homel/mbal0pcg/Alison/new_perox/*/*'):

    ppf_list = []

    for file in glob.glob(folder+'*'):
        file_name = (file.split('/'))
        f = file_name[-1]
        g = f.split()
        if '_c2.tif' in f:
            gf = f
        if '_c3.tif' in f:
            rf = f

    path_green = folder+gf
    path_red = folder+rf

    gpints = green_perox(path_green)
    rpints = red_perox(path_red)
    points_list = []
    non_colocal_dots = 0

    # -----
    # Match Green Perox to Red Perox

```

```

# -----
if gpoints:
    for gpoint in gpoints:
        dist_list = []
        points_dict = {}
        gp_s = gpoint.split()
        xg,yg = int(gp_s[0]), int(gp_s[1])
        for rpoint in rpoints:
            rp_s = rpoint.split()
            xr,yr = int(rp_s[0]), int(rp_s[1])
            dist = float(((xr-xg)**2)+((yr-yg)**2))
            dist_um = (0.08)*(math.sqrt(dist))
            dist_list.append(dist_um)
            points_dict[dist_um] = rpoint
        dist_list.sort()
        min_dist = dist_list[0]
        if dist_list:
            if min_dist < 0.5:
                points_list.append(min_dist), ppf_list.append(min_dist)
                rpointm = points_dict.get(min_dist)
                rpoints.remove(rpointm)
            else:
                non_colocal_dots += 1
        else:
            print 'OOPS'
ttl = float(0)
if points_list:
    for p in points_list:
        ttl+=p
print>>the_other_file, '\n', 'Average Distance per Stack =',float(ttl)/len(points_list), 'microns', '\n'
ttl_f = float(0)
if ppf_list:
    for p in ppf_list:
        ttl_f+=p
        if g[0] in '1alpha':
            onealphalist.append(p)
        if g[0] in '6alpha':
            sixalphalist.append(p)
        if g[0] in 'WT':
            WTlist.append(p)

s = path_green.split('/')
num_perox = len(ppf_list)
print>>the_file, '\n', s[-2], '\n', 'Average Distance =',float(ttl_f)/num_perox, 'microns', '\n', 'Number
of peroxisomes compared=',num_perox,'\n', 'Non-colocalising dots=', non_colocal_dots, '\n'
print>>the_other_file, '\n', s[-2], '\n', 'Average Distance =',float(ttl_f)/num_perox, 'microns', '\n',
'Number of peroxisomes compared=',num_perox, '\n', 'Non-colocalising dots=', non_colocal_dots, '\n'
if g[0] in '1alpha':
    onettl += (float(ttl_f)/len(ppf_list))
    onettlttl +=1
    onelttl += num_perox
if g[0] in '6alpha':
    sixttl += (float(ttl_f)/len(ppf_list))
    sixttlttl +=1
    sixlttl += num_perox
if g[0] in 'WT':
    WTttl += (float(ttl_f)/len(ppf_list))
    WTttlttl +=1
    WTlttl += num_perox

#####

print>>another_file, '1a=', onettl/onettlttl, median(onealphalist), onelttl, '6a=', sixttl/sixttlttl,
median(sixalphalist), sixlttl, 'WT=', WTttl/WTttlttl, median(WTlist), WTlttl
print>>another_file, onealphalist, '\n', sixalphalist, '\n', WTlist

```

D.2 Program to Analyse Number of Peroxisomes Per Cell

Although not presented as part of this body of work, this program has been utilised for other purposes; such as working out the difference in peroxisomal number based on the size of cells, and comparing the difference in the number of peroxisomes across several mutants for another student's thesis.

Several of the image analysis techniques that are described in the earlier sections were discovered through writing this program. It takes images of cells with fluorescent protein in the cytosol and green-labelled peroxisomes (such as those in Figure 3.9), and processes them

in order to extract the positional data of both the cells and peroxisomes, enabling them to be matched together.

Peroxisomal positional information was gathered using the maxima finder method (see section 3.8). Then, the image of the cells would be segmented and the list of ROIs obtained (see section 3.9). For each ROI (cell) located in the red fluorescent channel, the program looked if there were any matches between the XY co-ordinates of the cell and any of the peroxisomes in the previously acquired list of XY co-ordinates. A tally was kept for the number of peroxisomes matching to cells and any that were would be removed from the list of co-ordinates to be checked through (to speed up the processing).

The end result of this program would be a table listing all the cells contained within one image and how many peroxisomes were contained within each cell. This information could then be used to work out the average number of peroxisomes per cell if required. As ROIs also contain information relating to their size and circularity, one can also use this information to correlate the number of peroxisomes in a cell against its size. This was performed for several mutant strains of *S. cerevisiae*, and no correlation was found. The Python code for this program is displayed below.

```
import glob, string, time, sys, os, fnmatch, math
from ij import IJ, ImagePlus, WindowManager, ImageStack
from ij.plugin import ImageCalculator, Duplicator, ChannelSplitter
import ij.plugin.frame
from ij.plugin.frame import RoiManager
from ij.plugin.filter import ParticleAnalyzer, MaximumFinder
from ij.measure import Measurements, ResultsTable
from java.lang import Double
from ij.process import ImageProcessor
from loci.plugins import BF

# V1.2 Paul Galvin 8th December

##### DEFINE FUNCTIONS #####

# 1. PEROXISOME_ANALYSIS - gets co-ordinates of peroxisomes in image. MUST BE CALLED BEFORE BF or CYTO

def PEROXISOME_ANALYSIS(ImageTitle,which_channel,directory):

    imp_perox1 = IJ.selectWindow(ImageTitle+" - C=%d"%(which_channel))

    IJ.run(imp_perox1, "Subtract Background...", "rolling=1 sliding stack")
    IJ.run(imp_perox1, "Z Project...", "projection=[Sum Slices] copy")

    SUM_image = str("SUM_"+ImageTitle+" - C=%d"%(which_channel))

    # -----
    # Gaussian Blur

    imp_perox1 = IJ.selectWindow(SUM_image)
    imp_perox2 = IJ.run("Duplicate...", " ")
    imp_perox1 = IJ.selectWindow(SUM_image)
    IJ.run(imp_perox1, "Gaussian Blur...", "sigma=1")
    imp_perox2 = IJ.selectWindow(SUM_image+"-1")
    IJ.run(imp_perox2, "Gaussian Blur...", "sigma=2")

    ic = ImageCalculator()
    imp1 = WindowManager.getImage(SUM_image)
    imp2 = WindowManager.getImage(SUM_image+"-1")
    imp3 = ic.run("Subtract", imp1, imp2)

    # -----
    # Convert to 8-bit

    imp3 = IJ.selectWindow(SUM_image)

    IJ.run(imp3, "8-bit", "")
```

```

# -----
# Find Maxima

imp3 = IJ.selectWindow(SUM_image)
IJ.run(imp3, "Find Maxima...", "noise=3 output=[Single Points]")

IJ.selectWindow(SUM_image)
IJ.run("Close", "")
IJ.selectWindow(SUM_image+"-1")
IJ.run("Close", "")

imp4 = IJ.selectWindow(SUM_image+" Maxima")

if not os.path.exists(str(str(directory)+'/Results/')):
    os.makedirs(str(str(directory)+'/Results/'))

perox_file =
str(str(directory)+'/Results/'+str(ImageTitle).strip()+str(which_channel)+'perox_co_ords_results'+'.txt')

# -----
# Extract XY co-ordinates

IJ.run(imp4, "Save XY Coordinates...", "background=0 invert suppress save=[$s]" %(perox_file))

IJ.selectWindow(SUM_image+" Maxima")
IJ.run("Close", "")

# -----
# Number of peroxisomes based on length of list of points - list used later on for matching perox to cells

perox_path = open(perox_file).readlines()

ppoints = []

for linep in perox_path:
    f = linep.split()
    ppoints.append(f[0]+' '+f[1])

    perox_count = len(ppoints)

# if perox_count > 2000:
#     ppoints = []

os.remove(perox_file) # Sometimes can be useful to see co-ords so can be commented out

return ppoints

#####
#####

# 2. BRIGHTFIELD ANALYSIS - segments brightfield images of cells and matches peroxisomes to cells
# Unreliable - I suggest using cytoplasmic labelling for cells!

def BRIGHTFIELD_PROCESSING_PT1 (ImageTitle, which_channel, directory, ppoints):

# -----
# Brightfield Segmentation Part 1
# -----

imp_BF = IJ.selectWindow(ImageTitle+" - C=%d"%(which_channel))

IJ.run(imp_BF, "Z Project...", "projection=[Max Intensity] copy")
MAX_image = str("MAX_"+ImageTitle+" - C=%d"%(which_channel))

# -----
# Process Image

IJ.run(imp_BF, "Subtract Background...", "rolling=10 sliding")
IJ.run(imp_BF, "Convert to Mask", "")
IJ.run(imp_BF, "Invert", "")
IJ.run(imp_BF, "Fill Holes", "")
IJ.run(imp_BF, "Watershed", "")

# -----
# Analyse Particles

table1 = ResultsTable()
roi1 = RoiManager(True)
ParticleAnalyzer.setRoiManager(roi1)
pa = ParticleAnalyzer(ParticleAnalyzer.ADD_TO_MANAGER+ParticleAnalyzer.EXCLUDE_EDGE_PARTICLES,
Measurements.AREA+Measurements.CENTER_OF_MASS, table1, 200.00, 6000.00, 0.65, 1.0)
pa.setHideOutputImage(True)

imp_BF_max = WindowManager.getImage(MAX_image)
pa.analyze(imp_BF_max)

rois = roi1.getRoisAsArray()
roi_count = len(rois)

if not os.path.exists(str(str(directory)+'/Results/')):
    os.makedirs(str(str(directory)+'/Results/'))

cell_path = str(str(directory)+'/Results/'+str(ImageTitle[:-5])+'_Cell_Results'+'.txt')
cell_file = open(cell_path, 'w')

roic, match, empty_cells, perox_in_cells, cell_no, areas = 0,0,0,0,0,0
PEROX_IN_CELLS_LIST = []

roimask=imp_BF_max.duplicate()
roi=roimask.getProcessor()

print>>cell_file, "CellID", "Area", "Num_Perox", "X_Centre", "Y_Centre"

```

```

# -----
# Match peroxisomes to cells

for roi in rois:
    roip.setRoi(roi)
    area = int(table1.getValueAsDouble(0, roic))
    XM = round(table1.getValueAsDouble(8, roic),1)
    YM = round(table1.getValueAsDouble(9, roic),1)
    poly_roi = roi.getPolygon()
    x_points = (str(roi.getPolygon().xpoints)[12:-2]).split(',')
    y_points = (str(roi.getPolygon().ypoints)[12:-2]).split(',')
    for y in range(int(min(y_points, key=lambda x:int(x))), int(max(y_points, key=lambda x:int(x)))):
        for x in range(int(min(x_points, key=lambda x:int(x))), int(max(x_points, key=lambda x:int(x)))):
            if poly_roi.contains(x,y):
                for point in ppoints:
                    f = point.split()
                    if f[0] == str(x) and f[1] == str(y):
                        match += 1
                        ppoints.remove(point)

    if match == 0:
        empty_cells += 1
        print>>cell_file, str(roic).rjust(6), str(area).rjust(4), str(match).center(9), str(XM).rjust(8),
str(YM).rjust(8)

    if match > 0 :
        cell_no += 1
        print>>cell_file, str(roic).rjust(6), str(area).rjust(4), str(match).center(9), str(XM).rjust(8),
str(YM).rjust(8)
        perox_in_cells += match

    PEROX_IN_CELLS_LIST.append(match)
    roic += 1
    match = 0

# -----
# Reset Roi Manager and Save Data

if roi_count > 0:
    roiM1.runCommand('Delete')

    print>>cell_file, "\nNumber of cells with peroxisomes = %s" %(cell_no), "Total peroxisomes = %s"
%(perox_in_cells), "Empty cells = %s" %(empty_cells)
    if perox_in_cells != 0:
        print>>cell_file, "Average number of peroxisomes/cell = %s"
%(float(perox_in_cells)/float((cell_no+empty_cells)))
    print>>cell_file, "Average Area of cells = %s" %(float(areas)/float((cell_no+empty_cells)))

cell_file.close()

IJ.selectWindow(MAX_image)
IJ.run("Close", "")

return roi_count, PEROX_IN_CELLS_LIST

# -----
# Brightfield Segmentation Part 2 - called if Part 1 did not process image correctly
# -----

def BRIGHTFIELD_PROCESSING_PT2(ImageTitle,which_channel,directory,ppoints):

    imp_BF = IJ.selectWindow(ImageTitle+" - C=%d"%(which_channel))

    # -----
    # Process Image

    IJ.run(imp_BF, "Z Project...", "projection=[Max Intensity] copy")
    MAX_image = str("MAX_"+ImageTitle+" - C=%d"%(which_channel))

    IJ.run(imp_BF, "Subtract Background...", "rolling=30 sliding")
    IJ.run(imp_BF, "16-bit", "")
    IJ.run(imp_BF, "Auto Threshold", "method=Otsu white")
    IJ.run(imp_BF, "Find Edges", "")
    IJ.run(imp_BF, "Invert", "")
    IJ.run(imp_BF, "Fill Holes", "")
    IJ.run(imp_BF, "Watershed", "")

    # -----
    # Analyse Particles

    table1 = ResultsTable()
    roiM1 = RoiManager(True)
    ParticleAnalyzer.setRoiManager(roiM1)
    pa = ParticleAnalyzer(ParticleAnalyzer.ADD_TO_MANAGER+ParticleAnalyzer.EXCLUDE_EDGE_PARTICLES,
Measurements.AREA+Measurements.CENTER_OF_MASS, table1, 200.00, 6000.00, 0.5, 1.0)
    pa.setHideOutputImage(True)

    imp_BF_max = WindowManager.getImage(MAX_image)
    pa.analyze(imp_BF_max)

    rois = roiM1.getRoisAsArray()
    roi_count = len(rois)

    if not os.path.exists(str(str(directory)+'/Results/')):
        os.makedirs(str(str(directory)+'/Results/'))

    cell_path = str(str(directory)+'/Results/'+str(ImageTitle[:-5])+'_Cell_Results+'.txt')
    cell_file = open(cell_path,'w')

    roic, match, empty_cells, perox_in_cells, cell_no = 0,0,0,0,0
    PEROX_IN_CELLS_LIST = []

    roimask=imp_BF_max.duplicate()
    roip=roimask.getProcessor()

```

```

print>>cell_file, "CellID", "Area", "Num_Perox", "X_Centre", "Y_Centre"

# -----
# Match peroxisomes to cells

for roi in rois:
    roip.setRoi(roi)
    area = int(table1.getValueAsDouble(0, roic))
    XM = round(table1.getValueAsDouble(8, roic),1)
    YM = round(table1.getValueAsDouble(9, roic),1)
    poly_roi = roi.getPolygon()
    x_points = (str(roi.getPolygon().xpoints)[12:-2]).split(',')
    y_points = (str(roi.getPolygon().ypoints)[12:-2]).split(',')
    for y in range(int(min(y_points, key=lambda x:int(x))), int(max(y_points, key=lambda x:int(x)))):
        for x in range(int(min(x_points, key=lambda x:int(x))), int(max(x_points, key=lambda x:int(x)))):
            if poly_roi.contains(x,y):
                for point in ppoints:
                    f = point.split()
                    if f[0] == str(x) and f[1] == str(y):
                        match += 1
                        ppoints.remove(point)

    if match == 0:
        empty_cells += 1
        print>>cell_file, str(roic).rjust(6), str(area).rjust(4), str(match).center(9), str(XM).rjust(8),
str(YM).rjust(8)

    if match > 0 :
        cell_no += 1
        print>>cell_file, str(roic).rjust(6), str(area).rjust(4), str(match).center(9), str(XM).rjust(8),
str(YM).rjust(8)
        perox_in_cells += match

    PEROX_IN_CELLS_LIST.append(match)
    roic += 1
    match = 0

# -----
# Reset Roi Manager and Save Data

if roi_count > 0:
    roiM1.runCommand('Delete')

    print>>cell_file, "\nNumber of cells with peroxisomes = %s" %(cell_no), "Total peroxisomes = %s"
%(perox_in_cells), "Empty cells = %s" %(empty_cells)
    if perox_in_cells != 0:
        print>>cell_file, "Average number of peroxisomes/cell = %s"
%(float(perox_in_cells)/float((cell_no+empty_cells)))

    cell_file.close()

    IJ.selectWindow(MAX_image)
    IJ.run("Close", "")

    return roi_count, PEROX_IN_CELLS_LIST

# 2b BRIGHTFIELD_ANALYSIS - calls cyto_processing and checks for weird low roi count
def BRIGHTFIELD_ANALYSIS(ImageTitle,which_channel,directory,ppoints):

    IT = ImageTitle
    W_C = which_channel
    D = directory
    PP = ppoints

    imp_cyto = IJ.selectWindow(ImageTitle+" - C=%d"%(which_channel))
    # IJ.run(imp_cyto, "Subtract Background...", "rolling=30 sliding stack")

    roi_count, PEROX_IN_CELLS_LIST = BRIGHTFIELD_PROCESSING_PT1(IT,W_C,D,PP)

    if roi_count < 12:
        print 'ROI count too low, trying alternative processing'
        roi_count, PEROX_IN_CELLS_LIST = BRIGHTFIELD_PROCESSING_PT2(IT,W_C,D,PP)

    return PEROX_IN_CELLS_LIST

#####

# 3a CYTOPLASMIC_PROCESSING - segments images with cyto staining and matches perox to cells - called by 3b
def CYTOPLASMIC_PROCESSING(run,ImageTitle,which_channel,directory,ppoints):

    imp_cyto = IJ.selectWindow(ImageTitle+" - C=%d"%(which_channel))
    IJ.selectWindow(ImageTitle+" - C=%d"%(which_channel))

    IJ.run(imp_cyto, "Z Project...", "projection=[Sum Slices] copy")

    SUM_image = str("SUM_"+ImageTitle+" - C=%d"%(which_channel))

    # -----
    # Process Image

    imp_cyto = WindowManager.getImage(SUM_image)
    IJ.run(imp_cyto, "Enhance Local Contrast (CLAHE)", "blocksize=127 histogram=256 maximum=2 mask=None*
fast_(less_accurate)")
    IJ.run(imp_cyto, "8-bit", "")
    IJ.run(imp_cyto, "Auto Local Threshold", "method=Mean radius=10 parameter_1=0 parameter_2=0 white") # If image
doesn't segregate well, consider changing the radius
    IJ.run(imp_cyto, "Invert", "")

    if run in [2,3]: # 2nd attempt inverts and solves problem of strange thresholding
        IJ.run(imp_cyto, "Convert to Mask", "")

```

```

if run in [1,2]:
    IJ.run(imp_cyto, "Fill Holes", "")

if run in [4]:
    IJ.run(imp_cyto, "Dilate", "")

# -----
# Analyse Particles

table1 = ResultsTable()
roiM1 = RoiManager(True)
ParticleAnalyzer.setRoiManager(roiM1)
pa = ParticleAnalyzer(ParticleAnalyzer.ADD_TO_MANAGER+ParticleAnalyzer.EXCLUDE_EDGE_PARTICLES,
Measurements.AREA+Measurements.CENTER_OF_MASS, table1, 200.00, 100000.00, 0.25, 1.0)
pa.setHideOutputImage(True)

imp_cyto_max = WindowManager.getImage(SUM_image)
pa.analyze(imp_cyto_max)

rois = roiM1.getRoisAsArray()
roi_count = len(rois)

if not os.path.exists(str(str(directory)+'/Results/')):
    os.makedirs(str(str(directory)+'/Results/'))

cell_path = str(str(directory)+'/Results/'+str(ImageTitle[:-5])+'_Cell_Results'+'.txt')
cell_file = open(cell_path, 'w')

roic, match, empty_cells, perox_in_cells, cell_no, areas = 0,0,0,0,0,0
PEROX_IN_CELLS_LIST, AREA_OF_CELLS_LIST = [],[]

roimask=imp_cyto_max.duplicate()
roip=roimask.getProcessor()

# -----
# Match peroxisomes to cells

print>>cell_file, "CellID", "Area", "Num_Perox", "X_Centre", "Y_Centre"

for roi in rois:
    roip.setRoi(roi)
    area = int(table1.getValueAsDouble(0, roi))
    XM = round(table1.getValueAsDouble(8, roi),1)
    YM = round(table1.getValueAsDouble(9, roi),1)
    poly_roi = roi.getPolygon()
    x_points = (str(roi.getPolygon().xpoints)[12:-2]).split(',')
    y_points = (str(roi.getPolygon().ypoints)[12:-2]).split(',')
    for y in range(int(min(y_points, key=lambda x:int(x))), int(max(y_points, key=lambda x:int(x)))):
        for x in range(int(min(x_points, key=lambda x:int(x))), int(max(x_points, key=lambda x:int(x)))):
            if poly_roi.contains(x,y):
                for point in ppoints:
                    f = point.split()
                    if f[0] == str(x) and f[1] == str(y):
                        match += 1
                        ppoints.remove(point)

    if match == 0:
        empty_cells += 1
        print>>cell_file, str(roi).rjust(6), str(area).rjust(4), str(match).center(9), str(XM).rjust(8),
str(YM).rjust(8)

    if match > 0 :
        cell_no += 1
        print>>cell_file, str(roi).rjust(6), str(area).rjust(4), str(match).center(9), str(XM).rjust(8),
str(YM).rjust(8)
        perox_in_cells += match

    PEROX_IN_CELLS_LIST.append(match)
    AREA_OF_CELLS_LIST.append(area)
    roic += 1
    match = 0
    area += area

# -----
# Reset Roi Manager and Save Data

if roi_count > 0:
    roiM1.runCommand('Delete')

print>>cell_file, "\nNumber of cells with peroxisomes = %s" %(cell_no), "Total peroxisomes = %s"
%(perox_in_cells), "Empty cells = %s" %(empty_cells)
if perox_in_cells != 0:
    print>>cell_file, "Average number of peroxisomes/cell = %s"
%(float(perox_in_cells)/float((cell_no+empty_cells)))
print>>cell_file, "Average area of cells = %s" %(float()/float((cell_no+empty_cells)))

cell_file.close()

perox_number_threshold = float(len(ppoints))/20

if roi_count < perox_number_threshold:

    IJ.selectWindow(SUM_image)
    IJ.run("Close", "")

return roi_count, PEROX_IN_CELLS_LIST, AREA_OF_CELLS_LIST

#####
# 3b CYTOPLASMIC ANALYSIS - calls cyto_processing and checks for weird low roi count

def CYTOPLASMIC_ANALYSIS(ImageTitle, which_channel, directory, ppoints):

```

```

IT = ImageTitle
W_C = which_channel
D = directory
PP = ppoints

imp_cyto = IJ.selectWindow(ImageTitle+" - C=%d"%(which_channel))
IJ.run(imp_cyto, "Subtract Background...", "rolling=20 sliding stack")

perox_number_threshold = float(len(ppoints))/20

roi_count, PEROX_IN_CELLS_LIST, AREA_OF_CELLS_LIST = CYTOPLASMIC_PROCESSING(1,IT,W_C,D,PP)

if roi_count < perox_number_threshold:
    roi_count, PEROX_IN_CELLS_LIST, AREA_OF_CELLS_LIST = CYTOPLASMIC_PROCESSING(2,IT,W_C,D,PP)
    if roi_count < perox_number_threshold:
        roi_count, PEROX_IN_CELLS_LIST, AREA_OF_CELLS_LIST = CYTOPLASMIC_PROCESSING(3,IT,W_C,D,PP)
        if roi_count < perox_number_threshold:
            roi_count, PEROX_IN_CELLS_LIST, AREA_OF_CELLS_LIST = CYTOPLASMIC_PROCESSING(4,IT,W_C,D,PP)

return PEROX_IN_CELLS_LIST, AREA_OF_CELLS_LIST

#####
##### CALL FUNCTIONS #####
#####

# 4 & 5 - The parts that can be called
# 4. ANALYSE_PEROXISOMES - the function that will be called for a file that calls the other functions

def ANALYSE_PEROXISOMES(filename, PEROX_CH, BF_CH, CYTO_CH):

    the_file = IJ.run("Bio-Formats Importer", " open=[%s] autoscale split_channels color_mode=Composite
view=Hyperstack stack_order=XYCZT" %filename) #using Bio_formats importer splits channels for you

    imp = WindowManager.getCurrentImage()

    if 1 == imp.getNSlices():
        IJ.showMessage("Not a stack!")
        raise RuntimeError("Not a stack!")

    ImageTitle = filename.split('/')[ -1] #filename of the image file
    directory = os.path.dirname(os.path.realpath(filename)) #directory which it is in

    # -----
    # Call the analysis parts

    PPOINTS = PEROXISOME_ANALYSIS(ImageTitle, PEROX_CH, directory)

    #PEROX_IN_CELLS_LIST = BRIGHTFIELD_ANALYSIS(ImageTitle, BF_CH, directory, PPOINTS)

    PEROX_IN_CELLS_LIST, AREA_OF_CELLS_LIST = CYTOPLASMIC_ANALYSIS(ImageTitle, CYTO_CH, directory, PPOINTS)

    # -----
    # Housekeeping

    IJ.run("Close All", "") # Close all FIJI windows
    return PEROX_IN_CELLS_LIST, AREA_OF_CELLS_LIST

    # -----

#####
#####

# 5. ANALYSE_SET - function that calls ANALYSE_PEROXISOMES for multiple files if given directory and pattern
# e.g. ANALYSE_SET('/home1/mbal0pog/ygr/*' ((glob syntax)), 'mspl+pna78+peh010 *.liff' ((fnmatch syntax), 1,0,2)

def ANALYSE_SET(folder, pattern, PEROX_CH, BF_CH, CYTO_CH):

    TOTAL_PEROX_IN_CELLS_LIST, TOTAL_AREA_OF_CELLS_LIST = [], []

    for filename in glob.glob(folder):
        f = filename.split('/')[ -1]
        if fnmatch.fnmatch(f, pattern):
            PEROX_IN_CELLS_LIST, AREA_OF_CELLS_LIST = ANALYSE_PEROXISOMES(filename, PEROX_CH, BF_CH, CYTO_CH)
            TOTAL_PEROX_IN_CELLS_LIST.extend(PEROX_IN_CELLS_LIST)
            TOTAL_AREA_OF_CELLS_LIST.extend(AREA_OF_CELLS_LIST)

    MEAN_PEROX = float(sum(TOTAL_PEROX_IN_CELLS_LIST))/len(TOTAL_PEROX_IN_CELLS_LIST)
    MEAN_AREA = float(sum(TOTAL_AREA_OF_CELLS_LIST))/len(TOTAL_AREA_OF_CELLS_LIST)
    VARIANCE_PEROX = sum([(i-MEAN_PEROX)**2 for i in TOTAL_PEROX_IN_CELLS_LIST])/len(TOTAL_PEROX_IN_CELLS_LIST)
    STD_PEROX = math.sqrt(VARIANCE_PEROX)
    print pattern, MEAN_PEROX, STD_PEROX, MEAN_AREA

    cell_path = str(str(folder)+'/Results/'+str(pattern[: -6])+'_SET_RESULTS'+'.txt')
    cell_file = open(cell_path, 'w')

    print>>cell_file, pattern, MEAN, STD

#####
##### PROGRAM START #####
#####

print 'Analyse Peroxisomes v1.2.'

# -----
# If looking at set these must be defined - call ANALYSE_SET

folder = '' # What folder are the images in? (must be in glob syntax)
pattern = '' # What set of images should be looked at? (must be in fnmatch syntax)

# -----

```

```

# If looking at one file this should be defined - call ANALYSE_PEROXISOMES
filename = ''          # Must be full path

# -----
# These channel variables must be defined regardless of looking at one or many images
PEROX_CH = 2          # What image channel contains peroxisomes?
BF_CH = 0             # What image channel is brightfield?
CYTO_CH = 1          # What image channel is cytoplasmic labelling?

# -----
# Call for one image
# e.g. ANALYSE_PEROXISOMES(filename,PEROX_CH,BF_CH,CYTO_CH)

# -----
# Call for a set of images
# Can call multiple times for different sets by changing variables in function call
# e.g. ANALYSE_SET('/home1/mbal0pcg/ygr/*','msp1+pna78+peh010 *.liff',1,0,2)

# I/O error message needed

#ANALYSE_SET()

print 'Finished'

```

D.3 Program to Analyse Genome Wide Screen of Peroxisomal Mutants

Another large program worth mentioning is a program that analyses a large genome wide screen. The screen that it used for was of *vps1/dnm1* mutant yeast that also contained a mutation in another gene. Like the previous program, this program was written to extract the number of peroxisomes per cell. However, the peroxisomes in *vps1/dnm1* mutant yeast form into elongated structures (as shown in Figures 4.6 and 4.8), so the second method of segmenting peroxisomes was used. This was also done to extract any differences in the size and circularity of the peroxisomes between the mutants.

In order to match these peroxisomes to cells, the centre pixel that constituted a peroxisomal ROI was used to localise them to cells. The ROI was then deleted from a list of peroxisomes so it was not counted twice, and to speed up processing. The end result of this program was a long table containing the name of the mutant, the average number of peroxisomes per cell, the average area of the peroxisomes and the average circularity of the peroxisomes. This data is still being analysed by colleagues. The Python code for this program (for use on a Windows machine, the Linux code is slightly different) is displayed below.

```

import glob, string, time, sys, os
from ij import IJ, ImagePlus, WindowManager, ImageStack
import ij.plugin.frame
from ij.plugin.frame import RoiManager
from ij.plugin.filter import ParticleAnalyzer
from ij.measure import Measurements, ResultsTable
from java.lang import Double
from ij.process import ImageProcessor

# Dear user,
#
# Remember that \ in windows filenames are a pain and need either 'raw string' modification by adding r in front of
# the filename or double backward slashes '\\' to force python to accept the \ as real and not throw errors
# os.path.normpath is required to turn a filepath into something python can read but the backward slashes still
# need to be dealt with
#
#####
#####

```

```

# 1. PEROXISOME_ANALYSIS - gets co-ordinates of peroxisomes in image.
def PEROXISOME_ANALYSIS(ImageTitle):

    imp_perox = IJ.openImage(ImageTitle)

    IT = ImageTitle.split('\')[ -1]

    IJ.run(imp_perox, "Subtract Background...", "rolling=3 sliding")
    IJ.run(imp_perox, "Gaussian Blur...", "sigma=1");
    IJ.run(imp_perox, "8-bit", "")
    IJ.run(imp_perox, "Auto Threshold", "method=Triangle white") # Auto Threshold using the Triangle method.
    White means white objects on a black background

    table1 = ResultsTable() # Generate a new results table
    roiM1 = RoiManager(True)
    ParticleAnalyzer.setRoiManager(roiM1) # This is the table that the results will be
    stored in

    pa = ParticleAnalyzer(ParticleAnalyzer.ADD_TO_MANAGER+ParticleAnalyzer.EXCLUDE_EDGE_PARTICLES,
    Measurements.AREA+Measurements.CENTER_OF_MASS+Measurements.SHAPE_DESCRIPTOR, table1, 20, 1000, 0.00, 1.0)
    # Sets parameters for particle analyser, excluding objects on the edge. Measurements taken are area, XY centre, and
    shape descriptors (of which circularity is one)
    pa.setHideOutputImage(True)
    pa.analyze(imp_perox) # Call particle analyser for image

    time.sleep(0.1)

    rois = roiM1.getRoisAsArray()
    roi_dict = {}

    for table_row, roi in enumerate(rois):

        poly_roi = roi.getPolygon()
        x_points = (str(roi.getPolygon().xpoints)[12:-2]).split(',')
        y_points = (str(roi.getPolygon().ypoints)[12:-2]).split(',')

        row = str(table1.getRowAsString(table_row)).split()[1:]

        roi_dict[table_row] = [(row)]
        points_list = []

        for n,x in enumerate(x_points):
            points_list.append((x_points[n].strip(), y_points[n].strip()))

        roi_dict[table_row].append(points_list)

    if len(rois) > 0:
        roiM1.runCommand('Delete')
    IJ.run("Close All", "")

    return roi_dict

#####
#####

# 2a CYTOPLASMIC_PROCESSING - segments images with cyto staining and matches perox to cells - called by
def CYTOPLASMIC_PROCESSING(ImageTitle,run):

    imp_cyto = IJ.openImage(ImageTitle)

    IJ.run(imp_cyto, "Subtract Background...", "rolling=50 sliding")
    IJ.run(imp_cyto, "Gaussian Blur...", "sigma=1")

    if run in [1,2]:
        IJ.run(imp_cyto, "8-bit", "")
        IJ.run(imp_cyto, "Auto Local Threshold", "method=Mean radius=5 parameter_1=0 parameter_2=0 white") # If
        image doesn't segregate well, consider changing the radius
        IJ.run(imp_cyto, "Convert to Mask", "")

    time.sleep(0.1)

    if run in [2]: # 2nd attempt inverts and solves problem of strange thresholding
        IJ.run(imp_cyto, "Invert", "")

    if run in [1,2]:
        IJ.run(imp_cyto, "Fill Holes", "")

    if run in [3]:
        IJ.run(imp_cyto, "Subtract Background...", "rolling=50 sliding")
        IJ.run(imp_cyto, "Gaussian Blur...", "sigma=1")
        IJ.run(imp_cyto, "Auto Threshold", "method=IsoData white")
        IJ.run(imp_cyto, "Convert to Mask", "")
        IJ.run(imp_cyto, "Fill Holes", "")
        IJ.run(imp_cyto, "Watershed", "")

    IJ.run(imp_cyto, "Translate...", "x=0 y=-4 interpolation=None")

    table1 = ResultsTable()
    roiM1 = RoiManager(True)
    ParticleAnalyzer.setRoiManager(roiM1)
    pa = ParticleAnalyzer(ParticleAnalyzer.ADD_TO_MANAGER+ParticleAnalyzer.EXCLUDE_EDGE_PARTICLES,
    Measurements.AREA+Measurements.CENTER_OF_MASS, table1, 300.00, 10000.00, 0.35, 1.0)
    pa.setHideOutputImage(True)
    pa.analyze(imp_cyto)

    rois = roiM1.getRoisAsArray()
    roi_count = len(rois)

    roi_dict = {}

```

```

if roi_count > 0:
    for table_row, roi in enumerate(rois):
        x_points = (str(roi.getPolygon().xpoints)[12:-2]).split(',')
        y_points = (str(roi.getPolygon().ypoints)[12:-2]).split(',')

        points_list = []

        for y in range(int(min(y_points, key=lambda x:int(x))), int(max(y_points, key=lambda x:int(x)))):
            for x in range(int(min(x_points, key=lambda x:int(x))), int(max(x_points, key=lambda x:int(x)))):
                if roi.getPolygon().contains(x,y):
                    points_list.append((str(x), str(y)))

        row = str(table1.getRowAsString(table_row)).split()
        row.append(0)
        row.append('No')

        roi_dict[table_row] = [(row)]
        roi_dict[table_row].append(points_list)

    roim1.runCommand('Delete')
    IJ.run("Close All", "")

    return roi_count, roi_dict

# 2b CYTOPLASMIC_ANALYSIS - calls CYTOPLASMIC_PROCESSING and checks for weird low roi count
def CYTOPLASMIC_ANALYSIS(ImageTitle):
    roi_count, cell_dict = CYTOPLASMIC_PROCESSING(ImageTitle,1)
    cell_threshold = 10

    if roi_count < cell_threshold:
        roi_count, cell_dict = CYTOPLASMIC_PROCESSING(ImageTitle,2)
        if roi_count < cell_threshold:
            roi_count, cell_dict = CYTOPLASMIC_PROCESSING(ImageTitle,3)

    return cell_dict

#####

# 3. MAKE_PLATE_DICTIONARY - Sorts out filenames for processing
def MAKE_PLATE_DICTIONARY(directory):
    well_dict = {}
    directory = os.path.normpath(directory)

    for f in glob.glob(directory+'*.tif'):
        f_split = f.split('\\')

        pic_filename = f_split[-1]
        pic_filename_split = pic_filename.split('--')

        well_id = pic_filename_split[0]
        pic_id = pic_filename_split[2]

        if well_id not in well_dict.keys():
            well_dict[well_id] = {}

        if pic_id not in (well_dict[well_id]).keys():
            well_dict[well_id][pic_id] = []

        well_dict[well_id][pic_id].append(f)

    return well_dict

#####

# 4. RUN_PROCESSING - Actually runs the processing, calling the other functions to do their jobs
def RUN_PROCESSING(directory):
    # -----
    # Makes a dictionary of dictionaries which contains a list of filenames
    well_dict = MAKE_PLATE_DICTIONARY(directory)

    # -----
    # Make directory for results and set up results file for whole plate
    results_folder_path = '\\'.join(directory.split('\\')[:-1])+'/results/'

    if not os.path.exists(results_folder_path):
        os.makedirs(results_folder_path)

    plate = (results_folder_path.split('\\')[-1]).split('/')[0]
    plate_results_file = open(results_folder_path+str(plate)+'_results'+'.tsv', 'w')

    print>>>plate results file, '%7s \t %15s \t %20s \t %17s \t %8s \t %8s \t %20s \t %15s \t %15s'
    % ('WELL_ID', 'CELLS_COUNTED', 'AVG_PEROX_PER_CELL',
      'NUM_PEROX_COUNTED', 'MIN_PEROX', 'MAX_PEROX', 'AVG_CIRCULARITY_PEROX', 'AVG_AREA_PEROX', 'NOTES')

    # -----
    # For each well perform analysis
    for well_id, pic_id in well_dict.iteritems():

```

```

        cells_in_well_list = [] # This is a list which will contain a readout of each cell in each of the 3
pictures per well
        circularity_list = [] # This list will contain the circularity readings of all peroxisomes in each of the
wells (note that it does not mean that they were matched to any cells and therefore could be slightly inaccurate)
        perox_area_list = []
        notes = ''

        cell_file = open(results_folder_path+str(well_id)+'.tsv','w')
        print>>cell_file, '%3s \t %5s \t %9s \t %9s \t %9s \t %15s'
%('ID','AREA','X_CENTRE','Y_CENTRE','NUM_PEROX','CONTAINS_PEROX')

        # -----
        # For each pair of pictures (3 per well) perform analysis

        for picture_no, channel_list in pic_id.iteritems():

            cherry_file = [x for x in channel_list if 'Cherry' in x][0]
            gfp_file = [y for y in channel_list if 'GFP' in y][0]

            cyto_dict = CYTOPLASMIC_ANALYSIS(cherry_file)

            if cyto_dict:
                perox_dict = PEROXISOME_ANALYSIS(gfp_file)

            # -----
            # For each cell in the picture check for peroxisomes

            for cell, cell_values in cyto_dict.iteritems():

                cell_points = cell_values[1]

                if len(permox_dict) > 1000:
                    notes = 'PROBABLY CYTOSOLIC'

                for perox, perox_values in perox_dict.iteritems():

                    centroid_perox = [str(int(float(permox_values[0][1])),), str(int(float(permox_values[0][2])))] #
Centre in X,Y

                    cell_set = set(map(tuple, cell_values[1])) # List of points in cell
                    perox_set = set(map(tuple, perox_values[1])) # List of points in perox (only outline of
perox actually) (see code above)

                    if perox_set.intersection(cell_set):
                        if centroid_perox in cell_points:
                            cyto_dict[cell][0][4] += 1
                            cyto_dict[cell][0][5] = 'Yes'
                            circularity_list.append(float(permox_values[0][3]))
                            perox_area_list.append(float(permox_values[0][0]))
                        else:
                            cyto_dict[cell][0][5] = 'Yes'

                    cells_in_well_list.append(cell_values[0]) # Dump info about this cell to list

                    cells_in_well_list.append('### %s END ###' % (picture_no)) # Denote end of the pic (when it has run
out cells to look at)

            # -----
            # After looking through the 3 pictures, can now work out the average perox per cell and dump the rest of
the data into a file per well

            num_perox_list = [] # This list will store info about number of
peroxisomes per cell
            for item in cells_in_well_list: # Dump contents of the list into a file
                if '###' in item: # Straight print the line denoting end of a
section
                    print>>cell_file, item
                else:
                    print>>cell_file, '%3s \t %5s \t %9s \t %9s \t %9s \t %15s'
%(item[0],item[1],item[2],item[3],item[4],item[5]) # Format nicely the lines, with one line per cell showing
Cell_ID (arbitrary number but can be used to go back to the picture), X, Y, Perox in cell, and note if cell
contains bits of peroxisome but not its centre
                    num_perox_list.append(int(item[4]))

            cell_file.close() # Close the cell file as to be nice on the
CPU

            if len(num_perox_list) > 0:
                num_perox_counted = float(sum(num_perox_list))
                num_of_cells = int(len(num_perox_list))
                avg_perox_per_cell = num_perox_counted/num_of_cells
                min_perox_per_cell = min(num_perox_list)
                max_perox_per_cell = max(num_perox_list)
                if len(circularity_list) > 0:
                    avg_c_perox = sum(circularity_list)/len(circularity_list)
                else:
                    avg_c_perox = 0
                if len(permox_area_list) > 0:
                    avg_area_perox = sum(permox_area_list)/len(permox_area_list)
                else:
                    avg_area_perox = 0

                print>>plate_results_file, '%-7s \t %15s \t %-20s \t %17s \t %8s \t %8s \t %-20s \t %-15s \t %15s'
%(well_id, num_of_cells, avg_perox_per_cell, num_perox_counted, min_perox_per_cell, max_perox_per_cell,
avg_c_perox, avg_area_perox, notes) # Work out average number of perox per cell based on number of cells, min and
max number and circularity of peroxisomes
                else:
                    notes = 'INVIABLE'
                print>>plate_results_file, '%-7s \t %15s \t %-20s \t %17s \t %8s \t %8s \t %-20s \t %15s \t %15s'
%(well_id, 0, 0, 0, 0, 0, 0, 0, notes)

            plate_results_file.close() # Close the file for this well when

```

```
everything done
    print 'Finished %s' % (plate)                                # Tell the user that its finished (last
line of code to execute)

# Adapted from ANALYSE_PEROXISOMES v1.2WIN
#####
##### PROGRAM START #####
#####

print 'Analyse Peroxisomes v1.3WIN'
print 'October 2016'

RUN_PROCESSING(r'')
```

Appendix E: Resolution Limits

Spatially, there is a limit to the resolution one can acquire in both XY (lateral) and Z (axial) dimensions in widefield light microscopy. The resolution here being an estimate of the minimum distance required to distinguish between two point objects. An estimate of the theoretical lateral resolution is given by the Abbe diffraction limit, as given by the equation:

$$d = \frac{\lambda}{2NA}$$

Where d is the resolution, λ is the wavelength of the light being imaged, and NA is the numerical aperture of the objective. The numerical aperture is a dimensionless number that characterises the range of angles over which the objective can accept light. Taking the wavelength of light to be the peak emission of the fluorescent protein, 518nm for mNeonGreen, and using the numerical aperture of the oil-immersion objective, which is 1.45, the resultant distance is 178nm. In reality this is closer to 200nm when taking into account the transmission of the light through the glass of the lens and the coverslip. The theoretical axial resolution is worse, and is given by the equation:

$$d = \frac{2\lambda}{(NA)^2}$$

Which using the same numbers comes out at 492nm, and again in reality the value is more likely over 500nm. These numbers are quite large relative to the size of a yeast cell ($\sim 5\mu\text{m}$), and very large compared to the size of a yeast peroxisome ($0.1 - 0.5\mu\text{m}$).

Appendix F: Re-evaluation of the role of Pex1 and dynamin-related proteins in peroxisome membrane biogenesis

Motley, A.M., Galvin, P.C., Ekal, L., Nuttall, J.M., and Hettema, E.H.
(2015). *The Journal of Cell Biology*. 211, 1041–1056.

Reevaluation of the role of Pex1 and dynamin-related proteins in peroxisome membrane biogenesis

Alison M. Motley, Paul C. Galvin, Lakhan Ekal, James M. Nuttall, and Ewald H. Hettema

Department of Molecular Biology and Biotechnology, University of Sheffield, Sheffield S10 2TN, England, UK

A recent model for peroxisome biogenesis postulates that peroxisomes form de novo continuously in wild-type cells by heterotypic fusion of endoplasmic reticulum-derived vesicles containing distinct sets of peroxisomal membrane proteins. This model proposes a role in vesicle fusion for the Pex1/Pex6 complex, which has an established role in matrix protein import. The growth and division model proposes that peroxisomes derive from existing peroxisomes. We tested these models by reexamining the role of Pex1/Pex6 and dynamin-related proteins in peroxisome biogenesis. We found that induced depletion of Pex1 blocks the import of matrix proteins but does not affect membrane protein delivery to peroxisomes; markers for the previously reported distinct vesicles colocalize in *pex1* and *pex6* cells; peroxisomes undergo continued growth if fission is blocked. Our data are compatible with the established primary role of the Pex1/Pex6 complex in matrix protein import and show that peroxisomes in *Saccharomyces cerevisiae* multiply mainly by growth and division.

Introduction

For many years, peroxisomes were thought to be autonomous organelles that multiply by growth and division and that import membrane and matrix proteins posttranslationally from the cytosol (Lazarow, 2003). Most peroxisomal matrix proteins contain a C-terminal peroxisomal targeting signal type 1 (PTS1; Gould et al., 1987). PTS1-containing proteins (cargo) are recognized in the cytosol by a soluble receptor (Pex5), which delivers its cargo by binding the docking complex (Pex13/14/17) on the peroxisomal membrane (Otera et al., 2002; Agne et al., 2003). The receptor and its cargo dissociate, and the receptor is recycled to the cytosol (Liu et al., 2012). Recycling requires the receptor to be monoubiquitinated (Platta et al., 2007; Okumoto et al., 2011) by the RING finger complex (Pex2/10/12; Williams et al., 2008; Platta et al., 2009) and extracted from the peroxisomal membrane by the AAA⁻ ATPases Pex1 and Pex6 (Platta et al., 2004, 2005; Miyata and Fujiki, 2005). The docking complex and RING finger complex are physically linked via Pex8 and together form the importomer (Agne et al., 2003). After deubiquitination, the receptor is ready for another round of import (Debelyy et al., 2011; Miyata et al., 2012).

Targeting and insertion of peroxisomal membrane proteins (PMPs) does not require the machinery used for matrix protein import. Targeting of most PMPs (class 1) depends on the predominantly cytoplasmic Pex19, which has a chaperone function that helps it to function as a targeting signal receptor; Pex19 binds targeting signals in newly synthesized PMPs and delivers them to the peroxisomal membrane by docking onto Pex3 (Sacksteder et

al., 2000; Fang et al., 2004; Rottensteiner et al., 2004; Pinto et al., 2006; Yagita et al., 2013; Chen et al., 2014). Some PMPs (class 2), including Pex3, contain targeting signals that are not recognized by Pex19, and these proteins follow an alternative route to peroxisomes (Jones et al., 2004; Hoepfner et al., 2005; Tam et al., 2005; Kim et al., 2006; Matsuzaki and Fujiki, 2008; Halbach et al., 2009; Fakieh et al., 2013; Knoops et al., 2014).

Most yeast mutants that lack functional peroxisomes (i.e., that are unable to import PTS1 proteins) contain peroxisomal membranes. However, two mutants, *pex3* and *pex19*, appear to lack peroxisomal membranes altogether (Hettema et al., 2000; Koek et al., 2007). Upon complementation of these mutants, peroxisomes form from the ER (Fig. 1; Hoepfner et al., 2005; Tam et al., 2005). This process was visualized by inducing the expression of Pex3-GFP in *Saccharomyces cerevisiae pex3* cells. Pex3 was first observed in ER-associated puncta, which subsequently dissociated from the ER and matured into peroxisomes (Hoepfner et al., 2005). Since then, the involvement of the ER in de novo peroxisome formation has been confirmed in various experimental setups (Haan et al., 2006; Toro et al., 2009).

Two models for peroxisome multiplication in wild-type (WT) yeast cells have been proposed (Fig. 1). In the first, peroxisomes multiply predominantly by growth and division, with the ER providing membrane lipids and a subset of PMPs, including Pex3 and Pex22 (Motley and Hettema, 2007; Halbach et al., 2009; Hettema and Motley, 2009; Nuttall et al., 2011; Fakieh et al., 2013), via vesicles that fuse with existing peroxisomes.

Correspondence to Ewald H. Hettema: e.hettema@sheffield.ac.uk

Abbreviations used in this paper: BiFC, bimolecular fluorescence complementation; DRP, dynamin-related protein; mRFP, monomeric RFP; pER, peroxisomal ER; PMP, peroxisomal membrane protein; PTS, peroxisomal targeting signal; WT, wild type; YPD, yeast peptone dextrose.

© 2015 Motley et al. This article is distributed under the terms of an Attribution-NonCommercial-Share Alike-No Mirror Sites license for the first six months after the publication date [see <http://www.rupress.org/terms>]. After six months it is available under a Creative Commons license [Attribution-NonCommercial-Share Alike 3.0 Unported license, as described at <http://creativecommons.org/licenses/by-nc-sa/3.0/>].

Supplemental Material can be found at:
<http://jcb.rupress.org/content/suppl/2015/12/07/jcb.201412066.DC1.html>

The Rockefeller University Press \$30.00
J. Cell Biol. Vol. 211 No. 5 1041–1056
www.jcb.org/cgi/doi/10.1083/jcb.201412066

JCB 1041

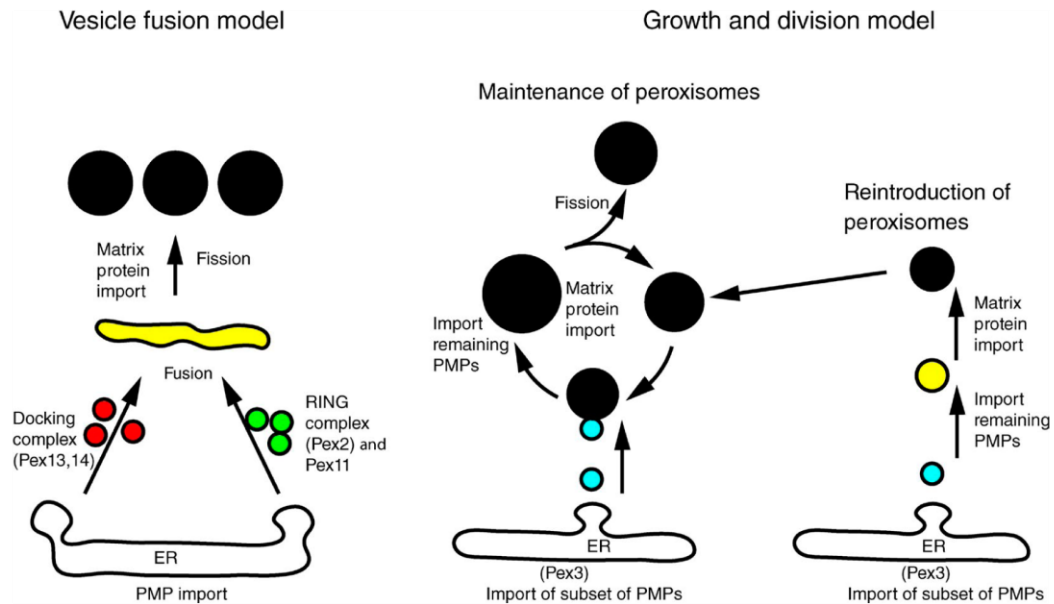


Figure 1. **Schematic representation of models for peroxisome multiplication in *S. cerevisiae*.** The vesicle fusion model proposes all PMPs traffic via the ER and exit in distinct vesicles containing Pex11 and RING finger proteins (Pex2/10/12; green) or docking complex proteins (Pex13/14/17; red). Heterotypic fusion between these vesicles requires the Pex1/6 complex and results in an intermediate compartment (yellow) in which the importomer is fully functional and matrix protein import commences. Peroxisomes form continuously, regardless of whether peroxisomes are already present. According to the growth and division model, preexisting peroxisomes receive newly synthesized membrane and matrix proteins and multiply by DRP-dependent fission. Pex1 and Pex6 are required for matrix protein import by the recycling of the PTS receptors. Only a subset of membrane proteins traffic via the ER (cyan), the remainder being inserted directly into peroxisomes (black). Peroxisomes form de novo only if no peroxisomes are present (reintroduction of peroxisomes): Pex3 localizes first to ER-associated puncta, which subsequently lose ER association (cyan) and acquire other PMPs (yellow), eventually importing matrix (PTS1 containing) proteins (black). Once a cell has formed peroxisomes de novo, they continue to multiply by growth and division.

Other PMPs are inserted directly into the peroxisomal membrane (Fang et al., 2004). The finding that newly synthesized PMPs are transported to existing peroxisomes supports this model (Motley and Hettema, 2007; Fakieh et al., 2013; Menendez-Benito et al., 2013). Fission of peroxisomes is mediated by the direct action of the dynamin-related proteins (DRPs) Vps1 and Dnm1 (Hoepfner et al., 2001; Kuravi et al., 2006; Vizeacoumar et al., 2006; Motley and Hettema, 2007; Motley et al., 2008; Williams et al., 2015). Most *vps1/dnm1* cells contain a single enlarged peroxisome (Kuravi et al., 2006; Motley and Hettema, 2007; Nagotu et al., 2008). The elongated peroxisome of *vps1/dnm1* cells passes through the bud neck and divides upon cytokinesis, resulting in efficient segregation between mother and daughter cells (Hoepfner et al., 2001; Kuravi et al., 2006; Motley and Hettema, 2007). DRPs are not required for the reintroduction of peroxisomes in cells that temporarily lack them (Motley and Hettema, 2007).

An alternative model postulates that all PMPs insert first into the ER (van der Zand et al., 2010), where docking complex proteins (Pex13/14) are sorted away from Pex11 and RING finger complex proteins (Pex2/10/12) before the exit of these complexes in distinct vesicles (Fig. 1; van der Zand et al., 2012). Heterotypic vesicle fusion is proposed to result in the formation of an active translocon, after which the import of matrix proteins can occur (van der Zand et al., 2012). According to this model, vesicle fusion requires the AAA⁺ ATPases Pex1 and Pex6 and gives rise to a continuous stream of new peroxisomes in WT cells that add to the existing population as well as being the mechanism of peroxisome formation in cells lacking peroxisomes (van der Zand et al., 2012; Tabak et al., 2013; van der Zand and Tabak, 2013). DRPs are proposed to act after the Pex1/Pex6-mediated vesicle fusion event. Pex1 and Pex6 have also

been suggested to mediate membrane fusion reactions of preperoxisomal structures during the maturation of peroxisomes in *Yarrowia lipolytica* (Titorenko and Rachubinski, 2000).

Studies in plants, yeast, and mammals have revealed that peroxisomes do not fuse homotypically (Arimura et al., 2004; Motley and Hettema, 2007; Bonekamp et al., 2012). However, both models described above require delivery of membrane material (lipids and proteins). Whereas the vesicle fusion model proposes heterotypic fusion of distinct ER-derived vesicles, the growth and division model proposes that ER-derived vesicles fuse with peroxisomes.

In this study, we reexamined the role of Pex1, Pex6, and the DRPs Vps1 and Dnm1 in peroxisome biogenesis. We found that depletion of Pex1 rapidly blocks matrix protein import but does not affect membrane protein delivery to peroxisomes. We show by genetic analysis that peroxisomal membranes are not maintained by a linear pathway whereby Pex1 acts upstream of DRPs and that reintroduction of peroxisomal membranes does not require Pex1. We find markers previously reported to be present in distinct vesicles localize to the same membranes in *pex1* and *pex6* cells. We show that peroxisomes undergo continued growth if fission is blocked and do not form de novo if peroxisomes are already present. These data support a model whereby peroxisomes multiply mainly by growth and division, and whereby Pex1/Pex6 has a direct role in matrix protein import and not in PMP biogenesis.

To understand the discrepancy between our conclusions and those of van der Zand et al. (2012), we replicated their experimental (bimolecular fluorescence complementation [BiFC]) setup. We found an increased turnover of peroxisomal membranes in *pex1* and *pex6* cells caused by pexophagy, and BiFC-positive peroxisomes divide asymmetrically. We discuss the implications of these new findings.

Results

Peroxisomes grow in the absence of DRP-dependent fission

According to the growth and division model, DRPs are required for fission of peroxisomes that grow as they continue to receive PMPs (and other membrane constituents). To test this, we forced cells lacking DRPs to form peroxisomes de novo (Fig. 2). We replaced the *PEX19* promoter with the *GALI* promoter (in WT and *vps1/dnm1* backgrounds) so that de novo formation is driven by conditional Pex19 expression. When cells are grown on glucose, Pex19 is not expressed, and the peroxisomal matrix marker HcRed-PTS1 is cytosolic. Pex19 expression is induced by switching cells to galactose medium. Import of HcRed-PTS1 first becomes detectable after ~3.5 h on this carbon source, the minimum time required to form peroxisomes de novo (Hoepfner et al., 2005; Tam et al., 2005; Motley and Hettema, 2007). At the early time points of de novo formation, both strains form multiple small peroxisomes per cell. The cultures were kept under conditions of exponential growth, with images being captured at intervals (shown for 4.5 h onwards). The frequency of *vps1/dnm1* cells with more than four peroxisomes decreased with time. After 16 h, >80% of *vps1/dnm1* cells contained a single enlarged peroxisome. That this reduction in peroxisome number is not a consequence of fusion of peroxisomes in *vps1/dnm1* cells is shown in Video 1, Fig. 2 C, and Fig. S1. In the video, we show that the newly formed peroxisomes in *vps1/dnm1* cells segregate until there is just one peroxisome, which becomes elongated as both mother and daughter try to inherit it. In Fig. S1, we pulse labeled peroxisomes in *Mata* or *MatA* cells with HcRed-PTS1 or GFP-PTS1, respectively. After mating, the red and green peroxisomes remained separate, in contrast to mitochondria, which fuse readily (Fig. S1; Nunnari et al., 1997). We have previously shown that peroxisomes in *vps1/dnm1* cells do not fuse (Motley et al., 2008). We conclude that the reduction of peroxisome number in *vps1/dnm1* cells is caused by dilution of peroxisomes by segregation in the absence of fission. We have tested a variety of PMPs (Pex3, Pex11, and Pex13-GFP) in this de novo assay, and as for the PTS1 protein, the number of puncta decreases until there is just a single peroxisome per cell in the *vps1/dnm1* background at the later time points (Fig. S2). We conclude that peroxisomes in dividing *vps1/dnm1* cells, once formed, proceed to grow into enlarged structures. The presence of a single enlarged peroxisome per *vps1/dnm1* cell strongly suggests that new peroxisomes do not form if a peroxisome is already present and is in line with our previous observations (Motley and Hettema, 2007).

Genetic analysis shows Pex1 does not act upstream of DRPs in peroxisomal membrane biogenesis

The vesicle fusion model proposes a role for Pex1/6-mediated vesicle fusion before fission of peroxisomes by DRPs (Fig. 1). To test this, we determined the number of peroxisomal membrane structures in various mutant backgrounds (Fig. 3). Because *pex1* cells are deficient in matrix protein import, we used the peroxisomal membrane markers Pex11- and Pex13-GFP.

pex1 cells have a reduced number of peroxisomal membrane puncta (>70% have one to three puncta; Fig. 3) caused by increased turnover (Nuttall et al., 2014). Peroxisomal membrane structures are more abundant in *pex1* cells lacking the pexophagy receptor Atg36 (>90% of *pex1/atg36* cells have four or more fluorescent puncta; Motley et al., 2012). Cells with quadruple

deletion of *vps1/dnm1/pex1/atg36* have strongly reduced numbers of membrane structures (i.e., their phenotype resembles that of *vps1/dnm1* and not *pex1/atg36* cells; Fig. 3). This cannot be explained by a linear model whereby Pex1 acts upstream of DRPs.

Pex1 is not required for de novo formation of peroxisomal membranes

We tested the role of Pex1 in the formation of peroxisomal membranes using an approach similar to that described above for Fig. 2, in which we forced cells to form peroxisomes de novo by replacing the *PEX19* promoter with the *GALI* promoter. We used Pex13-GFP and Pex11-monomeric RFP (mRFP) as markers for the distinct vesicles (van der Zand et al., 2012), which should persist in the absence of Pex1. Both PMPs show very faint signals at early time points, as PMPs are unstable in the absence of peroxisomes (Hettema et al., 2000), with Pex11-mRFP faintly labeling a tubular network and Pex13-GFP labeling puncta (Fig. 4 A). In *pex19* cells, these puncta also contain Pex3 (Fig. 4 C). Pex3-GFP has previously been seen in the peroxisomal ER (pER) in cells forming peroxisomes de novo (Hoepfner et al., 2005; Tam et al., 2005). The tubular network faintly labeled by Pex11-mRFP in peroxisome-deficient cells colocalizes with MitoTracker (Fig. 4 B). After 3-h growth on a galactose medium, Pex11-mRFP becomes detectable in the Pex13-GFP puncta both in the presence or the absence of Pex1. Therefore, during de novo peroxisome formation (peroxisome reintroduction), peroxisomal membrane structures containing both Pex11-mRFP and Pex13-GFP are formed independently of Pex1.

Induced degradation of Pex1 confirms its role in matrix protein import

We depleted Pex1 using an auxin-inducible degron tag (Nishimura et al., 2009; Nuttall et al., 2014). Degron-tagged Pex1 is undetectable 60 min after the addition of auxin (Fig. 5 A). We induced fluorescent reporter proteins after Pex1 depletion and examined their localization. 90 min after auxin addition, newly synthesized PMPs were transported to preexisting peroxisomes (labeled with HcRed), whereas the import of newly synthesized GFP-PTS1 was blocked. This shows that PMPs still reach peroxisomes in Pex1-depleted cells and are not trapped in the ER or a preperoxisomal compartment. A role for Pex1 and Pex6 in PTS1 import has been well documented (Miyata and Fujiki, 2005; Platta et al., 2005) and is confirmed by our depletion experiment. We noticed occasional PMP-GFP puncta that did not contain detectable matrix marker in both WT and Pex1-depleted cells (Fig. 5 C). We think this arises because of asymmetric fission of peroxisomes (see Fig. 6).

Colocalization of PMPs in *pex1* and *pex6* cells

The experiments in Fig. 4 indicate that Pex1 is not required for de novo formation of peroxisomal membranes or for PMPs to reach existing peroxisomes. To investigate this further, we quantified colocalization of Pex11-mRFP and Pex13-GFP by comparing the coordinates of the center of each fluorescent spot in *pex1*, *pex6*, *pex1/pex6*, and WT cells (see Materials and methods subsection Image acquisition and processing; Fig. 6). We found that the absence of Pex1 or Pex6, or both, does not significantly decrease the degree of colocalization of these markers (Fig. 6, A and B), with the median distance between them being 113, 113, 160, and 160 nm for *pex1*, *pex6*, *pex1/pex6*, and WT, respectively. This is below the resolution of our setup.

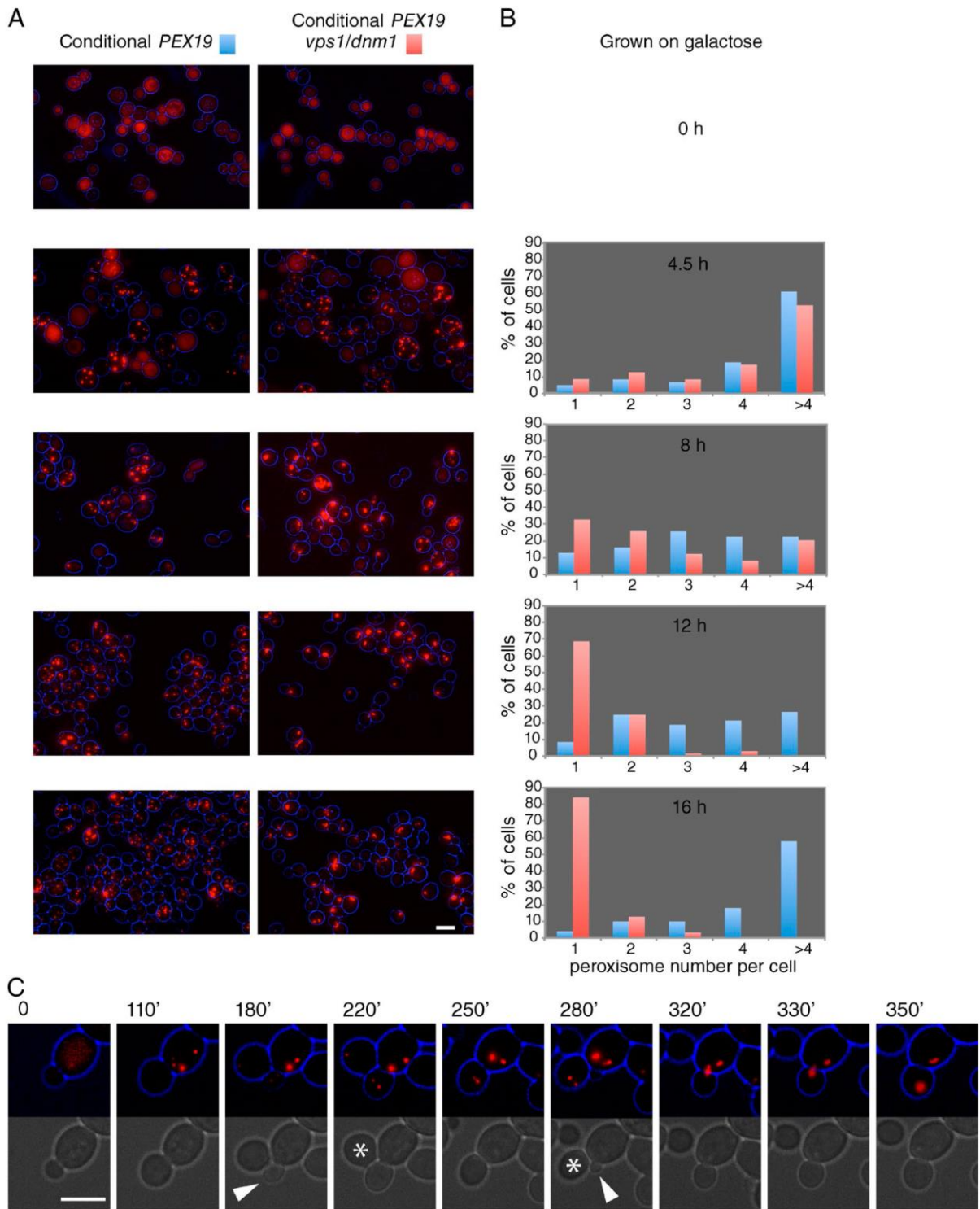


Figure 2. De novo–formed peroxisomes grow into elongated peroxisomes in DRP-deficient cells. (A) Galactose-controllable *PEX19* strains transformed with constitutive HcRed-PTS1 were grown on raffinose (top) or galactose medium for the times indicated in B. (B) Peroxisome number per cell was determined for at least 200 cells for each time point. Blue, conditional *pex19* expression in WT background. Red, conditional *pex19* expression in *vps1Δ/dnm1Δ* background. (C) Stills of a time-lapse video (Video 1): peroxisomes formed de novo in *vps1/dnm1* cells expressing HcRed-PTS1 segregate on cell division, until a single enlarged peroxisome remained. Asterisks indicate cells that move away. Unit of measure is in minutes. Arrows indicate new buds forming. Bars, 5 μ m.

Furthermore, we show that Pex11-mRFP and Pex13-GFP clearly colocalize in the extended membranes of *vps1/dnm1/pex1/atg36* cells (i.e., the absence of Pex1 does not prevent their trafficking

to the same membrane; Fig. 6 C) and that a short (15 min) pulse of Pex11-GFP reaches Pex13-mCherry–labeled peroxisomal membranes in *pex1/pex6* cells (Fig. 6 D).

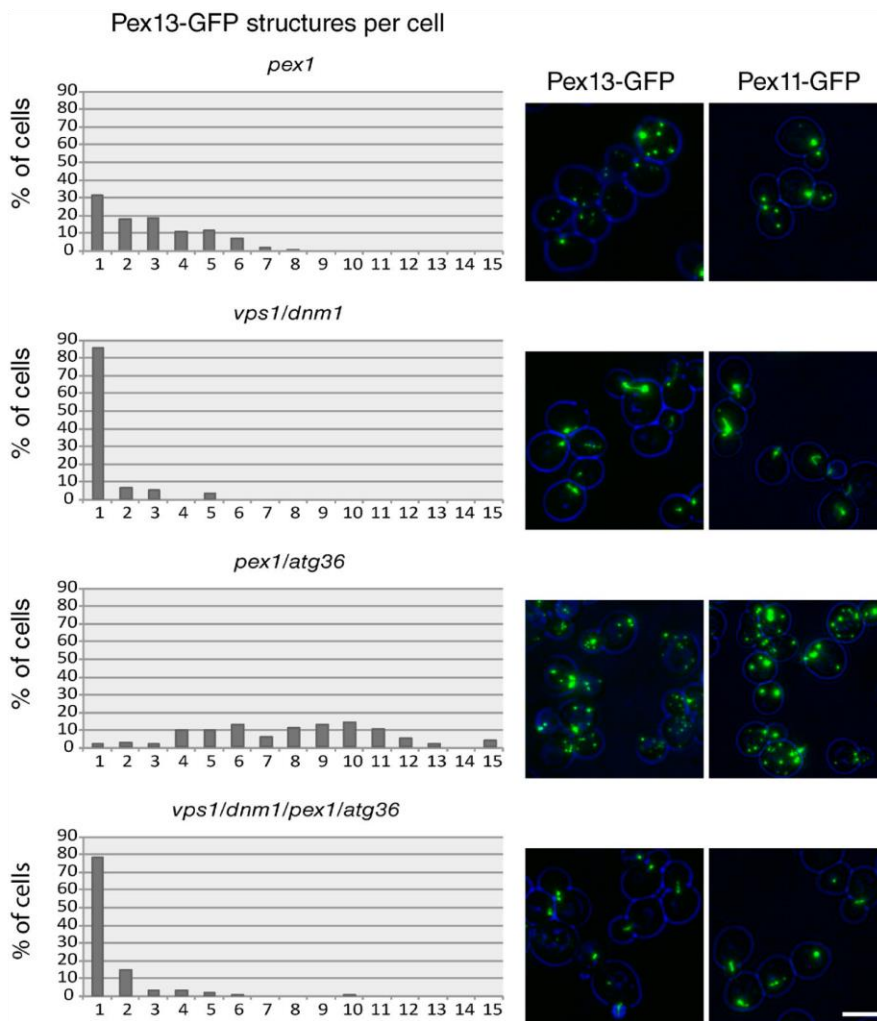


Figure 3. **Quantitation of membrane structures in *pex1Δ*, *pex1Δ/atg36Δ*, *vps1Δ/dnm1Δ*, and *vps1Δ/dnm1Δ/pex1Δ/atg36Δ* cells.** Mutants expressing Pex11- or Pex13-GFP from their endogenous promoters (on plasmids) were imaged by epifluorescence microscopy. Cells were kept in a log phase on glucose-containing medium for 18 h before imaging. The doubling time of WT, *vps1Δ/dnm1Δ*, *pex1Δ/atg36Δ*, and *vps1Δ/dnm1Δ/pex1Δ/atg36Δ* strains under this condition was 101 min, 100 min, 106 min, and 115 min, respectively. The number of Pex13-GFP puncta per cell was determined for at least 200 cells per strain. Bar, 5 μ m.

Homogenates of WT and *pex1*, *pex6*, and *pex1/pex6* cells were analyzed by flotation equilibrium density gradient centrifugation (Fig. 7). Tagged Pex11 and Pex13 cofractionated with each other in all strains analyzed. Endogenous Pex13 floats to the same density as Pex13-GFP and Pex11-GFP in transformed and untransformed cells, indicating that tagging Pex11 and Pex13 does not affect the fractionation of peroxisomal membranes. The distribution of PMPs within the gradients is different in WT cells compared with mutants: the bulk of the PMPs (tagged or untagged) are present in fractions 4 + 5 in WT cells and in fractions 4–7 in *pex1*, *pex6*, and *pex1/pex6* cells (Fig. 7). The shift to lower density fractions of peroxisomal membranes (ghosts) has been reported before (Santos et al., 1988; Gärtner et al., 1991; van Roermund et al., 1991; Motley et al., 1994; Hettema et al., 2000). Furthermore, differential centrifugation experiments (Fig. 7) show that the 25,000 *g* pellet contains the bulk of Pex11-GFP, Pex13-GFP, and Pex13 in both WT and *pex1/pex6* cells, whereas the bulk of the cytoplasmic marker (P_{gk1}) is present in the 25,000 *g* supernatant. A small but reproducible amount of Pex13, Pex11-GFP, and Pex13-GFP was observed in the supernatant fraction of *pex1/pex6* cells. The subcellular fractionation experiments support the fluorescence microscopy observations that Pex11 and Pex13 are present in the same membrane structures in cells lacking Pex1 and/or Pex6.

As our conclusions contrast with those of a previous study (van der Zand et al., 2012), we replicated their experimental setup by reconstructing some of their strains and BiFC Venus tags. We generated identical strains (same tags, linker length, and parental strains) and used the same experimental conditions. To detect interactions between peroxins as a measure of importomer assembly, van der Zand et al. (2012) used BiFC after mating haploid yeast tagged in the genome with Venus GFP N- and C-terminal halves (VN and VC). BiFC occurs when nonfluorescent GFP halves are brought together by interaction between the proteins they are fused to. The presence of a signal was interpreted as the presence of complex formation (i.e., that the proteins are present in the same membrane structure). The absence of a signal was interpreted as the proteins being present in distinct membrane structures (van der Zand et al., 2012).

As markers for the docking complex, we used Pex13-VN and Pex14-VC, and for the RING finger complex, we used Pex2-VN. As shown in Fig. S3, peroxisomes formed within 3 h of mating *pex1* with *pex6* cells, but the BiFC signals took longer to develop. Similar to the observations of van der Zand et al. (2012), 24 h after mating, BiFC was evident in all combinations of Pex13-VN and Pex14-VC (*pex1* \times 6, 6 \times 6, and 1 \times 1), and a weak signal between Pex2-VN and Pex14-VC was observed in the *pex1* \times *pex6* mating combination, although, in our hands, only in a minority (<10%) of mating cells. This signal is very

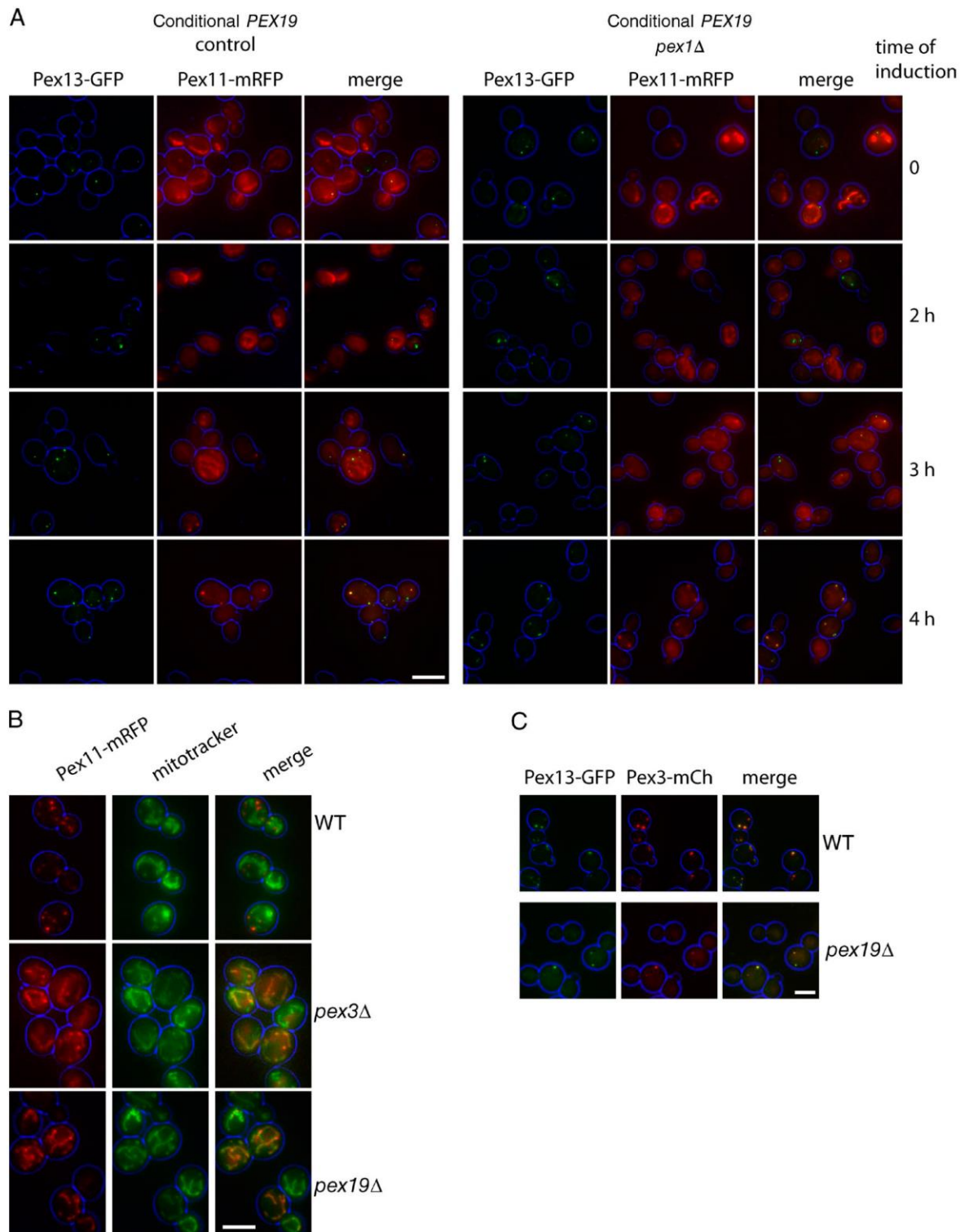


Figure 4. **Pex1 is not required for de novo formation of peroxisomal membranes.** (A) Galactose-controllable *PEX19* strains expressing Pex13-GFP and Pex11-mRFP from their endogenous promoters (on plasmids) were grown on raffinose (top) or galactose medium for the times indicated. The Pex11-mRFP signal was weak and was enhanced strongly to show localization. (B) WT, *pex3Δ*, and *pex19Δ* cells expressing Pex11-mRFP from its endogenous promoter on plasmid were grown to log phase and stained with MitoTracker green. (C) WT and *pex19Δ* cells expressing Pex13-GFP and Pex3-mCherry (Pex3-mCH) from endogenous promoters (on plasmids) were grown to log phase. Bars, 5 μ m.

weak and varies between experiments. The lack of Pex2-VN/Pex14-VC BiFC in *pex1* \times *pex1* and *pex6* \times *pex6* mating combinations was previously interpreted as an indication that Pex2

and Pex14 are present in distinct vesicles. However, the lack of an already faint signal could also be a consequence of enhanced pexophagy that occurs in *pex1* and *pex6* cells (Nuttall et al.,

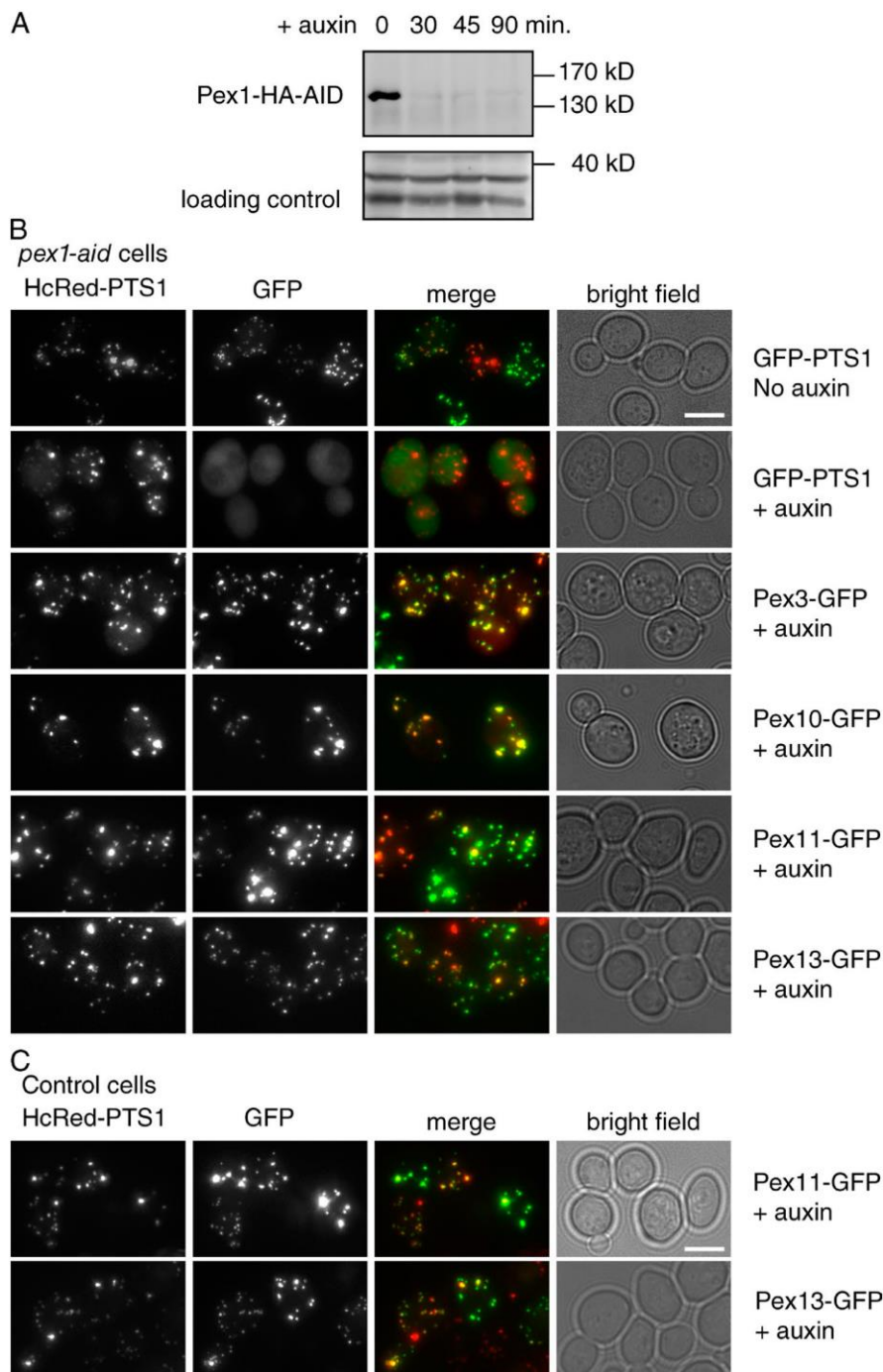


Figure 5. Short-term depletion of Pex1 affects matrix protein import but not PMP transport. (A) Western blot analysis of Pex1-HA-AID levels in cells as grown in <0–90 min after addition of 0.5-mM auxin. (B) Pex1-HA-AID cells expressing the peroxisomal matrix marker HcRed-PTS1 were transformed with various PMP-GFP expression plasmids driven by the *GAL1* promoter. Cells were grown to log phase on raffinose medium, and auxin was added to 0.5 mM. 45 min later, cells were resuspended in a galactose medium + auxin for 15 min (Pex3, Pex11, and Pex13) or 45 min (Pex10) to induce PMP-GFP expression and imaged by epifluorescence microscopy. (C) WT cells expressing HcRed-PTS1 constitutively and Pex11- or Pex13-GFP from the *GAL1* promoter were grown as described in B in the presence of auxin. Bars, 5 μ m.

2014). Furthermore, the significance of BiFC signals forming from constitutively expressed tags after such long incubations (24–72 h; van der Zand et al., 2012) in cells that have peroxisomes after 3 h is not clear. We therefore tested for these interactions in haploid *pex1* and *pex6* cells.

Fig. 8 A shows BiFC between Pex2-VN and Pex14-VC in haploid cells. This BiFC is readily detectable in WT cells, but interestingly, we also see a signal in *pex1* and *pex6* cells, although only in a minority of cells (~25%). Double labeling with the PMP marker Ant1-mCherry stains the vacuole in many *pex1* and *pex6* cells, which we would expect as a result of enhanced pexophagy. When the pexophagy receptor is disrupted in these haploid strains, vacuolar labeling of Ant1 is prevented

and Pex14-VC is stabilized to near-WT levels (by Western blotting; Fig. 8 B). BiFC between Pex2-VN and Pex14-VC now becomes evident in most *pex1/atg36* and *pex6/atg36* cells. We conclude that the weak signal of Pex2/Pex14 BiFC in *pex1* and *pex6* cells is a consequence of increased peroxisome turnover.

To control for specificity, we tested for BiFC in haploid cells between all combinations of Pex2-VN, Pex14-VC, and mitochondrial outer membrane proteins Tom20-VN and Tom70-VC. As shown in Fig. 8 C, the Tom20/Tom70 pair shows mitochondrial BiFC, and as expected, the Tom70/Pex2 pair is negative. Surprisingly, however, the Pex14/Tom20 pair gives a signal. Furthermore, this BiFC is stronger than that between Pex14 and Pex2. Whether this signal is meaningful is not

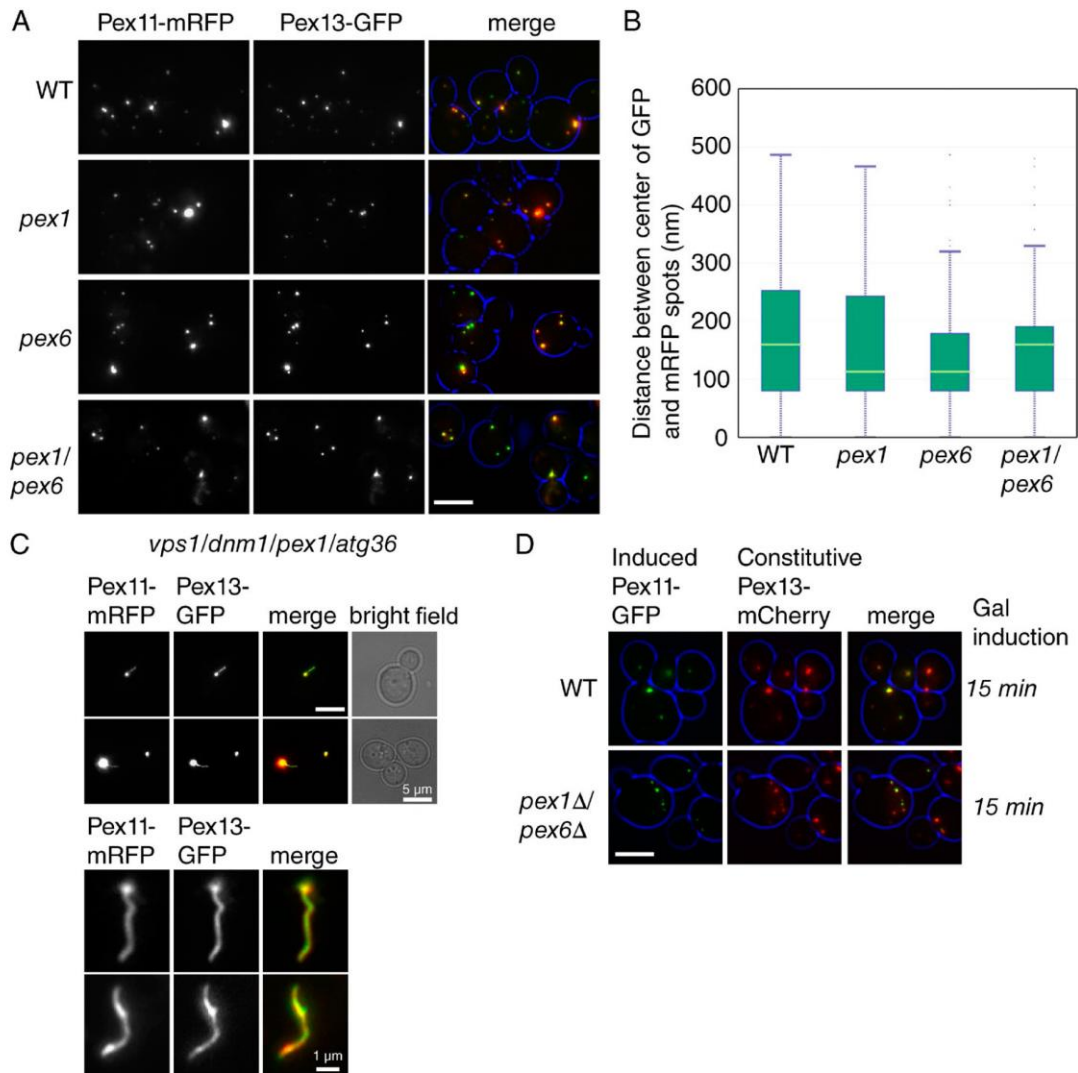


Figure 6. **Colocalization of Pex11 and Pex13 in *pex1* and *pex6* cells.** (A) *pex1*, *pex6*, *pex1/pex6*, and WT cells expressing Pex11-RFP and Pex13-GFP (from endogenous promoters on plasmids) were imaged after 3-h growth in log phase. (B) The distance between the center of each fluorescent Pex11-RFP and Pex13-GFP spot was calculated as described in the Materials and methods subsection Image acquisition and processing and is depicted as a box plot. $n > 400$ spots for each strain. The pale green line across each box indicates the median. (C) *vps1/dnm1/pex1/atg36* cells expressing Pex11-RFP and Pex13-GFP (from endogenous promoters on plasmid) were imaged after 18 h in exponential growth phase. (D) WT and *pex1/pex6* cells expressing plasmid-based Pex13-mCherry constitutively and Pex11-GFP from the *GAL1* promoter were given a short pulse of Pex11-GFP as indicated. Bars, 5 μ m.

clear. BiFC signals between proteins in different membranes have been previously reported (Pu et al., 2011; Mattiazzi Ušaj et al., 2015). The strength of the BiFC signal correlates with the level of expression of the proteins tested: quantification of C-tagged proteins indicates the number of molecules per cell is 339 for Pex2, 2,570 for Pex14, 5,680 for Tom20, and 45,300 for TOM70 (Ghaemmaghami et al., 2003). The strength of the BiFC signal may be influenced more by the relative abundance of the proteins tested than by an interaction between them or even their presence in the same membrane.

Asymmetric segregation of BiFC signal with matrix marker

In agreement with van der Zand et al. (2012), we noticed that some peroxisomes lack a BiFC signal when mating WT VC- and VN-tagged strains (Fig. 9 A and their Figs. 1 and 6). Although the formation of BiFC puncta without matrix content may reflect

de novo formation (van der Zand et al., 2012; and their Fig. 6), an alternative explanation is that BiFC and peroxisomal matrix marker do not segregate equally. In support of this, red-only peroxisomes are evident in haploid WT cells expressing VN and VC tags and HcRed-PTS1 (Fig. 9 B), which is striking because we and others have shown that newly synthesized PMPs traffic to existing peroxisomes (Motley and Hettema, 2007; Fakieh et al., 2013; Menendez-Benito et al., 2013). If unequal segregation of BiFC and red-PTS1 content explains the occurrence of red-only peroxisomes, we would expect such a segregation defect to be more evident on the elongated peroxisomes of *vps1* cells, and this is what we saw: BiFC signals appear as puncta on the extended peroxisomes of haploid (Fig. 9, C and D) and diploid (Fig. 9 E) *vps1* cells. In contrast, Pex13-GFP and Pex14-GFP label the whole peroxisomal structure (Fig. 9 F), although high magnification reveals that this labeling is not evenly spread over the peroxisomal membrane, particularly in the case of Pex14-GFP.

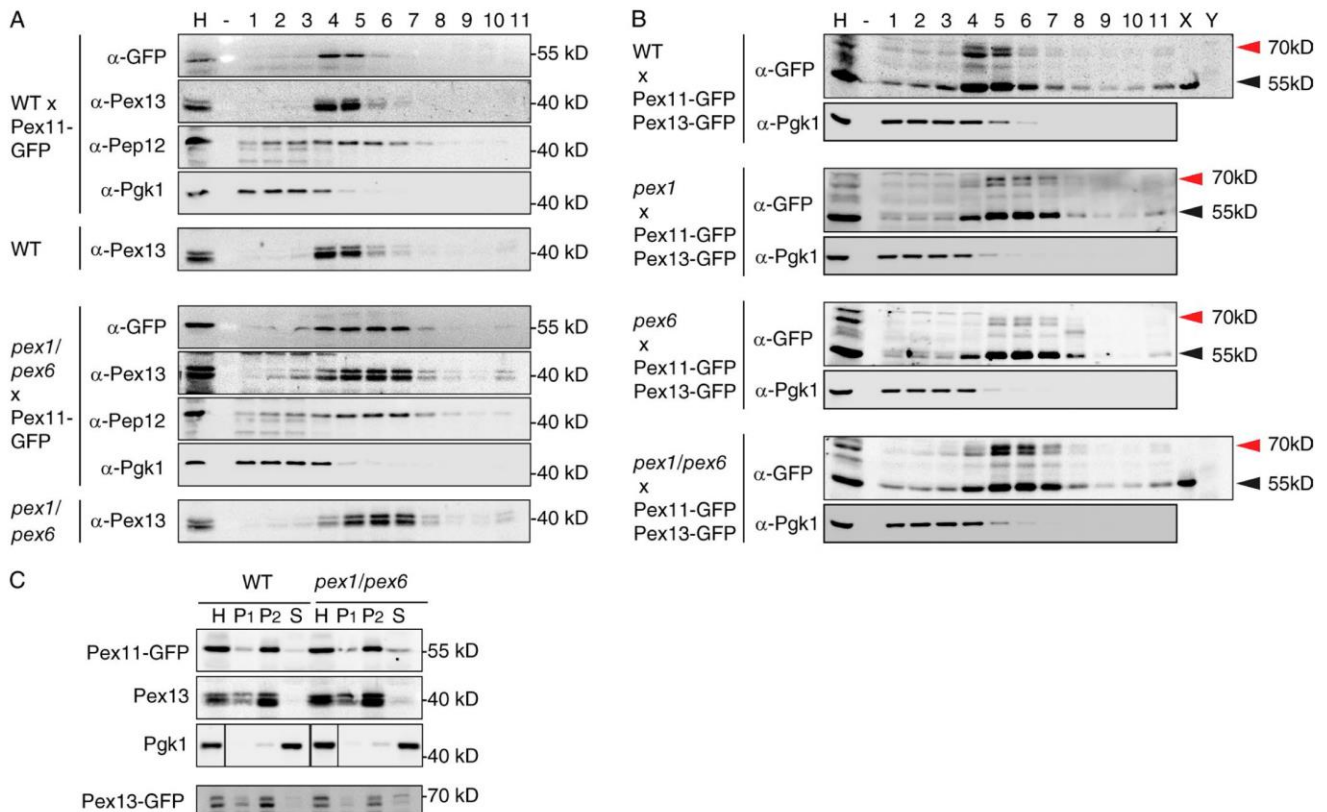


Figure 7. Cofractionation of Pex11-GFP with Pex13 and Pex13-GFP in WT, *pex1*, *pex6*, and *pex1/pex6* cells. (A and B) Homogenates (H; 800 g postnuclear supernatant) adjusted to 60% sucrose were separated by flotation analysis through sucrose equilibrium density gradient centrifugation. Fractions were collected from the bottom, and equal volumes were analyzed by Western blotting. Homogenates were prepared from glucose-grown cells of the strains as indicated. Cytosolic (Pgk1; A and B) and endosomal (Pep12; A) markers were included as the control for separation of membranes from cytosol. Pex13 is detected as a doublet, as Pex13 is prone to partial breakdown by proteolysis during subcellular fractionation (Elgersma et al., 1996). The samples in B were TCA precipitated and concentrated fourfold, as Pex13-GFP signals were weak. X and Y indicate control samples containing a P2 fraction of WT or *pex1/pex6* cells expressing Pex11-GFP only and untransformed WT or *pex1/pex6* cells. Red arrowheads indicate doublets of Pex13-GFP. Black arrowheads indicate Pex11-GFP. (C) Homogenates from WT and *pex1/pex6* cells transformed with either Pex11-GFP or Pex13-GFP were separated by centrifugation first at 2,500 g and then at 25,000 g into a 2,500 g pellet (P1), a 25,000 g pellet (P2), and a 25,000 g supernatant fraction (S). Equivalent portions of each fraction were analyzed by Western blotting. Black lines indicate that intervening lanes have been spliced out.

We imaged diploid *vps1* cells expressing Pex13-VN and Pex14-VC, as this BiFC pair resulted in the strongest signal and allowed for time-lapse microscopy over several cell divisions (Fig. 9 G and Video 2). The time-lapse analysis illustrates that BiFC signal frequently fails to segregate when the HcRed-PTS1-labeled peroxisome divides on cytokinesis. We conclude that red-only peroxisomes arise because the BiFC complex often fails to segregate when peroxisomes divide.

Discussion

By studying the role of DRPs and AAA⁺ ATPases, we have tested two models of peroxisome multiplication. The first model proposes that peroxisomes multiply by growth and division. According to this model, peroxisome growth is the result of delivery from the ER of vesicles carrying lipids and a subset of PMPs. Other PMPs and matrix proteins are imported directly into peroxisomes, and division is mediated by DRPs. When peroxisomes are absent, they can be reintroduced by de novo formation from the ER (Fig. 1).

The second model proposes that peroxisomes form de novo regardless of whether peroxisomes are already present.

All PMPs enter the ER and exit in distinct preperoxisomal vesicles that undergo heterotypic fusion, bringing together components of the import machinery. Fusion is mediated by the AAA ATPases Pex1 and Pex6. After fusion and assembly of the importomer, matrix protein import commences, resulting in a new peroxisome. This linear maturation model ends with fission of peroxisomes by DRPs (Fig. 1; van der Zand et al., 2012; Tabak et al., 2013; van der Zand and Tabak, 2013).

The results reported here indicate that peroxisomes multiply mainly by growth and division in *S. cerevisiae*. We found that peroxisomes can grow in size and receive newly synthesized PMPs, and that membrane growth and delivery of PMPs occurs independent of Pex1 and Pex6. Our data support previous findings of the direct involvement of Pex1 and Pex6 in matrix protein import. We do not find evidence to support the proposal that Pex1 and Pex6 are required for the formation of new peroxisomal membranes by fusion of ER-derived vesicles.

Most cells lacking the DRPs Vps1 and Dnm1 contain a single peroxisome. This phenotype is difficult to explain if new peroxisomes form continuously, unless these would form de novo as large structures that neither divide nor segregate between mother and daughter cell during cell division. Our results show this is not the case: multiple small peroxisomes appear

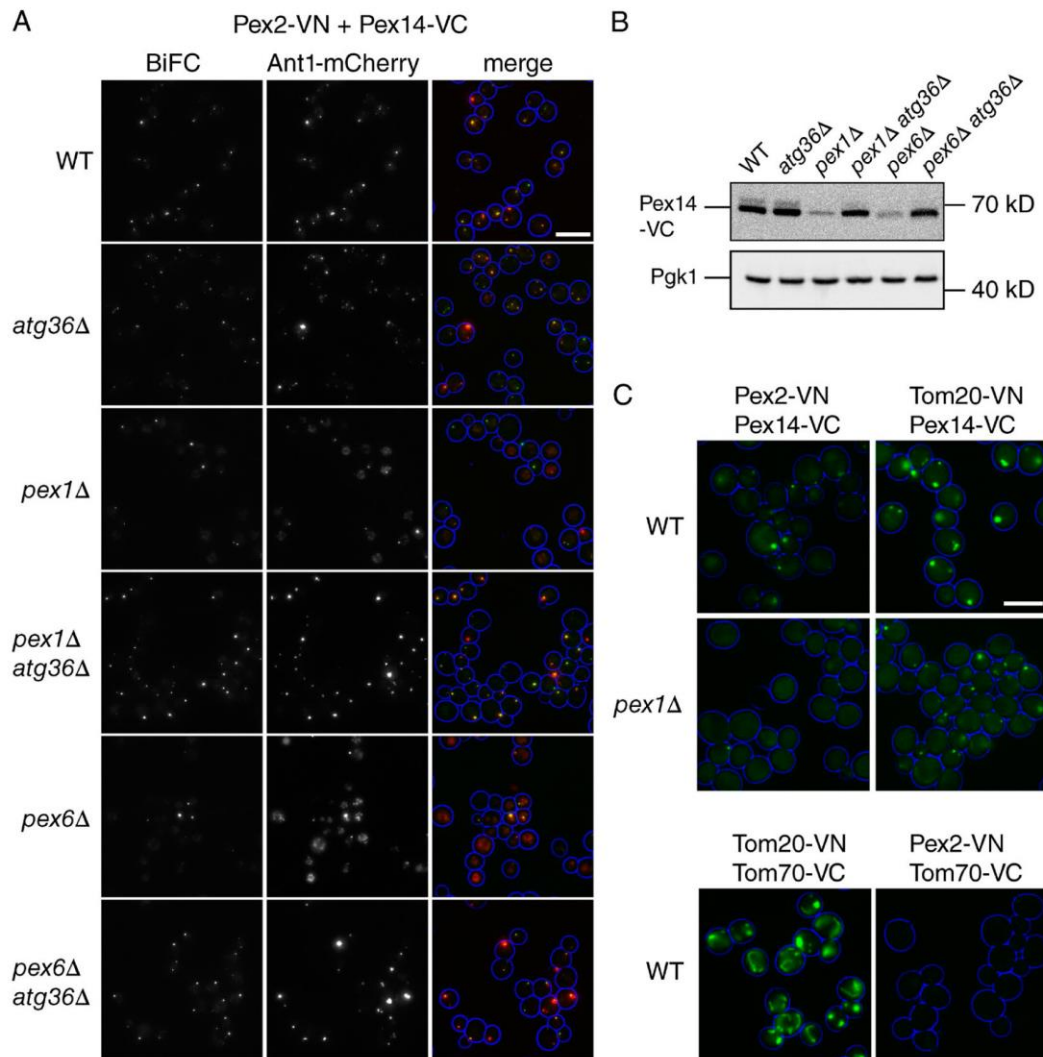


Figure 8. A block in pexophagy restores BiFC signals in *pex1* and *pex6* cells. (A) BiFC between Pex2-VN and Pex14-VC (genomically tagged) in haploid cells. Cells were transformed with a plasmid expressing Ant1-mCherry and grown on a glucose-containing medium to allow BiFC signals to develop. Mean number of Ant1-mCherry puncta per cell + SD were as follows: WT, 2.5 ± 1.6 ; *atg36Δ*, 3.5 ± 2.3 ; *pex1Δ*, 0.55 ± 0.6 ; *pex1Δ atg36Δ*, 1.4 ± 0.7 ; *pex6Δ*, 0.6 ± 0.6 ; and *pex6Δ atg36Δ*, 1.6 ± 0.9 . Percentage of cells showing colocalization between BiFC and Ant1 were as follows: WT, 84%; *atg36Δ*, 89%; *pex1Δ*, 95%; *pex1Δ atg36Δ*, 93%; *pex6Δ*, 98%; and *pex6Δ atg36Δ*, 90%. At least 100 cells were analyzed. (B) Western blot showing Pex14-VC in strains as indicated. PGK1 was used as a loading control. (C) BiFC between mitochondrial and peroxisomal proteins in WT and *pex1Δ* cells as indicated. A single slice of each sample was captured so that the fluorescence intensity in the images reflects the BiFC signal strength in the samples. Bars, 5 μ m.

initially in *vps1/dnm1* cells forced (by conditional Pex19 expression) to form peroxisomes de novo. These new peroxisomes increase in size but decrease in number during several rounds of cell division as they distribute between mother and daughter cell until a single peroxisome per cell is observed. Upon cytokinesis, this single peroxisome is split into two, allowing segregation between mother and daughter cell. The single elongated peroxisome phenotype of *vps1/dnm1* cells is stably inherited over many cell generations (Video 2; Hoepfner et al., 2001; Kuravi et al., 2006; Motley and Hettema, 2007), implying that peroxisomes continue to receive new membrane and matrix constituents. This is consistent with pulse chase experiments showing that peroxisomal markers segregate between mother and daughter peroxisomes on fission (Motley and Hettema, 2007; Knoblauch et al., 2013; Menendez-Benito et al., 2013). Not all proteins distribute equally on peroxisome fission, however (Cepińska et al., 2011; Knoblauch et al., 2013), and this

is observed to some extent in *vps1/dnm1* cells for Pex14-GFP (Fig. 9 F). The asymmetric distribution in the membrane of Pex13/Pex14 BiFC is much greater than that of Pex13-GFP or Pex14-GFP (Fig. 9, E and F). Asymmetric fission most likely underlies the occasional occurrence of PMP-GFP puncta that lack detectable matrix content (Figs. 5 and 6), as PMP-GFP puncta without content are not observed in *vps1/dnm1* cells (Fig. 9 F). Distinct peroxisome populations are generated by asymmetric distribution of PMPs and content followed by membrane fission during Woronin body biogenesis (Managadze et al., 2007; Liu et al., 2008). Asymmetric segregation also underlies the removal of intraorganellar aggregates from peroxisomes (Manivannan et al., 2013). In accordance with van der Zand et al. (2012), we found that BiFC signals fail to label all peroxisomes. However, we show that this is not a consequence of de novo formation of peroxisomes, but of asymmetric fission of BiFC-positive peroxisomes.

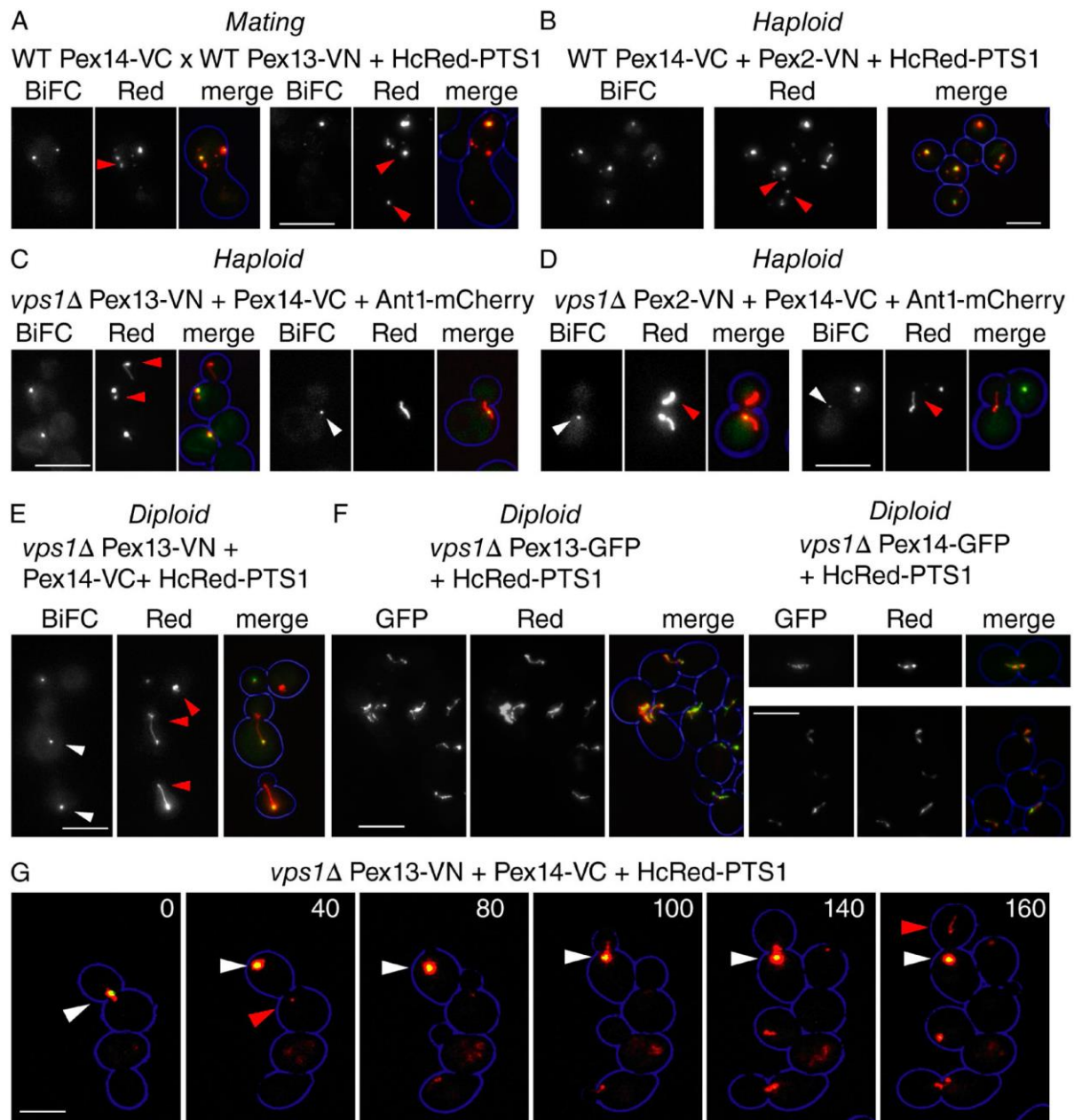


Figure 9. Failure of BiFC to segregate with peroxisomes in mating cells, haploid cells, and diploid cells. (A) WT MatA Pex14-VC cells containing red-PTS1 on a plasmid were mated with WT MatA Pex13-VN cells and imaged 24 h after mating. Two examples are shown. (B) BiFC between Pex2-VN and Pex14-VC in WT haploid cells expressing HcRed-PTS1 from a plasmid. (C and D) *VPS1* was disrupted in haploid cells double tagged as indicated, and peroxisomes were visualized using Ant1-mCherry. Two examples of each are shown. (E and F) Pex13-VN/14-VC BiFC (E) versus Pex13-GFP and Pex14-GFP (F) in diploid *vps1* cells expressing HcRed-PTS1 from a plasmid. VN, VC, and GFP tags were genomically integrated (i.e., a WT copy in addition to tagged protein was present in diploid cells). Red arrowheads indicate peroxisomes or parts of peroxisomes without a BiFC signal. White arrowheads indicate punctate BiFC signals colocalizing with the elongated peroxisomes. White arrowheads in G indicate peroxisome with BiFC signal from which a peroxisome without BiFC signal splits off (red arrowheads). Bars, 5 μ m.

A recent modeling study (Mukherji and O'Shea, 2014) proposed that peroxisomes form mainly de novo when *S. cerevisiae* cells are grown on glucose, whereas under conditions of peroxisome proliferation, the DRPs contribute to multiplication by peroxisome fission. In that study, the effect of disruption of DRPs on peroxisome abundance in cells grown on glucose was not tested. We (Motley and Hettema, 2007; Motley et al., 2008) and others (Kuravi et al., 2006) have shown that peroxisome

abundance is severely reduced in DRP-deficient cells grown on glucose (Fig. S4). Therefore, at least under our experimental conditions, peroxisomes multiply mainly by growth and division. In plants and mammals, there is support for the multiplication of peroxisomes by growth and division (Huybrechts et al., 2009; Delille et al., 2010; Barton et al., 2013), although both forms of multiplication have been reported to occur simultaneously in mammalian cells (Kim et al., 2006).

Although we have not detected de novo peroxisome formation in *S. cerevisiae* cells containing peroxisomes, we may have missed low levels of this. There may be conditions whereby de novo formation is induced in WT cells. A complex of ER reticulons and Pex30 has been reported to form a site of close contact between ER and peroxisomes. The absence of this complex enhances the rate at which new peroxisomes form during peroxisome reintroduction. This suggests a link between regulation of de novo peroxisome formation and ER morphology (Yan et al., 2007; David et al., 2013).

That the ER plays a central role in peroxisome biogenesis is supported by studies in many different organisms (Dimitrov et al., 2013; Agrawal and Subramani, 2015; Kim and Hettema, 2015). In *S. cerevisiae*, there is strong support for a role for the ER during reintroduction of peroxisomes in mutants temporarily lacking them (Hoepfner et al., 2005; Kragt et al., 2005; Tam et al., 2005; Haan et al., 2006). When Pex3-GFP expression is induced in *pex3*-deficient yeast cells, new peroxisomes form from a subdomain of the ER, the pER. In *S. cerevisiae*, the pER was reported to be ER associated (Bascom et al., 2003; Hoepfner et al., 2005), although no continuation with the ER was found in *Hansenula polymorpha* (Knoops et al., 2014). Other PMPs localized to this compartment in *pex3* or *pex19* cells, including Pex3, Pex13, Pex14, and Pex22 (Figs. 4 and 6; Faber et al., 2002; Bascom et al., 2003; Hoepfner et al., 2005; Kragt et al., 2005; Tam et al., 2005; Haan et al., 2006; Kim et al., 2006; Toro et al., 2009; van der Zand et al., 2010; Fakieh et al., 2013; Knoops et al., 2014). Some PMPs do not enter the pER, but insert late when new peroxisomes are formed in *H. polymorpha* (Knoops et al., 2014). We observe this for Pex11-GFP in *S. cerevisiae*. In the absence of peroxisomes, Pex11 is unstable (Hettema et al., 2000; Motley et al., 2012), and the low levels of Pex11-GFP that remain mislocalize to mitochondria (Fig. 4; Mattiazzi Ušaj et al., 2015). Upon peroxisome reintroduction, Pex11-GFP appears in puncta with Pex13 close to the time that GFP-PTS1 import commences (3–4 h; Figs. 2 and 4). These observations are compatible with a previously proposed model of de novo formation from the ER (during peroxisome reintroduction) by a process of maturation: a subset of PMPs traffic via the ER to the pER, preperoxisomes form from this specialized part of the ER, other PMPs are inserted, and a final maturation step is the import of matrix proteins (Hoepfner et al., 2005; Knoops et al., 2014).

In cells multiplying peroxisomes by growth and division (for example, in WT *S. cerevisiae* cells), we favor a model whereby peroxisomes receive lipids and a subset of PMPs via vesicular transport from the ER, whereas other PMPs are inserted into peroxisomes directly (Fig. 1). This model is supported by the following findings: that Pex15 appended with a glycosylation site is fully glycosylated in WT cells (Lam et al., 2010), that pER-trapped Pex3 can be transported to existing peroxisomes (Motley and Hettema, 2007), and that signals for Pex3 insertion into the ER, its sorting within the ER, and its subsequent sorting from pER to peroxisomes are required both during reintroduction of peroxisomes (de novo formation from the ER) and for transport of Pex3 to peroxisomes in WT cells (Fakieh et al., 2013). Many PMPs are recognized by Pex19 and could, after docking onto Pex3, be directly inserted into the peroxisomal membrane as has been shown to occur in mammalian cells and *Neurospora crassa* (Pinto et al., 2006; Matsuzaki and Fujiki, 2008; Yagita et al., 2013; Chen et al., 2014). Besides the direct route to peroxisomes, there

is also a PMP trafficking route via the ER in mammals and plants (Kim et al., 2006; Karnik and Trelease, 2007; Toro et al., 2009; Aranovich et al., 2014).

The triple ATPases, Pex1 and Pex6, are important for matrix protein import. A series of studies have uncovered a role for these proteins in the recycling of PTS1 and PTS2 targeting receptors (Platta et al., 2004, 2005; Miyata and Fujiki, 2005; Debelyy et al., 2011; Miyata et al., 2012). Additional roles for these proteins have been proposed, including maturation of precursor peroxisomes in *Y. lipolytica* (Titorenko et al., 2000) and heterotypic fusion of distinct ER-derived vesicles in *S. cerevisiae* (van der Zand et al., 2012). Our data are compatible with a role for Pex1 and Pex6 in matrix protein import. We did not find evidence to support a role for these proteins in membrane protein biogenesis as proposed in the vesicle fusion model (van der Zand et al., 2012). This model is in part based on the observation that markers for the distinct ER exit routes label separate structures in *pex1* and *pex6* cells. We could not reproduce this observation (Figs. 4, 6, and 7). We found that these markers colocalize and cofractionate in WT, *pex1*, *pex6*, and *pex1/pex6* cells. We expressed bright fluorescent proteins and fixed cells to reduce exposure times and movement. This may explain the discrepancy.

BiFC studies were used to show that Pex1 and Pex6 are required for assembly of the importomer (van der Zand et al., 2012). However, increased pexophagy in *pex1* and *pex6* cells (Nuttall et al., 2014) may have precluded detection of BiFC: we show by blocking pexophagy that importomer subunits Pex2 and Pex14 do give BiFC in *pex1* and *pex6* cells. This is in line with previous studies that indicate importomer assemblies in *pex1* and *pex6* cells (Agne et al., 2003; Kiel et al., 2004; Platta et al., 2004; Rosenkranz et al., 2006; Hensel et al., 2011). We show that depletion of Pex1 blocks matrix protein import (despite the presence of importomer in the membrane) but does not affect PMP delivery to peroxisomes. Furthermore, we find no role for Pex1 in the assembly of peroxisomal membranes during their reintroduction to conditional *pex19* cells. We conclude that, within the boundaries of our experimental framework, peroxisomes multiply mainly by growth and division, and that the AAA⁺ ATPases Pex1 and Pex6 are involved in matrix protein import.

Materials and methods

Yeast strains used are shown in Table S1, and the oligonucleotides used are shown in Table S2. Yeast strains used for Figs. 2, 3, 4, 5, 6, 7, S1, S2, and S4 and Video 1 were derivatives of BY4741 (*MATA his3-Δ1 leu2-Δ0 met15-Δ0 ura3-Δ0*) or BY4742 (*MATα his3-Δ1 leu2-Δ0 lys2-Δ0 ura3-Δ0*) and for Figs. 8, 9, and S3 and Video 2 were derivatives of FY1679-08A (*MATA*) and FY1679-06C (*MATα*), all obtained from the EUROSCARF (European *Saccharomyces Cerevisiae* Archive for Functional Analysis) consortium. Gene deletions were made by replacing the entire coding sequence with *Schizosaccharomyces pombe* *HIS5* or *Klebsiella pneumoniae* hygromycin B phosphotransferase gene cassette that confers resistance to hygromycin B (Goldstein and McCusker, 1999); BiFC or split GFP plasmids used as templates to genomically C-terminal tag Pex2- and 13-VN and Pex14-VC were pFA6a-VN173-HIS3MX6, pFA6a-VN155-HIS3MX6, and pFA6a-VN173-TRP1 (Bioneer Corporation). *URA3* and *LEU2* centromere plasmids were derived from Ycplac33 and Ycplac111 (Gietz and Sugino, 1988). GFP-PTS1 and RFP-PTS1 are peroxisomal luminal

marker proteins appended with the well-characterized PTS1 (Gould et al., 1988). The constitutive expression of HcRed-PTS1 was under the control of the *HIS3* promoter (Figs. 2, 4, 6, and 8). The majority of constructs used in this study were generated by homologous recombination in yeast (Uetz et al., 2000). The ORF of interest was amplified by PCR. The 5' ends of the primers included 18-nt extensions homologous to plasmid sequences flanking the intended insertion site, to enable repair of gapped plasmids by homologous recombination. For expression of genes under control of their endogenous promoter, 500 nt upstream from the ORF were included. Galactose-inducible constructs contained the *GALI* and *GALI0* intragenic region. All yeast constructs contain the *PGK1* terminator. Conditional expression constructs contained the *GALI* promoter.

Growth conditions and mating assay

Cells were grown overnight in selective glucose medium and diluted to OD 0.1 in either selective glucose medium (Figs. 3, 6 [A–C], 7, 8, 9, and S4 and Video 1) or in selective raffinose medium for 4 h followed by resuspension in galactose medium (Figs. 2, 4, 5, S1, and S2 and Video 1) for the times indicated. For mating, 10^7 cells of each mating type grown to logarithmic phase on yeast peptone dextrose (YPD) were mixed, pelleted, and spotted onto a prewarmed YPD plate and incubated at 30°C for the times indicated. For each experiment, >100 (mating) cells were examined, and images are representative.

Image acquisition and processing

Cells were analyzed with a microscope (Axiovert 200M; Carl Zeiss) equipped with an Exfo X-cite 120 excitation light source, band pass filters (Carl Zeiss and Chroma Technology Corp.), an α Plan-Fluar 100 \times 1.45 NA, Plan-Apochromat 63 \times 1.4 NA, or α -Plan 40 \times 0.65 NA Ph2 objective lens (Carl Zeiss) and a digital camera (Orca ER; Hamamatsu Photonics). Image acquisition was performed using Volocity software (PerkinElmer). Fluorescence images were collected as 0.5- μ m Z stacks using exposures of up to 300 ms, merged into one plane in Openlab (PerkinElmer), and processed further in Photoshop (Adobe). Bright-field images were collected in one plane and processed where necessary to highlight circumference of the cells.

For quantitation of colocalization, images were acquired using an Axio Observer (Carl Zeiss) microscope with a 100 \times 1.45 NA α Plan-Fluar objective with an electron-multiplying charge-coupled device camera (EM-C2; Rolera) using ZEN software. Single slices were taken of Pex13-GFP and Pex11-mRFP. Colocalization analysis was performed computationally using a Jython script for FIJI (<http://fiji.sc/Fiji>). Images were processed with a Fast-Fourier transform bandpass filter before subtracting the background and converting to 8-bit images. Per channel, the center of each fluorescent spot was then located by finding maxima in the image. The coordinates of the center of each fluorescent spot in the green channel was then compared with the coordinates of spots in the red channel. The distance between these coordinates was then found using a measure of 0.08 microns/pixel. The green and red coordinates with the minimum distance between them was then recorded, and they were both removed from the list of coordinates to be compared. More than 400 spots were counted in this manner.

For the live cell imaging, images for video were acquired using an Axio Observer microscope with a 100 \times 1.45 NA α Plan-Fluar objective with an EM-C2 electron-multiplying charge coupled device camera using ZEN software. Stacks were taken every 20 min at 27°C. Images were then processed to give extended depth of field and manually thresholded, and a Gaussian filter with a kernel of 3 \times 3 pixels was applied to remove noise using ZEN. Videos run at one frame per second. Cells were grown in a CellASIC Microfluidic system in 2%

galactose (Video 1) or 2% glucose (Video 2) for 14 h. Stills of Video 1 are shown in Fig. 2 C of peroxisomes forming de novo in *vps1/dnm1* cells (expressing HcRed-PTS1 from a plasmid) and segregating to daughter cells. Stills of Video 2, showing Pex13-VN/Pex14-VC in diploid *vps1* cells expressing HcRed-PTS1 from a plasmid, are shown in Fig. 9 G.

Subcellular fractionation

Cells grown overnight on selective glucose medium (OD₆₀₀ = 4–5) were converted to spheroplasts with Zymolyase 20T (5 mg/g cells). The spheroplasts were washed twice in 1.2-M sorbitol, 5-mM MES, pH 6, 1-mM EDTA, 1-mM KCl before resuspension in 0.65-M sorbitol, 5-mM MES, pH 6, 1-mM EDTA, and 1-mM KCl (fractionation buffer) containing 1-mM PMSF and protease inhibitor cocktail. Cell breakage was achieved by 10 strokes with a tight-fitting douncer. Intact cells and nuclei were removed by two centrifugation steps (800 g for 10 min). 1 ml homogenate was mixed with 3 ml of 80% sucrose in a fractionation buffer. The sample was loaded on the bottom of an SW41 tube over which a sucrose step gradient was loaded consisting of 1-ml fractions of 50, 45, 40, 35, 32.5, 30, and 25% sucrose (wt/vol). These gradients were centrifuged for 18 h at 100,000 g in an SW41 rotor at 4°C. 1-ml fractions were collected from the bottom of the tube and analyzed by SDS-PAGE and immunoblotting. All sucrose solutions were made in fractionation buffer.

3 ml homogenate was fractionated by sequential differential centrifugation, from which we obtained a 2,500 g pellet, a 25,000 g pellet, and a 25,000 g supernatant. Pellet fractions were resuspended in a 3-ml fractionation buffer. Equivalent volumes of these fractions were analyzed by SDS-PAGE and immunoblotting.

Immunoblotting

For preparation of extracts by alkaline lysis, cells were centrifuged and pellets resuspended in 0.2-M NaOH and 0.2% β -mercaptoethanol and left on ice for 10 min. Soluble protein was precipitated by addition of 5% TCA for a further 10 min. After centrifugation (13,000 g for 5 min at 4°C), soluble protein was resuspended in 10 μ l of 1-M Tris-HCl, pH 9.4, and boiled in 90 μ l of 1 \times SDS-PAGE sample loading buffer for 10 min. Samples (0.25–1 OD₆₀₀ equivalent) were resolved by SDS-PAGE followed by immunoblotting. Monoclonal anti-GFP antibody was obtained from Roche (11814460001), and secondary antibody was HRP-linked anti-mouse polyclonal (1706516; Bio-Rad Laboratories). Pex13 antiserum was provided by R. Erdmann (Ruhr University, Bochum, Germany). Blots were blocked in 2% (wt/vol) fat-free Marvel milk in TBS-Tween 20 (50-mM Tris-HCl, pH 7.5, 150-mM NaCl, and 0.1% [vol/vol] Tween 20). Tagged proteins were detected using enhanced chemiluminescence (Biological Industries) and chemiluminescence imaging.

Online supplemental material

Fig. S1 presents a mating assay revealing that peroxisomes in *vps1/dnm1* cells do not fuse. Fig. S2 presents additional data using peroxisomal membrane markers showing that peroxisomes in *vps1/dnm1* cells grow into elongated structures. Fig. S3 presents additional data showing that upon mating of *pex1* and *pex6* cells, matrix protein import is restored much faster than the development of BiFC signals. Fig. S4 shows quantitation of peroxisome number in WT, *vps1*, and *vps1/dnm1* cells grown on glucose. Video 1 presents a time-lapse analysis of peroxisome dynamics in *vps1/dnm1* cells. Video 2 presents time-lapse analysis of asymmetric segregation of a peroxisomal membrane BiFC signal in support of Fig. 9. Table S1 shows yeast strains used in this study. Table S2 shows oligonucleotides used in this study. Online supplemental material is available at <http://www.jcb.org/cgi/content/full/jcb.201412066/DC1>.

Acknowledgments

We would like to thank Jeremy Craven for discussion throughout the project. We would also like to thank various members of the Hettema lab (University of Sheffield, Sheffield, England, UK), including Pawel Gardzielewski for construction of the conditional pex19 strains, Joanne Lacey for construction of Gal-inducible Pex13 and Pex14-GFP plasmids, and Marzieh Radi for the running of Western blots. We would also like to thank Ralf Erdmann for Pex13 antiserum. We would also like to thank Kevin Knoops and Ida van der Klei for their constructive comments on the manuscript and for sharing unpublished data.

This work was funded in part by a Wellcome Trust senior research fellowship in basic biomedical science awarded to E.H. Hettema (WT084265MA).

The authors declare no competing financial interests.

Submitted: 12 December 2014

Accepted: 3 November 2015

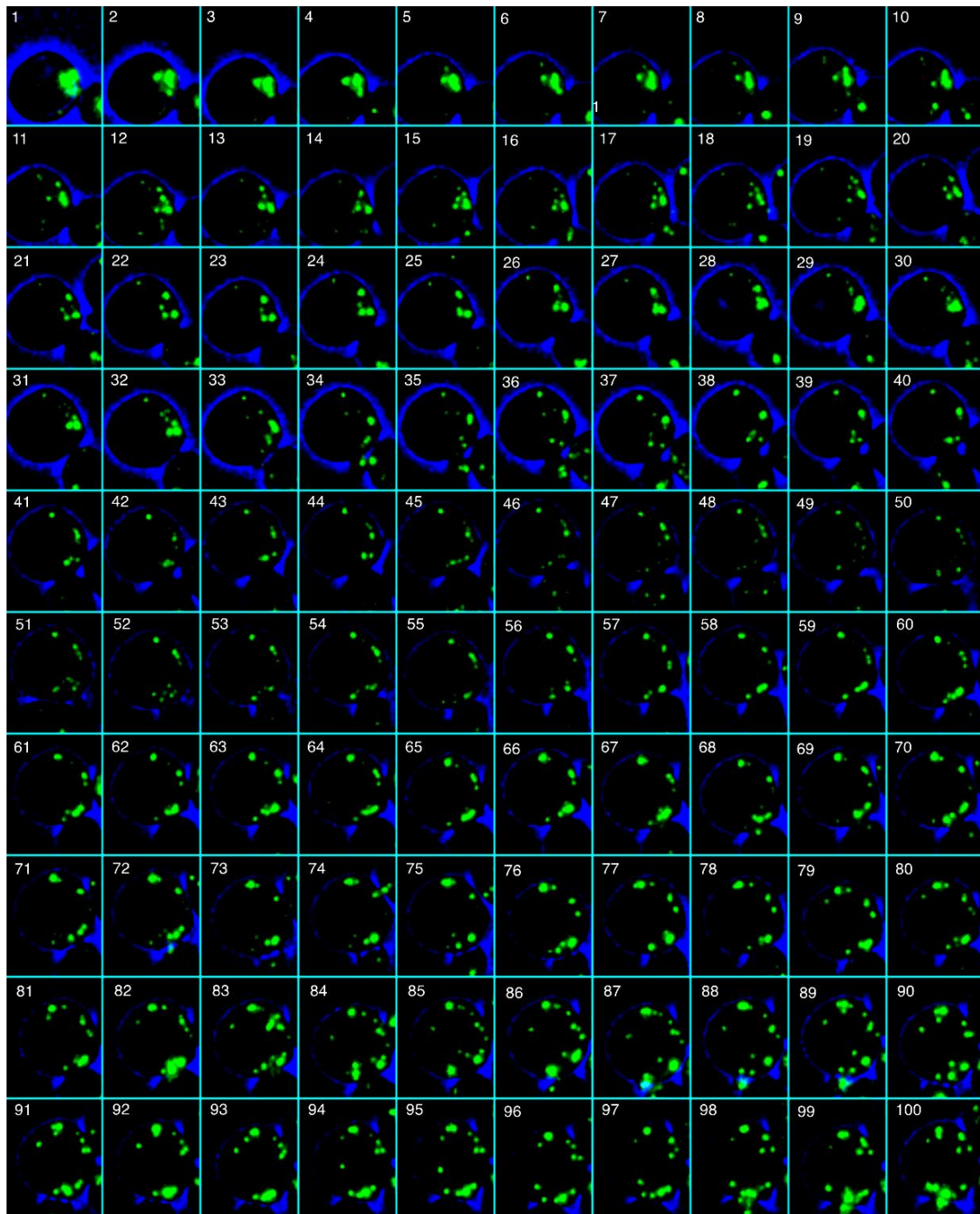
References

- Agne, B., N.M. Meindl, K. Niederhoff, H. Einwächter, P. Rehling, A. Sickmann, H.E. Meyer, W. Girzalsky, and W.H. Kunau. 2003. Pex8p: an intraperoxisomal organizer of the peroxisomal import machinery. *Mol. Cell.* 11:635–646. [http://dx.doi.org/10.1016/S1097-2765\(03\)00062-5](http://dx.doi.org/10.1016/S1097-2765(03)00062-5)
- Agrawal, G., and S. Subramani. 2015. De novo peroxisome biogenesis: Evolving concepts and conundrums. *Biochim. Biophys. Acta.* <http://dx.doi.org/10.1016/j.bbamcr.2015.09.014>
- Aranovich, A., R. Hua, A.D. Rutenberg, and P.K. Kim. 2014. PEX16 contributes to peroxisome maintenance by constantly trafficking PEX3 via the ER. *J. Cell Sci.* 127:3675–3686. <http://dx.doi.org/10.1242/jcs.146282>
- Arimura, S., J. Yamamoto, G.P. Aida, M. Nakazono, and N. Tsutsumi. 2004. Frequent fusion and fission of plant mitochondria with unequal nucleoid distribution. *Proc. Natl. Acad. Sci. USA.* 101:7805–7808. <http://dx.doi.org/10.1073/pnas.0401077101>
- Barton, K., N. Mathur, and J. Mathur. 2013. Simultaneous live-imaging of peroxisomes and the ER in plant cells suggests contiguity but no luminal continuity between the two organelles. *Front. Physiol.* 4:196. <http://dx.doi.org/10.3389/fphys.2013.00196>
- Bascom, R.A., H. Chan, and R.A. Rachubinski. 2003. Peroxisome biogenesis occurs in an unsynchronized manner in close association with the endoplasmic reticulum in temperature-sensitive *Yarrowia lipolytica* Pex3p mutants. *Mol. Biol. Cell.* 14:939–957. <http://dx.doi.org/10.1091/mbe.E02-10-0633>
- Bonekamp, N.A., P. Sampaio, F.V. de Abreu, G.H. Lüers, and M. Schrader. 2012. Transient complex interactions of mammalian peroxisomes without exchange of matrix or membrane marker proteins. *Traffic.* 13:960–978. <http://dx.doi.org/10.1111/j.1600-0854.2012.01356.x>
- Cepińska, M.N., M. Veenhuis, I.J. van der Klei, and S. Nagotu. 2011. Peroxisome fission is associated with reorganization of specific membrane proteins. *Traffic.* 12:925–937. <http://dx.doi.org/10.1111/j.1600-0854.2011.01198.x>
- Chen, Y., L. Pieuchot, R.A. Loh, J. Yang, T.M. Kari, J.Y. Wong, and G. Jedd. 2014. Hydrophobic handoff for direct delivery of peroxisome tail-anchored proteins. *Nat. Commun.* 5:5790. <http://dx.doi.org/10.1038/ncomms6790>
- David, C., J. Koch, S. Oeljeklaus, A. Laemsack, S. Melchior, S. Wiese, A. Schummer, R. Erdmann, B. Warscheid, and C. Brocard. 2013. A combined approach of quantitative interaction proteomics and live-cell imaging reveals a regulatory role for endoplasmic reticulum (ER) reticulon homology proteins in peroxisome biogenesis. *Mol. Cell. Proteomics.* 12:2408–2425. <http://dx.doi.org/10.1074/mcp.M112.017830>
- Debely, M.O., H.W. Platta, D. Saffian, A. Hensel, S. Thoms, H.E. Meyer, B. Warscheid, W. Girzalsky, and R. Erdmann. 2011. Ubp15p, a ubiquitin hydrolase associated with the peroxisomal export machinery. *J. Biol. Chem.* 286:28223–28234. <http://dx.doi.org/10.1074/jbc.M111.238600>
- Delille, H.K., B. Agricola, S.C. Guimaraes, H. Borta, G.H. Lüers, M. Fransen, and M. Schrader. 2010. Pex11p β -mediated growth and division of mammalian peroxisomes follows a maturation pathway. *J. Cell Sci.* 123:2750–2762. <http://dx.doi.org/10.1242/jcs.062109>
- Dimitrov, L., S.K. Lam, and R. Schekman. 2013. The role of the endoplasmic reticulum in peroxisome biogenesis. *Cold Spring Harb. Perspect. Biol.* 5:a013243. <http://dx.doi.org/10.1101/cshperspect.a013243>
- Elgersma, Y., L. Kwast, A. Klein, T. Voorn-Brouwer, M. van den Berg, B. Metzger, T. America, H.F. Tabak, and B. Distel. 1996. The SH3 domain of the *Saccharomyces cerevisiae* peroxisomal membrane protein Pex13p functions as a docking site for Pex5p, a mobile receptor for the import PTS1-containing proteins. *J. Cell Biol.* 135:97–109. <http://dx.doi.org/10.1083/jcb.135.1.97>
- Faber, K.N., G.J. Haan, R.J. Baerends, A.M. Kram, and M. Veenhuis. 2002. Normal peroxisome development from vesicles induced by truncated *Hansenula polymorpha* Pex3p. *J. Biol. Chem.* 277:11026–11033. <http://dx.doi.org/10.1074/jbc.M112347200>
- Fakieh, M.H., P.J. Drake, J. Lacey, J.M. Munck, A.M. Motley, and E.H. Hettema. 2013. Intra-ER sorting of the peroxisomal membrane protein Pex3 relies on its luminal domain. *Biol. Open.* 2:829–837. <http://dx.doi.org/10.1242/bio.20134788>
- Fang, Y., J.C. Morrell, J.M. Jones, and S.J. Gould. 2004. PEX3 functions as a PEX19 docking factor in the import of class I peroxisomal membrane proteins. *J. Cell Biol.* 164:863–875. <http://dx.doi.org/10.1083/jcb.200311131>
- Gärtner, J., W.W. Chen, R.I. Kelley, S.J. Mihalik, and H.W. Moser. 1991. The 22-kD peroxisomal integral membrane protein in Zellweger syndrome—presence, abundance, and association with a peroxisomal thiolase precursor protein. *Pediatr. Res.* 29:141–146. <http://dx.doi.org/10.1203/00006450-199102000-00007>
- Ghaemmaghami, S., W.K. Huh, K. Bower, R.W. Howson, A. Belle, N. Dephoure, E.K. O’Shea, and J.S. Weissman. 2003. Global analysis of protein expression in yeast. *Nature.* 425:737–741. <http://dx.doi.org/10.1038/nature02046>
- Gietz, R.D., and A. Sugino. 1988. New yeast-*Escherichia coli* shuttle vectors constructed with in vitro mutagenized yeast genes lacking six-base pair restriction sites. *Gene.* 74:527–534. [http://dx.doi.org/10.1016/0378-1119\(88\)90185-0](http://dx.doi.org/10.1016/0378-1119(88)90185-0)
- Goldstein, A.L., and J.H. McCusker. 1999. Three new dominant drug resistance cassettes for gene disruption in *Saccharomyces cerevisiae*. *Yeast.* 15:1541–1553. [http://dx.doi.org/10.1002/\(SICI\)1097-0061\(199910\)15:14<1541::AID-YEA476>3.0.CO;2-K](http://dx.doi.org/10.1002/(SICI)1097-0061(199910)15:14<1541::AID-YEA476>3.0.CO;2-K)
- Gould, S.G., G.A. Keller, and S. Subramani. 1987. Identification of a peroxisomal targeting signal at the carboxy terminus of firefly luciferase. *J. Cell Biol.* 105:2923–2931. <http://dx.doi.org/10.1083/jcb.105.6.2923>
- Gould, S.J., G.A. Keller, and S. Subramani. 1988. Identification of peroxisomal targeting signals located at the carboxy terminus of four peroxisomal proteins. *J. Cell Biol.* 107:897–905. <http://dx.doi.org/10.1083/jcb.107.3.897>
- Haan, G.J., R.J. Baerends, A.M. Krikken, M. Otzen, M. Veenhuis, and I.J. van der Klei. 2006. Reassembly of peroxisomes in *Hansenula polymorpha* pex3 cells on reintroduction of Pex3p involves the nuclear envelope. *FEMS Yeast Res.* 6:186–194. <http://dx.doi.org/10.1111/j.1567-1364.2006.00037.x>
- Halbach, A., R. Rucktäschel, H. Rottensteiner, and R. Erdmann. 2009. The N-domain of Pex22p can functionally replace the Pex3p N-domain in targeting and peroxisome formation. *J. Biol. Chem.* 284:3906–3916. <http://dx.doi.org/10.1074/jbc.M806950200>
- Hensel, A., S. Beck, F. El Magraoui, H.W. Platta, W. Girzalsky, and R. Erdmann. 2011. Cysteine-dependent ubiquitination of Pex18p is linked to cargo translocation across the peroxisomal membrane. *J. Biol. Chem.* 286:43495–43505. <http://dx.doi.org/10.1074/jbc.M111.286104>
- Hettema, E.H., and A.M. Motley. 2009. How peroxisomes multiply. *J. Cell Sci.* 122:2331–2336. <http://dx.doi.org/10.1242/jcs.034363>
- Hettema, E.H., W. Girzalsky, M. van den Berg, R. Erdmann, and B. Distel. 2000. *Saccharomyces cerevisiae* pex3p and pex19p are required for proper localization and stability of peroxisomal membrane proteins. *EMBO J.* 19:223–233. <http://dx.doi.org/10.1093/emboj/19.2.223>
- Hoepfner, D., M. van den Berg, P. Philippsen, H.F. Tabak, and E.H. Hettema. 2001. A role for Vps1p, actin, and the Myo2p motor in peroxisome abundance and inheritance in *Saccharomyces cerevisiae*. *J. Cell Biol.* 155:979–990. <http://dx.doi.org/10.1083/jcb.200107028>
- Hoepfner, D., D. Schildknecht, I. Braakman, P. Philippsen, and H.F. Tabak. 2005. Contribution of the endoplasmic reticulum to peroxisome formation. *Cell.* 122:85–95. <http://dx.doi.org/10.1016/j.cell.2005.04.025>
- Huybrechts, S.J., P.P. Van Veldhoven, C. Brees, G.P. Mannaerts, G.V. Los, and M. Fransen. 2009. Peroxisome dynamics in cultured mammalian cells. *Traffic.* 10:1722–1733. <http://dx.doi.org/10.1111/j.1600-0854.2009.00970.x>
- Jones, J.M., J.C. Morrell, and S.J. Gould. 2004. PEX19 is a predominantly cytosolic chaperone and import receptor for class I peroxisomal membrane proteins. *J. Cell Biol.* 164:57–67. <http://dx.doi.org/10.1083/jcb.200304111>
- Karnik, S.K., and R.N. Trelease. 2007. Arabidopsis peroxin 16 trafficks through the ER and an intermediate compartment to pre-existing peroxisomes

- via overlapping molecular targeting signals. *J. Exp. Bot.* 58:1677–1693. <http://dx.doi.org/10.1093/jxb/erm018>
- Kiel, J.A., K. Emmrich, H.E. Meyer, and W.H. Kunau. 2004. Ubiquitination of the peroxisomal targeting signal type 1 receptor, Pex5p, suggests the presence of a quality control mechanism during peroxisomal matrix protein import. *J. Biol. Chem.* 280:1921–1930. <http://dx.doi.org/10.1074/jbc.M403632200>
- Kim, P.K., and E.H. Hettema. 2015. Multiple pathways for protein transport to peroxisomes. *J. Mol. Biol.* 427:1176–1190. <http://dx.doi.org/10.1016/j.jmb.2015.02.005>
- Kim, P.K., R.T. Mullen, U. Schumann, and J. Lippincott-Schwartz. 2006. The origin and maintenance of mammalian peroxisomes involves a de novo PEX16-dependent pathway from the ER. *J. Cell Biol.* 173:521–532. <http://dx.doi.org/10.1083/jcb.200601036>
- Knoblach, B., X. Sun, N. Coquelle, A. Fagarasanu, R.L. Poirier, and R.A. Rachubinski. 2013. An ER-peroxisome tether exerts peroxisome population control in yeast. *EMBO J.* 32:2439–2453. <http://dx.doi.org/10.1038/emboj.2013.170>
- Knoops, K., S. Manivannan, M.N. Cepinska, A.M. Krikken, A.M. Kram, M. Veenhuis, and I.J. van der Klei. 2014. Preperoxisomal vesicles can form in the absence of Pex3. *J. Cell Biol.* 204:659–668. <http://dx.doi.org/10.1083/jcb.201310148>
- Koek, A., M. Komori, M. Veenhuis, and I.J. van der Klei. 2007. A comparative study of peroxisomal structures in *Hansenula polymorpha* pex mutants. *FEMS Yeast Res.* 7:1126–1133. <http://dx.doi.org/10.1111/j.1567-1364.2007.00261.x>
- Kragt, A., T. Voorn-Brouwer, M. van den Berg, and B. Distel. 2005. Endoplasmic reticulum-directed Pex3p routes to peroxisomes and restores peroxisome formation in a *Saccharomyces cerevisiae* pex3Δ strain. *J. Biol. Chem.* 280:34350–34357. <http://dx.doi.org/10.1074/jbc.M505432200>
- Kuravi, K., S. Nagotu, A.M. Krikken, K. Sjollem, M. Deckers, R. Erdmann, M. Veenhuis, and I.J. van der Klei. 2006. Dynamin-related proteins Vps1p and Dnm1p control peroxisome abundance in *Saccharomyces cerevisiae*. *J. Cell Sci.* 119:3994–4001. <http://dx.doi.org/10.1242/jcs.03166>
- Lam, S.K., N. Yoda, and R. Schekman. 2010. A vesicle carrier that mediates peroxisome protein traffic from the endoplasmic reticulum. *Proc. Natl. Acad. Sci. USA.* 107:21523–21528. <http://dx.doi.org/10.1073/pnas.1013397107>
- Lazarow, P.B. 2003. Peroxisome biogenesis: advances and conundrums. *Curr. Opin. Cell Biol.* 15:489–497. [http://dx.doi.org/10.1016/S0955-0674\(03\)00082-6](http://dx.doi.org/10.1016/S0955-0674(03)00082-6)
- Liu, F., S.K. Ng, Y. Lu, W. Low, J. Lai, and G. Jedd. 2008. Making two organelles from one: Woronin body biogenesis by peroxisomal protein sorting. *J. Cell Biol.* 180:325–339. <http://dx.doi.org/10.1083/jcb.200705049>
- Liu, X., C. Ma, and S. Subramani. 2012. Recent advances in peroxisomal matrix protein import. *Curr. Opin. Cell Biol.* 24:484–489. <http://dx.doi.org/10.1016/j.ceb.2012.05.003>
- Managadze, D., C. Würtz, M. Sichtung, G. Niehaus, M. Veenhuis, and H. Rottensteiner. 2007. The peroxin PEX14 of *Neurospora crassa* is essential for the biogenesis of both glyoxysomes and Woronin bodies. *Traffic.* 8:687–701. <http://dx.doi.org/10.1111/j.1600-0854.2007.00560.x>
- Manivannan, S., R. de Boer, M. Veenhuis, and I.J. van der Klei. 2013. Lumenal peroxisomal protein aggregates are removed by concerted fission and autophagy events. *Autophagy.* 9:1044–1056. <http://dx.doi.org/10.4161/auto.24543>
- Matsuzaki, T., and Y. Fujiki. 2008. The peroxisomal membrane protein import receptor Pex3p is directly transported to peroxisomes by a novel Pex19p- and Pex16p-dependent pathway. *J. Cell Biol.* 183:1275–1286. <http://dx.doi.org/10.1083/jcb.200806062>
- Mattiuzzi Ušaj, M., M. Brložnik, P. Kaferle, M. Žitnik, H. Wolinski, F. Leitner, S.D. Kohlwein, B. Zupan, and U. Petrovič. 2015. Genome-wide localization study of yeast Pex11 identifies peroxisome-mitochondria interactions through the ERMES complex. *J. Mol. Biol.* 427:2072–2087. <http://dx.doi.org/10.1016/j.jmb.2015.03.004>
- Menendez-Benito, V., S.J. van Deventer, V. Jimenez-Garcia, M. Roy-Luzarraga, F. van Leeuwen, and J. Neeffjes. 2013. Spatiotemporal analysis of organelle and macromolecular complex inheritance. *Proc. Natl. Acad. Sci. USA.* 110:175–180. <http://dx.doi.org/10.1073/pnas.1207424110>
- Miyata, N., and Y. Fujiki. 2005. Shuttling mechanism of peroxisome targeting signal type 1 receptor Pex5: ATP-independent import and ATP-dependent export. *Mol. Cell Biol.* 25:10822–10832. <http://dx.doi.org/10.1128/MCB.25.24.10822-10832.2005>
- Miyata, N., K. Okumoto, S. Mukai, M. Noguchi, and Y. Fujiki. 2012. AWP1/ZFA ND6 functions in Pex5 export by interacting with cys-monoubiquitinated Pex5 and Pex6 AAA ATPase. *Traffic.* 13:168–183. <http://dx.doi.org/10.1111/j.1600-0854.2011.01298.x>
- Motley, A.M., and E.H. Hettema. 2007. Yeast peroxisomes multiply by growth and division. *J. Cell Biol.* 178:399–410. <http://dx.doi.org/10.1083/jcb.200702167>
- Motley, A., E. Hettema, B. Distel, and H. Tabak. 1994. Differential protein import deficiencies in human peroxisome assembly disorders. *J. Cell Biol.* 125:755–767. <http://dx.doi.org/10.1083/jcb.125.4.755>
- Motley, A.M., G.P. Ward, and E.H. Hettema. 2008. Dnm1p-dependent peroxisome fission requires Caf4p, Mdv1p and Fis1p. *J. Cell Sci.* 121:1633–1640. <http://dx.doi.org/10.1242/jcs.026344>
- Motley, A.M., J.M. Nuttall, and E.H. Hettema. 2012. Pex3-anchored Atg36 tags peroxisomes for degradation in *Saccharomyces cerevisiae*. *EMBO J.* 31:2852–2868. <http://dx.doi.org/10.1038/emboj.2012.151>
- Mukherji, S., and E.K. O'Shea. 2014. Mechanisms of organelle biogenesis govern stochastic fluctuations in organelle abundance. *eLife.* 3:e02678. <http://dx.doi.org/10.7554/eLife.02678>
- Nagotu, S., A.M. Krikken, M. Otzen, J.A. Kiel, M. Veenhuis, and I.J. van der Klei. 2008. Peroxisome fission in *Hansenula polymorpha* requires Mdv1 and Fis1, two proteins also involved in mitochondrial fission. *Traffic.* 9:1471–1484. <http://dx.doi.org/10.1111/j.1600-0854.2008.00772.x>
- Nishimura, K., T. Fukagawa, H. Takisawa, T. Kakimoto, and M. Kanemaki. 2009. An auxin-based degron system for the rapid depletion of proteins in nonplant cells. *Nat. Methods.* 6:917–922. <http://dx.doi.org/10.1038/nmeth.1401>
- Nunnari, J., W.F. Marshall, A. Straight, A. Murray, J.W. Sedat, and P. Walter. 1997. Mitochondrial transmission during mating in *Saccharomyces cerevisiae* is determined by mitochondrial fusion and fission and the intramitochondrial segregation of mitochondrial DNA. *Mol. Biol. Cell.* 8:1233–1242. <http://dx.doi.org/10.1091/mbc.8.7.1233>
- Nuttall, J.M., A. Motley, and E.H. Hettema. 2011. Peroxisome biogenesis: recent advances. *Curr. Opin. Cell Biol.* 23:421–426. <http://dx.doi.org/10.1016/j.ceb.2011.05.005>
- Nuttall, J.M., A.M. Motley, and E.H. Hettema. 2014. Deficiency of the export components Pex1, Pex6, and Pex15 causes enhanced pexophagy in *Saccharomyces cerevisiae*. *Autophagy.* 10:835–845. <http://dx.doi.org/10.4161/auto.28259>
- Okumoto, K., S. Misono, N. Miyata, Y. Matsumoto, S. Mukai, and Y. Fujiki. 2011. Cysteine ubiquitination of PTS1 receptor Pex5p regulates Pex5p recycling. *Traffic.* 12:1067–1083. <http://dx.doi.org/10.1111/j.1600-0854.2011.01217.x>
- Otera, H., K. Setoguchi, M. Hamasaki, T. Kumashiro, N. Shimizu, and Y. Fujiki. 2002. Peroxisomal targeting signal receptor Pex5p interacts with cargoes and import machinery components in a spatiotemporally differentiated manner: conserved Pex5p WXXXF/Y motifs are critical for matrix protein import. *Mol. Cell Biol.* 22:1639–1655. <http://dx.doi.org/10.1128/MCB.22.6.1639-1655.2002>
- Pinto, M.P., C.P. Grou, I.S. Alencastre, M.E. Oliveira, C. Sá-Miranda, M. Fransens, and J.E. Azevedo. 2006. The import competence of a peroxisomal membrane protein is determined by Pex19p before the docking step. *J. Biol. Chem.* 281:34492–34502. <http://dx.doi.org/10.1074/jbc.M607183200>
- Platta, H.W., W. Girzalsky, and R. Erdmann. 2004. Ubiquitination of the peroxisomal import receptor Pex5p. *Biochem. J.* 384:37–45. <http://dx.doi.org/10.1042/BJ20040572>
- Platta, H.W., S. Grunau, K. Rosenkranz, W. Girzalsky, and R. Erdmann. 2005. Functional role of the AAA peroxins in dislocation of the cycling PTS1 receptor back to the cytosol. *Nat. Cell Biol.* 7:817–822. <http://dx.doi.org/10.1038/ncb1281>
- Platta, H.W., F. El Magraoui, D. Schlee, S. Grunau, W. Girzalsky, and R. Erdmann. 2007. Ubiquitination of the peroxisomal import receptor Pex5p is required for its recycling. *J. Cell Biol.* 177:197–204. <http://dx.doi.org/10.1083/jcb.200611012>
- Platta, H.W., F. El Magraoui, B.E. Bäumer, D. Schlee, W. Girzalsky, and R. Erdmann. 2009. Pex2 and pex12 function as protein-ubiquitin ligases in peroxisomal protein import. *Mol. Cell Biol.* 29:5505–5516. <http://dx.doi.org/10.1128/MCB.00388-09>
- Pu, J., C.W. Ha, S. Zhang, J.P. Jung, W.K. Huh, and P. Liu. 2011. Interactomic study on interaction between lipid droplets and mitochondria. *Protein Cell.* 2:487–496. <http://dx.doi.org/10.1007/s13238-011-1061-y>
- Rosenkranz, K., I. Birschmann, S. Grunau, W. Girzalsky, W.H. Kunau, and R. Erdmann. 2006. Functional association of the AAA complex and the peroxisomal importomer. *FEBS J.* 273:3804–3815. <http://dx.doi.org/10.1111/j.1742-4658.2006.05388.x>
- Rottensteiner, H., A. Kramer, S. Lorenzen, K. Stein, C. Landgraf, R. Volkmer-Engert, and R. Erdmann. 2004. Peroxisomal membrane proteins contain common Pex19p-binding sites that are an integral part of their targeting signals. *Mol. Cell Biol.* 15:3406–3417. <http://dx.doi.org/10.1091/mbc.E04-03-0188>

- Sacksteder, K.A., J.M. Jones, S.T. South, X. Li, Y. Liu, and S.J. Gould. 2000. PEX19 binds multiple peroxisomal membrane proteins, is predominantly cytoplasmic, and is required for peroxisome membrane synthesis. *J. Cell Biol.* 148:931–944. <http://dx.doi.org/10.1083/jcb.148.5.931>
- Santos, M.J., T. Imanaka, H. Shio, and P.B. Lazarow. 1988. Peroxisomal integral membrane proteins in control and Zellweger fibroblasts. *J. Biol. Chem.* 263:10502–10509.
- Tabak, H.F., I. Braakman, and A. van der Zand. 2013. Peroxisome formation and maintenance are dependent on the endoplasmic reticulum. *Annu. Rev. Biochem.* 82:723–744. <http://dx.doi.org/10.1146/annurev-biochem-081111-125123>
- Tam, Y.Y., A. Fagarasanu, M. Fagarasanu, and R.A. Rachubinski. 2005. Pex3p initiates the formation of a preperoxisomal compartment from a subdomain of the endoplasmic reticulum in *Saccharomyces cerevisiae*. *J. Biol. Chem.* 280:34933–34939. <http://dx.doi.org/10.1074/jbc.M506208200>
- Titorenko, V.I., and R.A. Rachubinski. 2000. Peroxisomal membrane fusion requires two AAA family ATPases, Pex1p and Pex6p. *J. Cell Biol.* 150:881–886. <http://dx.doi.org/10.1083/jcb.150.4.881>
- Titorenko, V.I., H. Chan, and R.A. Rachubinski. 2000. Fusion of small peroxisomal vesicles in vitro reconstructs an early step in the in vivo multistep peroxisome assembly pathway of *Yarrowia lipolytica*. *J. Cell Biol.* 148:29–44. <http://dx.doi.org/10.1083/jcb.148.1.29>
- Toro, A.A., C.A. Araya, G.J. Cordova, C.A. Arredondo, H.G. Cardenas, R.E. Moreno, A. Venegas, C.S. Koenig, J. Cancino, A. Gonzalez, and M.J. Santos. 2009. Pex3p-dependent peroxisomal biogenesis initiates in the endoplasmic reticulum of human fibroblasts. *J. Cell. Biochem.* 107:1083–1096.
- Uetz, P., L. Giot, G. Cagney, T.A. Mansfield, R.S. Judson, J.R. Knight, D. Lockshon, V. Narayan, M. Srinivasan, P. Pochart, et al. 2000. A comprehensive analysis of protein-protein interactions in *Saccharomyces cerevisiae*. *Nature.* 403:623–627. <http://dx.doi.org/10.1038/35001009>
- van der Zand, A., and H.F. Tabak. 2013. Peroxisomes: offshoots of the ER. *Curr. Opin. Cell Biol.* 25:449–454. <http://dx.doi.org/10.1016/j.ceb.2013.05.004>
- van der Zand, A., I. Braakman, and H.F. Tabak. 2010. Peroxisomal membrane proteins insert into the endoplasmic reticulum. *Mol. Biol. Cell.* 21:2057–2065. <http://dx.doi.org/10.1091/mbc.E10-02-0082>
- van der Zand, A., J. Gent, I. Braakman, and H.F. Tabak. 2012. Biochemically distinct vesicles from the endoplasmic reticulum fuse to form peroxisomes. *Cell.* 149:397–409. <http://dx.doi.org/10.1016/j.cell.2012.01.054>
- van Roermund, C.W., S. Brul, J.M. Tager, R.B. Schutgens, and R.J. Wanders. 1991. Acyl-CoA oxidase, peroxisomal thiolase and dihydroxyacetone phosphate acyltransferase: aberrant subcellular localization in Zellweger syndrome. *J. Inherit. Metab. Dis.* 14:152–164. <http://dx.doi.org/10.1007/BF01800588>
- Vizeacoumar, F.J., W.N. Vreden, M. Fagarasanu, G.A. Eitzen, J.D. Aitchison, and R.A. Rachubinski. 2006. The dynamin-like protein Vps1p of the yeast *Saccharomyces cerevisiae* associates with peroxisomes in a Pex19p-dependent manner. *J. Biol. Chem.* 281:12817–12823. <http://dx.doi.org/10.1074/jbc.M600365200>
- Williams, C., M. van den Berg, E. Geers, and B. Distel. 2008. Pex10p functions as an E3 ligase for the Ubc4p-dependent ubiquitination of Pex5p. *Biochem. Biophys. Res. Commun.* 374:620–624. <http://dx.doi.org/10.1016/j.bbrc.2008.07.054>
- Williams, C., L. Opalinski, C. Landgraf, J. Costello, M. Schrader, A.M. Krikken, K. Knoops, A.M. Kram, R. Volkmer, and I.J. van der Klei. 2015. The membrane remodeling protein Pex11p activates the GTPase Dnm1p during peroxisomal fission. *Proc. Natl. Acad. Sci. USA.* 112:6377–6382. <http://dx.doi.org/10.1073/pnas.1418736112>
- Yagita, Y., T. Hiromasa, and Y. Fujiki. 2013. Tail-anchored PEX26 targets peroxisomes via a PEX19-dependent and TRC40-independent class I pathway. *J. Cell Biol.* 200:651–666. <http://dx.doi.org/10.1083/jcb.201211077>
- Yan, M., D.A. Rachubinski, S. Joshi, R.A. Rachubinski, and S. Subramani. 2007. Dysferlin domain-containing proteins, Pex30p and Pex31p, localized to two compartments, control the number and size of oleate-induced peroxisomes in *Pichia pastoris*. *Mol. Biol. Cell.* 19:885–898. <http://dx.doi.org/10.1091/mbc.E07-10-1042>

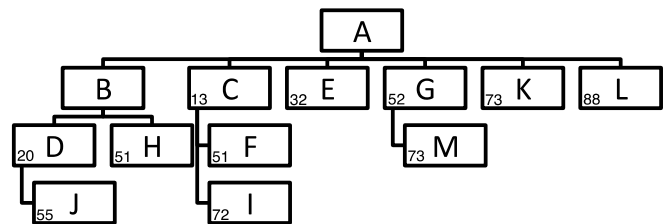
Appendix G: 100 Frame-Montage of Cell A



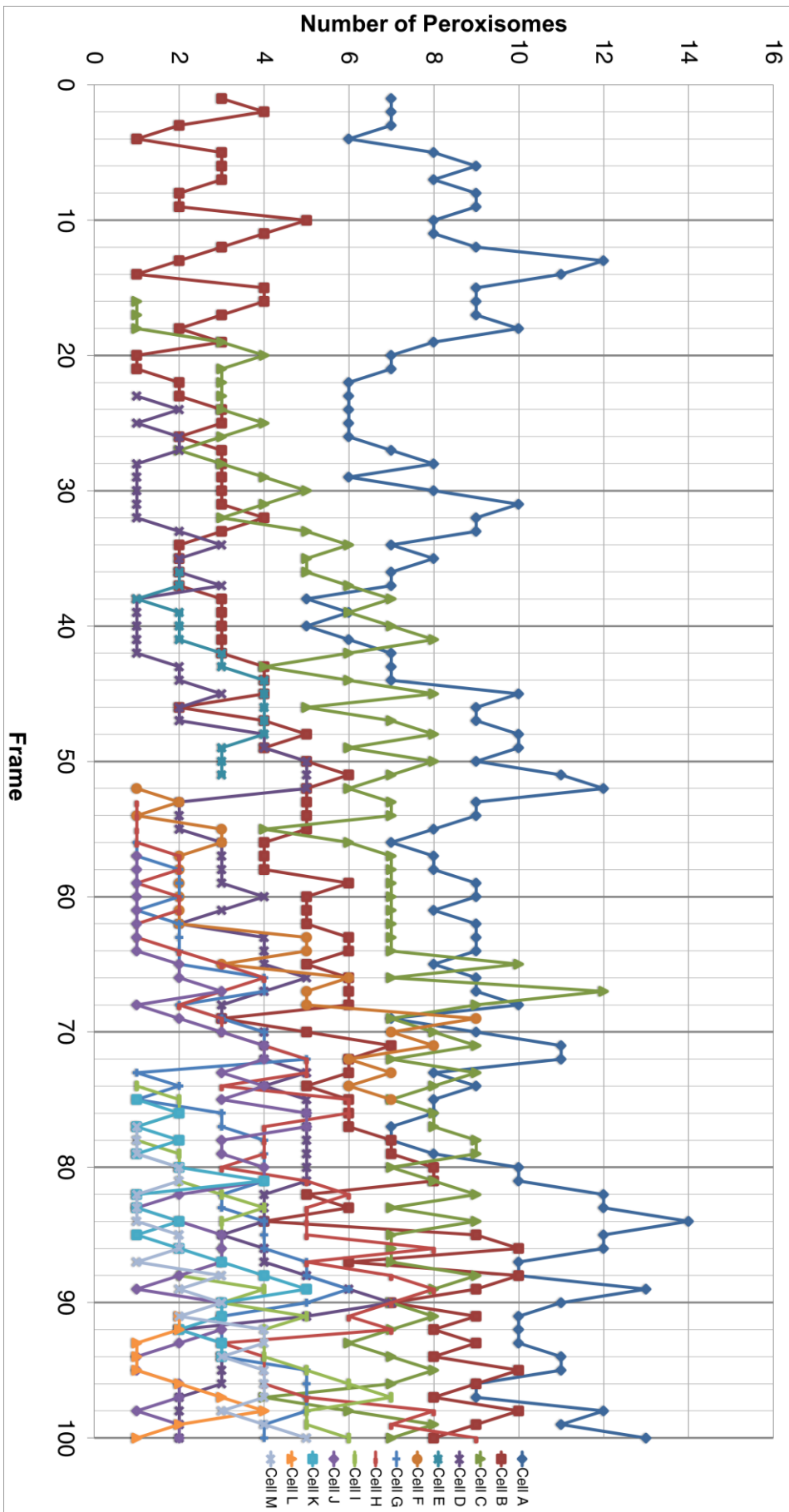
Appendix H: Non-annotated Versions of Figures 6.6 and 6.7a-e for KPPC Model

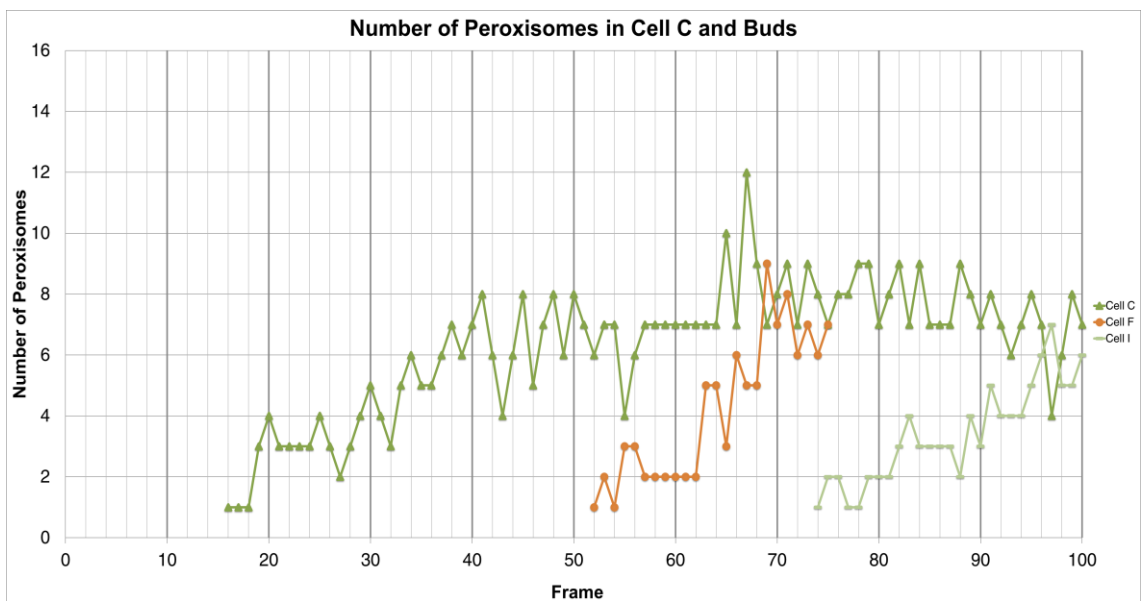
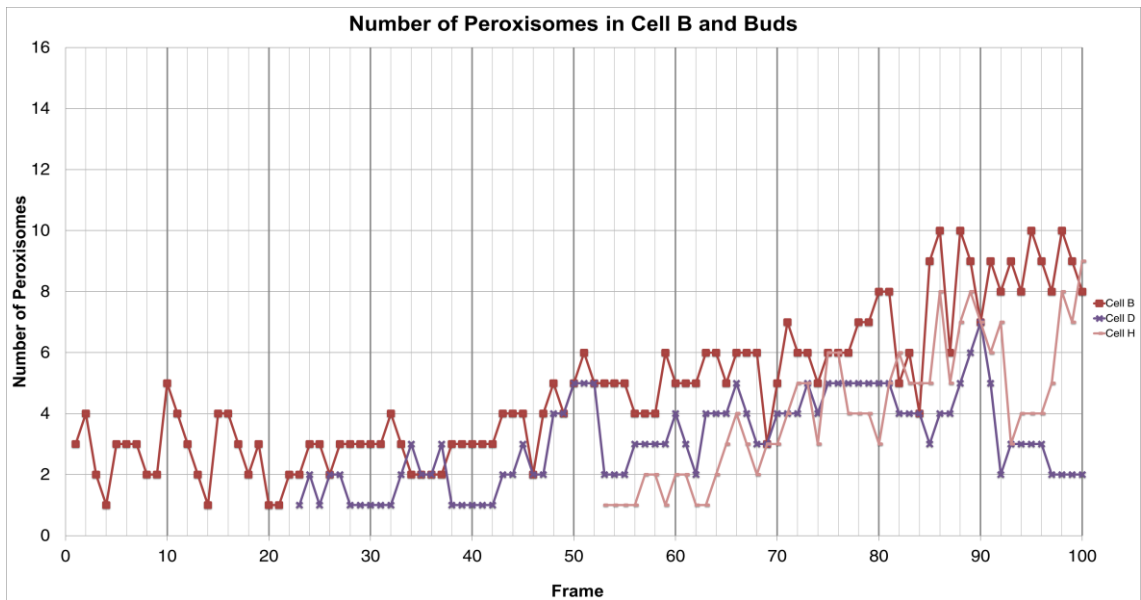
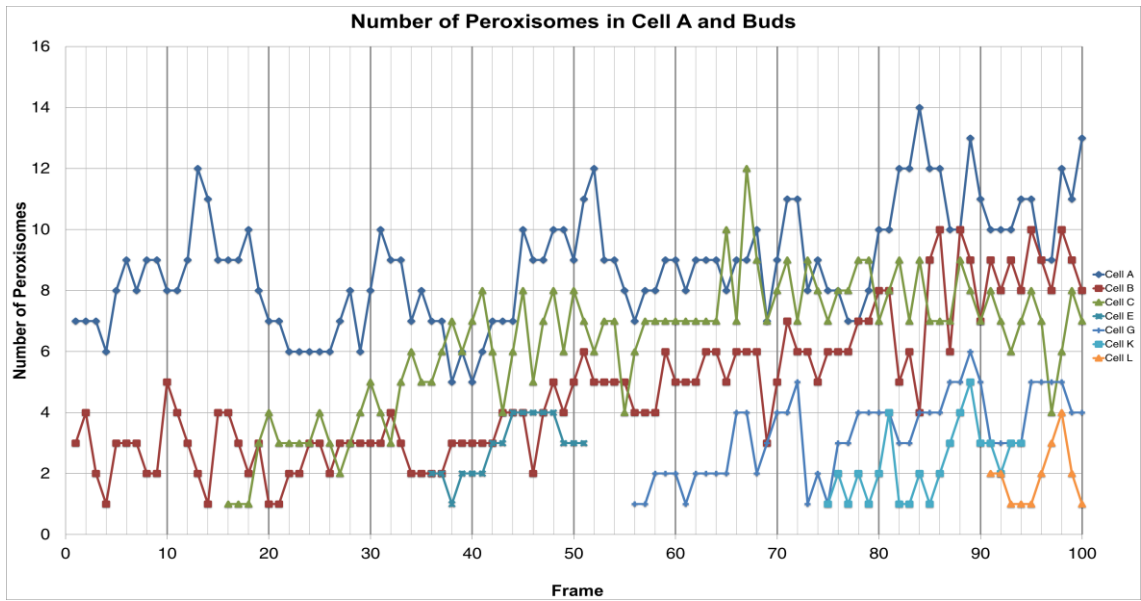
Figures repeated here to allow one to make a less biased judgement about peaks etc. Cluster 1 table and lineage repeated here so that all lineages can be found in the same place for ease of reference.

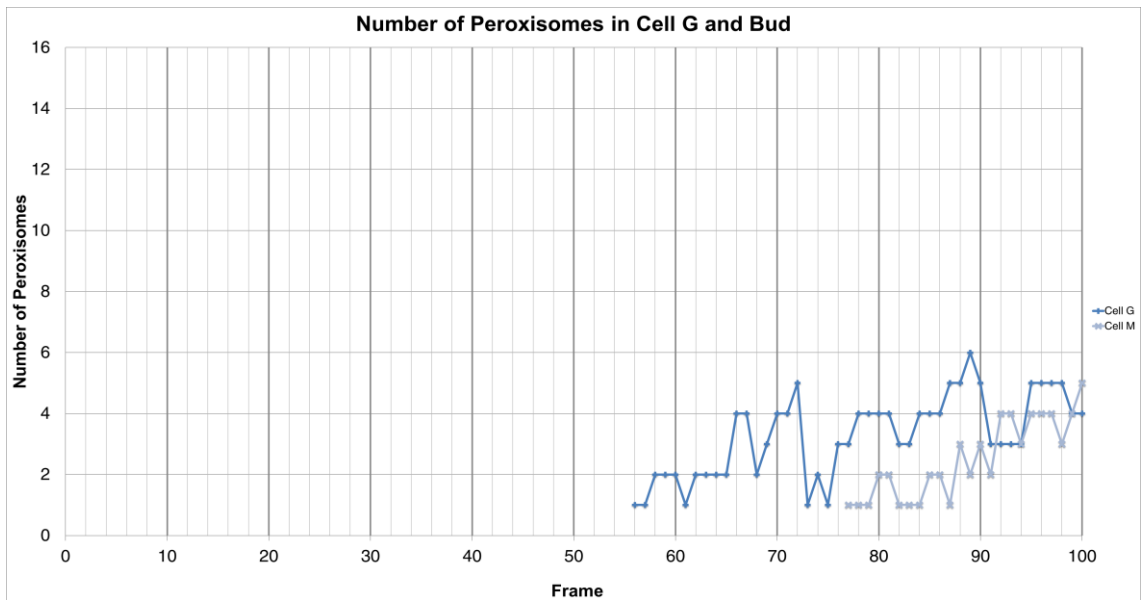
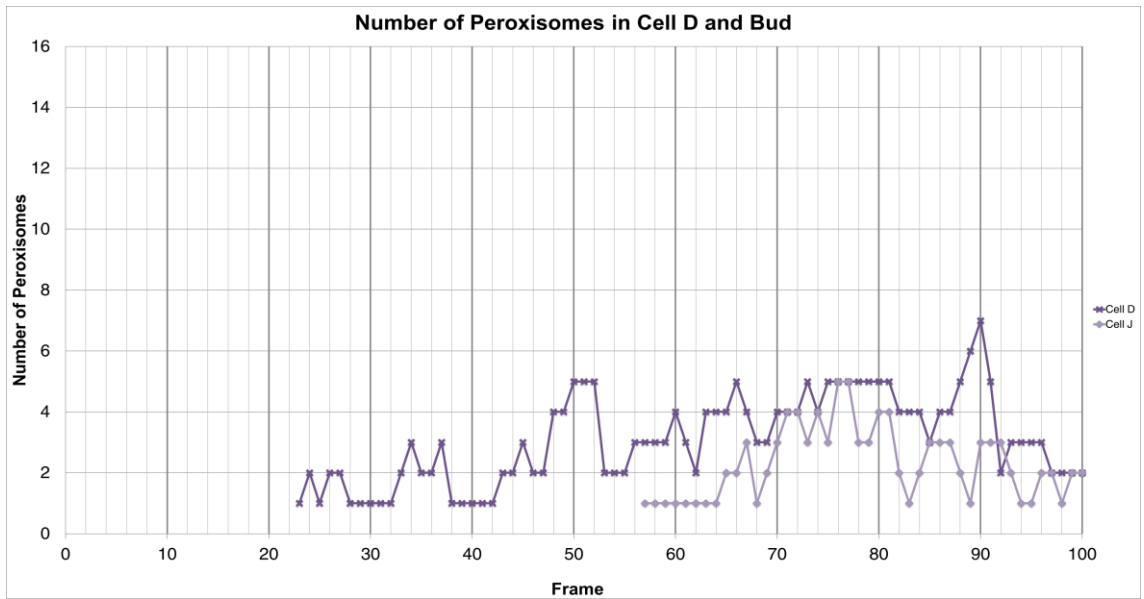
Cell	Frames	Buds
A	1-100	B,C,E,G,K,L
B	1-100	D,H
C	13-100	F,I
D	20-100	J
E	32-51	
F	51-76	
G	52-100	M
H	51-100	
I	72-100	
J	55-100	
K	73-94	
L	88-100	
M	73-100	



Number of Peroxisomes in All Cells



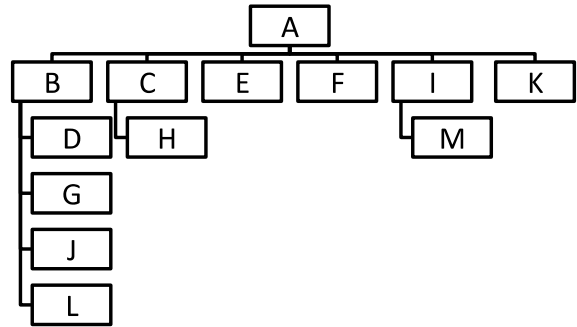




**Appendix I: Cluster Lineages and Graphs of
Peroxisomal Number Per Frame For Each
Cell in Clusters 2-5 for Evaluation of Yeast
Peroxisome Population Control Model**

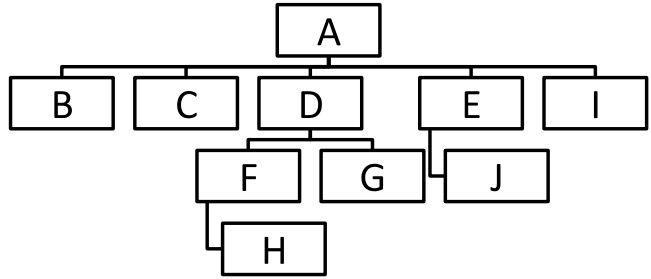
Cluster 2

Cell	Frames Present	Buds
A	1-100	B,C,E,F,I,K
B	1-100	D,G,J,L
C	7-100	H
D	19-42	
E	30-51	
F	47-67	
G	41-64	
H	49-100	
I	64-100	M
J	63-84	
K	83-100	
L	85-100	
M	92-100	



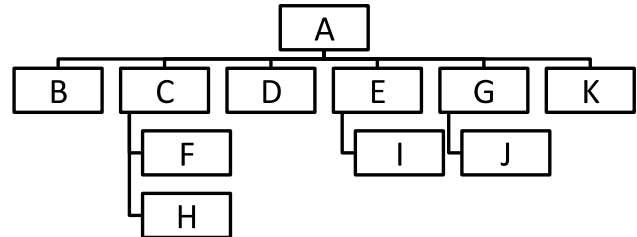
Cluster 3

Cell	Frames Present	Buds
A	1-100	B,C,D,E,I
B	1-10	
C	5-29	
D	29-100	F,G
E	68-100	J
F	69-100	H
G	88-100	
H	89-100	
I	89-100	
J	89-100	



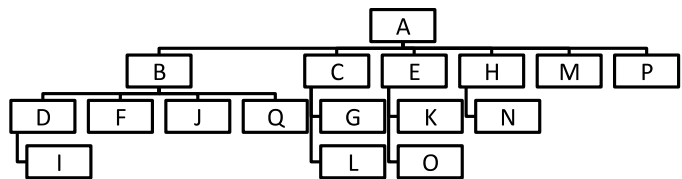
Cluster 4

Cell	Frames Present	Buds
A	1-100	B,C,D,E,G,K
B	1-15	
C	12-73	F,H
D	29-49	
E	48-100	I
F	44-67	
G	72-100	J
H	67-73	
I	74-100	
J	95-100	
K	95-100	

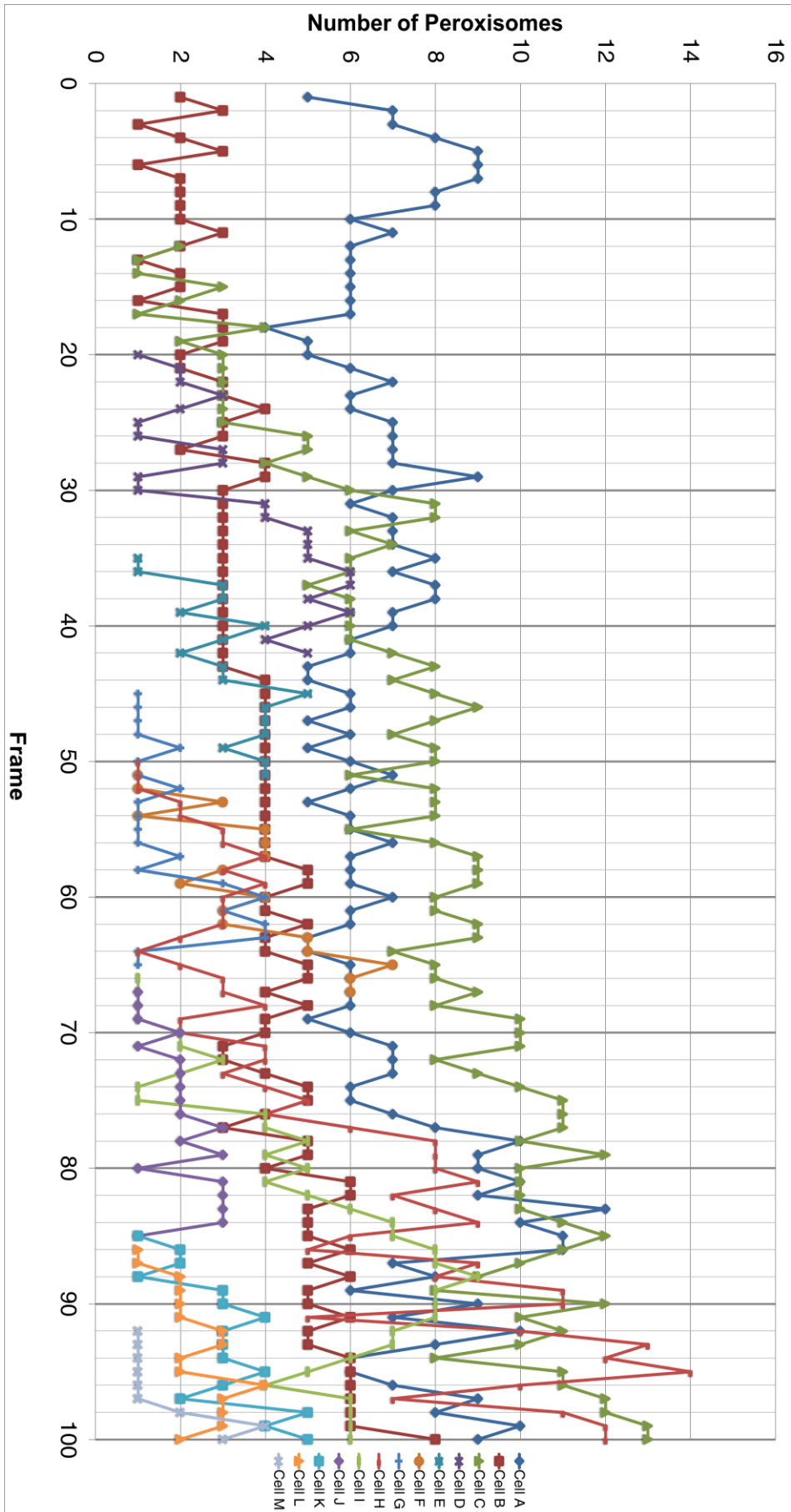


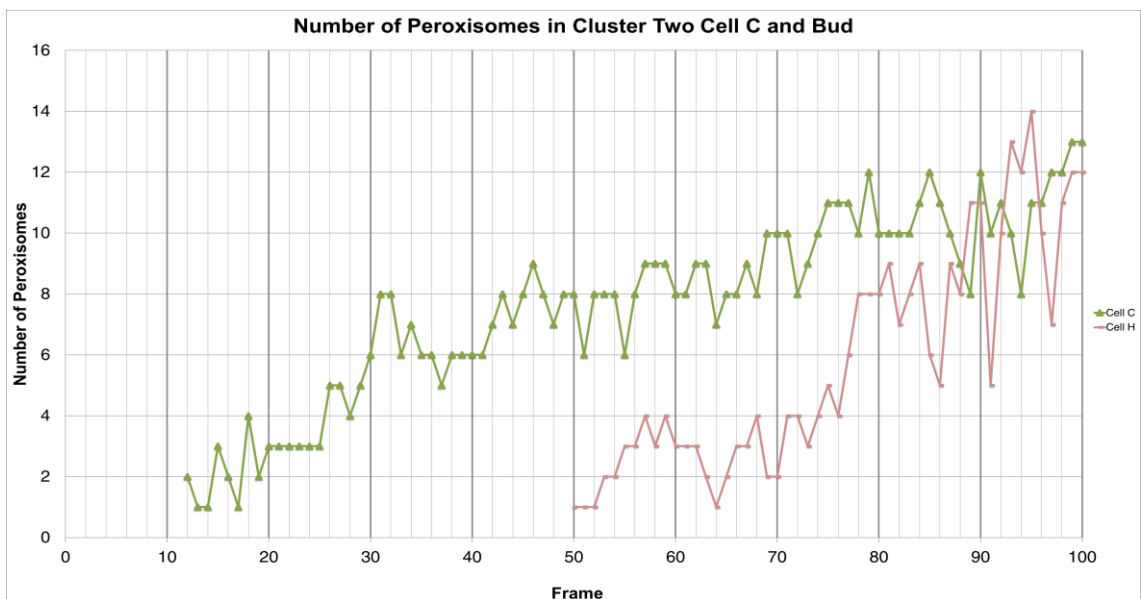
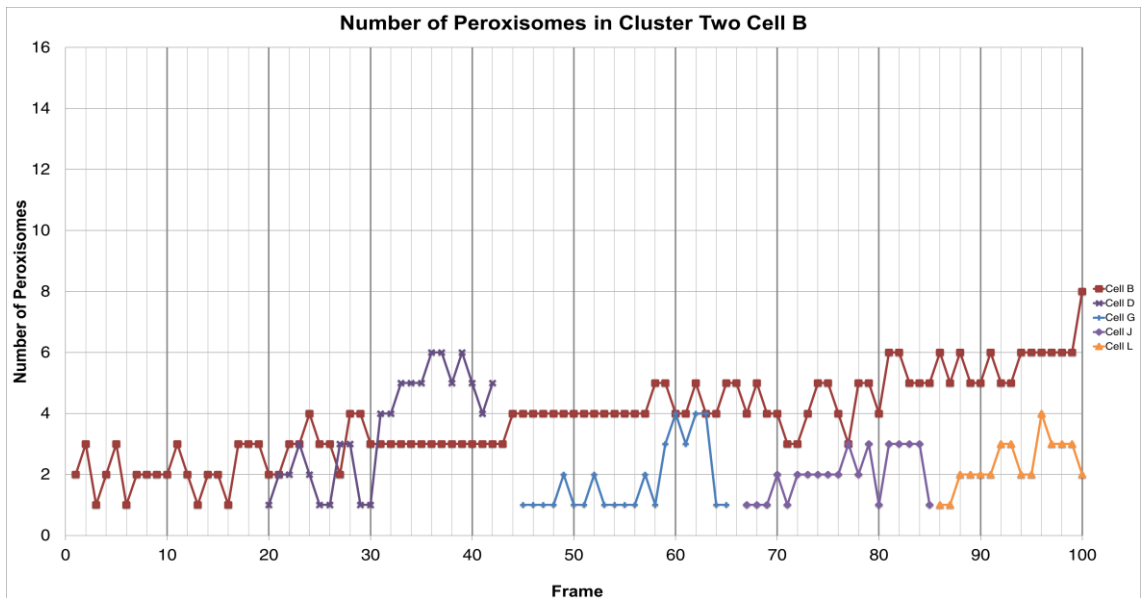
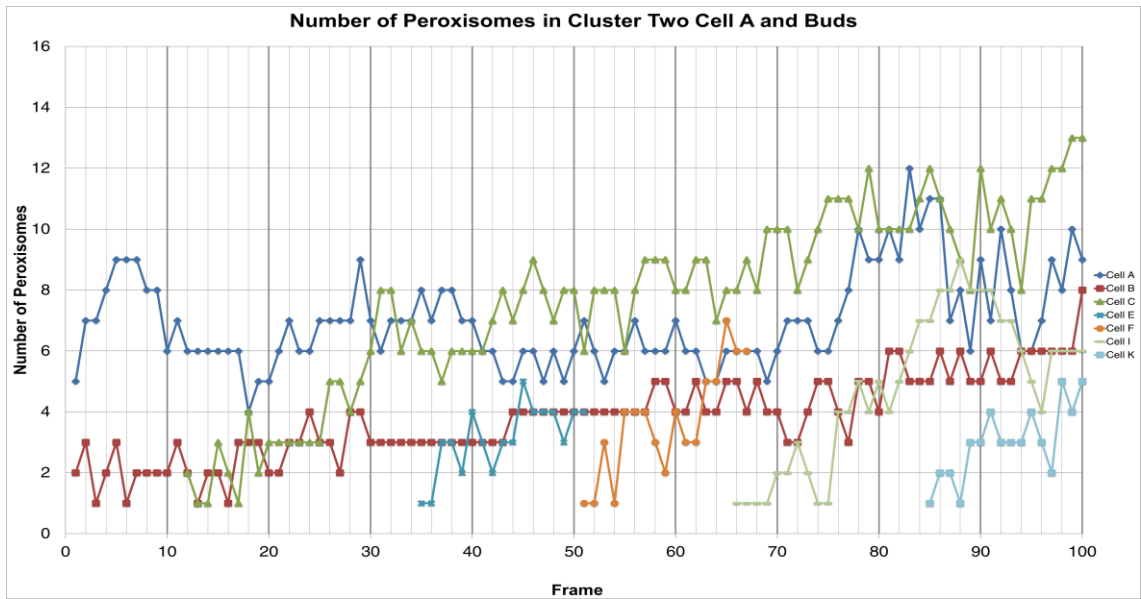
Cluster 5

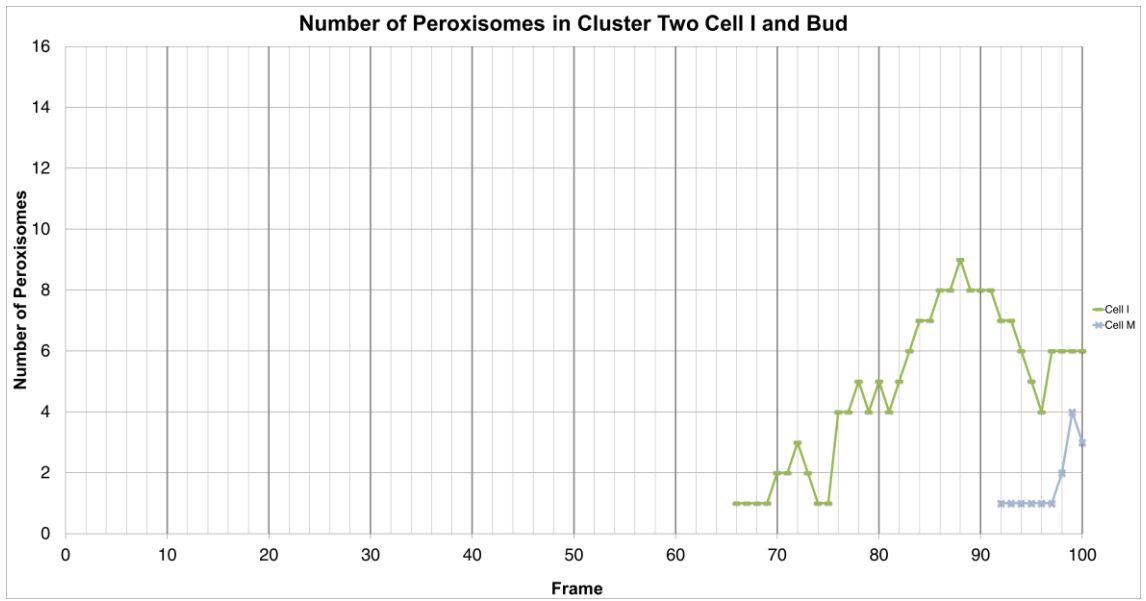
Cell	Frames Present	Buds
A	1-100	B,C,E,H,M,P
B	1-100	D,F,J,Q
C	19-100	G,L
D	22-100	I
E	38-100	K,O
F	47-65	
G	47-100	
H	56-100	N
I	57-100	
J	64-100	
K	65-87	
L	71-100	
M	73-100	
N	78-100	
O	88-100	
P	95-100	
Q	94-100	



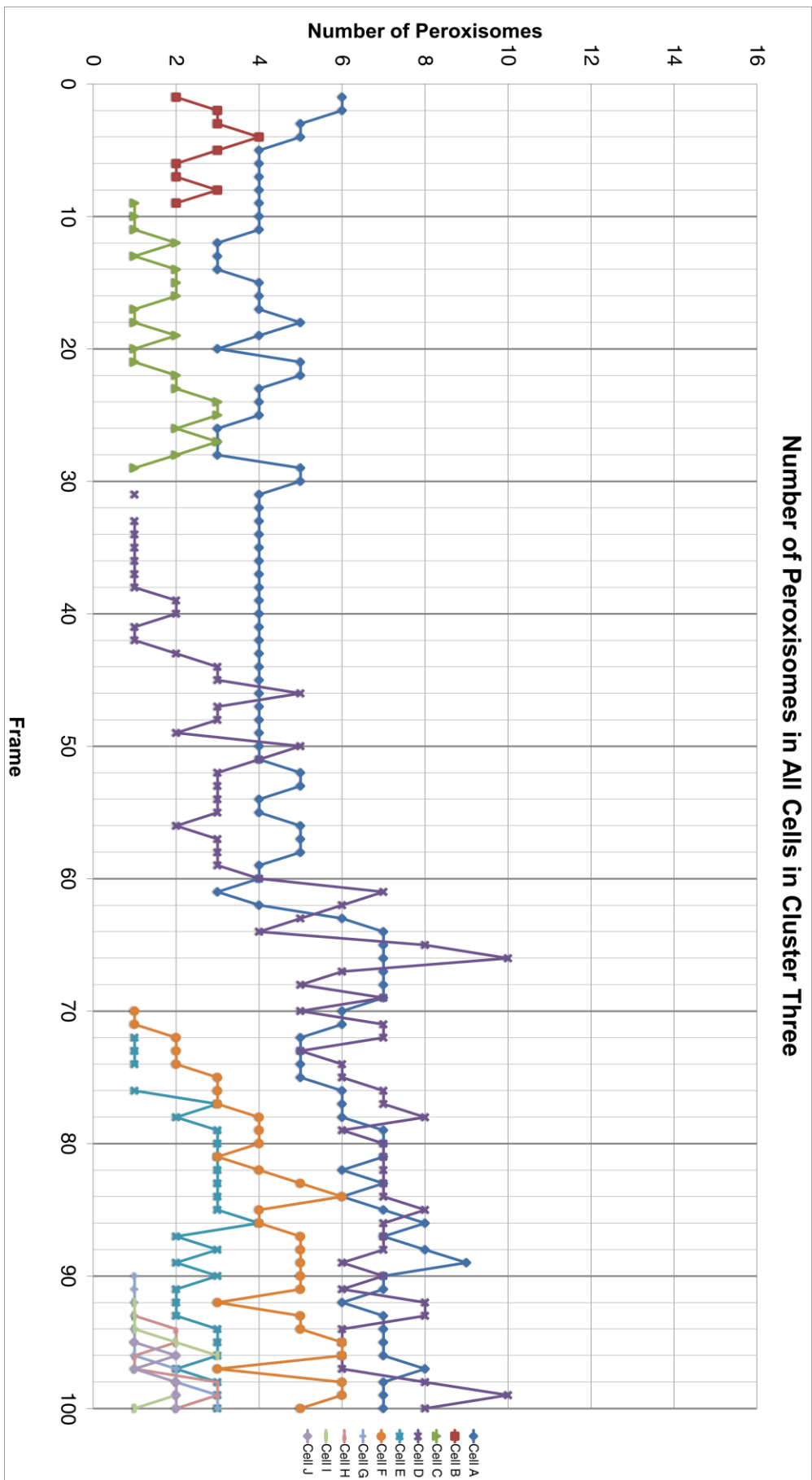
Number of Peroxisomes in All Cells in Cluster Two

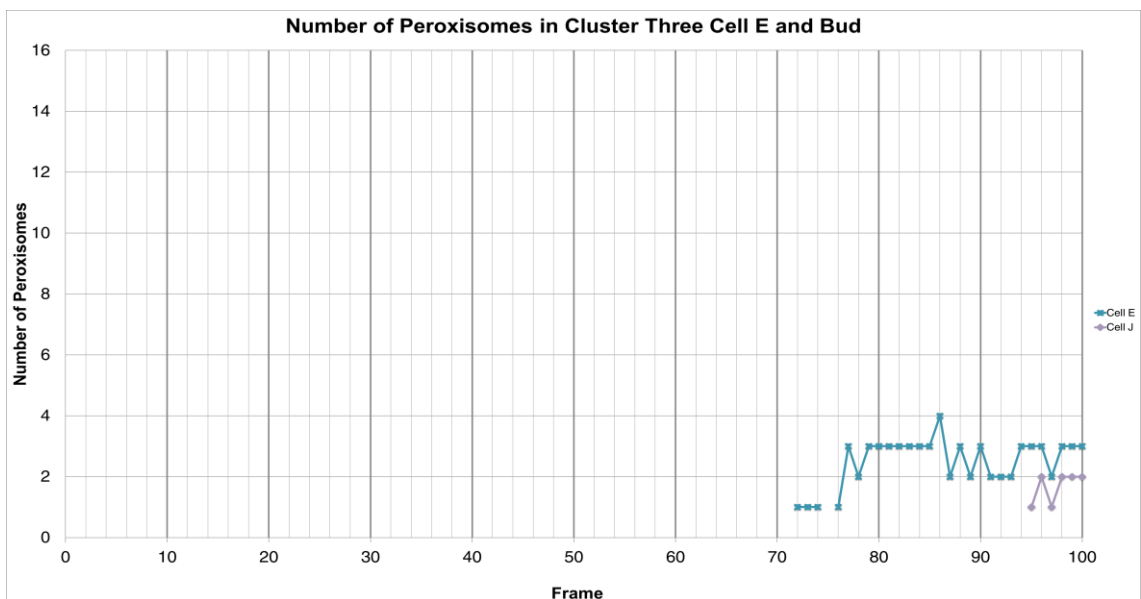
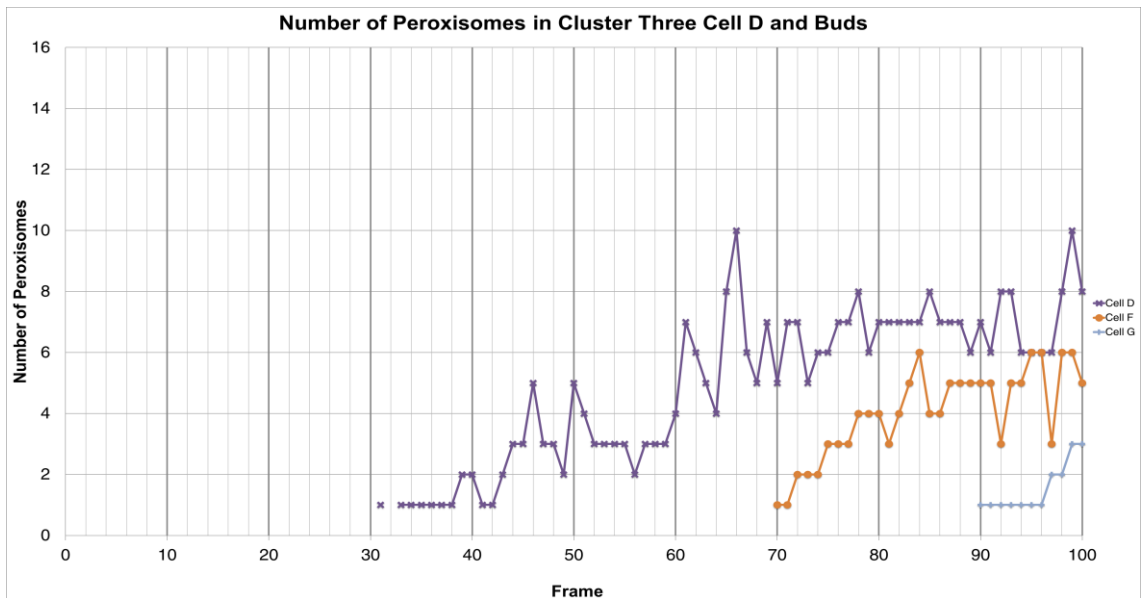
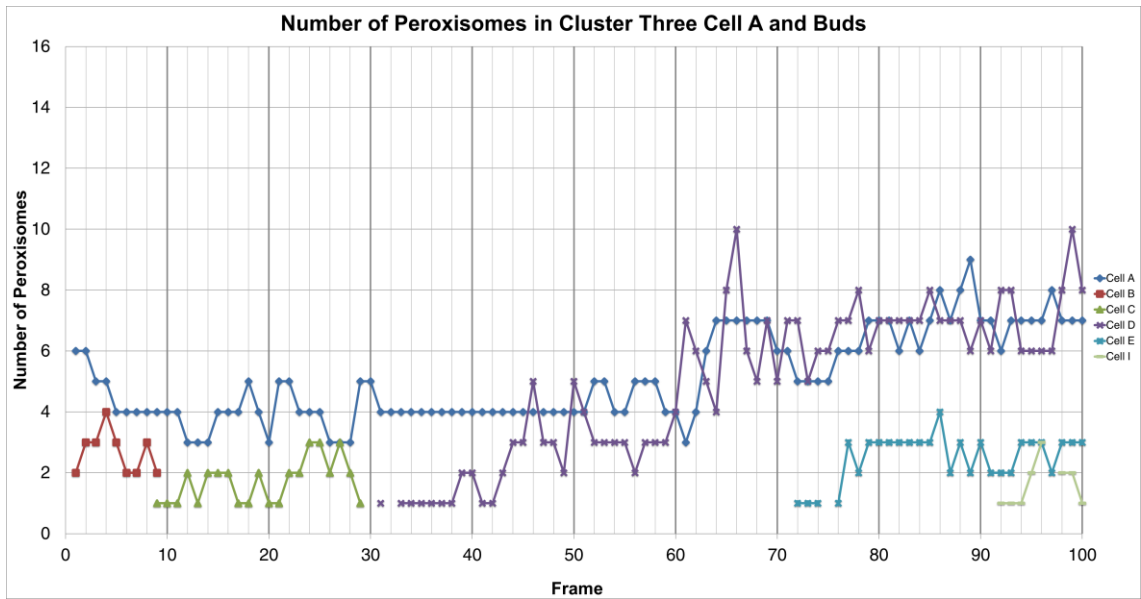


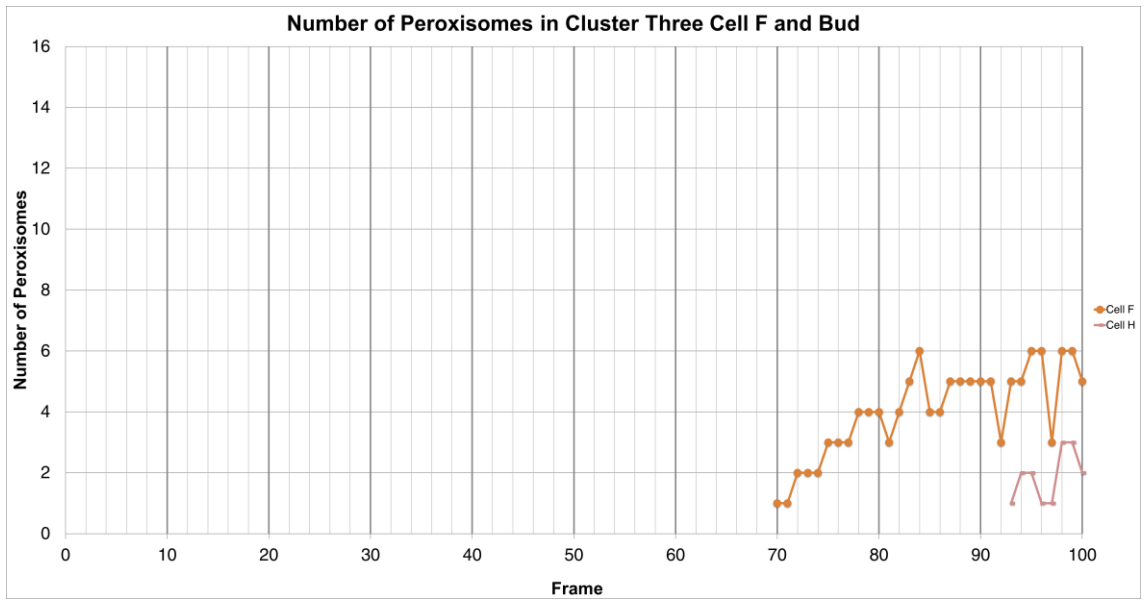




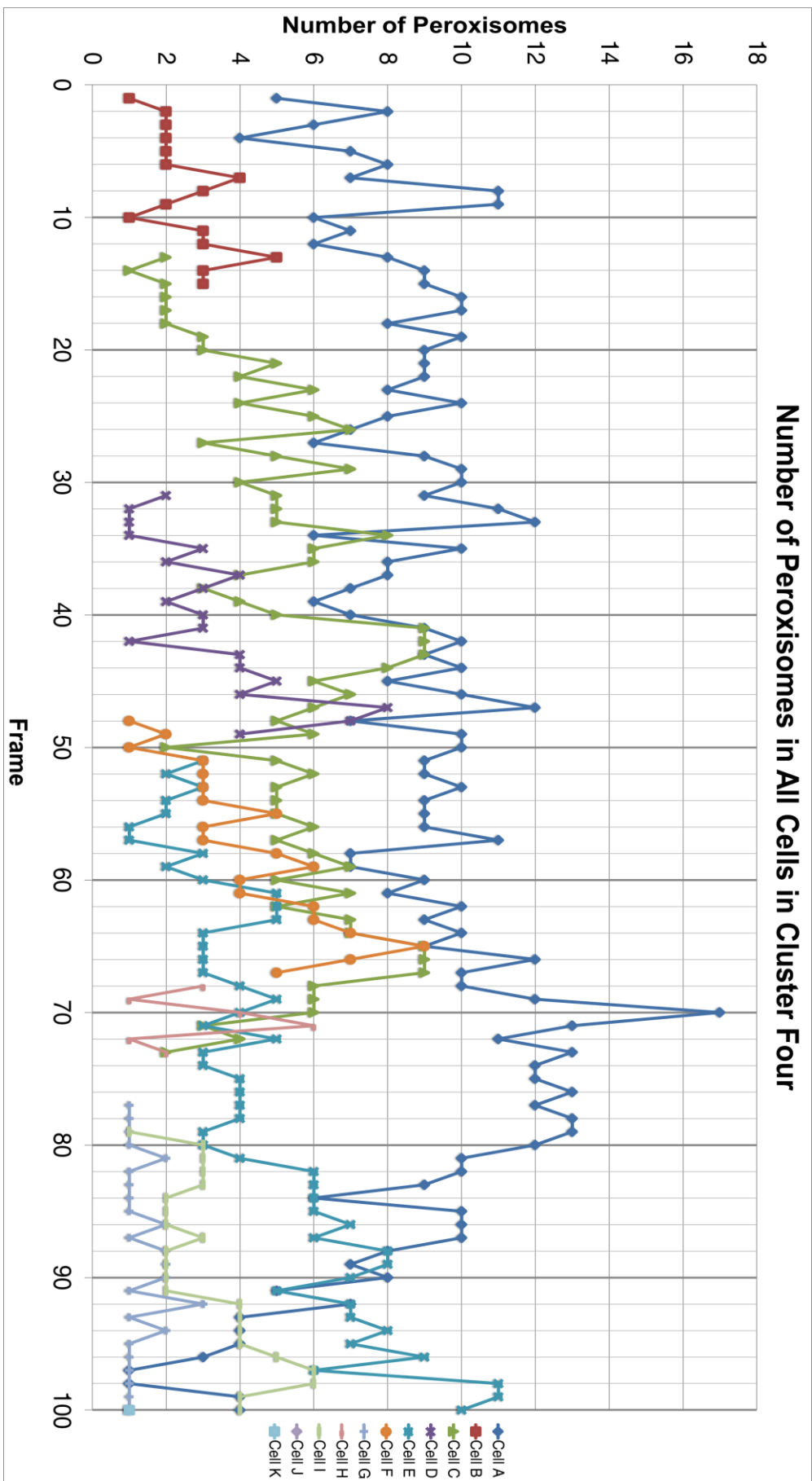
Number of Peroxisomes in All Cells in Cluster Three

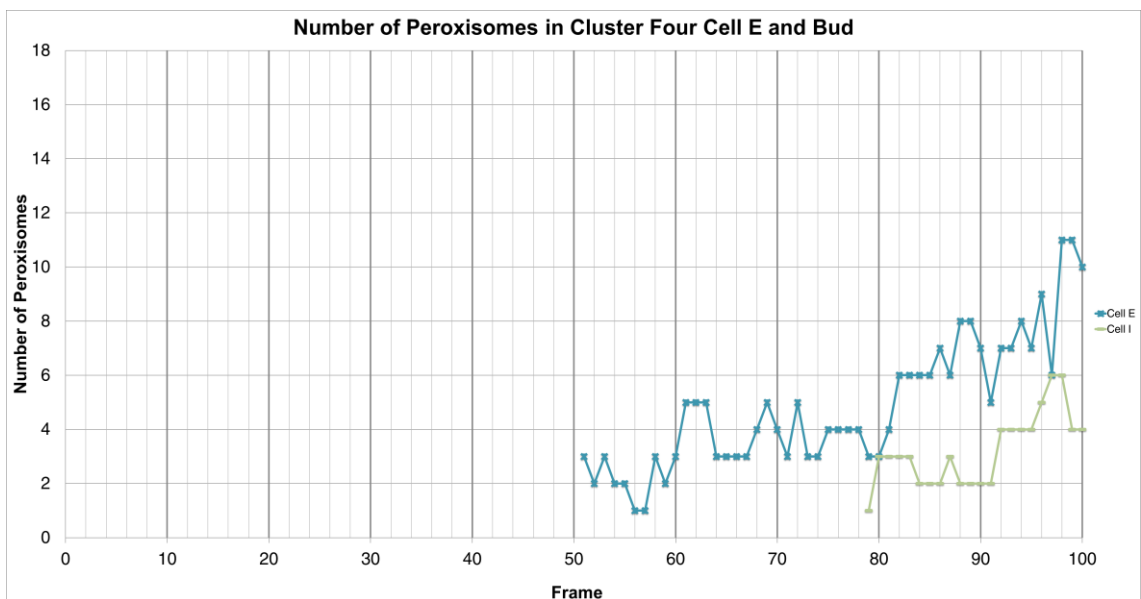
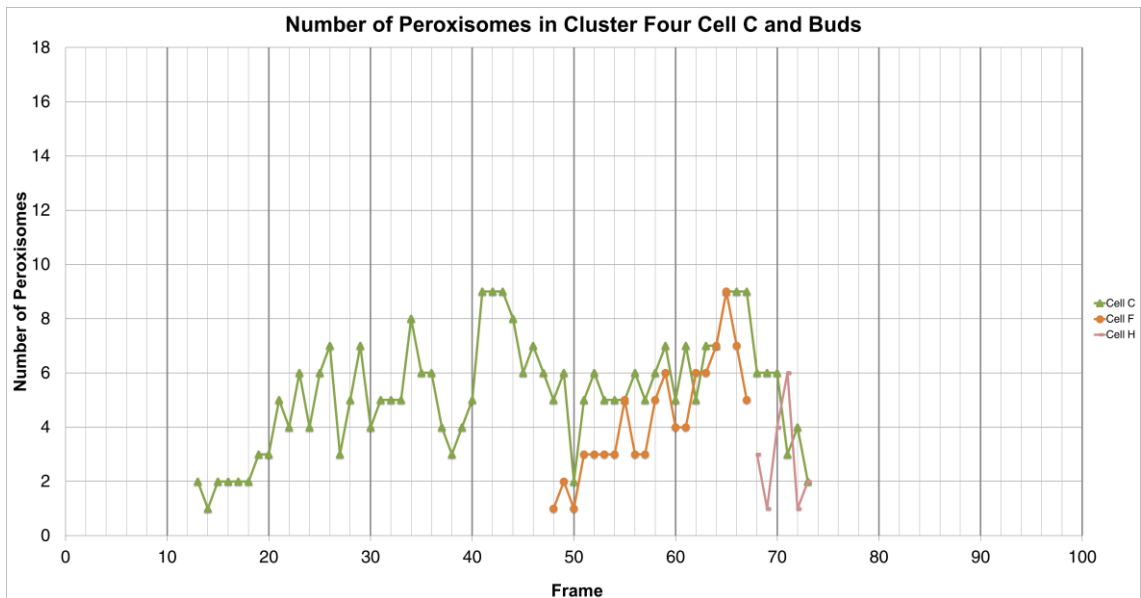
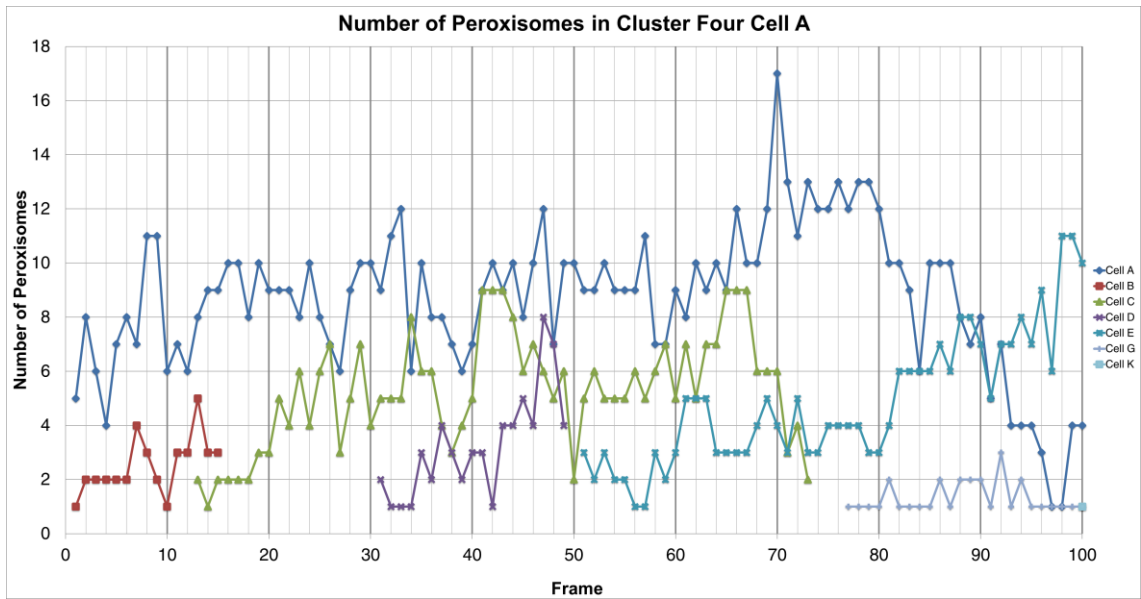


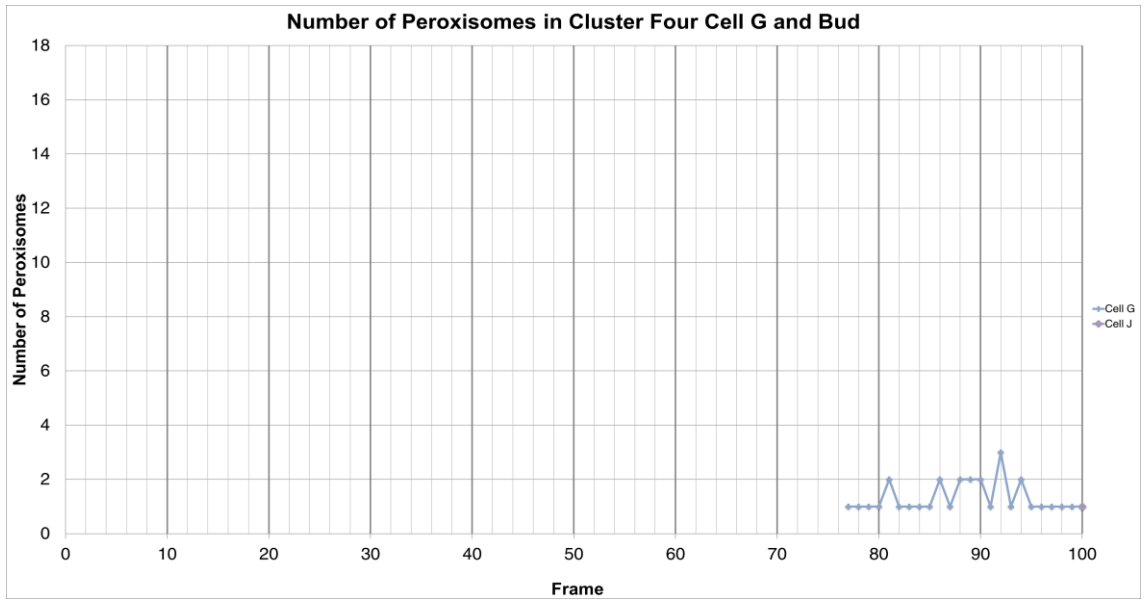




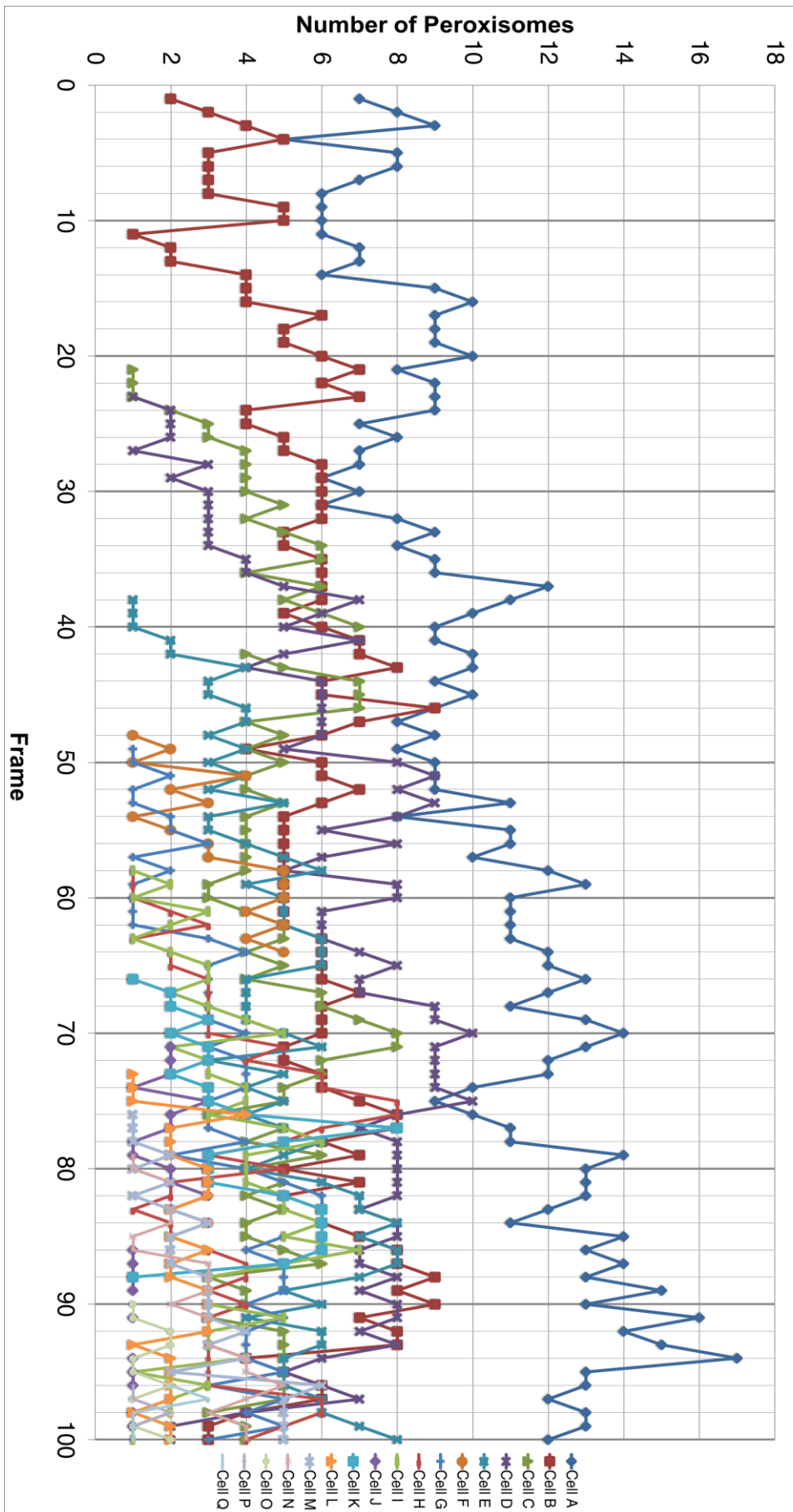
Number of Peroxisomes in All Cells in Cluster Four

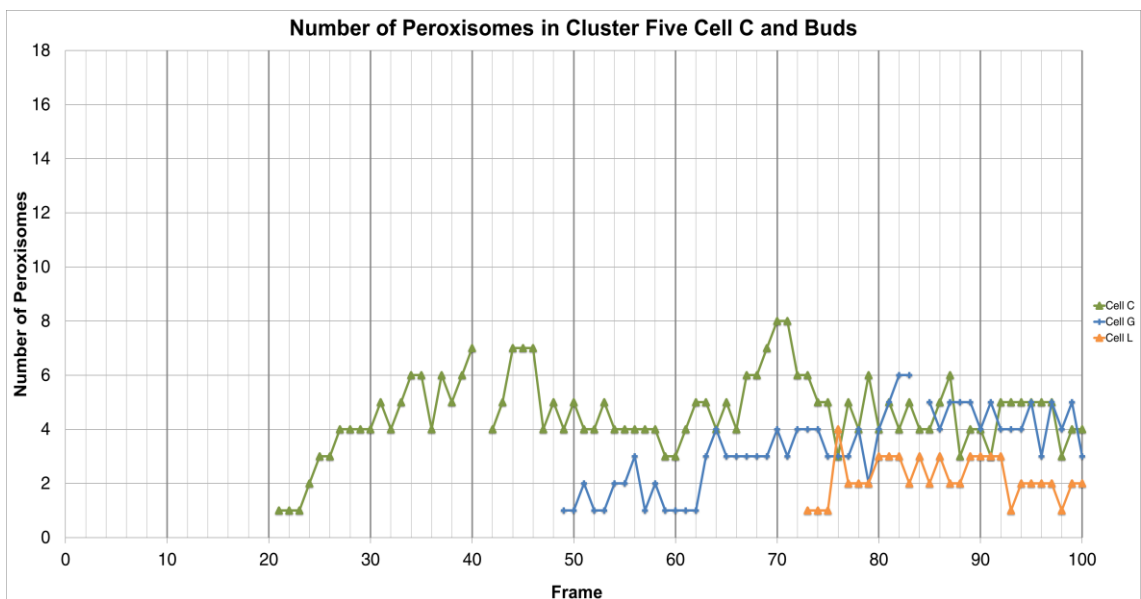
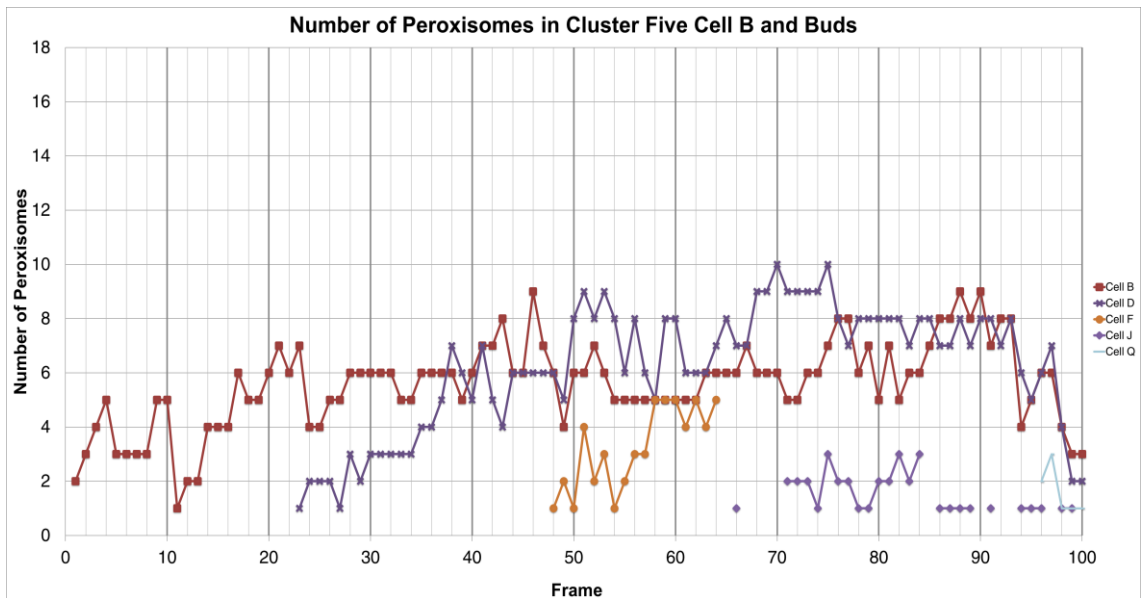
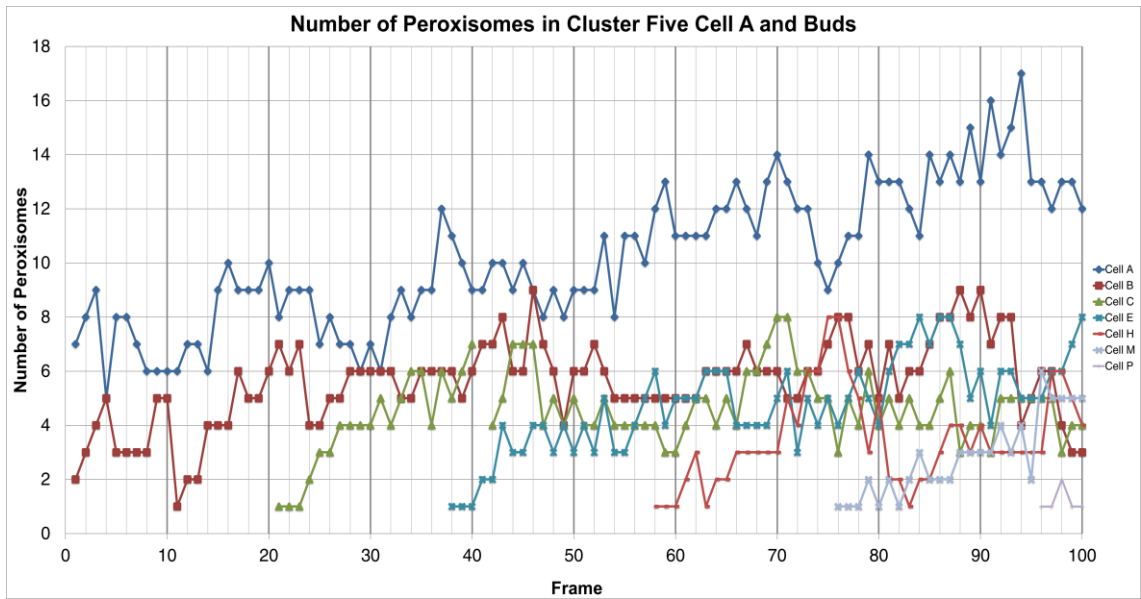


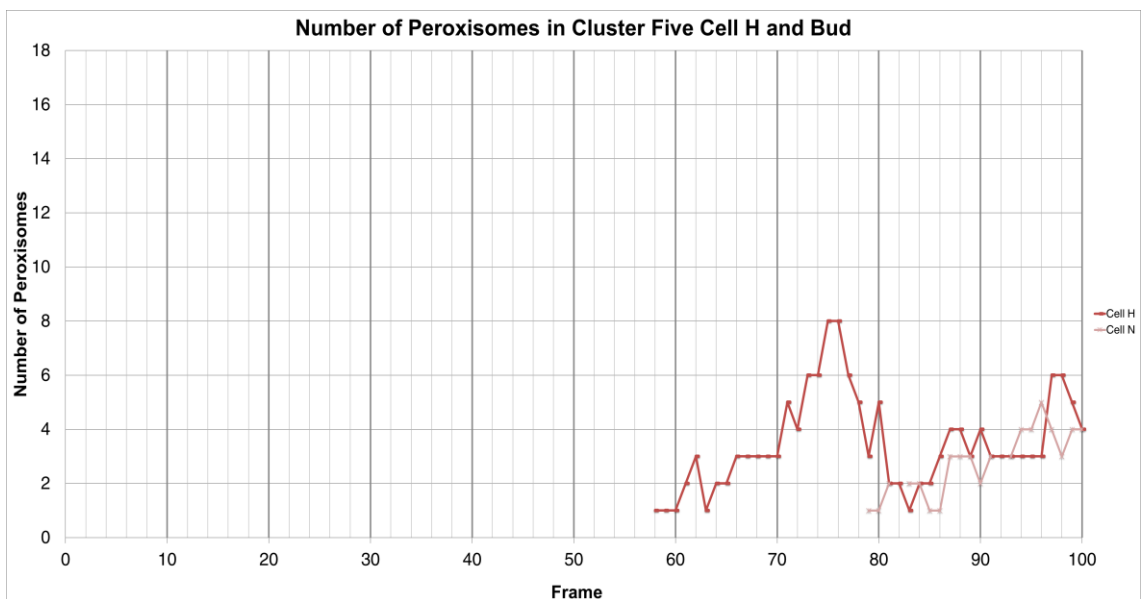
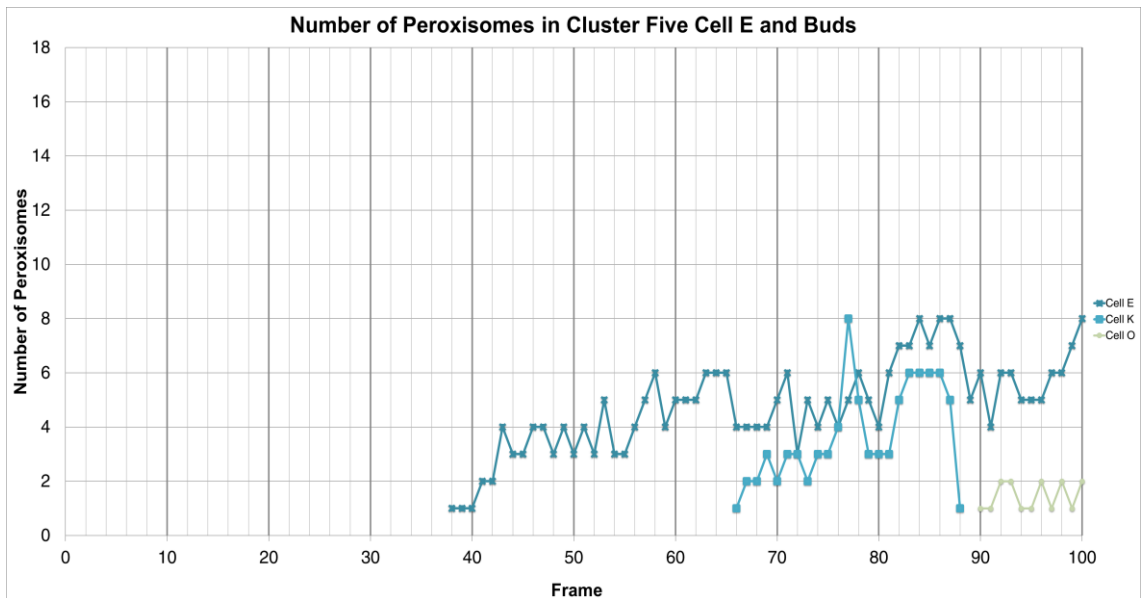
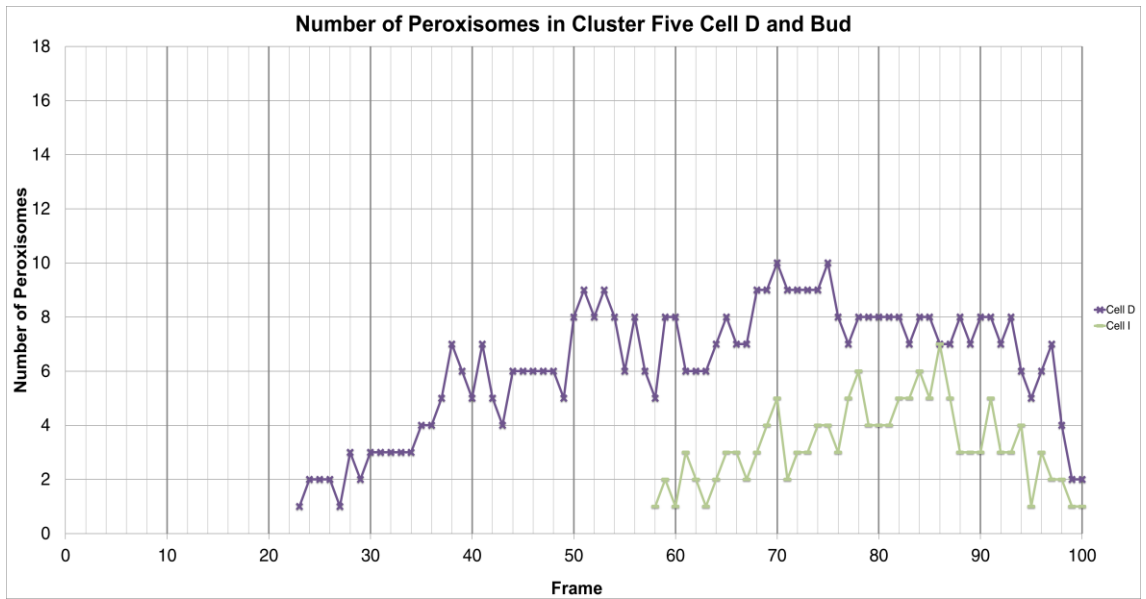




Number of Peroxisomes in All Cells in Cluster Five







References

- Agne, B., Meindl, N.M., Niederhoff, K., Einwächter, H., Rehling, P., Sickmann, A., Meyer, H.E., Girzalsky, W., and Kunau, W.H. (2003). Pex8p: An intraperoxisomal organizer of the peroxisomal import machinery. *Mol. Cell* *11*, 635–646.
- Altmann, K., Frank, M., Neumann, D., Jakobs, S., and Westermann, B. (2008). The class V myosin motor protein, Myo2, plays a major role in mitochondrial motility in *Saccharomyces cerevisiae*. *J. Cell Biol.* *181*, 119–130.
- Beier, K., and Fahimi, H.D. (1985). Automatic determination of labeling density in protein A-gold immunocytochemical preparations using an image analyzer - Application to peroxisomal enzymes. *Histochemistry* *82*, 99–100.
- Beier, K., and Fahimi, H.D. (1992). Application of automatic image analysis for quantitative morphological studies of peroxisomes in rat liver in conjunction with cytochemical staining with 3-3'-diaminobenzidine and immunocytochemistry. *Microsc. Res. Tech.* *21*, 271–282.
- Berger, J., Dorninger, F., Forss-Petter, S., and Kunze, M. (2016). Peroxisomes in brain development and function. *Biochim. Biophys. Acta - Mol. Cell Res.* *1863*, 934–955.
- Blobel, G. (1980). Intracellular protein topogenesis. *Proc. Natl. Acad. Sci. U. S. A.* *77*, 1496–1500.
- Boldogh, I.R., Ramcharan, S.L., Yang, H.-C., and Pon, L.A. (2004). A Type V Myosin (Myo2p) and a Rab-like G-Protein (Ypt11p) Are Required for Retention of Newly Inherited Mitochondria in Yeast Cells during Cell Division. *Mol. Biol. Cell* *15*, 3994–4002.
- van den Bosch, H., Schutgens, R.B., Wanders, R.J., and Tager, J.M. (1992). Biochemistry of peroxisomes. *Annu. Rev. Biochem.* *61*, 157–197.
- Braverman, N.E., D'Agostino, M.D., and MacLean, G.E. (2013). Peroxisome biogenesis disorders: Biological, clinical and pathophysiological perspectives. *Dev. Disabil. Res. Rev.* *17*, 187–196.
- Braverman, N.E., Raymond, G. V., Rizzo, W.B., Moser, A.B., Wilkinson, M.E., Stone, E.M., Steinberg, S.J., Wangler, M.F., Rush, E.T., Hacia, J.G., et al. (2016). Peroxisome biogenesis disorders in the Zellweger spectrum: An overview of current diagnosis, clinical manifestations, and treatment guidelines. *Mol. Genet. Metab.* *117*, 313–321.

- Brocard, C., and Hartig, A. (2006). Peroxisome targeting signal 1: is it really a simple tripeptide? *Biochim. Biophys. Acta* *1763*, 1565–1573.
- Budka, H., Sluga, E., and Heiss, W.-D. (1976). Spastic Paraplegia Associated with Addison's Disease: Adult Variant of Adreno-Leukodystrophy. *250*.
- Campbell, R.E., Campbell, R.E., Tour, O., Tour, O., Palmer, A.E., Palmer, A.E., Steinbach, P. a, Steinbach, P. a, Baird, G.S., Baird, G.S., et al. (2002). A monomeric red fluorescent protein. *Proc. Natl. Acad. Sci. U. S. A.* *99*, 7877–7882.
- Carlton, V.E.H., Harris, B.Z., Puffenberger, E.G., Batta, a K., Knisely, a S., Robinson, D.L., Strauss, K. a, Shneider, B.L., Lim, W. a, Salen, G., et al. (2003). Complex inheritance of familial hypercholanemia with associated mutations in TJP2 and BAAT. *Nat. Genet.* *34*, 91–96.
- Carpenter, A.E., Jones, T.R., Lamprecht, M.R., Clarke, C., Kang, I.H., Friman, O., Guertin, D. a, Chang, J.H., Lindquist, R. a, Moffat, J., et al. (2006). CellProfiler: image analysis software for identifying and quantifying cell phenotypes. *Genome Biol.* *7*, R100.
- de Chaumont, F., Dallongeville, S., Chenouard, N., Hervé, N., Pop, S., Provoost, T., Meas-Yedid, V., Pankajakshan, P., Lecomte, T., Le Montagner, Y., et al. (2012). Icy: an open bioimage informatics platform for extended reproducible research. *Nat. Methods* *9*, 690–696.
- Chenouard, N., Smal, I., de Chaumont, F., Maška, M., Sbalzarini, I.F., Gong, Y., Cardinale, J., Carthel, C., Coraluppi, S., Winter, M., et al. (2014). Objective comparison of particle tracking methods. *Nat. Methods* *11*, 281–289.
- Cherry, J.M., Hong, E.L., Amundsen, C., Balakrishnan, R., Binkley, G., Chan, E.T., Christie, K.R., Costanzo, M.C., Dwight, S.S., Engel, S.R., et al. (2012). *Saccharomyces* Genome Database: The genomics resource of budding yeast. *Nucleic Acids Res.* *40*, 700–705.
- Collins, T.. (2007). ImageJ for microscopy. *Biotechniques* *43*, 25–30.
- Cormack, B.P., Valdivia, R.H., and Falkow, S. (1996). FACS-optimized mutants of the green fluorescent protein (GFP). *Gene* *173*, 33–38.
- Cross, L.L., Ebeed, H.T., and Baker, A. (2015). Peroxisome biogenesis, protein targeting mechanisms and PEX gene functions in plants. *Biochim. Biophys. Acta* *1863*, 850–862.

- Danpure, C., and Jennings, P. (1986). Peroxisomal Alanine - Glyoxylate Aminotransferase Deficiency in Primary Hyperoxaluria Type-I. *Febs Lett.* *201*, 20–24.
- Debelyy, M.O., Platta, H.W., Saffian, D., Hensel, A., Thoms, S., Meyer, H.E., Warscheid, B., Girzalsky, W., and Erdmann, R. (2011). Ubp15p, a ubiquitin hydrolase associated with the peroxisomal export machinery. *J. Biol. Chem.* *286*, 28223–28234.
- Delille, H.K., Agricola, B., Guimaraes, S.C., Borta, H., Lüers, G.H., Fransen, M., and Schrader, M. (2010). Pex11p β -mediated growth and division of mammalian peroxisomes follows a maturation pathway. *J. Cell Sci.* *123*, 275027–275062.
- Demachy, I., Ridard, J., Laguitton-Pasquier, H., Durnerin, E., Vallverdu, G., Archirel, P., and Lévy, B. (2005). Cyan fluorescent protein: molecular dynamics, simulations, and electronic absorption spectrum. *J. Phys. Chem. B* *109*, 24121–24133.
- Diaspro, A., Chirico, G., Usai, C., Ramoino, P., and Dobrucki, J. (2006). Photobleaching. *Handb. Biol. Confocal Microsc.* 690–702.
- Distel, B., Erdmann, R., Gould, S.J., Blobel, G., Crane, D.I., Cregg, J.M., Dodt, G., Fujiki, Y., Goodman, J.M., Just, W.W., et al. (1996). A unified nomenclature for peroxisome biogenesis factors. *J. Cell Biol.* *135*, 1–3.
- de Duve, C. (1969). The peroxisome: a new cytoplasmic organelle. *Proc. R. Soc. London.*
- De Duve, C., and Baudhuin, P. (1966). Peroxisomes (microbodies and related particles). *Physiol. Rev.* *46*, 323–357.
- De Duve, C., Pressman, B.C., Gianetto, R., Wattiaux, R., and Appelmans, F. (1955). Tissue fractionation studies. 6. Intracellular distribution patterns of enzymes in rat-liver tissue. *Biochem. J.* *60*, 604–617.
- Ebberink, M.S., Mooijer, P.A.W., Gootjes, J., Koster, J., Wanders, R.J.A., and Waterham, H.R. (2011). Genetic classification and mutational spectrum of more than 600 patients with a Zellweger syndrome spectrum disorder. *Hum. Mutat.* *32*, 59–69.
- Einwächter, H., Sowinski, S., Kunau, W.H., and Schliebs, W. (2001). *Yarrowia lipolytica* Pex20p, *Saccharomyces cerevisiae* Pex18p/Pex21p and mammalian Pex5pL fulfil a common function in the early steps of the peroxisomal PTS2 import pathway. *EMBO Rep.* *2*, 1035–1039.

- Eliceiri, K.W., Berthold, M.R., Goldberg, I.G., Ibanez, L., Manjunath, B.S., Martone, M.E., Murphy, R.F., Peng, H., Plant, A.L., Roysam, B., et al. (2012). Biological imaging software tools. *Nat Methods* 9, 697–710.
- Engelen, M., Kemp, S., de Visser, M., van Geel, B.M., Wanders, R.J. a., Aubourg, P. a, and Poll-The, B.T. (2012). X-linked adrenoleukodystrophy (X-ALD): clinical presentation and guidelines for diagnosis, follow-up and management. *Orphanet J. Rare Dis.* 7, 51.
- Erdmann, R., Veenhuis, M., Mertens, D., and Kunau, W.H. (1989). Isolation of peroxisome-deficient mutants of *Saccharomyces cerevisiae*. *Proc. Natl. Acad. Sci.* 86, 5419–5423.
- Ernster, L., and Schatz, G. (1981). Mitochondria : A Historical Review. *J. Cell Biol.* 91.
- Estrada, P., Kim, J., Coleman, J., Walker, L., Dunn, B., Takizawa, P., Novick, P., and Ferro-Novick, S. (2003). Myo4p and She3p are required for cortical ER inheritance in *Saccharomyces cerevisiae*. *J. Cell Biol.* 163, 1255–1266.
- Fagarasanu, A., and Rachubinski, R.A. (2007). Orchestrating organelle inheritance in *Saccharomyces cerevisiae*. *Curr. Opin. Microbiol.* 10, 528–538.
- Fagarasanu, A., Fagarasanu, M., Eitzen, G. a., Aitchison, J.D., and Rachubinski, R. a. (2006a). The Peroxisomal Membrane Protein Inp2p Is the Peroxisome-Specific Receptor for the Myosin V Motor Myo2p of *Saccharomyces cerevisiae*. *Dev. Cell* 10, 587–600.
- Fagarasanu, A., Fagarasanu, M., and Rachubinski, R.A. (2007). Maintaining peroxisome populations: a story of division and inheritance. *Annu. Rev. Cell Dev. Biol.* 23, 321–344.
- Fagarasanu, A., Mast, F.D., Knoblach, B., Jin, Y., Brunner, M.J., Logan, M.R., Glover, J.N.M., Eitzen, G.A., Aitchison, J.D., Weisman, L.S., et al. (2009). Myosin-driven peroxisome partitioning in *S. cerevisiae*. *J. Cell Biol.* 186, 541–554.
- Fagarasanu, A., Mast, F.D., Knoblach, B., and Rachubinski, R. a (2010). Molecular mechanisms of organelle inheritance: lessons from peroxisomes in yeast. *Nat. Rev. Mol. Cell Biol.* 11, 644–654.
- Fagarasanu, M., Fagarasanu, A., Tam, Y.Y.C., Aitchison, J.D., and Rachubinski, R.A. (2005). Inp1p is a peroxisomal membrane protein required for peroxisome inheritance in *Saccharomyces cerevisiae*. *J. Cell Biol.* 169, 765–775.
- Fagarasanu, M., Fagarasanu, A., and Rachubinski, R.A. (2006b). Sharing the wealth:

Peroxisome inheritance in budding yeast. *Biochim. Biophys. Acta - Mol. Cell Res.* *1763*, 1669–1677.

Fahimi, H.D., Reich, D., Völkl, A., and Baumgart, E. (1996). Contributions of the immunogold technique to investigation of the biology of peroxisomes. *Histochem. Cell Biol.* *106*, 105–114.

Fakieh, M.H., Drake, P.J.M., Lacey, J., Munck, J.M., Motley, A.M., and Hettema, E.H. (2013). Intra-ER sorting of the peroxisomal membrane protein Pex3 relies on its luminal domain. *Biol. Open* *2*, 829–837.

Fang, Y., Morrell, J.C., Jones, J.M., and Gould, S.J. (2004). PEX3 functions as a PEX19 docking factor in the import of class I peroxisomal membrane proteins. *J. Cell Biol.* *164*, 863–875.

Fehrenbacher, K.L., Yang, H.-C., Gay, A.C., Huckaba, T.M., and Pon, L.A. (2004). Live Cell Imaging of Mitochondrial Movement along Actin Cables in Budding Yeast. *Curr. Biol.* *14*, 1996–2004.

Ferdinandusse, S., Denis, S., Clayton, P.T., Graham, a, Rees, J.E., Allen, J.T., McLean, B.N., Brown, a Y., Vreken, P., Waterham, H.R., et al. (2000). Mutations in the gene encoding peroxisomal alpha-methylacyl-CoA racemase cause adult-onset sensory motor neuropathy. *Nat. Genet.* *24*, 188–191.

Ferdinandusse, S., Denis, S., Mooyer, P.A.W., Dekker, C., Duran, M., Soorani-Lusing, R.J., Boltshauser, E., Macaya, A., Gärtner, J., Majoie, C.B.L.M., et al. (2006a). Clinical and biochemical spectrum of D-bifunctional protein deficiency. *Ann. Neurol.* *59*, 92–104.

Ferdinandusse, S., Kostopoulos, P., Denis, S., Rusch, H., Overmars, H., Dillmann, U., Reith, W., Haas, D., Wanders, R.J.A., Duran, M., et al. (2006b). Mutations in the gene encoding peroxisomal sterol carrier protein X (SCPx) cause leukoencephalopathy with dystonia and motor neuropathy. *Am. J. Hum. Genet.* *78*, 1046–1052.

Ferdinandusse, S., Denis, S., Hogenhout, E.M., Koster, J., van Roermund, C.W.T., IJlst, L., Moser, A.B., Wanders, R.J.A., and Waterham, H.R. (2007). Clinical, biochemical, and mutational spectrum of peroxisomal acyl-coenzyme A oxidase deficiency. *Hum. Mutat.* *28*, 904–912.

Fujiki, Y., Okumoto, K., Mukai, S., Honsho, M., and Tamura, S. (2014). Peroxisome

biogenesis in mammalian cells. *Front. Physiol.* 5 AUG, 1–8.

Gabaldon, T. (2010). Peroxisome diversity and evolution. *Philos. Trans. R. Soc. B Biol. Sci.* 365, 765–773.

Gerbert A., J., Ronald J.A., W., Paul A., W., and Stephanie J., M. (1997). Phytanoyl-Coenzyme a Hydroxylase Deficiency — The Enzyme Defect in Refsum's Disease. *N. Engl. J. Med.* 337, 127–128.

Girzalsky, W., Saffian, D., and Erdmann, R. (2010). Peroxisomal protein translocation. *Biochim. Biophys. Acta - Mol. Cell Res.* 1803, 724–731.

Goldfischer, S., Moore, C.L., Johnson, A.B., Spiro, A.J., Valsamis, M.P., Wisniewski, H.K., Ritch, R.H., Norton, W.T., Rapin, I., and Gartner, L.M. (1973). Peroxisomal and Mitochondrial Defects in the Cerebro-Hepato-Renal Syndrome. *Science* (80-.). 182, 62–64.

Golgi, C. (1898). Sur la structure des cellules nerveuses. *Arch Ital Biol* 30, 60–71.

Gootjes, J., Schmohl, F., Mooijer, P.A.W., Dekker, C., Mandel, H., Topcu, M., Huemer, M., Von Sch?tz, M., Marquardt, T., Smeitink, J.A., et al. (2004). Identification of the molecular defect in patients with peroxisomal mosaicism using a novel method involving culturing of cells at 40°C: Implications for other inborn errors of metabolism. *Hum. Mutat.* 24, 130–139.

Gould, S.J., Keller, G.A., Hosken, N., Wilkinson, J., and Subramani, S. (1989). A conserved tripeptide sorts proteins to peroxisomes. *J. Cell Biol.* 108, 1657–1664.

Haanstra, J.R., González-marcano, E.B., Gualdrón-lópez, M., and Michels, P.A.M. (2015). Biogenesis , maintenance and dynamics of glycosomes in trypanosomatid parasites. *BBA - Mol. Cell Res.*

Halbach, A., Rucktächel, R., Rottensteiner, H., and Erdmann, R. (2009). The N-domain of Pex22p can functionally replace the Pex3p N-domain in targeting and peroxisome formation. *J. Biol. Chem.* 284, 3906–3916.

Hawkins, J., Mahony, D., Maetschke, S., Wakabayashi, M., Teasdale, R.D., and Bodén, M. (2007). Identifying novel peroxisomal proteins. *Proteins Struct. Funct. Bioinforma.* 69, 606–616.

Hayashi, M., Toriyama, K., Kondo, M., Kato, A., Mano, S., De Bellis, L., Hayashi-Ishimaru,

- Y., Yamaguchi, K., Hayashi, H., and Nishimura, M. (2000). Functional transformation of plant peroxisomes. *Cell Biochem. Biophys.* *32*, 295–304.
- Heslot, H., and Gaillardin, C. (1991). *Molecular biology and genetic engineering of yeasts* (CRC Press).
- Hettema, E.H., and Motley, A.M. (2009). How peroxisomes multiply. *J. Cell Sci.* *122*, 2331–2336.
- Hettema, E.H., Girzalsky, W., Berg, M. Van Den, Erdmann, R., Distel, B., van Den Berg, M., Erdmann, R., and Distel, B. (2000). *Saccharomyces cerevisiae* pex3p and pex19p are required for proper localization and stability of peroxisomal membrane proteins. *EMBO J.* *19*, 223–233.
- Hoebe, R.A., Van Oven, C.H., Gadella, T.W.J., Dhonukshe, P.B., Van Noorden, C.J.F., and Manders, E.M.M. (2007). Controlled light-exposure microscopy reduces photobleaching and phototoxicity in fluorescence live-cell imaging. *Nat. Biotechnol.* *25*, 249–253.
- Hoepfner, D., Van Den Berg, M., Philippsen, P., Tabak, H.F., and Hettema, E.H. (2001). A role for Vps1p, actin, and the Myo2p motor in peroxisome abundance and inheritance in *Saccharomyces cerevisiae*. *J. Cell Biol.* *155*, 979–990.
- Hoepfner, D., Schildknecht, D., Braakman, I., Philippsen, P., and Tabak, H.F. (2005). Contribution of the endoplasmic reticulum to peroxisome formation. *Cell* *122*, 85–95.
- Honsho, M., Tamura, S., Shimozawa, N., Suzuki, Y., Kondo, N., and Fujiki, Y. (1998). Mutation in PEX16 is causal in the peroxisome-deficient Zellweger syndrome of complementation group D. *Am. J. Hum. Genet.* *63*, 1622–1630.
- Hu, J., Baker, A., Bartel, B., Linka, N., Mullen, R.T., Reumann, S., and Zolman, B.K. (2012). *Plant Peroxisomes: Biogenesis and Function*. *Plant Cell* *24*, 2279–2303.
- Hua, R., and Kim, P.K. (2016). Multiple paths to peroxisomes: Mechanism of peroxisome maintenance in mammals. *Biochim. Biophys. Acta - Mol. Cell Res.* *1863*, 881–891.
- Hua, R., Gidda, S.K., Aranovich, A., Mullen, R.T., and Kim, P.K. (2015). Multiple Domains in PEX16 Mediate Its Trafficking and Recruitment of Peroxisomal Proteins to the ER. *Traffic* n/a-n/a.
- Huffaker, T.C., Thomas, J.H., and Botstein, D. (1988). Diverse effects of beta-tubulin

- mutations on microtubule formation and function. *J. Cell Biol.* *106*, 1997–2010.
- Hunter, J.D. (2007). Matplotlib: A 2D graphics environment. *Comput. Sci. Eng.* *9*, 90–95.
- Huybrechts, S.J., Van Veldhoven, P.P., Brees, C., Mannaerts, G.P., Los, G. V., and Fransen, M. (2009). Peroxisome dynamics in cultured mammalian cells. *Traffic* *10*, 1722–1733.
- Islinger, M., Cardoso, M.J.R., and Schrader, M. (2010). Be different-The diversity of peroxisomes in the animal kingdom. *Biochim. Biophys. Acta - Mol. Cell Res.* *1803*, 881–897.
- Jacobs, C.W. (1988). Functions of microtubules in the *Saccharomyces cerevisiae* cell cycle. *J. Cell Biol.* *107*, 1409–1426.
- Jaqaman, K., Loerke, D., Mettlen, M., Kuwata, H., Grinstein, S., Schmid, S.L., and Danuser, G. (2008). Robust single-particle tracking in live-cell time-lapse sequences. *Nat. Methods* *5*, 695–702.
- Jeynov, B., Lay, D., Schmidt, F., Tahirovic, S., and Just, W.W. (2006). Phosphoinositide synthesis and degradation in isolated rat liver peroxisomes. *FEBS Lett.* *580*, 5917–5924.
- Jones, J.M., Morrell, J.C., and Gould, S.J. (2004). PEX19 is a predominantly cytosolic chaperone and import receptor for class 1 peroxisomal membrane proteins. *J. Cell Biol.* *164*, 57–67.
- Jongsma, M.L.M., Berlin, I., and Neefjes, J. (2015). On the move: Organelle dynamics during mitosis. *Trends Cell Biol.* *25*, 112–124.
- Kankaanpää, P., Paavolainen, L., Tiitta, S., Karjalainen, M., Päivärinne, J., Nieminen, J., Marjomäki, V., Heino, J., and White, D.J. (2012). BioImageXD: an open, general-purpose and high-throughput image-processing platform. *Nat. Methods* *9*, 683–689.
- Kerckaert, I., Claeys, A., Just, W., Cornelis, A., and Roels, F. (1989). Automated image analysis of rat liver peroxisomes after treatment with thyroid hormones: Changes in number, size and catalase reaction. *Micron Microsc. Acta* *20*, 9–18.
- Kiel, J.A.K.W., Veenhuis, M., and van der Klei, I.J. (2006). PEX genes in fungal genomes: Common, rare or redundant. *Traffic* *7*, 1291–1303.
- Kim, P.K., and Hettema, E.H. (2015). Multiple pathways for protein transport to peroxisomes. *J. Mol. Biol.* *427*, 1176–1190.

- Kim, P.K., Mullen, R.T., Schumann, U., and Lippincott-Schwartz, J. (2006). The origin and maintenance of mammalian peroxisomes involves a de novo PEX16-dependent pathway from the ER. *J. Cell Biol.* *173*, 521–532.
- Knoblach, B., and Rachubinski, R.A. (2015). Sharing with your children: Mechanisms of peroxisome inheritance. *Biochim. Biophys. Acta - Mol. Cell Res.* *1863*, 1014–1018.
- Knoblach, B., and Rachubinski, R.A. (2016). How peroxisomes partition between cells. A story of yeast, mammals and filamentous fungi. *Curr. Opin. Cell Biol.* *41*, 73–80.
- Knoblach, B., Sun, X., Coquelle, N., Fagarasanu, A., Poirier, R.L., and Rachubinski, R.A. (2013). An ER-peroxisome tether exerts peroxisome population control in yeast. *EMBO J.* *32*, 2439–2453.
- Kochupurakkal, B.S., and Iglehart, J.D. (2013). Nourseothricin N-Acetyl Transferase: A Positive Selection Marker for Mammalian Cells. *PLoS One* *8*, 8–11.
- Koek, A., Komori, M., Veenhuis, M., and Van Der Klei, I.J. (2007). A comparative study of peroxisomal structures in *Hansenula polymorpha* pex mutants. *FEMS Yeast Res.* *7*, 1126–1133.
- Kornmann, B., Currie, E., Collins, S.R., Schuldiner, M., Nunnari, J., Weissman, J.S., and Walter, P. (2009). An ER-mitochondria tethering complex revealed by a synthetic biology screen. *Science* *325*, 477–481.
- Kragt, A., Voorn-Brouwer, T., Van Den Berg, M., and Distel, B. (2005). Endoplasmic reticulum-directed Pex3p routes to peroxisomes and restores peroxisome formation in a *Saccharomyces cerevisiae* pex3^{??} strain. *J. Biol. Chem.* *280*, 34350–34357.
- Kredel, S., Oswald, F., Nienhaus, K., Deuschle, K., Röcker, C., Wolff, M., Heilker, R., Nienhaus, G.U., and Wiedenmann, J. (2009). mRuby, a bright monomeric red fluorescent protein for labeling of subcellular structures. *PLoS One* *4*, 1–7.
- Krügel, H., Fiedler, G., Smith, C., and Baumberg, S. (1993). Sequence and transcriptional analysis of the nourseothricin acetyltransferase-encoding gene *nat1* from *Streptomyces noursei*. *Gene* *127*, 127–131.
- Lakowicz, J.R. (2006). Principles of Fluorescence Spectroscopy Principles of Fluorescence Spectroscopy.

- Lam, A.J., St-Pierre, F., Gong, Y., Marshall, J.D., Cranfill, P.J., Baird, M. a., McKeown, M.R., Wiedenmann, J., Davidson, M.W., Schnitzer, M.J., et al. (2012). Improving FRET dynamic range with bright green and red fluorescent proteins. *Nat. Methods* *9*, 1005–1012.
- Langford, G.M. (2002). Myosin-V, a versatile motor for short-range vesicle transport. *Traffic* *3*, 859–865.
- Lazarow, P.B. (2003). Peroxisome biogenesis: Advances and conundrums. *Curr. Opin. Cell Biol.* *15*, 489–497.
- Lazarow, P.B. (2006). Chapter 3.1.7. The import receptor Pex7p and the PTS2 targeting sequence. *Biochim. Biophys. Acta - Mol. Cell Res.* *1763*, 1599–1604.
- Lazarow, P.B., and Fujiki, Y. (1985). Biogenesis of peroxisomes. *Annu. Rev. Cell Biol.* *1*, 489–530.
- Li, C.H., and Lee, C.K. (1993). Minimum cross entropy thresholding. *Pattern Recognit.* *26*, 617–625.
- El Magraoui, F., Schrötter, A., Brinkmeier, R., Kunst, L., Mastalski, T., Müller, T., Marcus, K., Meyer, H.E., Girzalsky, W., Erdmann, R., et al. (2014). The cytosolic domain of Pex22p stimulates the Pex4p-dependent ubiquitination of the PTS1-receptor. *PLoS One* *9*.
- Manford, A.G., Stefan, C.J., Yuan, H.L., MacGurn, J.A., and Emr, S.D. (2012). ER-to-Plasma Membrane Tethering Proteins Regulate Cell Signaling and ER Morphology. *Dev. Cell* *23*, 1129–1140.
- Marzioch, M., Erdmann, R., Veenhuis, M., and Kunau, W.H. (1994). PAS7 encodes a novel yeast member of the WD-40 protein family essential for import of 3-oxoacyl-CoA thiolase, a PTS2-containing protein, into peroxisomes. *EMBO J.* *13*, 4908–4918.
- Matsuzaki, T., and Fujiki, Y. (2008). The peroxisomal membrane protein import receptor Pex3p is directly transported to peroxisomes by a novel Pex19p- and Pex16p-dependent pathway. *J. Cell Biol.* *183*, 1275–1286.
- Matsuzono, Y., Kinoshita, N., Tamura, S., Shimosawa, N., Hamasaki, M., Ghaedi, K., Wanders, R.J., Suzuki, Y., Kondo, N., and Fujiki, Y. (1999). Human PEX19: cDNA cloning by functional complementation, mutation analysis in a patient with Zellweger syndrome, and potential role in peroxisomal membrane assembly. *Proc. Natl. Acad. Sci. U. S. A.* *96*, 2116–

2121.

Michels, P.A.M., Moyersoer, J., Krazy, H., Galland, N., Herman, M., and Hannaert, V. (2005). Peroxisomes, glyoxysomes and glycosomes (review). *Mol. Membr. Biol.* 22, 133–145.

Michels, P.A.M., Bringaud, F., Herman, M., and Hannaert, V. (2006). Metabolic functions of glycosomes in trypanosomatids. *Biochim. Biophys. Acta - Mol. Cell Res.* 1763, 1463–1477.

Miyata, N., and Fujiki, Y. (2005). Shuttling mechanism of peroxisome targeting signal type 1 receptor Pex5: ATP-independent import and ATP-dependent export. *Mol. Cell. Biol.* 25, 10822–10832.

Miyata, N., Okumoto, K., Mukai, S., Noguchi, M., and Fujiki, Y. (2012). AWP1/ZFAND6 functions in Pex5 export by interacting with cys-monoubiquitinated Pex5 and Pex6 AAA ATPase. *Traffic* 13, 168–183.

Motley, A.M., and Hettema, E.H. (2007). Yeast peroxisomes multiply by growth and division. *J. Cell Biol.* 178, 399–410.

Motley, A.M., Brites, P., Gerez, L., Hogenhout, E., Haasjes, J., Benne, R., Tabak, H.F., Wanders, R.J.A., and Waterham, H.R. (2002). Mutational spectrum in the PEX7 gene and functional analysis of mutant alleles in 78 patients with rhizomelic chondrodysplasia punctata type 1. *Am. J. Hum. Genet.* 70, 612–624.

Motley, A.M., Ward, G.P., and Hettema, E.H. (2008). Dnm1p-dependent peroxisome fission requires Caf4p, Mdv1p and Fis1p. *J. Cell Sci.* 121, 1633–1640.

Motley, A.M., Galvin, P.C., Ekal, L., Nuttall, J.M., and Hettema, E.H. (2015). Reevaluation of the role of Pex1 and dynamin-related proteins in peroxisome membrane biogenesis. *J. Cell Biol.* 211, 1041–1056.

Mullock, B.M., and Luzio, J.P. (2005). Theory of Organelle Biogenesis. In *The Biogenesis of Cellular Organelles*, (Boston, MA: Springer US), pp. 1–18.

Munck, J.M., Motley, A.M., Nuttall, J.M., and Hettema, E.H. (2009). A dual function for Pex3p in peroxisome formation and inheritance. *J. Cell Biol.* 187, 463–471.

Muntau, a C., Mayerhofer, P.U., Paton, B.C., Kammerer, S., and Roscher, a a (2000). Defective peroxisome membrane synthesis due to mutations in human PEX3 causes Zellweger syndrome, complementation group G. *Am. J. Hum. Genet.* 67, 967–975.

- Nagotu, S., Saraya, R., Otzen, M., Veenhuis, M., and van der Klei, I.J. (2008). Peroxisome proliferation in *Hansenula polymorpha* requires Dnm1p which mediates fission but not de novo formation. *Biochim. Biophys. Acta - Mol. Cell Res.* *1783*, 760–769.
- Neuhaus, A., Eggeling, C., Erdmann, R., and Schliebs, W. (2016). Why do peroxisomes associate with the cytoskeleton? *Biochim. Biophys. Acta* *1863*, 1019–1026.
- Niemisto, A., Selinummi, J., Saleem, R., Shmulevich, I., Aitchison, J., and Yli-Harja, O. (2006). Extraction of the Number of Peroxisomes in Yeast Cells by Automated Image Analysis. In 2006 International Conference of the IEEE Engineering in Medicine and Biology Society, (IEEE), pp. 2353–2356.
- Novikoff, P.M., and Novikoff, A.B. (1972). Peroxisomes in absorptive cells of mammalian small intestine. *J. Cell Biol.* *53*, 532–560.
- Novikoff, A.B., Beaufay, H., and De Duve, C. (1956). Electron microscopy of lysosomen rich fractions from rat liver. *J. Biophys. Biochem. Cytol.* *2*, 179–184.
- Nuttall, J.M., Motley, A., and Hettema, E.H. (2011). Peroxisome biogenesis: Recent advances. *Curr. Opin. Cell Biol.* *23*, 421–426.
- Ofman, R., Hettema, E.H., Hogenhout, E.M., Caruso, U., Muijsers, A.O., and Wanders, R.J.A. (1998). Acyl-CoA:Di-hydroxyacetonephosphate acyltransferase: Cloning of the human cDNA and resolution of the molecular basis in rhizomelic chondrodysplasia punctata type 2. *Hum. Mol. Genet.* *7*, 847–853.
- Ogata, M. (1991). *Acatlasemia*. 331–340.
- Otera, H., Harano, T., Honsho, M., Ghaedi, K., Mukai, S., Tanaka, A., Kawai, A., Shimizu, N., and Fujiki, Y. (2000). The mammalian peroxin Pex5pl, the longer isoform of the mobile peroxisome targeting signal (PTS) type 1 transporter, translocates the Pex7p??PTS2 protein complex into peroxisomes via its initial docking site, Pex14p. *J. Biol. Chem.* *275*, 21703–21714.
- Otera, H., Setoguchi, K., Hamasaki, M., Kumashiro, T., Shimizu, N., and Fujiki, Y. (2002). Peroxisomal targeting signal receptor Pex5p interacts with cargoes and import machinery components in a spatiotemporally differentiated manner: conserved Pex5p WXXXF/Y motifs are critical for matrix protein import. *Mol. Cell. Biol.* *22*, 1639–1655.

- Otsu, N. (1979). A threshold selection method from gray-level histograms. *IEEE Trans. Syst. Man. Cybern.* *9*, 62–66.
- Parsons, M., Furuya, T., Pal, S., and Kessler, P. (2001). Biogenesis and function of peroxisomes and glycosomes. *Mol. Biochem. Parasitol.* *115*, 19–28.
- Passarge, E., and McAdams, A.J. (1967). Cerebro-hepato-renal syndrome: A newly recognized hereditary disorder of multiple congenital defects, including sudanophilic leukodystrophy, cirrhosis of the liver, and polycystic kidneys. *J. Pediatr.* *71*, 691–702.
- Pieuchot, L., and Jedd, G. (2012). Peroxisome Assembly and Functional Diversity in Eukaryotic Microorganisms. *Annu. Rev. Microbiol.* *66*, 237–263.
- Pineda, M., Girós, M., Roels, F., Espeel, M., Ruiz, M., Moser, A., Moser, H.W., Wanders, R.J., Pavia, C., Conill, J., et al. (1999). Diagnosis and follow-up of a case of peroxisomal disorder with peroxisomal mosaicism. *J. Child Neurol.* *14*, 434–439.
- Pirulli, D., Marangella, M., and Amoroso, A. (2003). Primary hyperoxaluria: genotype–phenotype correlation. *J. Nephrol.* *16*, 357–361.
- Platta, H.W., Girzalsky, W., and Erdmann, R. (2004). Ubiquitination of the peroxisomal import receptor Pex5p. *Biochem. J.* *384*, 37–45.
- Platta, H.W., Grunau, S., Rosenkranz, K., Girzalsky, W., and Erdmann, R. (2005). Functional role of the AAA peroxins in dislocation of the cycling PTS1 receptor back to the cytosol. *Nat Cell Biol* *7*, 817–822.
- Platta, H.W., El Magraoui, F., Bäumer, B.E., Schlee, D., Girzalsky, W., and Erdmann, R. (2009). Pex2 and pex12 function as protein-ubiquitin ligases in peroxisomal protein import. *Mol. Cell. Biol.* *29*, 5505–5516.
- Poznanski, A.K., Nosanchuk, J.S., Baublis, J., and Holt, J.F. (1970). The Cerebro-Hepato-Renal Syndrome (CHRS). *Am. J. Roentgenol.* *109*, 313–322.
- Purdue, P.E., Zhang, J.W., Skoneczny, M., and Lazarow, P.B. (1997). Rhizomelic chondrodysplasia punctata is caused by deficiency of human PEX7, a homologue of the yeast PTS2 receptor. *Nat Genet* *15*, 381–384.
- Purdue, P.E., Yang, X., and Lazarow, P.B. (1998). Pex18p and Pex21p, a novel pair of related peroxins essential for peroxisomal targeting by the PTS2 pathway. *J. Cell Biol.* *143*, 1859–

1869.

Rapp, S., Saffrich, R., Anton, M., Jäkke, U., Ansorge, W., Gorgas, K., and Just, W.W. (1996). Microtubule-based peroxisome movement. *J. Cell Sci.* *109*, 837–849.

Rehling, P., Marzioch, M., Niesen, F., Wittke, E., Veenhuis, M., and Kunau, W.H. (1996). The import receptor for the peroxisomal targeting signal 2 (PTS2) in *Saccharomyces cerevisiae* is encoded by the PAS7 gene. *EMBO J.* *15*, 2901–2913.

Remington, S.J. (2006). Fluorescent proteins: maturation, photochemistry and photophysics. *Curr. Opin. Struct. Biol.* *16*, 714–721.

Rhodin J. (1954). Correlation of ultrastructural organization and function in normal and experimentally changed proximal tubule cells of the mouse kidney. Stock. Karolinska Inst.

del Rio, L.A., Sandalio, L.M., Palma, J.M., Bueno, P., and Corpas, F.J. (1992). Metabolism of oxygen radicals in peroxisomes and cellular implications. *Free Radic. Biol. Med.* *13*, 557–580.

Rossanese, O.W., Reinke, C.A., Bevis, B.J., Hammond, A.T., Sears, I.B., O'Connor, J., and Glick, B.S. (2001). A Role for Actin, Cdc1p, and Myo2p in the Inheritance of Late Golgi Elements in *Saccharomyces cerevisiae*. *J. Cell Biol.* *153*, 47–62.

Rottensteiner, H., Kramer, A., Lorenzen, S., Stein, K., Landgraf, C., Volkmer-Engert, R., and Erdmann, R. (2004). Peroxisomal membrane proteins contain common Pex19p-binding sites that are an integral part of their targeting signals. *Mol. Biol. Cell* *15*, 3406–3417.

Rucktäschel, R., Girzalsky, W., and Erdmann, R. (2011). Protein import machineries of peroxisomes. *Biochim. Biophys. Acta - Biomembr.* *1808*, 892–900.

Sacksteder, K.A., Jones, J.M., South, S.T., Li, X., Liu, Y., and Gould, S.J. (2000). PEX19 binds multiple peroxisomal membrane proteins, is predominantly cytoplasmic, and is required for peroxisome membrane synthesis. *J. Cell Biol.* *148*, 931–944.

Saleem, R. a., Long-O'Donnell, R., Dilworth, D.J., Armstrong, A.M., Jamakhandi, A.P., Wan, Y., Knijnenburg, T. a., Niemistö, A., Boyle, J., Rachubinski, R. a., et al. (2010). Genome-wide analysis of effectors of peroxisome biogenesis. *PLoS One* *5*, 1–11.

Santos, M.J., Imanaka, T., Shio, H., Small, G.M., and Lazarow, P.B. (1988). Peroxisomal membrane ghosts in Zellweger syndrome--aberrant organelle assembly. *Science* *239*, 1536–1538.

- Sbalzarini, I.F., and Koumoutsakos, P. (2005). Feature point tracking and trajectory analysis for video imaging in cell biology. *J. Struct. Biol.* *151*, 182–195.
- Schindelin, J., Arganda-Carreras, I., Frise, E., Kaynig, V., Longair, M., Pietzsch, T., Preibisch, S., Rueden, C., Saalfeld, S., Schmid, B., et al. (2012). Fiji: an open-source platform for biological-image analysis. *Nat. Methods* *9*, 676–682.
- Schneider, C. a, Rasband, W.S., and Eliceiri, K.W. (2012). NIH Image to ImageJ: 25 years of image analysis. *Nat. Methods* *9*, 671–675.
- Schrader, M., and Yoon, Y. (2007). Mitochondria and peroxisomes: Are the “Big Brother” and the “Little Sister” closer than assumed? *BioEssays* *29*, 1105–1114.
- Schrader, M., King, S.J., Stroh, T. a, and Schroer, T. a (2000). Real time imaging reveals a peroxisomal reticulum in living cells. *J. Cell Sci.* *113 (Pt 2)*, 3663–3671.
- Schrader, M., Bonekamp, N.A., and Islinger, M. (2012). Fission and proliferation of peroxisomes. *Biochim. Biophys. Acta - Mol. Basis Dis.* *1822*, 1343–1357.
- Schutgens, R.B.H., Heymans, H.S. a, Wanders, R.J. a, Bosch, H.V.D., and Tager, J.M. (1986). Peroxisomal disorders: A newly recognised group of genetic diseases. *Eur. J. Pediatr.* *144*, 430–440.
- Setchell, K.D.R., Heubi, J.E., Bove, K.E., O’Connell, N.C., Brewsaugh, T., Steinberg, S.J., Moser, A., and Squires, R.H. (2003). Liver disease caused by failure to racemize trihydroxycholestanoic acid: Gene mutation and effect of bile acid therapy. *Gastroenterology* *124*, 217–232.
- Shaner, N.C., Lambert, G.G., Chammas, A., Ni, Y., Cranfill, P.J., Baird, M. a, Sell, B.R., Allen, J.R., Day, R.N., Israelsson, M., et al. (2013). A bright monomeric green fluorescent protein derived from *Branchiostoma lanceolatum*. *Nat. Methods* *10*, 407–409.
- Sibirny, A.A. (2016). Yeast peroxisomes: Structure, functions and biotechnological opportunities. *FEMS Yeast Res.* *16*, 1–14.
- Sibirny, a. a. (2012). Molecular mechanisms of peroxisome biogenesis in yeasts. *Mol. Biol.* *46*, 11–26.
- Silfies, J.S., Lieser, E.G., Schwartz, S.A., and Michael W. Davidson (2016). Correcting Focus Drift in Live-Cell Microscopy.

- Smith, J.J., and Aitchison, J.D. (2013). Peroxisomes take shape. *Nat. Rev. Mol. Cell Biol.* *14*, 803–817.
- Steinberg, S.J., Dodt, G., Raymond, G. V, Braverman, N.E., Moser, A.B., and Moser, H.W. (2006). Peroxisome biogenesis disorders. *Biochim. Biophys. Acta* *1763*, 1733–1748.
- Sternberg, S.R. (1983). *Biomedical Image Processing. Computer* (Long. Beach. Calif). *16*, 22–34.
- Tabak, H.F., Hoepfner, D., Zand, A. v d, Geuze, H.J., Braakman, I., and Huynen, M.A. (2006). Formation of peroxisomes: Present and past. *Biochim. Biophys. Acta - Mol. Cell Res.* *1763*, 1647–1654.
- Tabak, H.F., Braakman, I., and van der Zand, A. (2013). Peroxisome formation and maintenance are dependent on the endoplasmic reticulum. *Annu. Rev. Biochem.* *82*, 723–744.
- Takizawa, P.A., and Vale, R.D. (2000). The myosin motor, Myo4p, binds Ash1 mRNA via the adapter protein, She3p. *Proc. Natl. Acad. Sci. U. S. A.* *97*, 5273–5278.
- Tam, Y.Y.C., Fagarasanu, A., Fagarasanu, M., and Rachubinski, R.A. (2005). Pex3p initiates the formation of a preperoxisomal compartment from a subdomain of the endoplasmic reticulum in *Saccharomyces cerevisiae*. *J. Biol. Chem.* *280*, 34933–34939.
- Thorn, K., and Lambert, T. (2017). Fluorescent protein properties.
- Tinevez, J.-Y., Perry, N., Schindelin, J., Hoopes, G.M., Reynolds, G.D., Laplantine, E., Bednarek, S.Y., Shorte, S.L., and Eliceiri, K.W. (2016). TrackMate: an open and extensible platform for single-particle tracking. *Methods*.
- Tsien, R.Y. (1998). The green fluorescent protein. *Annu. Rev. Biochem.* *67*, 509–544.
- Unsold, M., Marienfeld, J.R., Brandt, P., and Brennicke, A. (1997). Human PEX7 encodes the peroxisomal PTS2 receptor and is responsible for rhizomelic chondrodysplasia punctata. *Nat. Genet.* *15*, 57–61.
- Vale, R.D. (2003). Myosin V motor proteins: Marching stepwise towards a mechanism. *J. Cell Biol.* *163*, 445–450.
- van der Zand, A., Gent, J., Braakman, I., and Tabak, H.F. (2012). Biochemically Distinct

- Vesicles from the Endoplasmic Reticulum Fuse to Form Peroxisomes. *Cell* 149, 397–409.
- Veenhuis, M., Van Dijken, J.P., and Harder, W. (1983). The significance of peroxisomes in the metabolism of one-carbon compounds in yeasts. *Adv. Microb. Physiol.* 24, 1–82.
- Wanders, R.J. a (2014). Metabolic functions of peroxisomes in health and disease. *Biochimie* 98, 36–44.
- Wanders, R.J. a, and Poll-The, B.T. (2015). “Role of peroxisomes in human lipid metabolism and its importance for neurological development.” *Neurosci. Lett.* 637, 1–7.
- Wanders, R.J. a, and Waterham, H.R. (2005). Peroxisomal disorders I: biochemistry and genetics of peroxisome biogenesis disorders. *Clin. Genet.* 67, 107–133.
- Wanders, R.J. a, and Waterham, H.R. (2006). Biochemistry of mammalian peroxisomes revisited. *Annu. Rev. Biochem.* 75, 295–332.
- Wanders, R.J.A., Dekker, C., Hovarth, V.A.P., Schutgens, R.B.H., Tager, J.M., van Laer, P., and Lecoutere, D. (1994). Human alkyldihydroxyacetonephosphate synthase deficiency: A new peroxisomal disorder. *J. Inherit. Metab. Dis.* 17, 315–318.
- Warren, G., and Wickner, W. (1996). Organelle inheritance. *Cell* 84, 395–400.
- Waterham, H.R., and Ebberink, M.S. (2012). Genetics and molecular basis of human peroxisome biogenesis disorders. *Biochim. Biophys. Acta - Mol. Basis Dis.* 1822, 1430–1441.
- Weisman, L.S. (2003). Yeast vacuole inheritance and dynamics. *Annu. Rev. Genet.* 37, 435–460.
- Weller, S., Gould, S.J., and Valle, D. (2003). Peroxisome Biogenesis Disorders. *Annu. Rev. Genomics Hum. Genet.* 4, 165–211.
- White, J., and Stelzer, E. (1999). Photobleaching GFP reveals protein dynamics inside live cells. *Trends Cell Biol.* 9, 61–65.
- Wiemer, E.A.C., Wenzel, T., Deerinck, T.J., Ellisman, M.H., and Subramani, S. (1997). Visualization of the peroxisomal compartment in living mammalian cells: Dynamic behavior and association with microtubules. *J. Cell Biol.* 136, 71–80.
- Wierzbicki, A.S., Lloyd, M.D., Schofield, C.J., Feher, M.D., and Gibberd, F.B. (2002). Refsum’s disease: A peroxisomal disorder affecting phytanic acid ??-oxidation. *J.*

Neurochem. *80*, 727–735.

Williams, C., van den Berg, M., Geers, E., and Distel, B. (2008). Pex10p functions as an E3 ligase for the Ubc4p-dependent ubiquitination of Pex5p. *Biochem. Biophys. Res. Commun.* *374*, 620–624.

Williams, E.L., Acquaviva, C., Amoroso, A., Chevalier, F., Coulter-Mackie, M., Monico, C.G., Giachino, D., Owen, T., Robbiano, A., Salido, E., et al. (2009). Primary hyperoxaluria type 1: Update and additional mutation analysis of the AGXT gene. *Hum. Mutat.* *30*, 910–917.

Wilson, G.N., Holmes, R.G., Custer, J., Lipkowitz, J.L., Stover, J., Datta, N., and Hajra, a (1986). Zellweger syndrome: diagnostic assays, syndrome delineation, and potential therapy. *Am. J. Med. Genet.* *24*, 69–82.

Yang, T.T., Cheng, L., and Kain, S.R. (1996). Optimized codon usage and chromophore mutations provide enhanced sensitivity with the green fluorescent protein. *Nucleic Acids Res.* *24*, 4592–4593.

Yik, W.Y., Steinberg, S.J., Moser, A.B., Moser, H.W., and Hacia, J.G. (2009). Identification of novel mutations and sequence variation in the Zellweger syndrome spectrum of peroxisome biogenesis disorders. *Hum. Mutat.* *30*, E467–E480.

Zaar, K., Volkl, A., and Fahimi, H.D. (1991). Purification of marginal plates from bovine renal peroxisomes: Identification with L- α -hydroxyacid oxidase B. *J. Cell Biol.* *113*, 113–121.

Zack, G.W., Rogers, E., and Latt, S. (1977). AUTOMATIC-MEASUREMENT OF SISTER CHROMATID EXCHANGE FREQUENCY. *J. Histochem. Cytochem.* 11–14.

van der Zand, A., and Tabak, H.F. (2013). Peroxisomes: Offshoots of the ER. *Curr. Opin. Cell Biol.* *25*, 490–454.

van der Zand, A., Braakman, I., and Tabak, H. (2010). Peroxisomal Membrane Proteins Insert into the Endoplasmic Reticulum. *Mol. Biol. Cell* *21*, 2057–2065.

